Energy Research and Development Division
FINAL PROJECT REPORT

UTILITY SCALE SOLAR FORECASTING, ANALYSIS AND MODELING

Prepared for: California Energy Commission
Prepared by: EnerNex LLC

EnerNex

FEBRUARY 2017
CEC-500-2017-010

PREPARED BY:

Primary Author(s):
Kay Stefferud
Jens Schoene
Vadim Zheglov
Jan Kleissl
Jack Fraser
Hilal Katmale

EnerNex, LLC
620 Mabry Hood Road, Suite 300
Knoxville, TN 37922
Phone: 865-218-4600 | Fax: 865-218-8999
http://www.enernex.com
Contract Number: 500-10-060

Prepared for:

California Energy Commission

Gail Wiggett
Hassan Mohammed
Contract Manager

Aleecia Gutierrez
Office Manager
Energy Generation Research Office

Laurie ten Hope
Deputy Director
ENERGY RESEARCH AND DEVELOPMENT DIVISION

Robert P. Oglesby
Executive Director

ACKNOWLEDGEMENTS

The researchers thank Southern California Edison (SCE) for supporting the project, including hosting the sky imagers, providing and customizing data, assisting with the modeling, and providing insight into forecasting and distribution system requirements. Specifically the researchers thank Sunil Shah, George Rodriguez, Darrell Holmes, Jerry Isaac, and Jack Peterson.

PREFACE

The California Energy Commission Energy Research and Development Division supports public interest energy research and development that will help improve the quality of life in California by bringing environmentally safe, affordable, and reliable energy services and products to the marketplace.

The Energy Research and Development Division conduct public interest research, development, and demonstration (RD&D) projects to benefit California.

The Energy Research and Development Division strives to conduct the most promising public interest energy research by partnering with RD&D entities, including individuals, businesses, utilities, and public or private research institutions.

Energy Research and Development Division funding efforts are focused on the following RD&D program areas:

- Buildings End-Use Energy Efficiency
- Energy Innovations Small Grants
- Energy-Related Environmental Research
- Energy Systems Integration
- Environmentally Preferred Advanced Generation
- Industrial/Agricultural/Water End-Use Energy Efficiency
- Renewable Energy Technologies
- Transportation

Utility Scale Solar Forecasting, Analysis and Modeling is the final report for the Research Needs for Utility-Scale Renewable Energy project (contract number 500-10-060) conducted by EnerNex LLC. The information from this project contributes to Energy Research and Development Division's Renewable Energy Technologies Program.

When the source of a table, figure or photo is not otherwise credited, it is the work of the author of the report.

For more information about the Energy Research and Development Division, please visit the Energy Commission's website at www.energy.ca.gov/research/ or contact the Energy Commission at 916-327-1551.

ABSTRACT

The research team investigated how increased use of solar photovoltaic generation impacts electrical distribution systems in Southern California. Through computer simulations and measured solar irradiance data, the investigation quantified the effects of an estimated 200 megawatts of commercial-scale photovoltaic generation within Southern California Edison service territory. For this study, the researchers used Supervisory Control and Data Acquisition system data, cloud images, modeling, simulation, and analysis of two distribution feeders with high photovoltaic penetration from three large scale photovoltaic systems totaling 6.5 megawatts.

Significant project findings include: (1) reverse power flows occur during times of high photovoltaic generation, (2) voltages remain within acceptable ranges even when large loads are dropped, and (3) settings for the protective relays need to be adjusted to account for the reverse power flows. Solar forecasting is possible out to a 15 minute time frame, and ramp rate prediction is possible within one to two minutes accuracy. Limitations of solar forecasting include the range of the sky camera and restrictions early and late in the day when the sun is low on the horizon.

Technology transfer opportunities exist for the solar forecasting hardware systems and algorithms as well as for protection schemes for high penetration levels of utility scale photovoltaic systems.

Keywords: Renewable energy, solar forecasting, photovoltaic, distribution system, power quality, power system models, PV generation models Please use the following citation for this report:

Kay Stefferud, Jens Schoene, Vadim Zheglov; EnerNex LLC; Jan Kleissl, UCSD. 2015. ***Analysis and Modeling of Utility Scale Solar Forecasting.*** California Energy Commission. Publication number: CEC-500-2017-010.

TABLE OF CONTENTS

LIST OF FIGURES

LIST OF TABLES

EXECUTIVE SUMMARY

Introduction

The increasing popularity of solar photovoltaic (PV) installations in California requires utility companies to address issues that might affect the state's electrical distribution systems. Utility companies and the California Independent System Operator (CAISO) require accurate solar forecasts to maintain grid reliability, optimize overall production of renewables, and efficiently model forecasted loads throughout CAISO territory. To determine the effects of utility-scale solar PV systems on the electric grid, researchers performed modeling, simulation, and analysis of two high-use PV distribution feeders with three solar PV systems in Southern California Edison (SCE) service territory.

Project Purpose

This project helped utility companies prepare for issues and impacts caused by increased PV installations on their distribution systems. Since PV generation is driven by weather processes, it varies from moment to moment. Of particular interest to the electric power industry are these changes such as sudden changes in irradiance (amount of light hitting a square meter). These "ramp events" require ancillary services to ramp up or down to meet the change in electrical supply and maintain power quality. Cloud cover can also result in ramp events reducing output by 50 to 80 percent within seconds. Short-term irradiance fluctuations can cause voltage fluctuations triggering automated equipment and lead to larger maintenance costs for utilities. This project investigated and analyzed methods to improve accuracy of intra-hour solar production forecasts and quantify the effects of the estimated 200 megawatts (MW) of commercial-scale PV generation to be installed in SCE service territory.

Project Process

Through computer simulations, modeling, measured solar irradiance data, line voltages, line reactive power (VARs), and recorded PV system generation, the investigation quantified the effects of an estimated 200 MWs of commercial-scale PV generation to be installed in SCE territory.

The project installed two sky camera systems (University of California San Diego (UCSD) sky imagers) adjacent to the solar PV systems. The research team tested and verified the sky camera forecasting procedures (algorithms) ability by collecting and analyzing the sky images and solar system production data.

For more than two months, the research team investigated and analyzed zero to 15 minute power output forecasts for each of the solar PV systems. Forecast performance was analyzed against a one minute resolution satellite forecast. Forecasting ability is possible out to a 15 minute time frame and ramp rate prediction is possible within one to two minutes accuracy. Forecasting limitations include the range of the sky camera and sun restrictions early and late in the day when the sun is low on the horizon.

Project Results

Significant project findings include: (1) reverse power flows occur during times of high PV generation, requiring SCE to adjust their monitoring equipment to account for bi-directional power flow, and (2) voltages remain within permissible ranges even when large loads are dropped, indicating that the investigated SCE feeders do not require additional voltage regulation equipment. However, due to commercial buildings with large rooftops tending to be clustered together in relatively small commercially zoned areas, existing SCE distribution feeders serving these areas are already experiencing greater than 100 percent PV penetration and its effects, such as reverse power flows. The solar forecast errors for the UCSD sky imagers were comparable to the satellite forecasts with a slight advantage for the UCSD sky cameras.

Project Benefits

During the study, increasingly high levels of solar PV use occurred in California. The research showed that distribution feeders could successfully handle high levels of solar PV generation, allowing California meet its renewable energy goals and reduce greenhouse gas (GHG) emissions. Changes in protection schemes on some distribution feeders would be necessary where the additional short circuit contribution from the PV installations is significant. Forecasting ability 15 minutes in the future and ramp rate prediction can help utilities manage solar PV systems operationally. Accurate forecasting of solar PV output in cloudy conditions allow for more efficient integration and use of solar PV generation, helping California reduce GHG emissions. The research has two main potential areas of tecnology transfer: (1) Solar forecasting hardware systems and algorithms using cloud forecasts for intra-hour and other time frames, and (2) Impacts and recommended protection schemes for high penetration levels of utility scale PV systems.

Chapter 1:
Introduction

1.1 Project Background

Renewable generation is being incentivized in the United States and globally resulting in increasing numbers of solar photovoltaic (PV) systems being installed in residential, commercial, industrial and utility applications. Utilities must be prepared for potential issues caused by increased levels of PV penetration on their distribution systems. Utilities and the California Independent System Operator (CAISO) require accurate solar forecasts to maintain grid reliability and to optimize overall production of renewables as well as to efficiently model forecasted loads throughout CAISO territory. Goals of the project were to 1) improve the accuracy of intra-hour solar production forecasts and 2) quantify the effects of the estimated 200 megawatts (MW) of commercial-scale PV generation to be installed in SCE service territory.

PV generation is driven by meteorological processes and consequently it is inherently variable. Solar generation variability occurs on a wide range of utility operation time periods– from real-time minute-to-minute fluctuations through yearly variations affecting long term planning. A conceptual view of the time frames involved when considering the power system impacts of integrating solar energy is depicted in Figure 1.

Figure 1: Time Scales **of Importance - Power System Impacts of Integrating Renewable Energy**

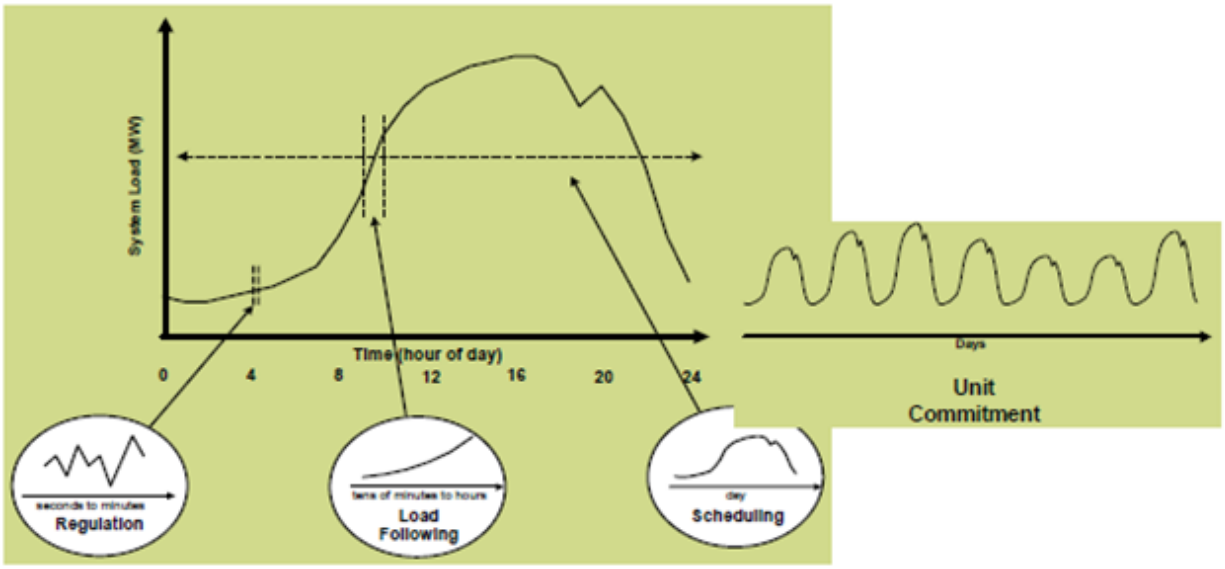

Appropriate system models are required to assess the implications of the uncertainty and variability of solar generation for operational and planning practices, and for system reliability.

Solar power presents a significant challenge because of high variability and uncertainty compared to conventional energy generation like natural gas or coal, while at the same time it is subject to environmental factors that are not controllable.

SCE has installed more than 30,000 PV systems on its distribution grid. The projected capacity for California-wide customer-installed PV systems is projected to be 3.2 gigawatts (GW) in 2016. Variability in solar irradiance makes regulating and maintaining power both more challenging and more costly, as the uncertainty requires larger regulation and spinning reserve capacities in order to meet ancillary service requirements. Reducing the uncertainty of solar power by solar forecasting methods can not only reduce the more expensive operating costs of ancillary services, but also allows utilities, CAISO and energy traders to make more reliable bids in the wholesale energy market.

Of particular interest to the electric power industry are sudden changes in irradiance, termed "ramp events"[1], as ramp events in turn require ancillary services to ramp up or down to meet the change in electrical supply and maintain power quality. Cloud cover can result in ramp events causing reductions in output by 50 to 80% within the time period it takes a large cloud to cover an array (typically on the order of 10 seconds). Short-term irradiance fluctuations can cause voltage fluctuations that can trigger operation of automated line equipment (e.g. tap changers) on distribution feeders leading to larger maintenance costs for utilities. Given constant load, counteracting such fluctuations would require dynamic inverter VAR control or a secondary power source (e.g. energy storage) that could ramp up or down at high frequencies to provide load following services. Such ancillary services are costly to operate, so reducing short-term variation is essential. Longer scale variations caused by cloud groups or weather fronts are also problematic as they lead to a large consistent reduction in power generation over a large area. These long-term fluctuations are easier to forecast and can be mitigated by slower ramping (but larger) supplementary power sources, but the ramping and scheduling of solar plants also adds costs to the operation of the electric grid. Grid operators are often concerned with worst-case scenarios, and it is important to understand the behavior of PV power output fluctuations over various timescales.

Therefore, solar forecasting plays a critical role in the integrating Utility Scale Renewable Energy (USRE). Accurate forecasts would allow load-following generation that is required to

---

[1] Pfister, G., McKenzie, R. L., Liley, J. B., Thomas, A., Forgan, B. W., Long, C. N., October 2003. Cloud coverage based on all-sky imaging and its impact on surface solar irradiance. Journal of Applied Meteorology and Climatology 42 (10), 1421 - 1434.

counteract ramps from USRE to be scheduled in the lower cost day-ahead market. Recent integration studies by National Renewable Energy Laboratory (NREL) and General Electric (GE) using 2020 renewable integration scenarios have shown economic values of renewable forecasting of $5 billion/year under 2020 USRE scenarios for the Western Electricity Coordinating Council (WECC) alone. With the advance of smart grid efforts the once autonomous operation of distribution systems will also benefit from solar forecasting and solar resource variability analysis.

1.2 Project Methodology Overview

For the Utility Scale Solar Forecasting, Analysis and Modeling (USRE) project, EnerNex, the University of California in San Diego (UCSD), Advantech, and Southern California Edison (SCE) investigated the effects of large scale solar PV on SCE's distribution systems. One part of the USRE project was to improve the accuracy of intra-hour solar production forecasts. A second part of the investigation quantified, through computer simulations and measured solar irradiance data, the effect of the estimated 200 MW of commercial-scale PV generation in SCE service territory.

1.2.1 Sky Imagers Forecasting Approach

The project installed two sky camera systems also known as sky imagers at two solar sites in SCE territory. Figure 2 shows the installation of the sky camera system at one site, adjacent to the utility-scale solar PV system.

Figure 2. Sky Camera Installation at SCE Utility Scale Solar PV Site

UCSD Sky Imagers (USI) were deployed for a year at a distribution feeder with utility-scale warehouse rooftop solar plants owned by SCE. Sky imager data and power output were available every 30 seconds. The largest one minute ramps in power output were 46% of DC capacity for the smallest 1.7 MW solar plant, while the largest plant (5 MW) solar plant only showed ramps up to 25% of PV capacity.

Zero to fifteen minute power output forecasts for each of the four rooftop solar plants were investigated over two months and two days were analyzed in greater depth. USI forecast performance was also analyzed against a one minute resolution satellite forecast. The forecast errors are comparable with slight advantages for the USI.

1.2.2 Distribution and PV Systems Modeling Approach

To determine the effects of utility-scale solar PV systems on the grid, modeling of two high-PV penetration distribution feeders in SCE's service territory along with 3 large scale PV systems was performed. Because commercial buildings with large rooftops tend to be clustered together in relatively small commercially zoned areas, existing SCE distribution feeders including the feeders studied are experiencing 100% PV penetration.

The study modeled and validated two SCE distribution circuits with high penetration levels of PV. The generation levels of each of the PV generators were individually determined from irradiance data taken from field measurements. Modeling scenarios included the loss of the two largest loads during high solar production periods augmenting reverse power flows. The model was used to investigate the following effects of the PV installed on the SCE distribution feeder: (1) voltage control, (2) effects of losing large loads, and (3) overcurrent and relay protection.

The data collection period was over a one-year time period which accounts for seasonal changes and cloud shading. Consequently, the time-of-day variation of the power generated by each PV generator was modeled in a highly realistic fashion. The distribution feeder included 3 large scale PV systems (2 MW, 2 MW and 2.5 MW) and the two largest loads totaled 934 MVA.

1.2.3 SCE Supplied Data

SCE provided distribution system models for the circuits in CYME format which were converted by EnerNex and used in the system modeling tasks. (CYME is a widely-used commercial power engineering distribution system modeling application.) SCE provided infromation on commerical inverter specifications for use in the models.

Supervisory Control And Data Acquisition (SCADA) data was acquired from SCE for the distribution feeders studied. SCADA data provided included time stamps, generation, line voltages, irrandiances, weather conditions such as wind speed and ambiant temperature as well as panel temperatures for the solar PV installations.

1.3 Standards Relevant to Operational Solar PV System

Standards, in particular inverter standards such as Institute of Electrical and Electronics Engineers (IEEE) 1547 define some operating characterteristics of the solar PV systems.

1.3.1 Current State of Institute of Electrical and Electronics Engineers (IEEE) Standard 1547

IEEE 1547-2008 is relevant to the evaluation of solar PV systems' impact on the distribution grid, because the current IEEE 1547 rules limit the ability of renewable generation, including

solar PV systems, to address issues that occur on systems with high penetration levels of solar PV.

IEEE standard 1547-2008 is the "Standard for Interconnecting Distributed Resources with Electric Power Systems". The 1547 standard was initially approved by the IEEE in 2003, and re-affirmed with no changes in 2008. The standard is technically voluntary, but has been referenced in the Federal Energy Policy Act of 2005 and by many state regulatory commissions. Many utility interconnection specifications, including those of the California IOUs and other California distribution utilities specifically reference the standard.

IEEE 1547 amendments under consideration permit, but do not require, voltage regulation, voltage ride-through and frequency ride-through, and were intended to address the changing system requirements due to the increased penetration of Distributed Generation (DG) on distribution systems. The consensus is that the revolution in power electronics and the integration of variable generation have continued at a rapid pace since the standard was written, and it is time to update the standard to address increasing levels of DG, including high penetrations of solar PV.

At the time of writing this report, there was considerable discussion of amendments to IEEE 1547-2003 and of a major revision for the 2018 deadline, if not sooner. A project authorization request (PAR) has been established to amend 1547-2003 to address three topics for change; voltage regulation, voltage ride-through, and frequency ride-through, and in August 2012 IEEE Standards Association approved this PAR. The amended IEEE 1547-2003 was in the balloting stage (as of February 2014). The comments to draft #3, issued in December 2013, were accepted in January 2014. The current intention is that these amendments to 1547-2003 will be completed, balloted, and approved by June, 2014. A PAR has been submitted to begin work on the full revision of 1547-2003 to be completed no later than 2018.

Proposed amendments to IEEE 1547 permit, but do not require, voltage regulation, voltage ride-through, and frequency ride-through, and were intended to address the changing system requirements due to the increased penetration of DG on distribution systems. The consensus is that the revolution in power electronics and the integration of variable generation have continued at a rapid pace in the eleven years since the standard was written, and it is time to re-write the standard for the new technology landscape.

1.3.2 Smart Inverter Working Group (SIWG)

The joint Energy Commission/ California Public Utilities Commission (CPUC) Smart Inverter Working Group (SIWG) recommendations are relevant to the evaluation of solar PV systems' impact on the distribution grid because the use of smart inverter functions can, to a large extent, mitigate the impact of large penetration levels of PV.

A joint effort between the CPUC and the Energy Commission is under way to develop recommendations to the CPUC to support advanced functionality of distributed generation system inverters. The recommendations include the technical steps to be taken to optimize distributed generation inverter functionality to support distribution system operations.

The joint CEC/CPUC SIWG published its list of recommendations in January 2014. The list of recommendations was filed with the CPUC in February 2014. The recommendations are available on the web at http://www.energy.ca.gov/electricity_analysis/rule21/documents/recommendations_and_test_plan_documents/Recommendations_for_updating_Technical_Requirements_for_Inverters_in_DER_2014-02-07-CPUC.pdf

SIWG recommendations of interest which can help control solar variability include:

- Ride-through of low/high voltage excursions beyond normal limits
- Ride-through of low/high frequency excursions beyond normal limits
- Volt/VAr control through dynamic reactive power injection through autonomous responses to local voltage measurements
- Define ramp rates
- Provide reactive power by a fixed power factor
- Soft-start reconnection
- Provide status and measurements on current energy and ancillary services
- Limit maximum real power output

1.4 Modeling of Control Area and Distribution System

1.4.1 General Description and Selection of Distribution Feeder

Simulation and modeling of two high-PV penetration distribution feeders in the SCE service territory were performed using OpenDSS. OpenDSS is an Electric Power Research Institute (EPRI) sponsored tool commonly used to analyze distributed generation connected to utility distribution systems. The distribution feeders were selected in coordination with SCE.

The first SCE feeder studied is identified as 'Feeder A' and is a feeder that predominantly provides power to large industrial customers. Figure 3 shows the locations and sizes of the 94 customers/loads on feeder A. In Figure 3 each circle represents a load bus with the size and color of the circle indicating the rating of the load.

Figure 3: Location and Sizes ofLoads on SCE's Feeder A

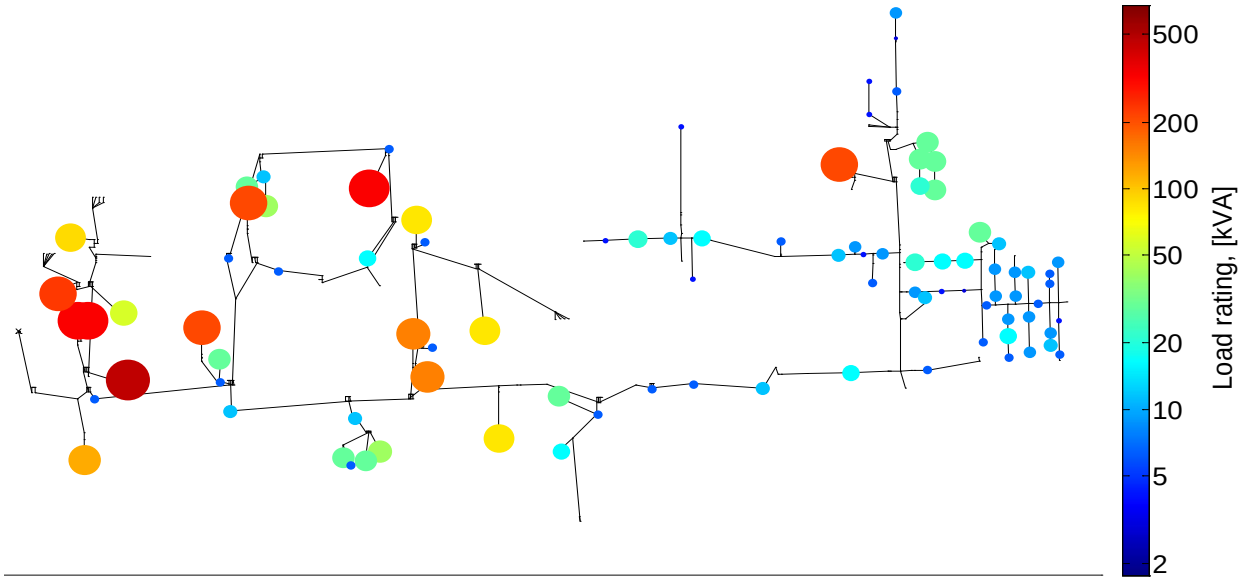

Figure 4: Locations and Sizes of Utility-scale PV Systems on SCE's Feeder A

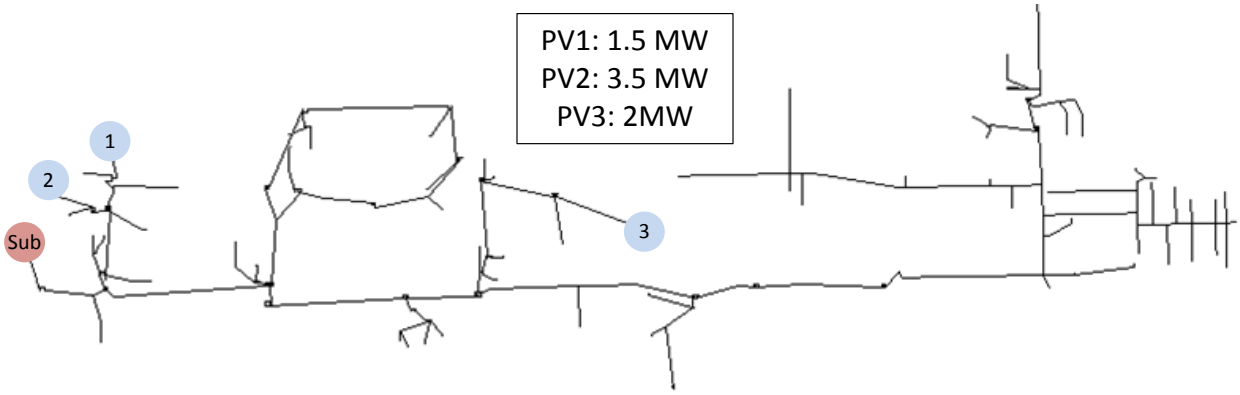

The feeder has three large utility-scale PV systems with a total rated power of 7 MW as illustrated in Figure 4. The rated size of the substation transformer is 10 megavolt amperes (MVA) and the total length of the feeder is 25570 feet (7.794 km).The characteristics of Feeder A are summarized in Table 1.

Table 1: Summary of Characteristics of Feeder A

Feeder A Parameters		Values
General	Buses	595
	Devices	688
Conductors	Length of three-phase lines	86.35 kft / 26.32 km
	Length of two-phase lines	0 kft/ 0 km
	Length of single-phase lines	0 kft/ 0 km
Substation	Voltage level	12 kVRMS (LL)
	Rating	10 MVA
Loads	Peak Demand (2012 - 2013)	9.1 MVA
	Number of three-phase loads	47
	Number of single-phase loads	47
PV	Number of PV generators	3
	Total rating	7 MW
Transformers	Number of transformers	14 (PV) + 1 (sub)
	Number of voltage regulators	0
Capacitor Banks	Total number of capacitor banks	2
	Rating	1200 MVAr

The second feeder is identified as 'Feeder B', and it provides power to predominantly large industrial customers. Figure 5 shows the locations and sizes of the 123 customers/load locations

on the feeder. Each circle represents a load bus with the size and color of the circle being indicative of the rating of the load. The aggregate rated load on the feeder is 8 MVA.

Figure 5: Location and Sizes of Loads on SCE's Feeder B

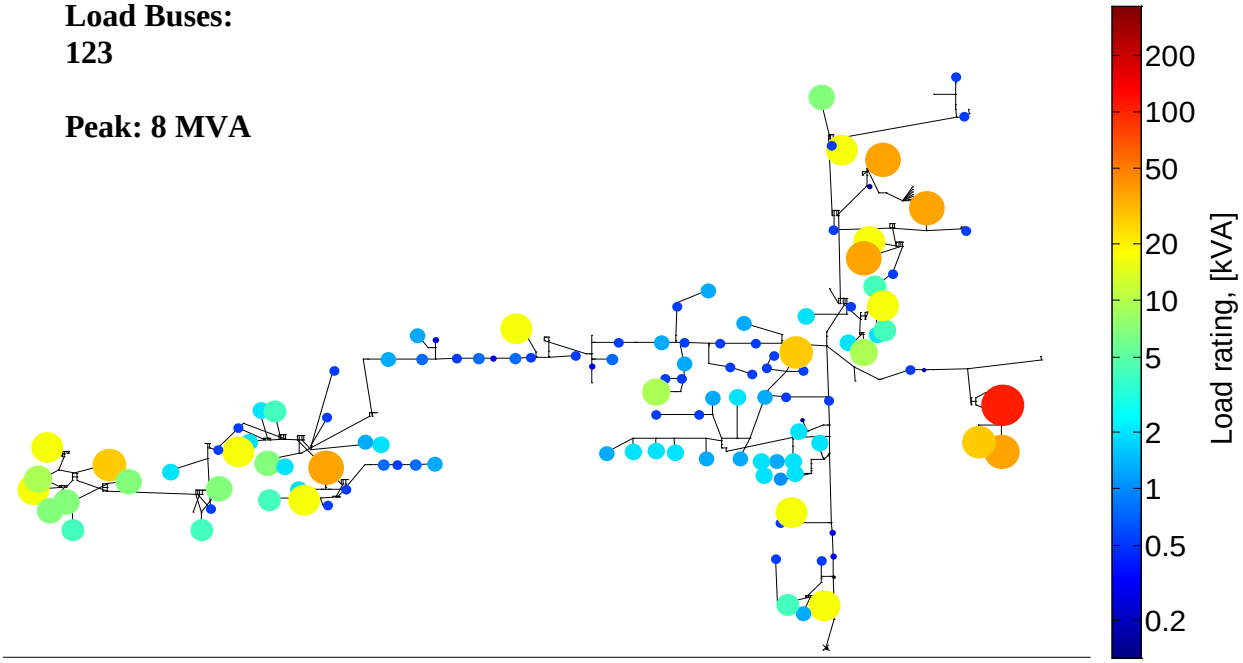

The feeder has one large utility-scale PV system of 3.5 MW illustrated in Figure 6. The rated size of the substation transformer is 10 MVA and the total length of the feeder is 17813 feet (5.429 km). The characteristics of Feeder B are summarized in Table 2.

Figure 6: Location and Sizes of Loads on SCE's Feeder B

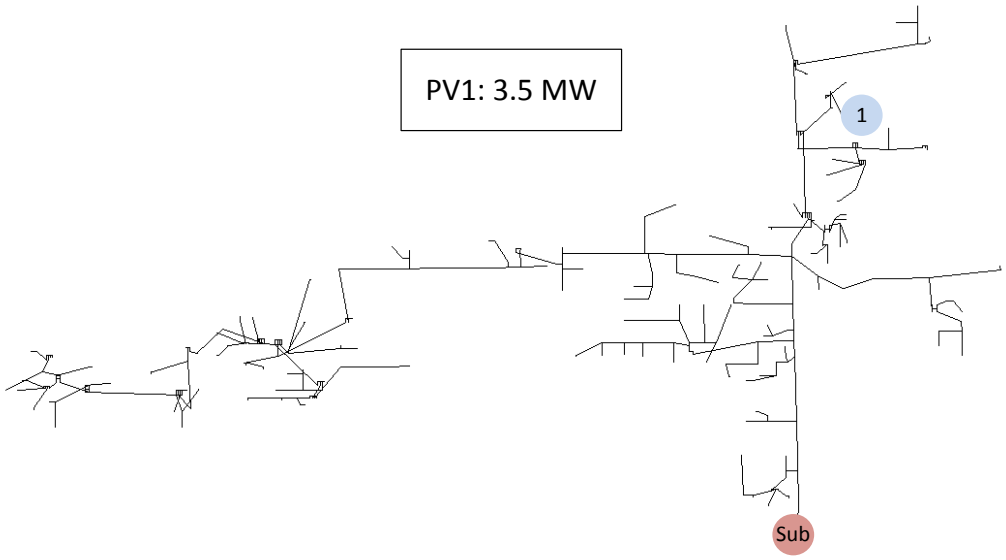

Table 2: Summary of Characteristics of Feeder B

Feeder B Parameters		Values
General	Buses	730
	Devices	597
Conductors	Length of three-phase lines	63.97 kft / 19.5 km
	Length of two-phase lines	6.7 kft/ 2.05 km
	Length of single-phase lines	5.34 kft/ 1.63 km
Substation	Voltage level	12 kVRMS (LL)
	Rating	10 MVA
Loads	Peak Demand (2012 - 2013)	8 MVA
	Number of three-phase loads	82
	Number of single-phase loads	41
PV	Number of PV generators	1
	Total rating	3.5 MW
Transformers	Number of transformers	7 (PV) + 1 (sub)
	Number of voltage regulators	0
Capacitor Banks	Total number of capacitor banks	2
	Rating	2400 MVAr

1.4.2 Modeling Approach, Assumptions, and Validation

In this section, the modeling approach, modeling assumptions, and validation process used are described to create the computer models of the Feeders A and B.

1.4.2.1 Modeling Approach

The simulation tool used in the analysis is OpenDSS[2]. Key features of OpenDSS relevant to the study include (1) multi-phase unbalanced power flow, short-circuit, and dynamics analysis, (2) time-sequenced simulation of overcurrent protective devices, regulator controls, and capacitor controls, (3) duration curve, duty cycle, and Monte Carlo simulation models for variable load and generation. In the spectrum of modeling complexity and capability, OpenDSS lies between a typical commercial distribution software package and Electromagnetic Transient (EMT) type programs.

The research team created OpenDSS models of SCE's Feeders A and B distribution feeders from CYME simulation files that were provided and validated by SCE. CYME is another power system analysis tool from Eaton's Cooper Power System. The validation process SCE used was as follows:

1) Select a high PV generation/low load case
2) Collect the following circuit loading and PV generation data from SCE's Supervisory Control And Data Acquisition (SCADA) system:
    a. Date/time for validation inputs
    b. PV site MW
    c. PV site Point of Common Connection (PCC) kilovolts (kV)
    d. PV site Mega Volt Ampere Reactive (MVAr). Not used in simulation as PV is set to unity power factor.
    e. Circuit amps per phase
    f. Circuit bank kV
    g. Circuit MVAr
3) Retrieve capacitor set points and capacitor status from SCE's Distribution Management System (DMS)
4) Check event log to ensure no events occurred during validation period
5) Retrieve circuit information from CYME database
6) Validate conductors
7) Set phase connection default types:

[2] OpenDSS has been tailored for distribution system studies. EnerNex staff has contributed to the development of OpenDSS.

a. All single-phase conductors and single-phase transformers default to A.
b. All two-phase conductors and two-phase transformers default to AB.
c. Change the default connection types based on a drawing that has the correct connection types.
d. Make assumptions for conductors/transformer for which information on connection type is not available. Assumptions are made so that the system is left partially unbalanced to match the transformer capacity ratios to the SCADA loading.

8) Validate source impedance and voltage
9) Check capacitor status and set to case conditions
10) Set PV generator models to desired output
11) Run load allocation for conditions
12) Run power flow
13) Run short circuit analysis
14) Check results versus SCADA data and source fault duty
15) Output:
    a. CYME simulation files for the validated case in text format
    b. Power flow results
    c. Short circuit report

SCE provided EnerNex the power flow results, short circuit report, and the CYME simulation files. The CYME simulation files contain the following information:

- Network topology: information on buses, equipment settings, and which types of equipment are connected to the buses,
- Equipment characteristics: specifications of capacitors, voltage regulators, and other utility equipment
- Load locations and characteristics

EnerNex developed Matlab code that (1) extracts the system information from the CYME database, (2) processes the information to generate all parameters needed for the OpenDSS model, and (3) creates files that can be used as input to the OpenDSS simulation. In addition, a visualization tool was developed that yields information about the location and properties of each object in the system. The OpenDSS model was benchmarked with the power flow and short circuit simulation results from the validated CYME models.

1.4.2.2 Assumptions

Some information was not included in the customer-provided CYME database. For instance, the information related to the substation transformers[3] and short circuit current contributions of the individual PV inverters. The data gaps were dealt with by using the customer-provided short circuit currents and power flow results from CYME model runs as a benchmark for the OpenDSS simulations, that is, the priority was to match the OpenDSS results to the CYME results[4]. This required some adjustments to the converted OpenDSS model, which was checked to ensure that the parameters used in the converted OpenDSS circuit, such as load impedances, source impedances, reactive compensation etc. are within the parameter ranges that are typical for actual feeder. It is believed the effects of these limitations are minor and do not impact the validity of the conclusions drawn from the simulation results.

1.4.2.3 Validation of Feeder A

In this section, the results of our validation process for the Feeder A were presented. The validation process encompasses a comparison of (1) the short-circuit currents and power flow results provided by SCE and (2) the respective results from our OpenDSS simulations. SCE obtained the power flow results from their validated CYME model. Both, the short-circuit currents and the power flow results were matched satisfactory.

Figure 7 shows a comparison of short circuit current between the provided CYME results and results from the OpenDSS simulation.

[3] It is common practice at the host utility to aggregate loads and other components, such as service transformers, to reduce the model complexity. Consequently, the transformer impedances are not resolved in the CYME models but are rather incorporated in the load impedances.

[4] The better approach is to verify the simulation results using measured data, but since these were not available to the team, they believe that achieving consistency with the host utility's simulation results is the second best approach, which is in line with the conceptual nature of this study.

Figure 7: Feeder A - Comparison of Short Circuit Currents

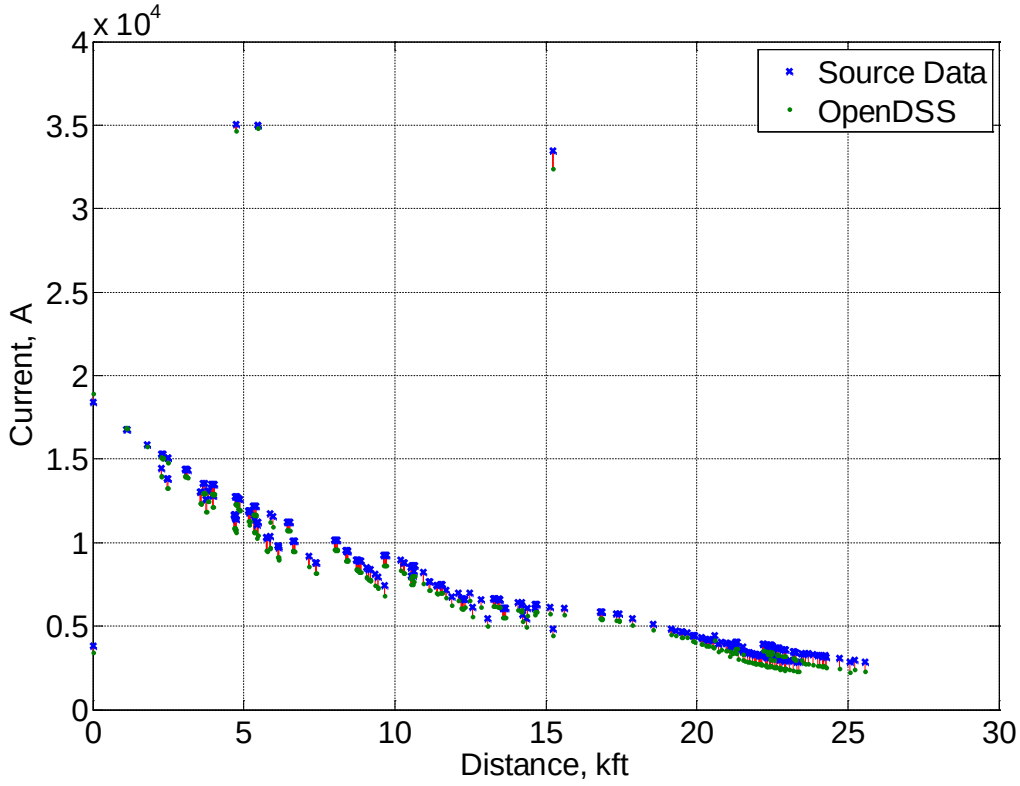

Obtained from simulation results from OpenDSS and CYME.

Figure 8 shows a comparison of the active powers between the provided CYME results and results from the OpenDSS simulation.

Figure 8: Feeder A - Comparison of Active Powers

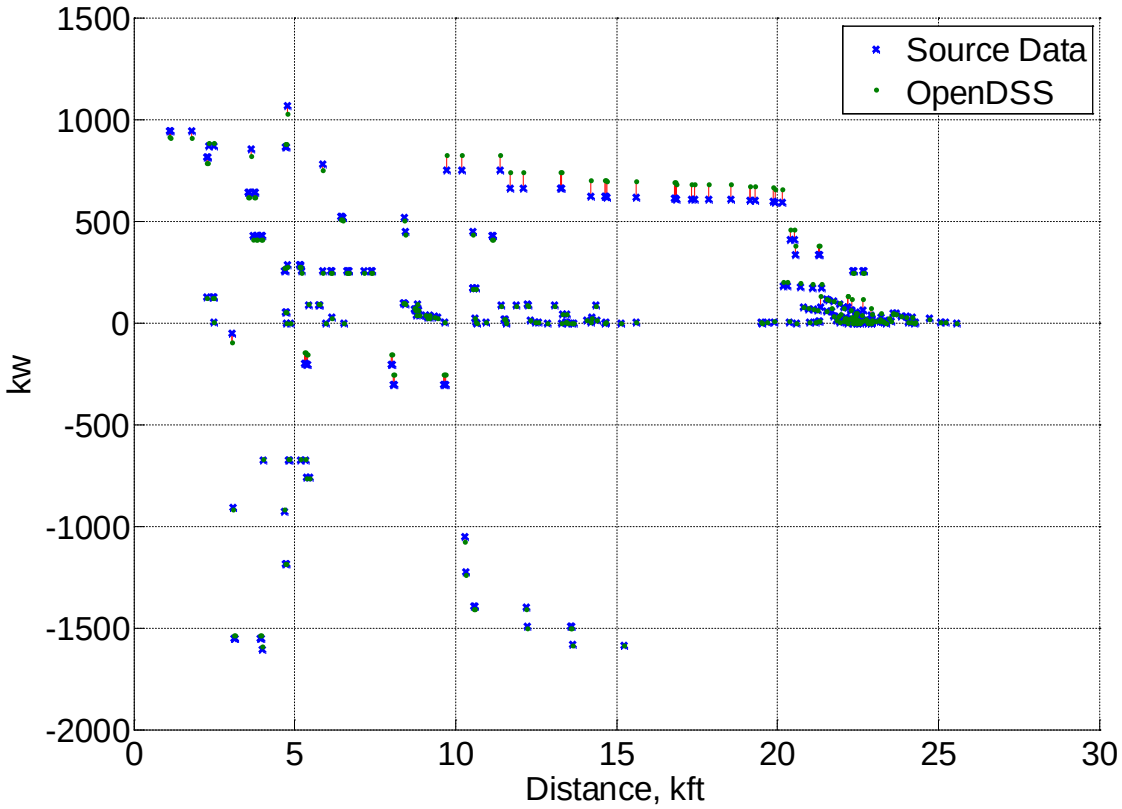

Obtained from OpenDSS and CYME power flow runs.

Figure 9 shows a comparison of the reactive powers between the provided CYME results and results from the OpenDSS simulation.

Figure 9: Feeder A - Comparison of Reactive Powers

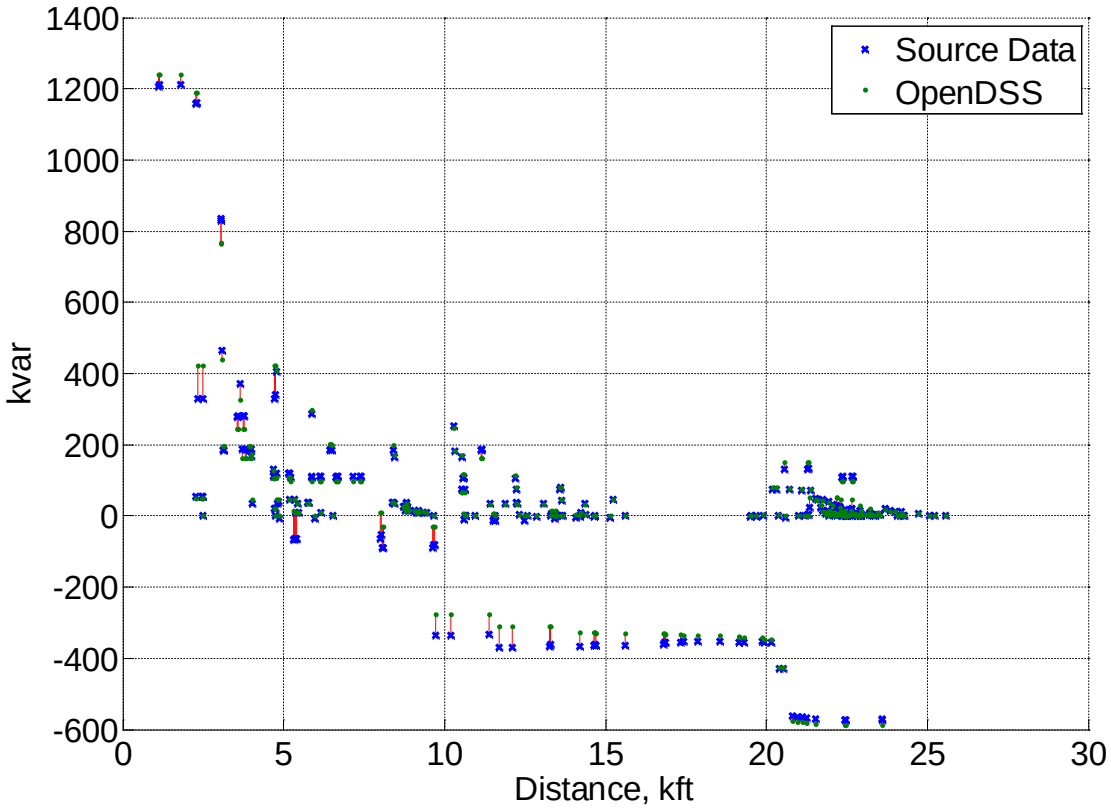

Obtained from OpenDSS and CYME power flow runs.

1.4.2.4 Validation of Feeder B

This section presents the results of the validation process for the Feeder B. As was done for Feeder A, this validation process encompasses a comparison of (1) the short-circuit current and power flow results provided by SCE and (2) the respective results from our OpenDSS simulations. SCE obtained the power flow results from their validated CYME model. Both, the short-circuit currents and the power flow results were matched satisfactory.

Figure 10 shows a comparison of the short circuit current between the provided CYME results and results from the OpenDSS simulation in Feeder B. Figure 11 shows a comparison of active powers obtained from OpenDSS and CYME power flow runs.

Figure 10: Feeder B -Comparison of Short Circuit Currents

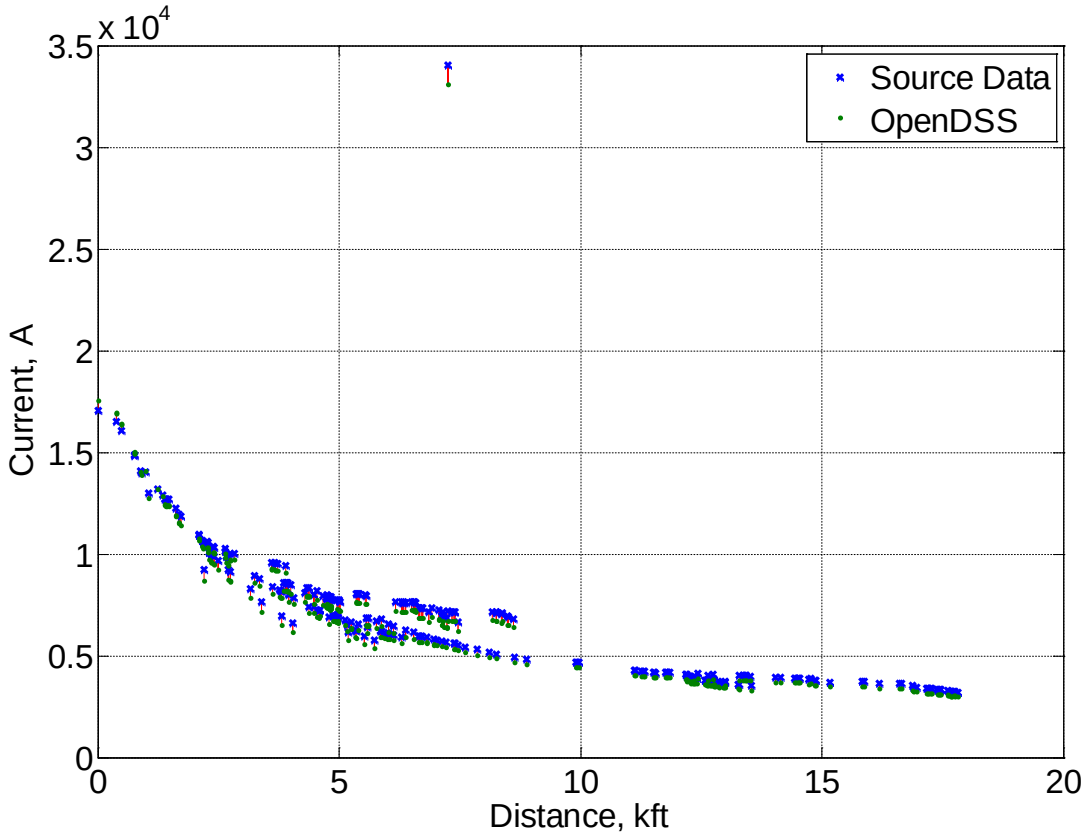

Obtained from simulation results from OpenDSS and CYME

Figure 11: Feeder B, comparison of active powers.

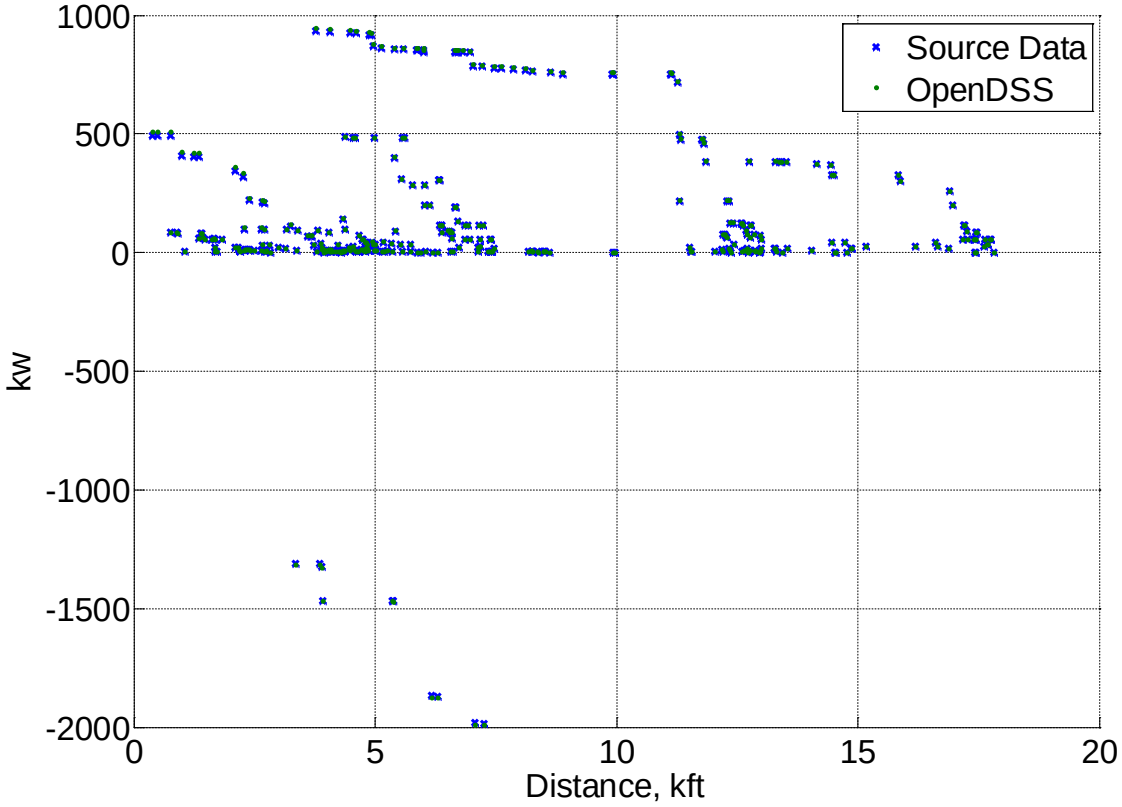

Obtained from OpenDSS and CYME power flow runs

Figure 12 shows a comparison of the reactive powers between the provided CYME results and results from the OpenDSS simulation.

Figure 12: Feeder B - Comparison of Reactive Powers

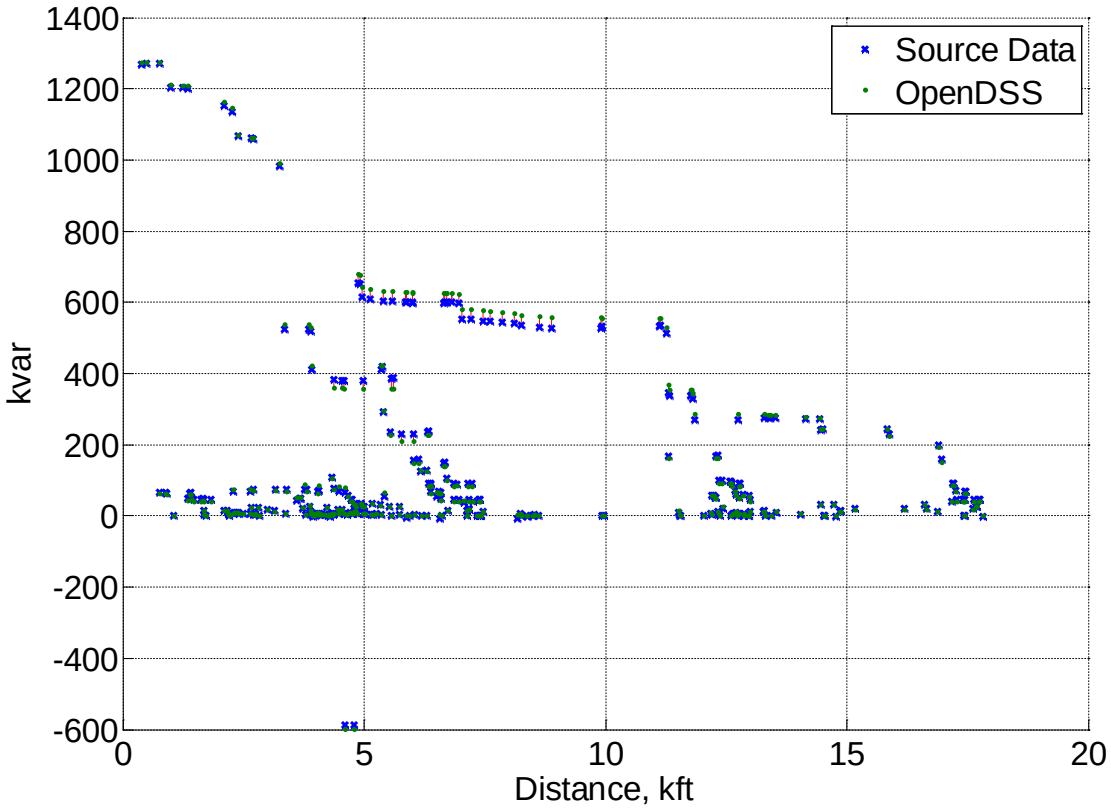

Obtained from OpenDSS and CYME power flow runs.

1.5 Modeling of PV Generators

This section describes the PV generator models developed for this study and used in the simulations. In Section 1.4.1, PV generators models were categorized and generally discussed their applications. In Section 1.4.2, the team described the build-in OpenDSS model, which was used in the steady-state and quasi-steady-state simulations. In Section 1.4.3, a transient PV model was described, which was developed and calibrated based on inverter test data provided by SCE.

1.5.1 Classification of PV Generator Models and General Modeling Considerations

PV generators are most commonly employed in distribution system and can be broadly classified in three categories [1]:

1) Utility-scale PV, are plants with three-phase PV generators that produce a combined power in the order of MWs. The plants are either directly connected to conventional feeders or to substations via a dedicated circuit.
2) Medium-scale PV, are units with capacities ranging from 10 kW to 10 MW that are often installed on or near commercial buildings, government sites, and residential

communities. The characteristics of this type of installation vary widely – larger installations resemble the utility-scale category in that they are three-phase and have a separate interconnection transformer, while smaller installations may connect to existing service transformers.

3) Small-scale PV with capacities of up to 10 kW are single-phase units that are installed on or near residential buildings and connect to the secondary side (120/240 V) of service transformers.

Connecting any of these PV types to a power system may require a system impact study and the choice of PV model employed in the study must be geared to the problem investigated. Commonly, there are two types of PV generator models used in system impact studies: (1) PV models that are suitable for steady-state and quasi-steady-state analysis and (2) models that are suitable for a dynamic and transient analysis. The former are relative simple model that are usually available as build-in models in modern distribution system analysis tools and require few input parameters. The latter are more complex models that, in order to build them, require detailed knowledge about the characteristics of the PV inverters that is hard to come by (most inverter manufacturer consider this information as proprietary and confidential). In the following paragraphs, the different types of studies are discussed in the context of selecting appropriate PV generator models for them.

1.5.2 PV Models for Steady-State Studies

Steady state in a power system means that the system is in equilibrium, that is, the system states and input conditions at any time 1 and 2 are identical. Consequently, a steady-state analysis can be performed fairly easily as it is sufficient to take a "snapshot" of the system at any time during steady state to determine its steady-state behavior. A typical application for a steady-state analysis is a load flow study, which determines the flow of fundamental-frequency currents in a system during normal operation. Incorporating PV generators in steady-state simulations is trivial as the PV generator simply need to provide a pre-set amount of power to the system (i.e., the PV-provided power at the time the "snapshot was taken"), which can be achieved by representing the PV generator as a constant voltage or constant current source.

1.1.1.1 PV Models for Quasi-Steady-State Studies

In a quasi-steady-state analysis, a sequence of steady-state calculations is executed. This technique is useful for a distribution system analysis, where the system state changes frequently due to different load conditions and in the case of variable generation, such as PV, different generation conditions. A quasi steady state analysis can be performed by any steady-state capable simulation software by simply manually executing cases that represent different scenarios, which is tedious if there are a large number of scenarios (e.g., analyzing the system for every minute of the day would require running 1440 cases). Some simulation programs, such as the OpenDSS used in this study, are designed for this type of analysis and have batch processing capability by allowing the user to specify load and/or generation profiles to account for load/generation variability. PV generator models employed in quasi-steady-state simulations are slightly more complex than PV models employed in steady-state simulations as they must account for changing irradiance conditions and the PVs response to them, which may

require incorporating Maximum-Power-Point Tracking (MPPT) algorithms into the simulations. An example for such a model can be found in Section 1.4.2 and describes the Open-DSS quasi-steady-state model, which was used in the simulations.

1.1.1.2 PV Models for Dynamic Studies

An investigation of the behavior of a power system when it is in a "fluctuating" state requires a dynamic analysis, which captures how the system parameters of interest change over time. Applications for a dynamic analysis are stability studies, e.g., the analysis of the system response to large system disturbances such as a line fault or the loss of a generator. Dynamic studies are often performed at the transmission level and are less relevant for distribution systems. One of the reasons for this is that they are typically designed to only model a positive sequence network and, consequently, cannot deal with imbalances often encountered in distribution systems. Dynamic simulation tools employ average or Root-Mean-Square (RMS) models, which neglect switching transients, but preserve other dynamics – e.g., dynamics resulting from the control system of PV inverters and DC-link dynamics. Examples for positive-sequence analysis tools are Siemens' PSS/E and GE's PSLF software application tools. The PSLF manual provides a detailed description of PV their build-in dynamic PV model. The Western Electricity Coordinating Council's (WECC) 'Data Preparation Manual' [2] [2] states that single generating units 10 MVA or higher, or aggregated capacity of 20 MVA connected to the transmission system (60kV and above) through a step-up transformer should be modeled as distinct generators in WECC base cases. It also states that collector-based system such as wind or solar plants connected to the transmission grid may be represented as an equivalent generator, low voltage to intermediate voltage transformer, equivalent collector circuit, and transformer, as recommended by the 'Wind Power Plant Power Flow Modeling Guide' of WECC's Renewable Energy System Task Force [3]. Because of similarities in the internal topology of central station PV plants and wind plants, the guidelines are very similar to wind power plants.

1.1.1.3 PV Models for Transient Studies

Electromagnetic transient programs calculate the instantaneous values of the system parameters, that is, the differential equations that describe the system are solved at each time step. Each electrical component can be represented explicitly, which facilitates the development of accurate and highly-detailed models that are capable of looking at transient problems occurring on a very short time frame (typically milliseconds to microseconds). In the case of PV generators, transient programs can be used to model inverters down to the switching level, which facilitates the investigation of harmonics from the modulation scheme or, possibly, other non-power frequency waveforms coming from the inverter (e.g., due to inverter control interaction/instabilities). Typical applications of transient models are the investigation of surges (e.g., switching surges or lightning surges) on the system. Transient models are required to study the initial (first few cycles) fault response of PV generators. The transient behavior of PV generators is highly dependent on the specifics of the PV generators and even PV generators from different manufacturer that are of the same type and rating can exhibit very different transient characteristics. This is because their behavior is governed by the manufacturer's choice

of control settings of the inverter, protection mechanism, modulation scheme, etc. In general, transient PV models are difficult to develop, require information that is not readily available (control block settings, modulation scheme, etc., MPPT algorithm, etc.) and unwieldy to use on large systems. For this study, a generic PV model was developed and calibrated with test data provided by SCE. This effort is described in Section 1.4.3.

1.5.3 Quasi-Steady-State PV Model

The PV generators in the simulations were represented using the OpenDSS PVSystem device model. This device model is available in OpenDSS V7.4.1 or later and is composed of elements that represent the PV array and the PV inverter. The PVSystem component is suitable for steady-state and quasi-steady-state analysis and, consequently, is sufficient for the investigation of most interconnection impact issues. A limitation of the PVSystem model is that it is unsuitable for transient and dynamic studies that require time-domain modeling, such as transient fault studies, detailed investigation of inverter behavior, flicker, etc. This is an inherent limitation of OpenDSS as this software application tool is only capable of frequency-domain analysis. Another limitation is that the inverter protection (e.g., inverter tripping on over-/undervoltage) is not inherently part of the PVSystem model. The inverter protection would need to be modeled separately.

The properties, capabilities, and assumptions of the PVSystem device models are summarized [4]:

- Applicable for simulations that have time steps larger than 1 second.
- A model assumption is that the inverter finds the Maximum Power Point (MPP) of the panel quickly.
- The active power is a function of (1) the irradiance, (2) temperature, (3) rated power at the MPP at a selected temperature and irradiance of 1.0 kW/m^2, and (4) the efficiency of the inverter at the operating power and voltage.
- The irradiance and temperature can be varied with each simulation step in a quasi-steady state analysis. This is achieved through the Loadshape and Tshape objects, which assign multiplication factors to the rated irradiance and rated temperature, respectively, at each simulation step. The result is that the output power of the PVSystem device varies with each step.
- XYcurve objects are used to describe how the active power at the MPP varies with temperature. The XYcurve is an object that is composed of x and y values that correlate two parameters – for the case above, power at the MPP and temperature. Values that lie between user-specified points are filled in through interpolation.
- XYcuve objects to correlate the inverter efficiency and dc bus voltage may be used in future versions of the PVSystem device. The current version uses only a single efficiency curve that is based on the typical operating voltage of a given array.
- The reactive power is specified separately from the active power. The PVSystem device can be set to either (1) constant VAr or (2) constant Power Factor (PF). In constant VAr

mode, the VAr output of the inverter fixed at the set value unless this value exceeds the rated VA value of the inverter – in this case the VAr output is reduced.

As described in the last item of the list above, the PVSystem device is not able to adjust VArs dynamically to regulate voltage – a capability that many PV inverters have, but that is not permitted according to IEEE 1547. Future version of the PVSystem device may incorporate voltage regulation modeling capability. A workaround for the current version of the PVSystem is to utilize the "kVAr" property of the PVSystem, which, when set, forces the inverter to operate in constant reactive power mode while the active power is changing based on the irradiance intensity. Voltage regulation can be simulated by pre-calculating the reactive compensation required from the PV generator and manually setting the kVAr value of the PVSystem object to this value. However, this method does not allow for dynamic voltage regulation, that is, in the real world the reactive power must be provided by PV generators with voltage regulation capability will change with changing load and generation conditions. OpenDSS can simulate the changing conditions with its quasi-steady state simulation mode, but the reactive power provided by the PVSystem will remain on its pre-set value and not dynamically adjust based on the changing load conditions.

1.5.4 Transient PV Model

This section discusses the transient PV model developed for this study, which was calibrated with data provided by SCE.

1.5.4.1 Description of Transient PV Model

A three-phase model of a solar module and inverter is presented for use in power system studies. This model can be used for both steady-state and transient simulations. The model is representative of a typical inverter used in distribution systems and of its control.

Model Overview

An overview of the EMTP-RV model is shown in Figure 13 and Figure 14. Figure 13 shows the irradiance model, the PV sub circuit block, the step up transformer, the equivalent grid and the block used for power measurement. Figure 14 shows the electrical components and the control blocks included in the PV sub circuit block: the inverter, the output reactor and the shunt filter. Each component of the circuit will be described in detail in the following sections.

Figure 13: Overview of Transient PV Inverter Model

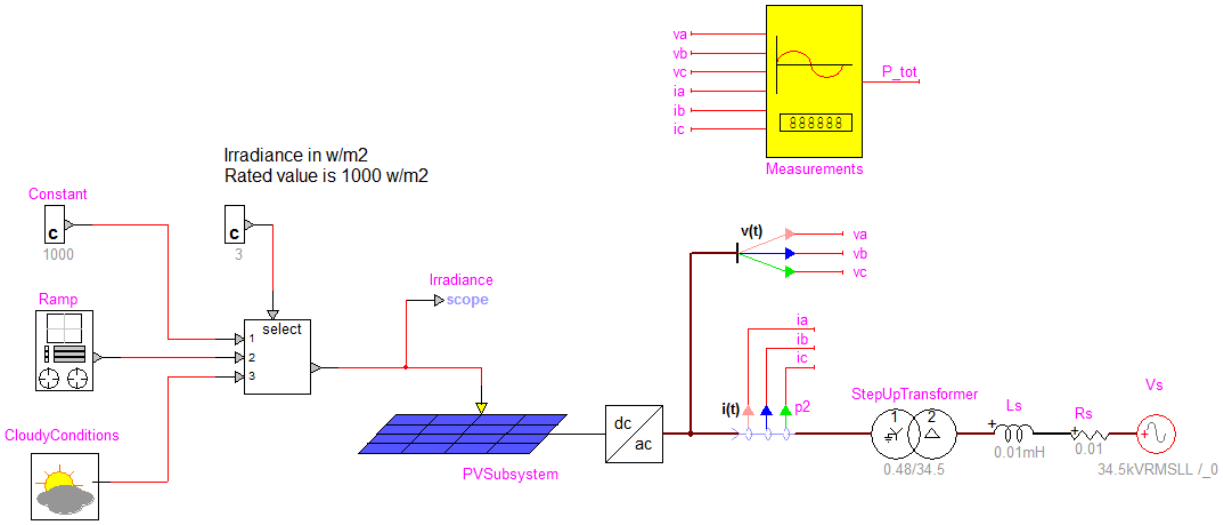

Figure 14: PV Subsystem: Inverter and Output Components

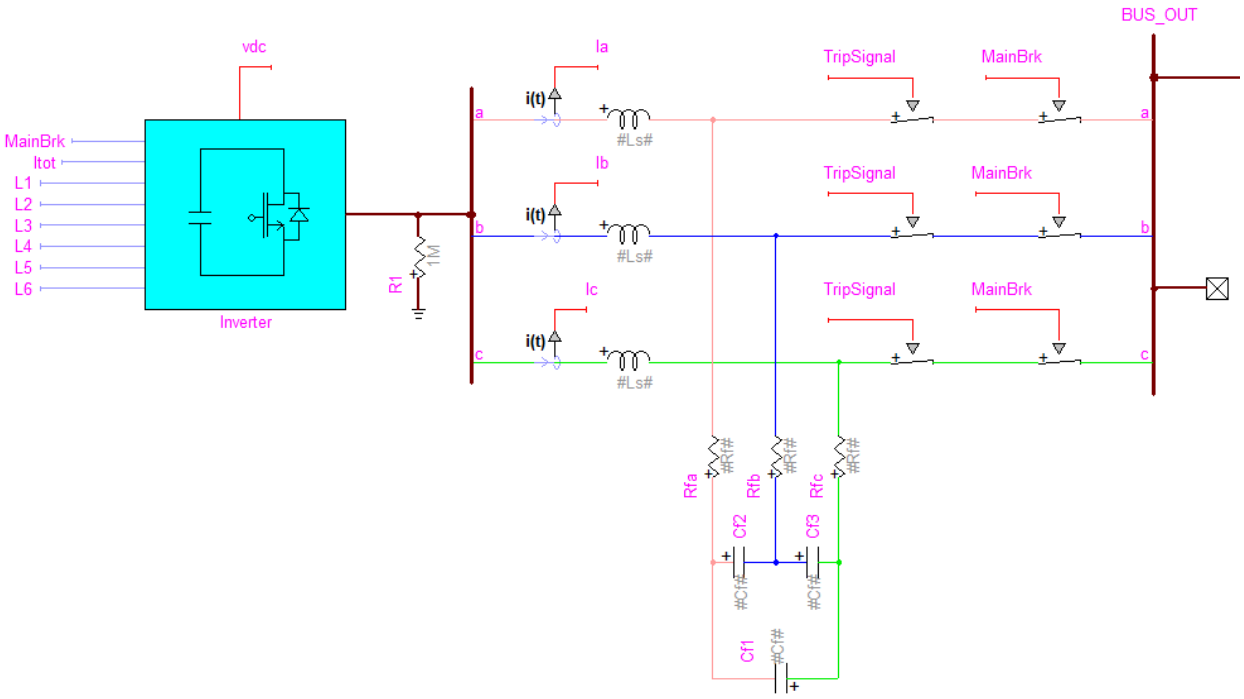

PV Subsystem and Parameters

The PV subsystem is shown in Figure 15. The input variable is the irradiance; the output of the dc-ac inverter is connected to the grid by means of a step-up transformer. The default model parameters are listed in Table 3.

Figure 15: PV Subsystem and Connection to Grid

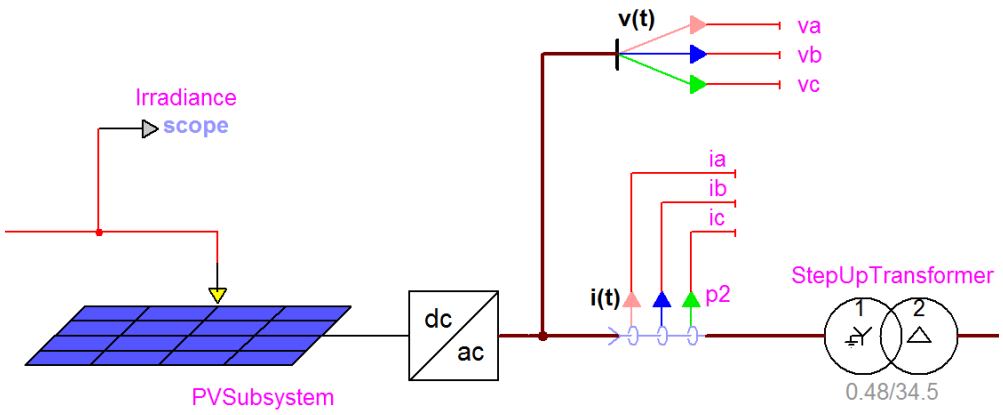

Table 3: Electrical Components Parameters

Quantity	Symbol	Value
Inverter Rated Power*	P	500 kW
Inverter Rated ac Voltage	V	480 V
Inverter Rated dc Voltage	Vdc	1260 V
Inverter Output Inductance	Lsb	1 mH
Inverter Filter Resistance	Rfb	0.2 Ω
Inverter Filter Capacitance	Cfb	600 µF
Transformer ratio	Vs/Vp	0.48/34.5
Transformer impedance	Zt	7%
Transformer Q ratio	X/R	70
Grid Reactance	X1	0.01 mH
Grid Resistance	R1	0.01 Ω
*Rated power is for irradiance equal to 1000 W/m^2		

Measurement block

The block performing voltage, current and power measurements is shown in Figure 16. This block has no links with the control blocks (therefore can be deleted from the model with no consequences on the performance). Its sole purpose is to measure voltage and current at the low side of the step-up transformer. The measurement block components are shown in Figure 17. To realistically represent the meter frequency response, single-pole low-pass filters are applied to the measured current and voltages. The filters time constants are user-adjustable.

Figure 16: Measurement Block, Container

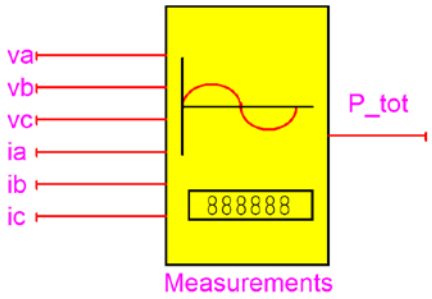

Figure 17: Measurement Block, Components

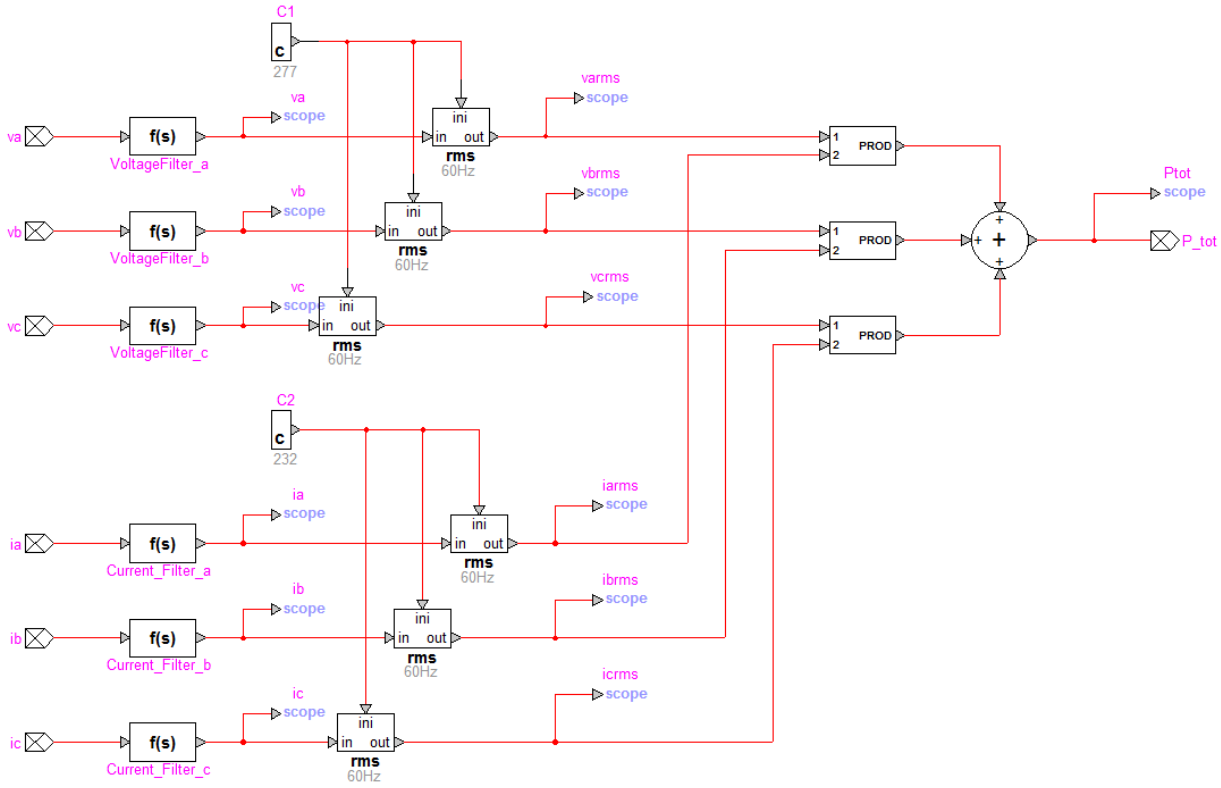

Inverter

The inverter block is shown in Figure 18. The input values are the total current from the solar array, the status of the disconnect switch (open or close) and the switching signals (L1 to L6). The output variables are the dc link voltage (vdc) and the three-phase inverter terminal. Figure 19 shows the inverter components.

Figure 18: Inverter Block, Container

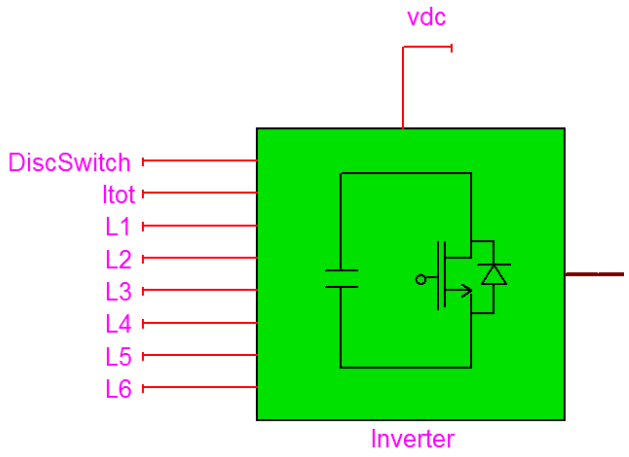

Figure 19: Inverter Block, Components

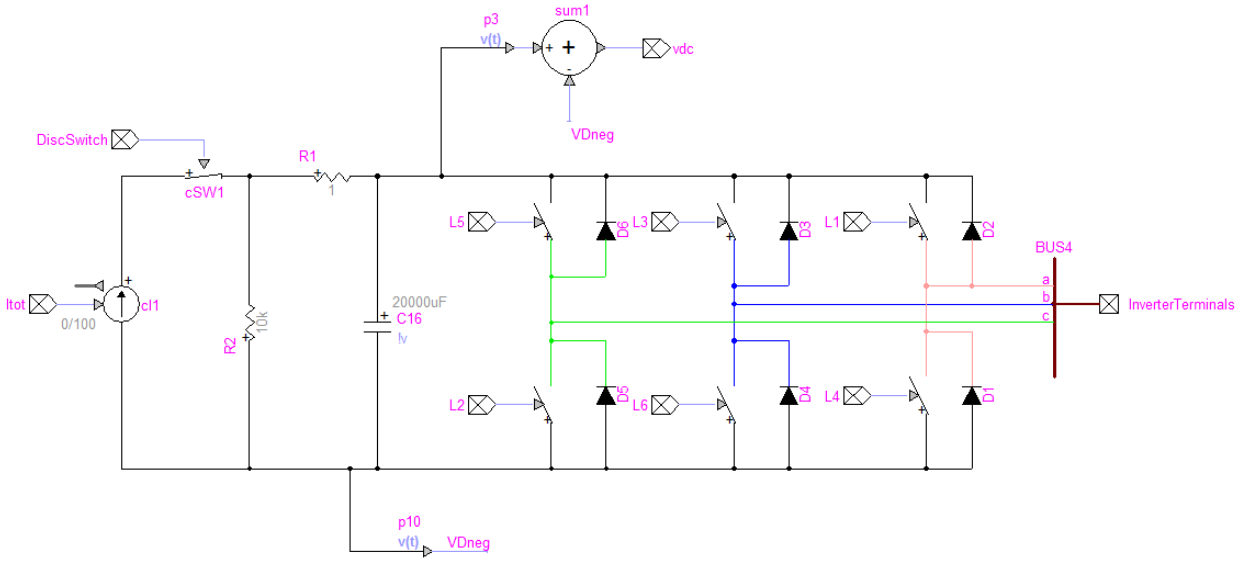

Solar Irradiance

Solar irradiance is measured in W/m². Typical values of irradiance vary from 0 to 1000 W/m². The model facilitates three different input modes for solar irradiance data (Figure 20):

1) Constant value

2) Ramp
3) Irradiance data from field measurement

Figure 20: Input Options for SolarIrradiance Data

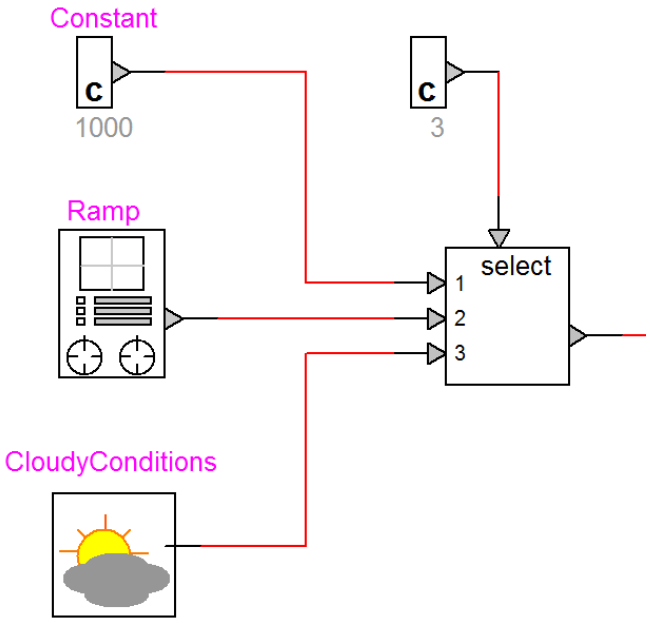

Solar Array

Solar arrays consist of modules that are composed of solar cells connected in series and in parallel. Figure 21 shows the equivalent electrical circuit of a solar cell. The rated power of the module is determined by the number of cells and rating of each cell. For the developed model, each solar cell has a maximum power output equal to 75 W. There are a total number of 79 cells connected in series and 90 in parallel for the base case resulting in a maximum theoretical power of 533 kW. The actual output power of the solar cell is reduced due to parasitic losses, which are accounted for in the model by means of the series and parallel resistance Rs and Rp shown in Figure 21.

Figure 21: Solar Cell Equivalent Electrical Circuit

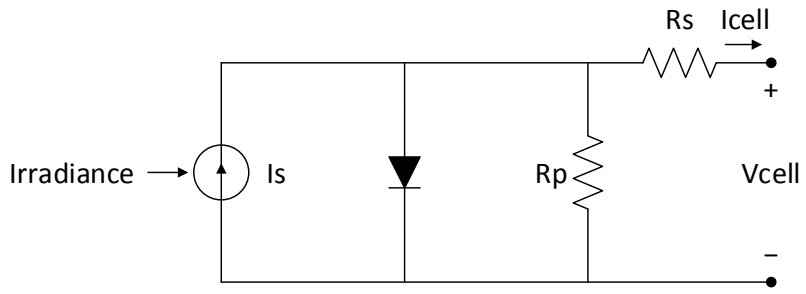

Figure 22 and Figure 23 show the developed EMTP-RV model of the solar array. This component has two input parameters: (1) the dc voltage at the inverter (labeled vdc) and (2) the irradiance. The output parameters are (1) the cell current I_{cell}, which is multiplied by the number of inverters (Ni) to give the total dc current and (2) the total output power from the solar array (ppv).

Figure 22: PV Array Block, Container

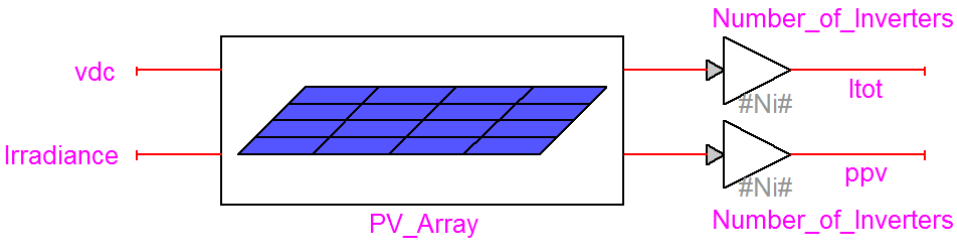

Figure 23: PV Array Block, Component.

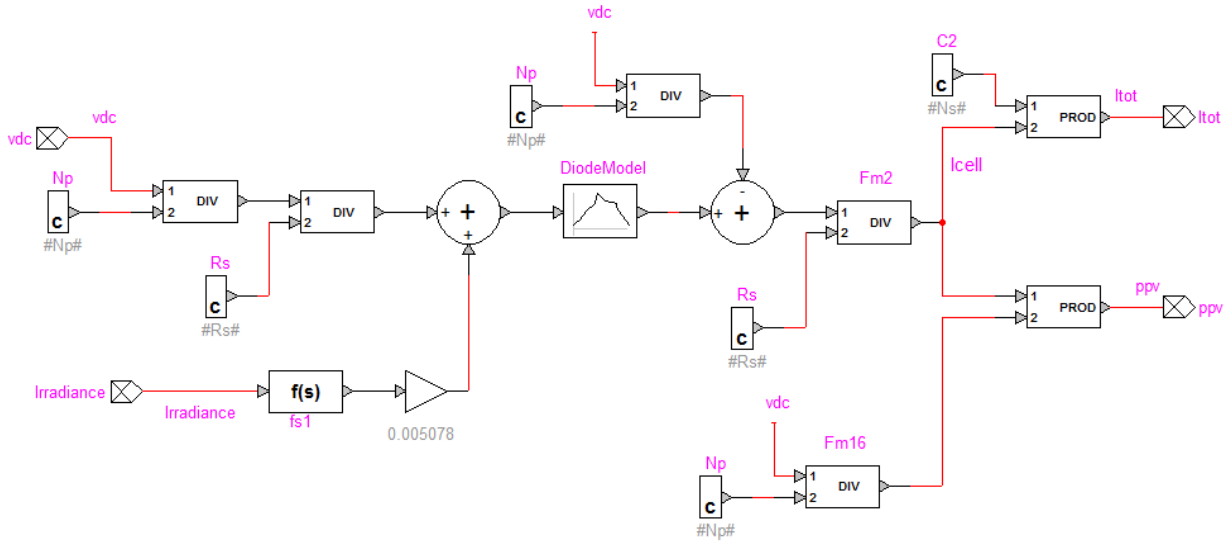

The cell current I_{cell} is uniquely determined by the solar irradiance and the circuit parameters, by solving the following loop equation[5]:

$$I_{SC} - \mathrm{I_{diode}} - \frac{\mathrm{Vdc}}{\mathrm{Rp}} - \mathrm{I}_{cell} = 0 \qquad (1)$$

I_{diode} is obtained by means of the VI relationship shown in Figure 24, which is incorporated into the model as a table lookup function. The only unknown in this equation is I_{cell}.

Figure 24: Diode VI Relationship

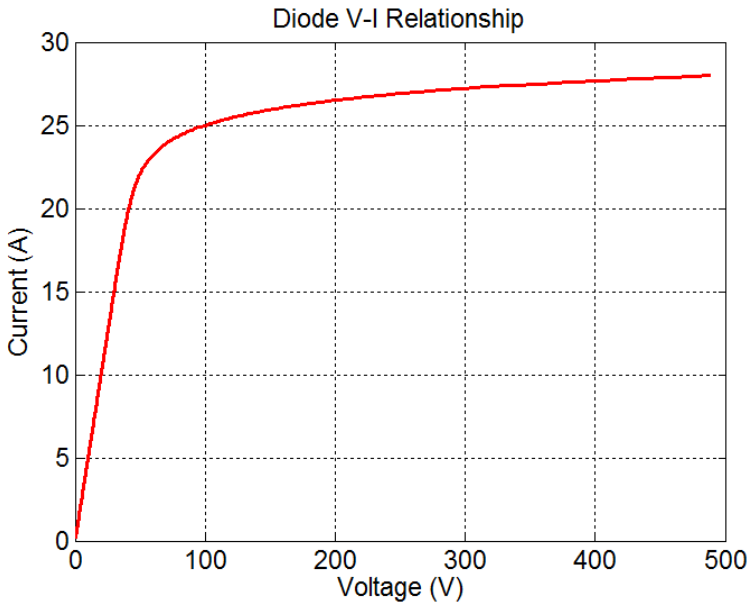

To obtain the variables to solve equation (1), the input variables are edited as follows:

- V_{dc} is divided by the number of cells in parallel, which yields the cell terminal voltage V_{cell}
- The irradiance is multiplied by a gain factor, which is representative of the energy conversion process inside the solar cell. The delay function is used to indicate that this process is not instantaneous, although very fast. The maximum irradiance corresponds to the solar cell producing maximum current.
- The current I_{cell} is multiplied by the number of cells in series to simulate the total current output of the next block, the Maximum Power Point Tracking (MPPT) block.

MPPT Algorithm

The Maximum Power Point Tracking (MPPT) algorithm adjusts the operating point of the solar cells to deliver maximum power based on the irradiance [6]. This is achieved by changing the dc link voltage reference. The non-linear I-V characteristic of solar cells necessitates the use of MPPT and, consequently, MPPT algorithms are always included in solar inverter control schemes. Figure 25 and

Figure 26 show the I-V (current-voltage) characteristic and the P-V (power-voltage) characteristic, respectively, which were incorporated into the developed model. In both figures, various curves are plotted as a function of different values of irradiance (1000, 800, 600, 400, 200 W/m^2).

The I-V characteristic shown in Figure 25 Figure 25 illustrates the non-linearity of this relationship, which is due to the semi-conductive nature of the solar cell. The short circuit current is close to 6 A, the open circuit voltage is 20 V. The open circuit voltage of the solar cell is limited by its characteristics and does not require an external regulator.

The P-V characteristic shown in

Figure 26 illustrates that for each irradiance value, there is one single power maximum, which corresponds to a specific voltage and current value. For lower irradiance values, an increasing voltage value is required to extract maximum power from the solar cell.

Figure 25: I-V Characteristic of the Solar Cell

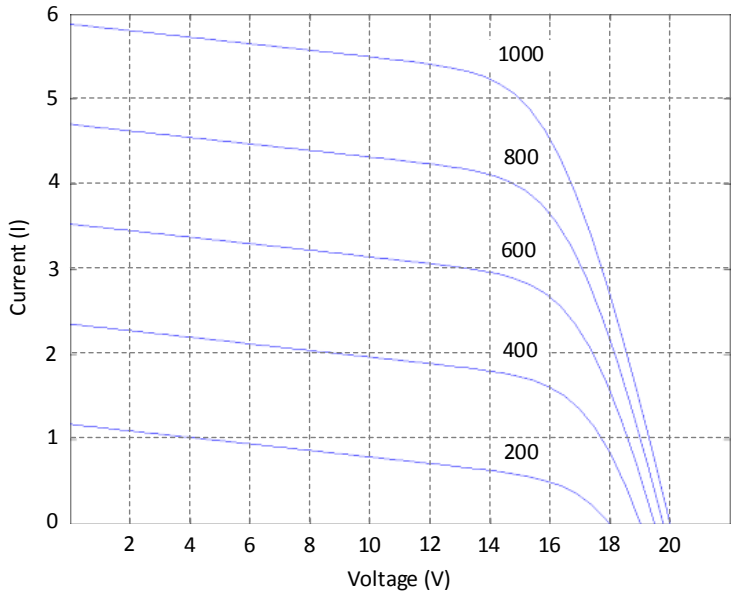

Figure 26: P-V Characteristic of the Solar Cell

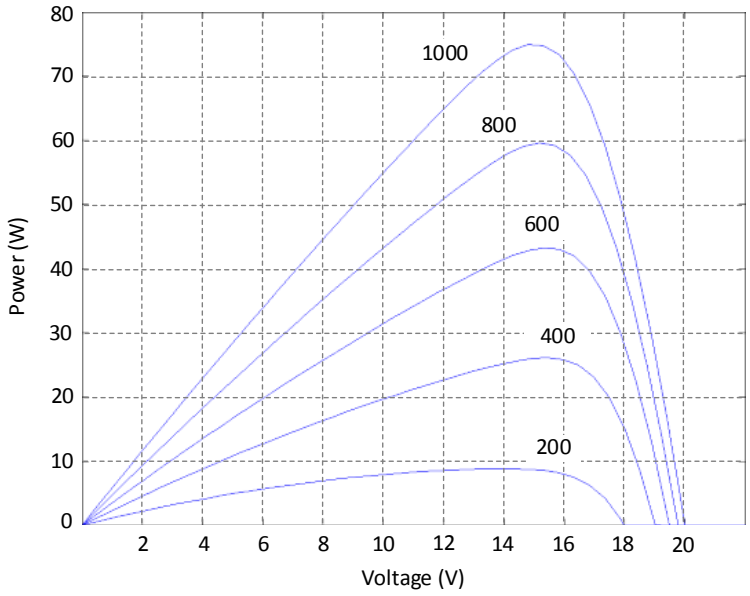

Figure 27 and Figure 28 show the block performing the MPPT algorithm in the EMPT-RV model. The input signals are the cell power and the dc link voltage, the output signal is the

reference current to the switching signals generator. It is apparent from Figure 28 that the model consists of two parts, which correspond to two different steps of the MPPT algorithm:

1) Part 1 (top part of Figure 28) defines a voltage correction value based on the output power of the solar module.
2) Part 2 (bottom part of Figure 28) calculates the current reference based on the new voltage set point.

Figure 27: MPPT Block, Container

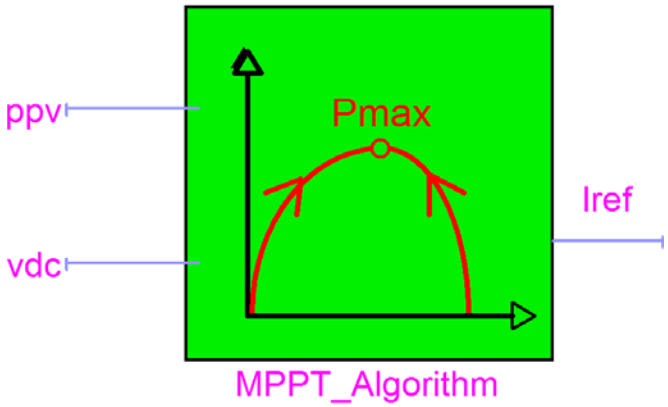

Figure 28: MPPT Block, Components

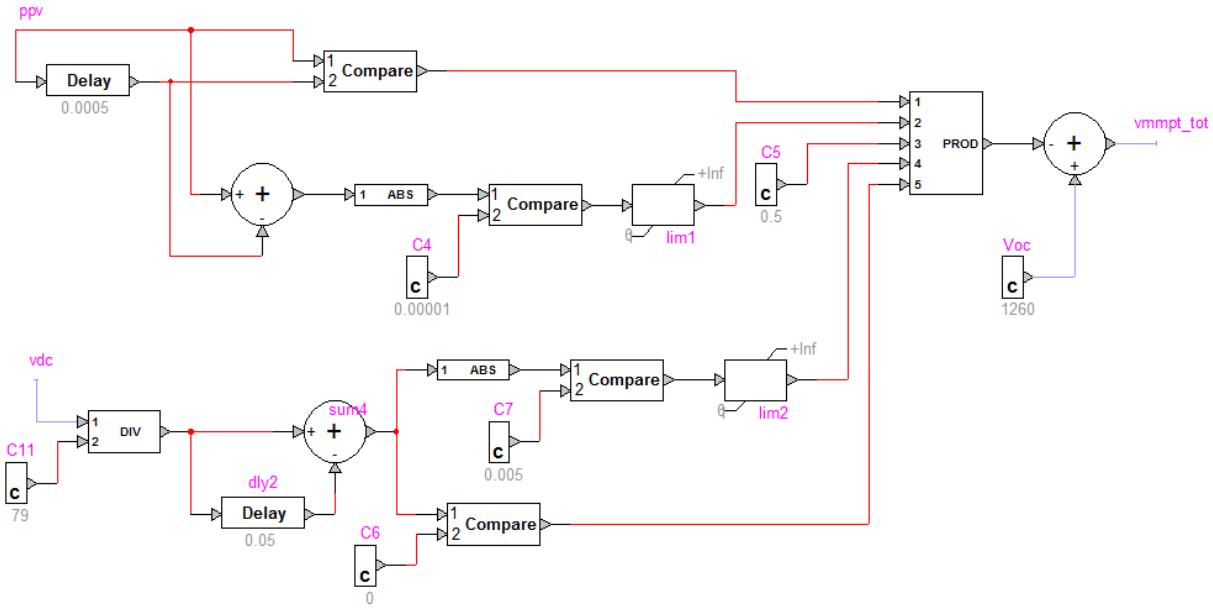

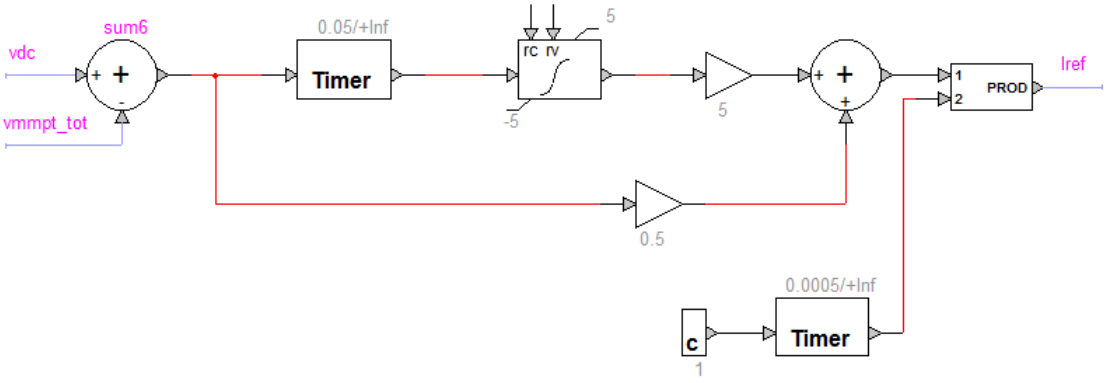
sum6
vdc
vmmpt_tot
+
+
-
0.05/+Inf
Timer
rc rv
5
-5
5
+
+
+
1
2
PROD
Iref
0.5
0.0005/+Inf
c
1
Timer

Switching Signal Generator, Overview

The switching signal generator is contained in the block shown in Figure 29. The inputs to the block are the measured currents and voltages, the reference currents and the trip signal. The output signals are the switching signals to the inverter switches. The power factor can be user-specified thus, changing the reactive power injected by the solar cell [5]. The switching block generator contains three distinguished sections that (1) generate a reference current, (2) modulate the switching signals, and (3) facilitate tripping upon opening of the main breaker. Each of these three sections is described in the following paragraph.

Figure 29: Switching Signal Generator, Container

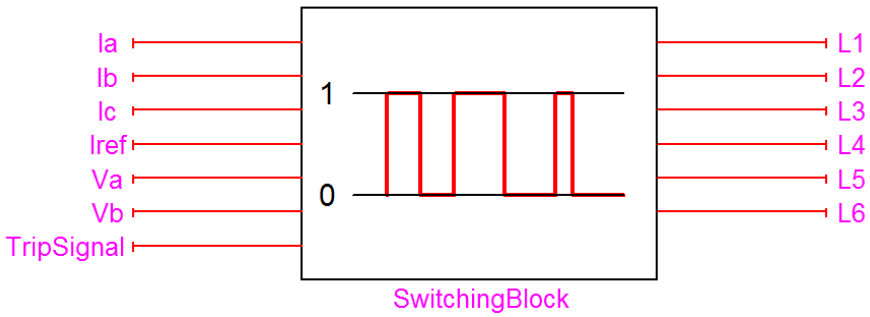

[5] Today's solar inverter typically operate at unity power factor since IEEE Std. 1547 does not allow distributed generators to control voltage. In spite of this, the option to adjust power factor is desirable because (1) the model might be employed for large solar generators which are outside of IEEE Std.1547 scope and/or (2) IEEE 1547 may allow voltage regulation of distributed generators in future revisions.

Switching Signal Generator, Reference Current Generation

Figure 30 shows the reference current waveform generator. The current waveforms at the inverter output are defined by two parameters: (1) magnitude and (2) phase angle. The magnitude is a function of irradiance, while the phase angle is a function of the power factor at the inverter terminals. In our model, current magnitude is defined by the parameter I_{ref}, which is generated by the MPPT block and fed into this block to generate is the output reference current for each of the three phases based on the user-adjustable power factor (the default value for the power factor is unity.

Figure 30: Switching Signal Generator, Reference Current Generation

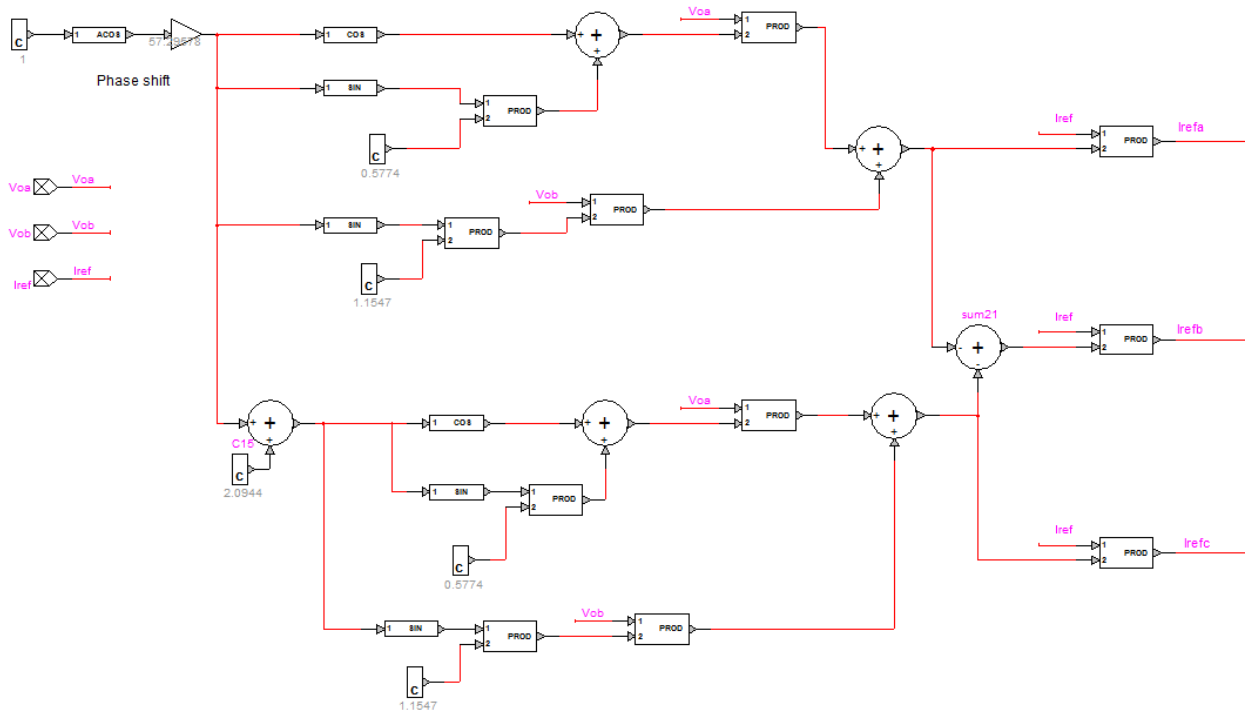

Switching Signal Generator, Modulation

The operations of the inverter switches are controlled by the modulation function to generate three-phase currents following the reference currents. The modulation scheme used in this model is hysteresis-band current control (also sometimes referred to as 'tolerance band control') [7] [8]. The hysteresis-band current control is implemented in our model by means of two comparators and a J-K flip-flop block as shown in Figure 31. Note that the signal 'initialize' is used to avoid instability of the controller. The switching signals are activated only for t> 0.5 ms.

Figure 31: Switching Signal Generator, Hysteresis-band Current Control

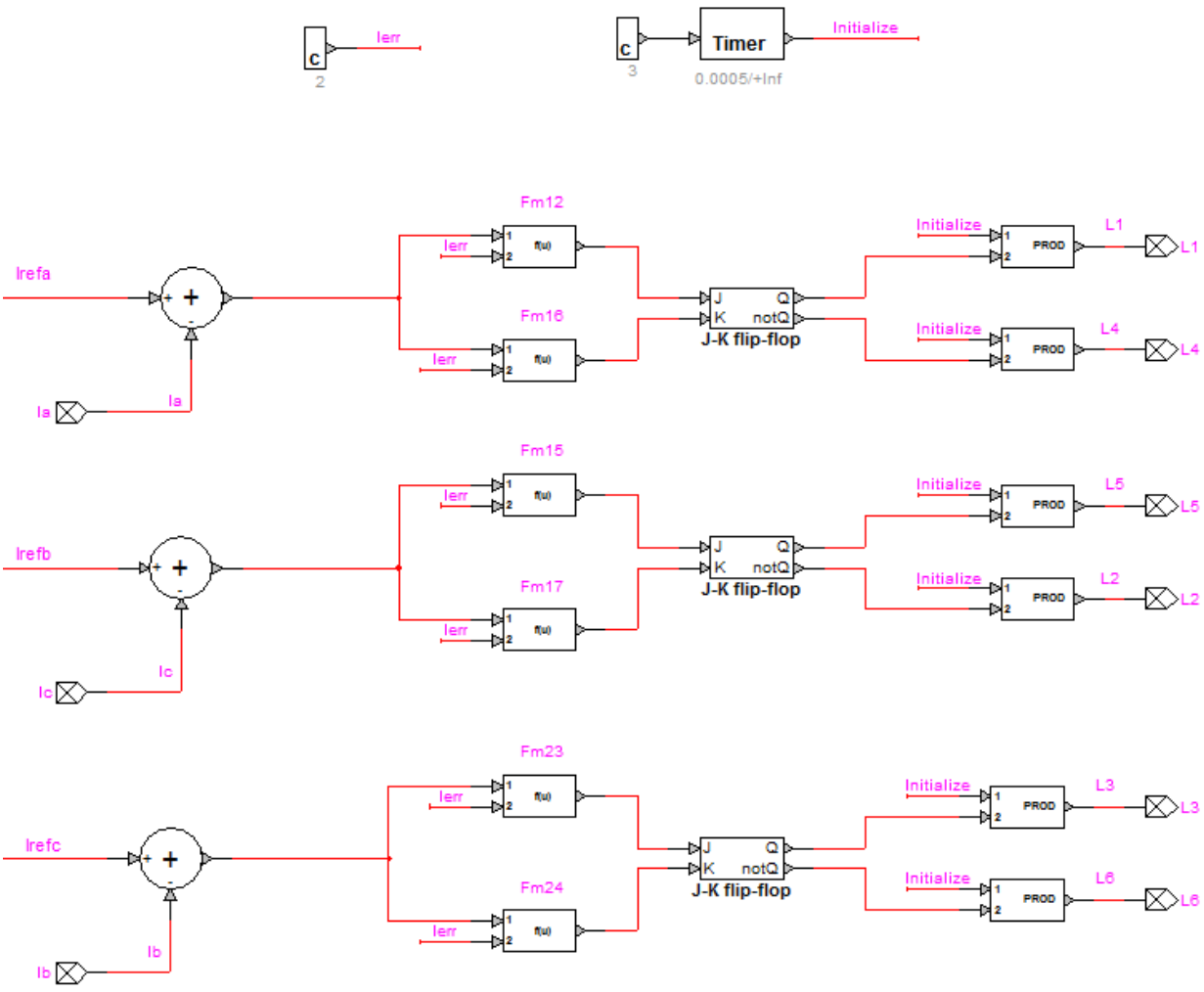

The hysteresis-band modulation scheme works by subtracting the current measured at the inverter terminal from the reference current, and using the resulting current difference as input to a tolerance band control scheme. The tolerance band control operates as shown in Figure 32. If the input is zero, the output will be maintained equal to zero until when the input increases up to the set error value e. At this point, the output will be held to unity until when the input will decrease to –e. At this point, the output value will return to zero and maintain that value

until when the input rises to +e, thus repeating the cycle [8]. The outputs of the control scheme are the switching signals to the inverter switches (0 for open, 1 for close).

Figure 32: Illustration of Hysteresis-band Current Control Scheme

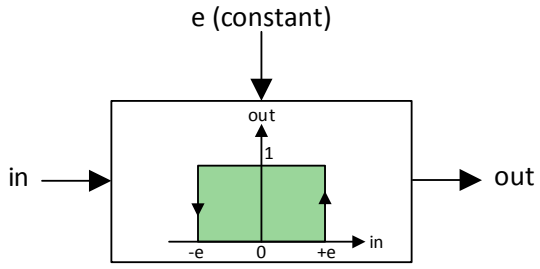

The error e to the controller is adjustable: smaller errors result in a cleaner waveform, but higher number of switching operation. This will increase the computational burden of the simulation, which is not much of a concern if modern computers and modeling tools are used. However, in the practical implementations the number of commutations cannot be excessive in order to keep switching losses and commutation losses of the inverter switches within reasonable limits.

Switching Signal Generator, Trip Function

The trip function generates tripping signals when the power flow from the inverter to the grid is interrupted by, for instance, opening of the main breaker. The tripping signals deactivate the switching operations. This mechanism is commonly implemented in inverters.

Figure 33 shows the model implementation of the trip function. The inputs to the trip function are (1) the trip signal and (2) the switching signals from the flip-flop blocks shown in Figure 31. The output of the product functions are the final switching signals (L1 to L6) sent to the inverter switches. Under normal conditions, 'TripSignal' is equal to unity, and the product block is in pass-through mode, i.e., the signals L1 to L6 are set by the hysteresis-band modulation scheme described in the previous section. When a tripping condition occurs (see the description of the 'Protection' functionality in the next section), the trip signal is set to zero and the output signals L1 to L6 become equal to zero, too (i.e., all switches are kept in an open state).

Figure 33: Switching Signal Generator, Tripping Function

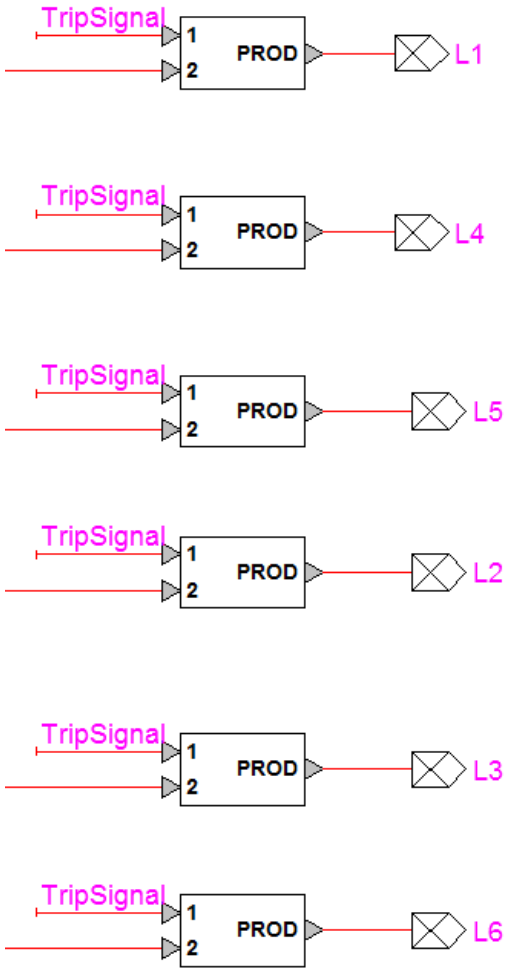

Protection

Figure 34 shows the protection block, which generates a trip signal during abnormal conditions. The inputs to the protection block are the phase a, phase b, and phase c voltages at the output of the inverter (before the step-up transformer). The output is the tripping signal for the protection breaker (0 for breaker open, 1 for breaker closed). An open breaker results in deactivation of the switching operation block, as described in the previous section. The protection settings are user-adjustable via the dialog box associated with the protection block. The default protection settings are as shown in Table 4 and Table 5.

Figure 34: Protection Block, Container

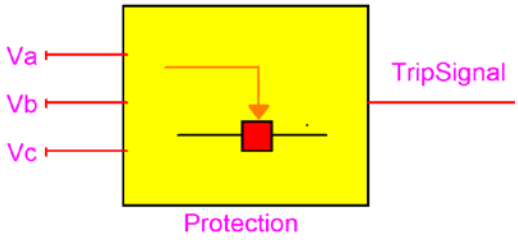

Table 4: Protection Settings – Voltage

Overvoltage		Undervoltage	
Variation	Time delay, s	Variation	Time delay, s
+10%	60	-25%	0.08
+12.5%	30	-15%	0.5
+15%	5	-10%	10
+20%	1	-5%	60

Table 5: Protection Settings – Frequency

Overfrequency		Underfrequency	
Value, Hz	Time delay, s	Value, Hz	Time delay, s
63	0.1	57	0.1

Figure 35 shows the components of the protection block that calculates the RMS values and frequency values of the monitored phase voltages. The calculated RMS and frequency values are inputs to voltage and frequency control function, which determine if the voltages/frequencies are within the set limits. Figure 36 shows the over-/underfrequency protection block. Figure 37 and Figure 38 show the overvoltage protection block and undervoltage protection block, respectively, for phase A. Similar blocks are used for phase B and phase C.

Figure 35: Protection Block, RMS and Frequency Calculations

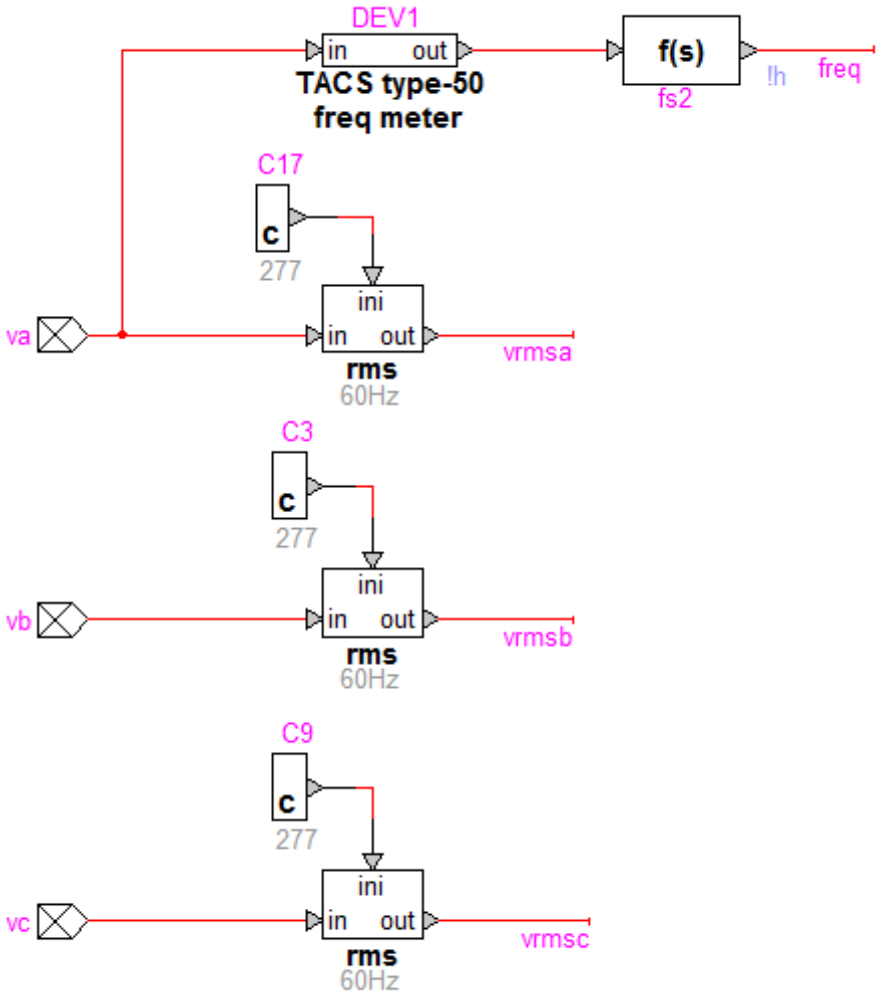

Figure 39 illustrates the logic used to calculate the Trip_Signal value. Trip_Signal is calculated from the individual trip signals from the voltage and frequency control blocks. If any of the individual trip signals is set to zero, the Trip_Signal becomes zero, which deactivates the switching signal generator (i.e., the inverter trips).

Figure 36: Protection Block, Frequency Protection

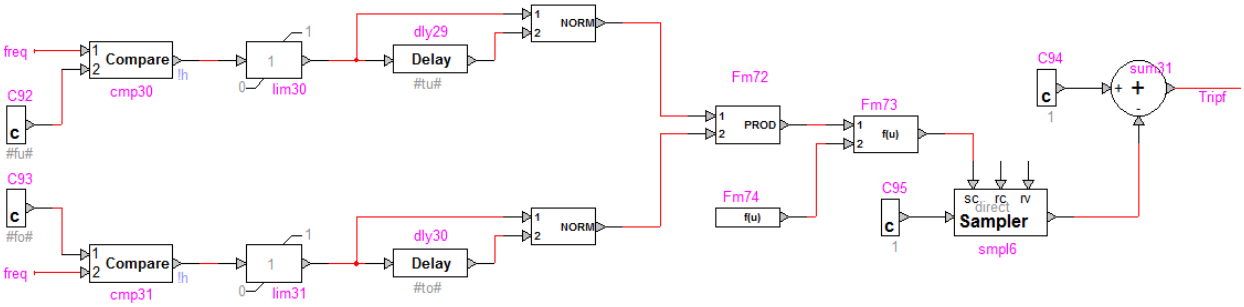

Figure 37: Protection Block, Overvoltage Protection for Phase A

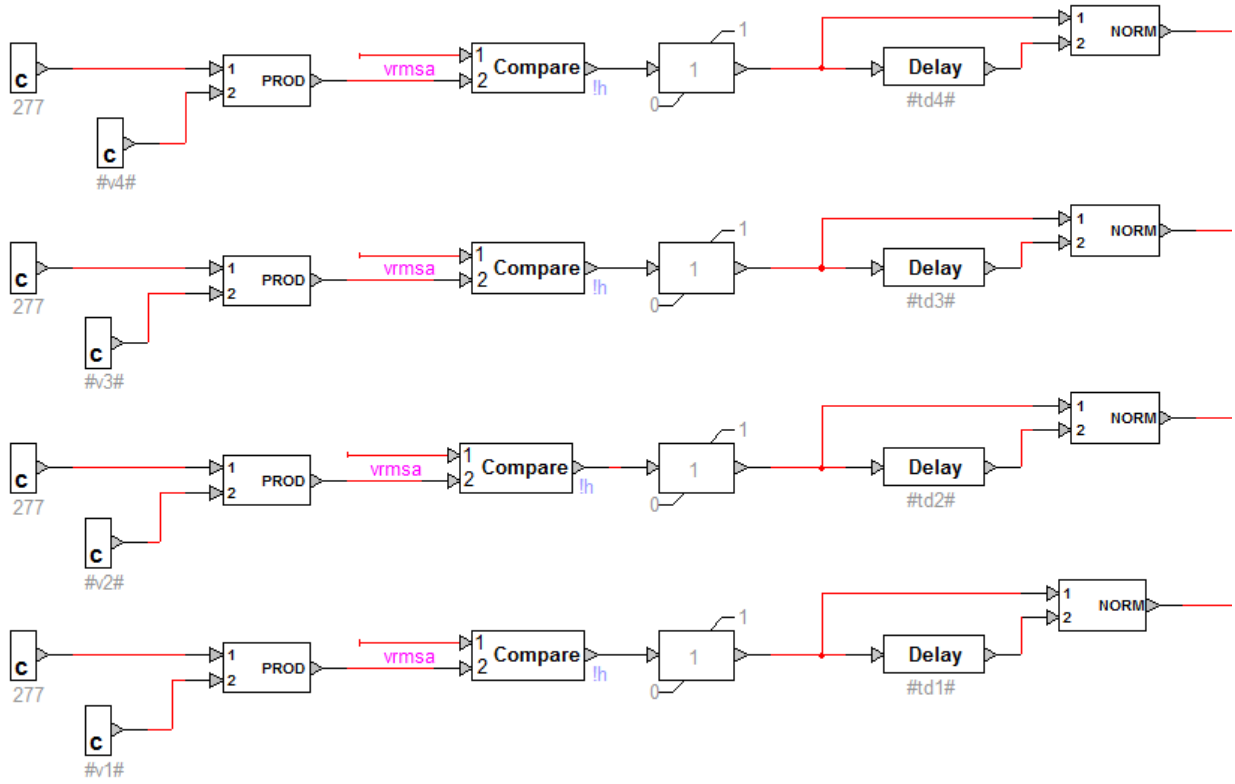

Figure 38: Protection Block, Overvoltage Protection for Phase B

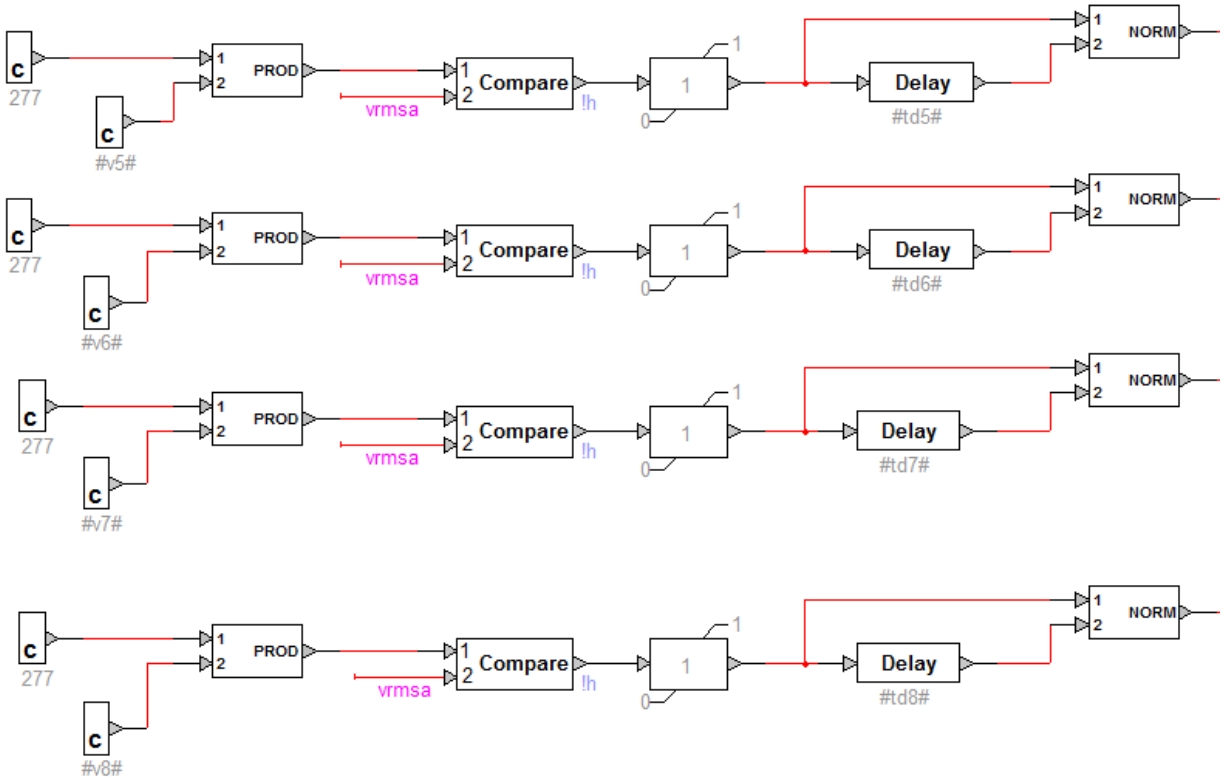

Figure 39: Protection Block, Trip Signal Calculation

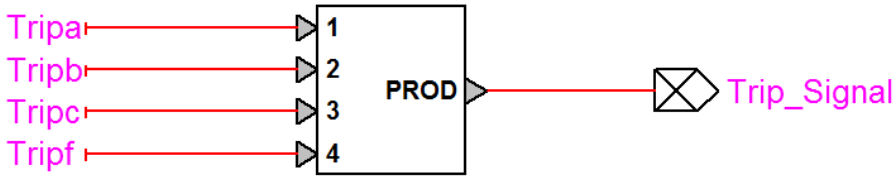

1.5.4.2 Calibration of Transient PV Model using SCE Test Data

The solar industry is faced with a continuing challenge of being able to develop transient PV models that exhibit realistic behavior, in particular during abnormal conditions such as faults (see Section 1.4.1.4). This difficulty is attributable to the need for highly detailed inverter information (modulation scheme, control parameters, filter specifications, etc.) when constructing transient PV models and the unavailability of these data to model builders. In this project, the researchers had the unique opportunity to create a transient PV model that exhibits realistic behavior, which was accomplished by "reverse engineering" a PV model from SCE's inverter test data. The generic transient PV model described in Section 1.4.3.1 was calibrated so its simulation output mimics the behavior of SCE's tested PV inverter. The modeled inverter is rated at 500 kW and has the following characteristics:

- The inverter operates as an AC current-controlled Voltage Source Inverter (VSI). It is synchronized with the phase of the line voltage automatically through a current-controlling reference signal that is synchronized with the line. This facilitates the control of power factor, real power, and reactive power.
- The inverter adjusts its reactive power to line reactive power (kVAr) or a reactive current demand signal. P and Q accuracy can be controlled to within +/- 2% of rated demand. The inverter can provide a limited amount of reactive power.
- The inverter has been tested by CSA to all applicable requirements in UL1741 and IEEE 1547, including (1) tripping on abnormal voltage and frequency and (2) voltage and current power quality.
- During normal operation, the inverter maximizes the PV output power by using Maximum Power Point Tracking (MPPT). The inverter controls the DC link voltage in small adjustable steps every 0.5 seconds. The DC input power is averaged over the 0.5 second time interval and the DC link voltage is adjusted based on the direction of change of the DC input power from one interval to the next. That is, if the DC input power increases, the DC link voltage will be increased and vice versa. Alternatively to the MPPT control mode, the inverter can be set to operate in constant current mode and in constant power mode.

The PV array was modeled as a controllable current source defined by the I-V characteristic shown in Figure 40.

Figure 40: Emulated PV VI Characteristic

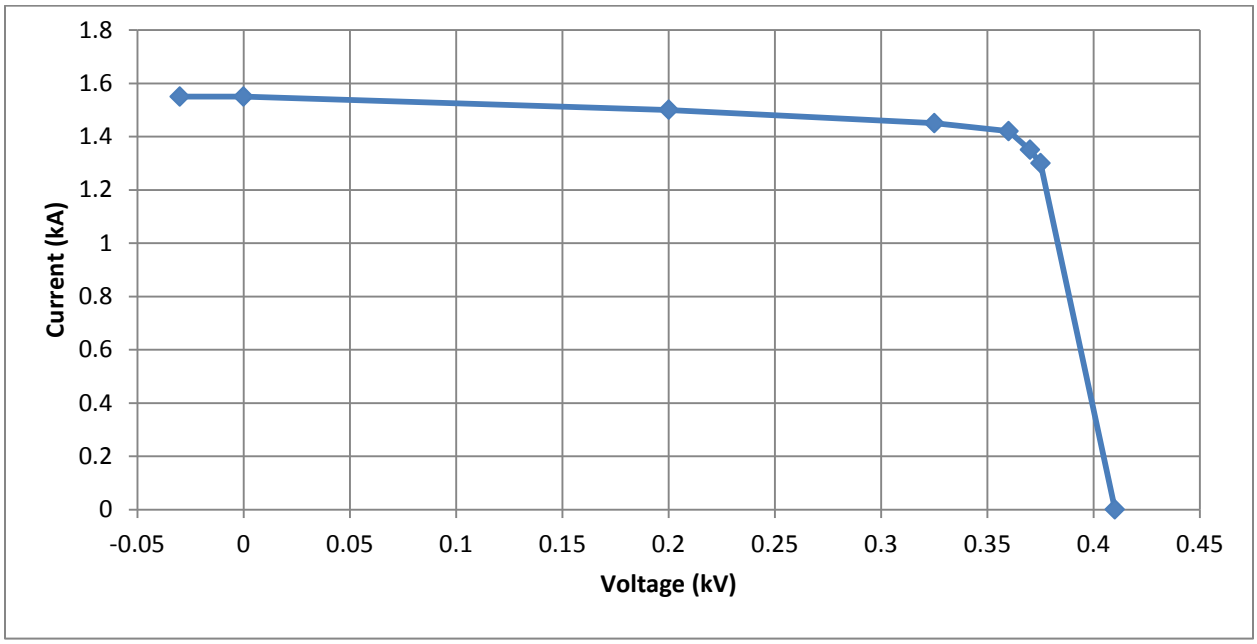

The following graphs show the results of our calibrated transient EMTP-RV model when the inverter operates at 0.25 pu of rated power. The following parameters are:

- Inverter line-line (phase a to phase b) output voltage, Figure 41
- DC link voltage, Figure 42
- Inverter phase a output current, Figure 43
- DC link currents, Figure 44
- DC link power, Figure 45
- Inverter power, Figure 46

Figure 41: Simulation Results from Calibrated EMTP-RV PV Model, InverterLine-Line Output Voltage

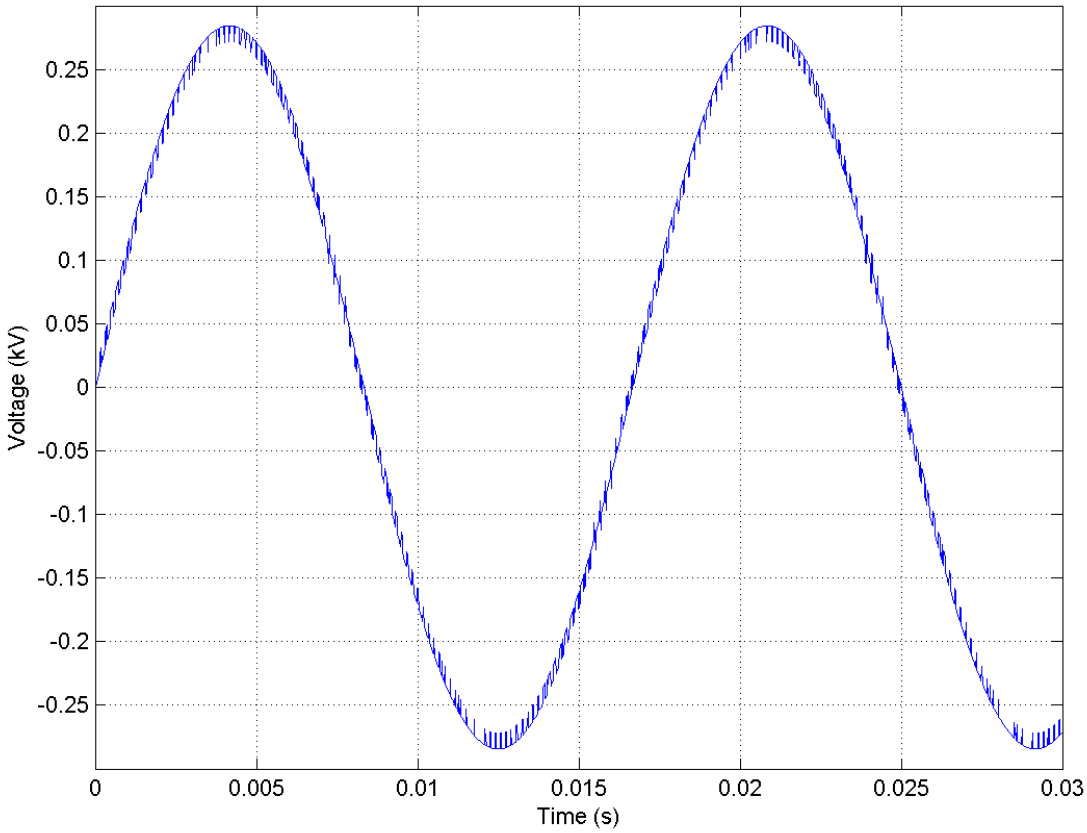

Figure 42: Simulation Results from Calibrated EMTP-RV PV Model, DC Link Voltage

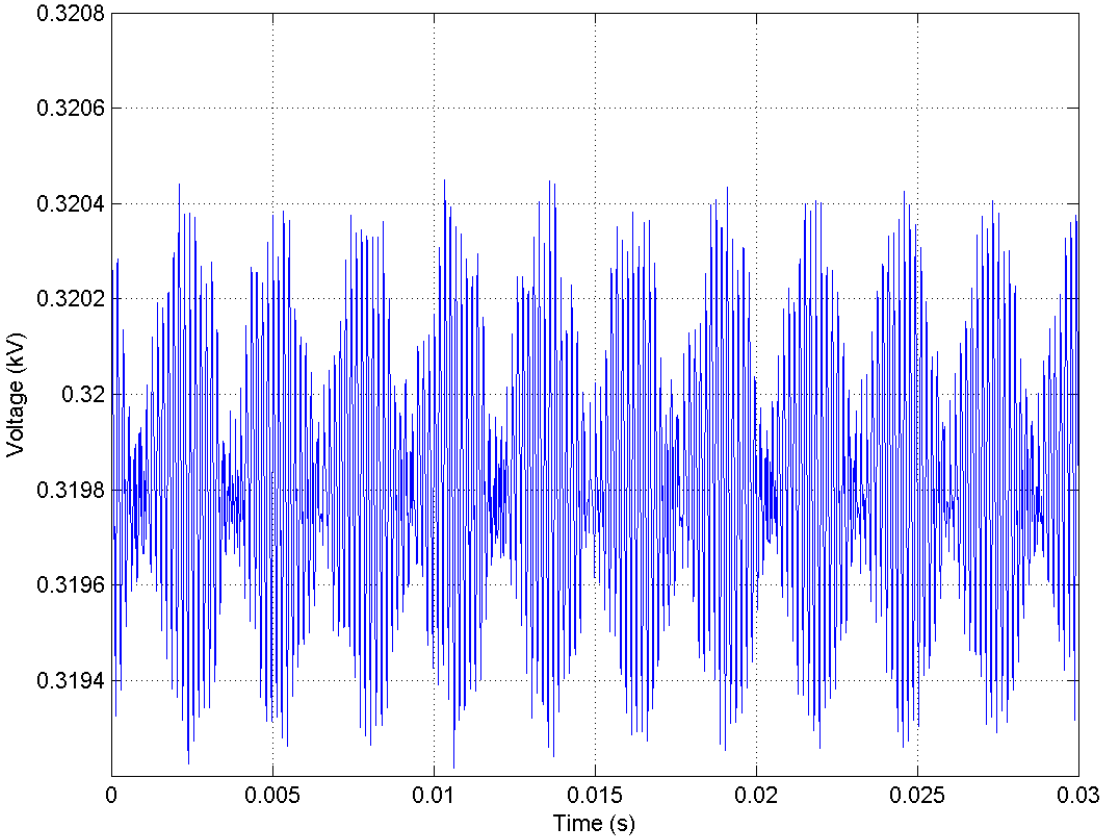

Figure 43: Simulation Results from Calibrated EMTP-RV PV Model, Inverter Phase an Output Current

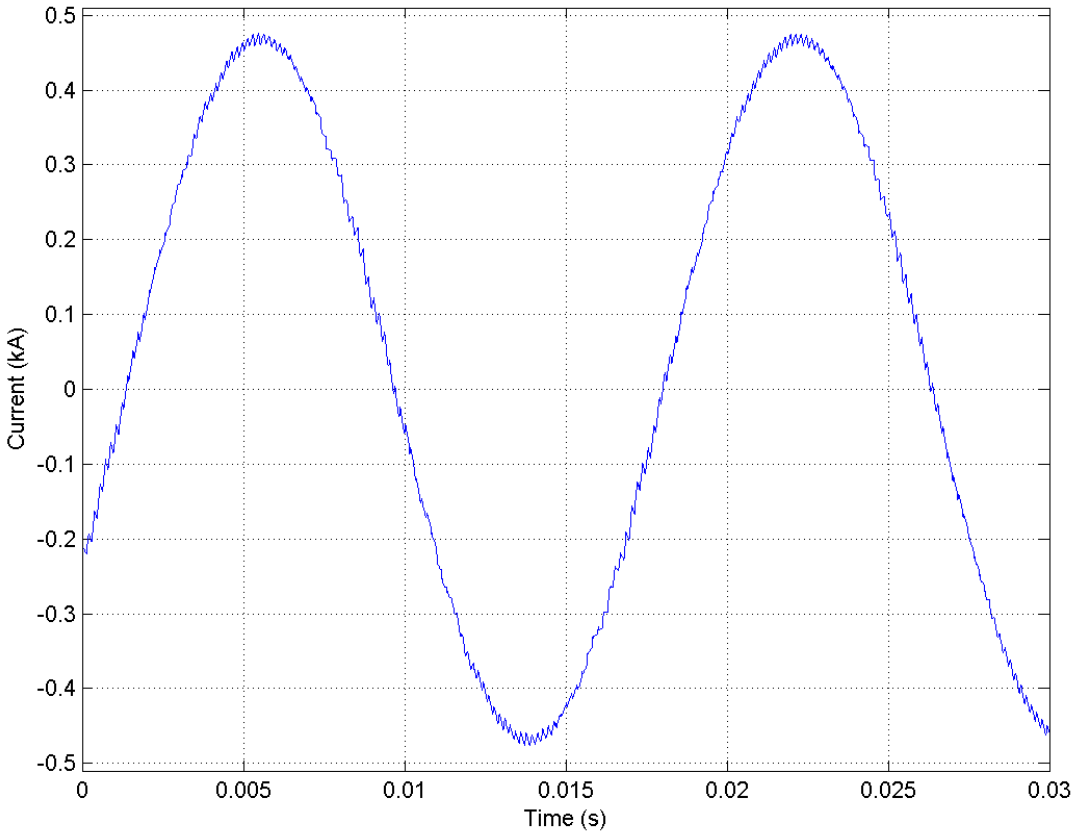

Figure 44: Simulation Results from Calibrated EMTP-RV PV Model, DC Link Current

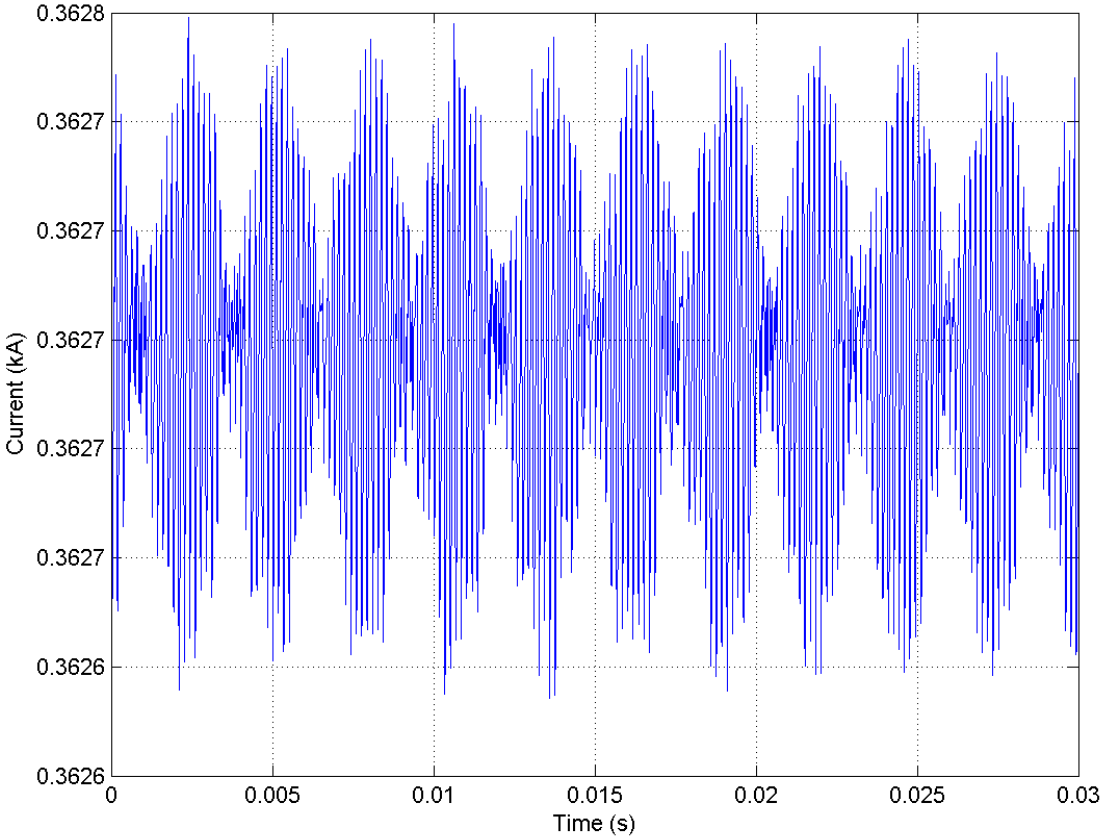

Figure 45: Simulation Results from Calibrated EMTP-RV PV Model, DC Link Power

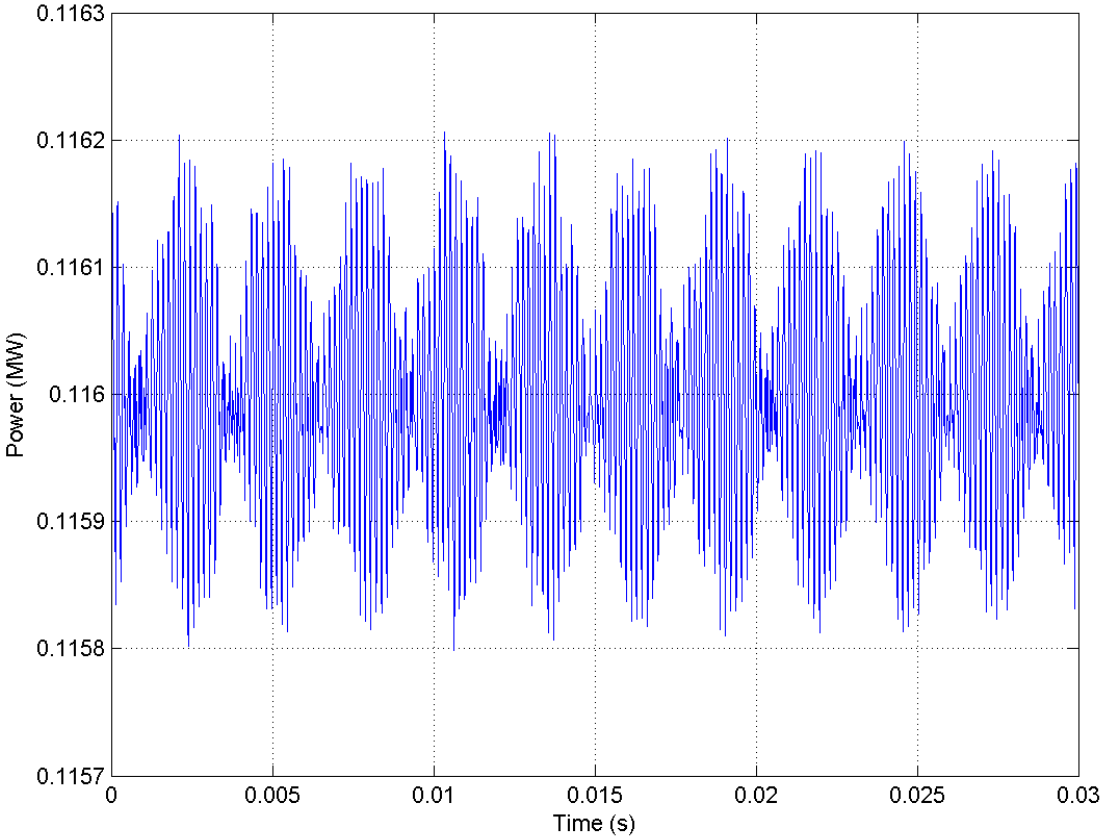

Figure 46: Simulation Results from Calibrated EMTP-RV PV Model, Inverter Output Power

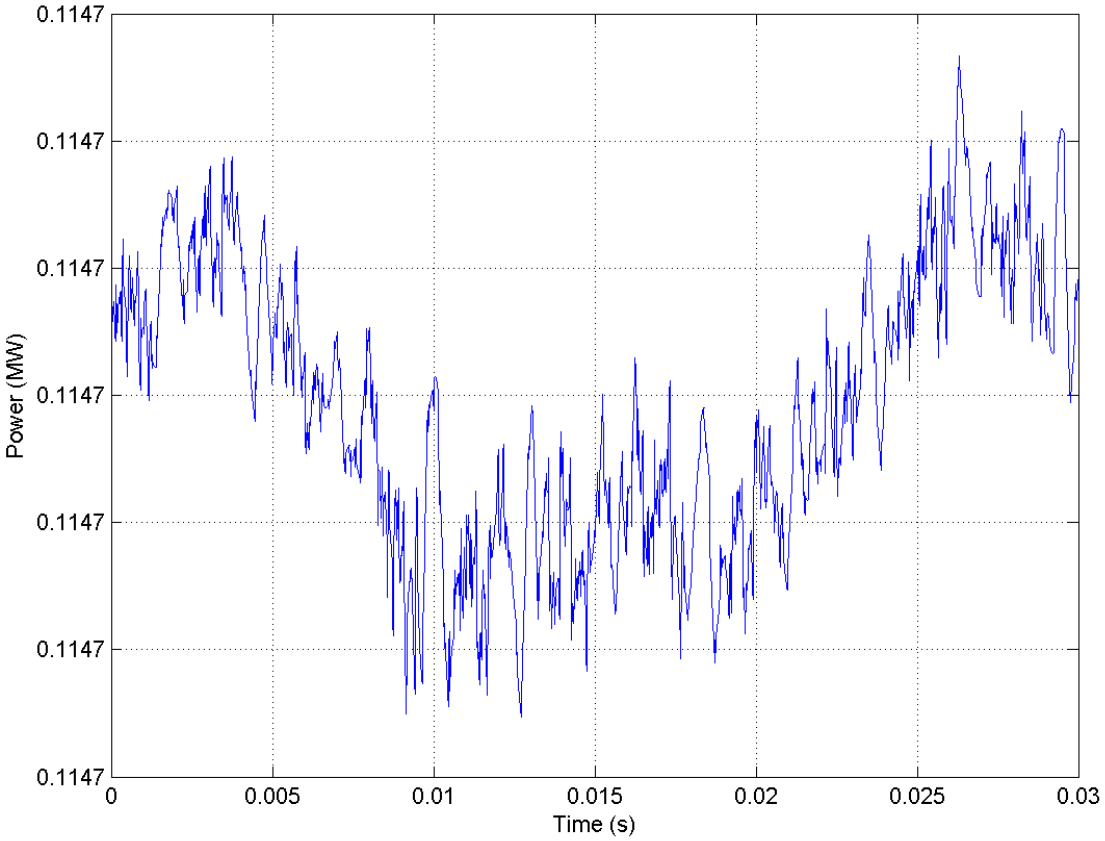

Chapter 2
Forecasting Methodology

2.1 Sky Imager Hardware Overview and Experimental Setup

In cooperation with Sanyo Electric Co. (now Panasonic), LTD., Smart Energy Systems Division, the University of California, San Diego designed and developed a sky imager system specifically for short-term solar forecasting applications. The USI captures images using an upward-facing charge-coupled device (CCD) image sensor sensing RGB channels at 12 bit intensity resolution per channel. A 4.5 mm focal length circular fisheye lens allows imaging of the entire sky hemisphere. Utilizing high dynamic range (HDR) imaging, the USI outputs images at 16 bits per channel with a dynamic range of over 80 dB[6]. Lossless PNG compression is used to store and transmit images for forecast analysis. Installation of the USI system is shown below. The two sky imagers used in this project are identified as USI1.5 and USI1.6.

Since cloud cover near the sun provides vital information for short-term solar forecasting, the USI does not employ a solar occulting device. The increased resolution and dynamic range, combined with the ability to image the entire sky hemisphere, has allowed the USI to overcome the primary shortcomings of the earlier TSI system.

In June 2009, Southern California Edison (SCE) received California Public Utilities Commission (CPUC) approval to install 500 MW of rooftop photovoltaic (PV) under its Solar Photovoltaic Program (SPVP), but it was later scaled back to 125 MW. For this project forecast data was generated for four multi-MW PV sites in the SCE Inland Empire (Table 1).

The images used in this analysis were taken by two rooftop-mounted USIs located at 34.0764° N, 117.2431° W, 338 m (marked as USI1.5 in Figure 47) and 34.0774° N, 117.2401° W, 345 m (marked as USI1.6 in Figure 48). The instrument captures images every 30 seconds during times when the sun is above an elevation of -3°.

[6] Urquhart, B., Ghonima, M., Nguyen, D., Kurtz, B., Chow, C. W., Kleissl, J., 2013. Sky imaging systems for short-term solar forecasting, Jan Kleissl (Editor): Solar Energy Forecasting and Resource Assessment, Elsevier.

Figure 47. Final Installation of the Imager

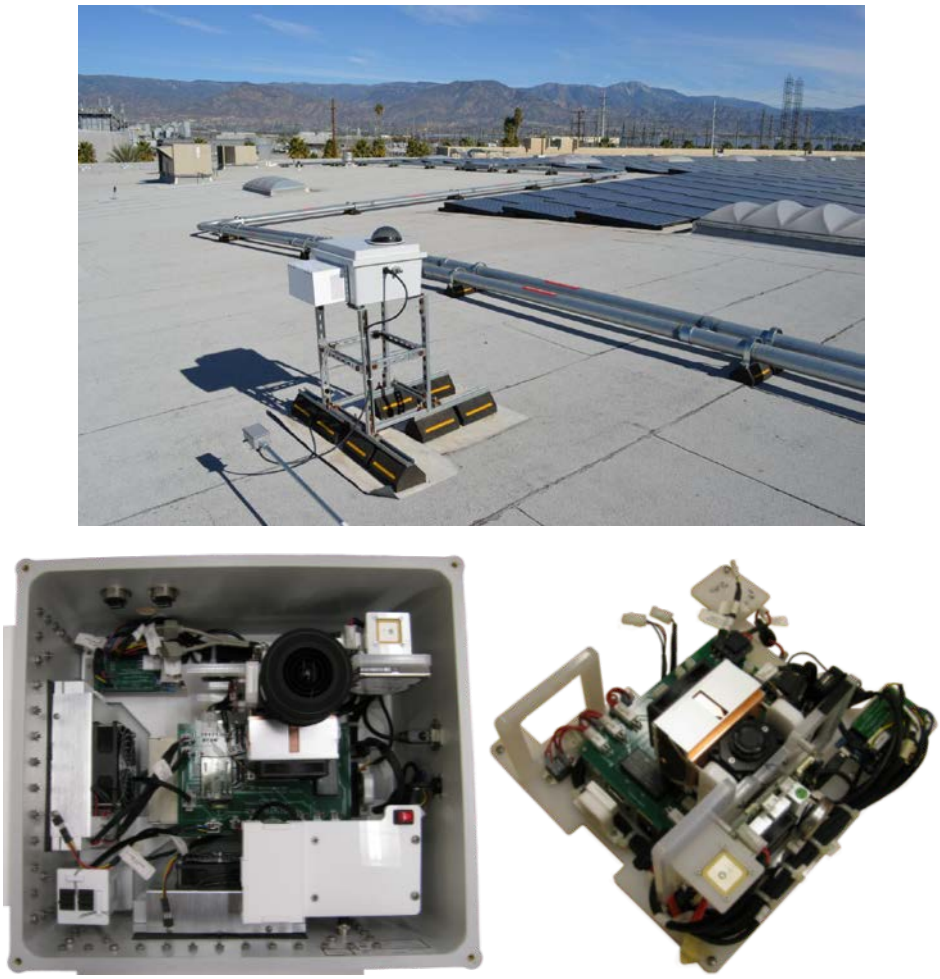

Near Power Plant SPVP011 (Top) and overview of the components of the imager (Bottom).

Table 6: Distances of Solar Plants Used for USI forecast Validation to the USI

Station name	Distance to USI1.5 (m)
SPVP011	176
SPVP013	1,071
SPVP016	1,277
SPVP022	2,883
METAR	2,804

Figure 48. Locations of Power Plants, METAR Station and USI Installations

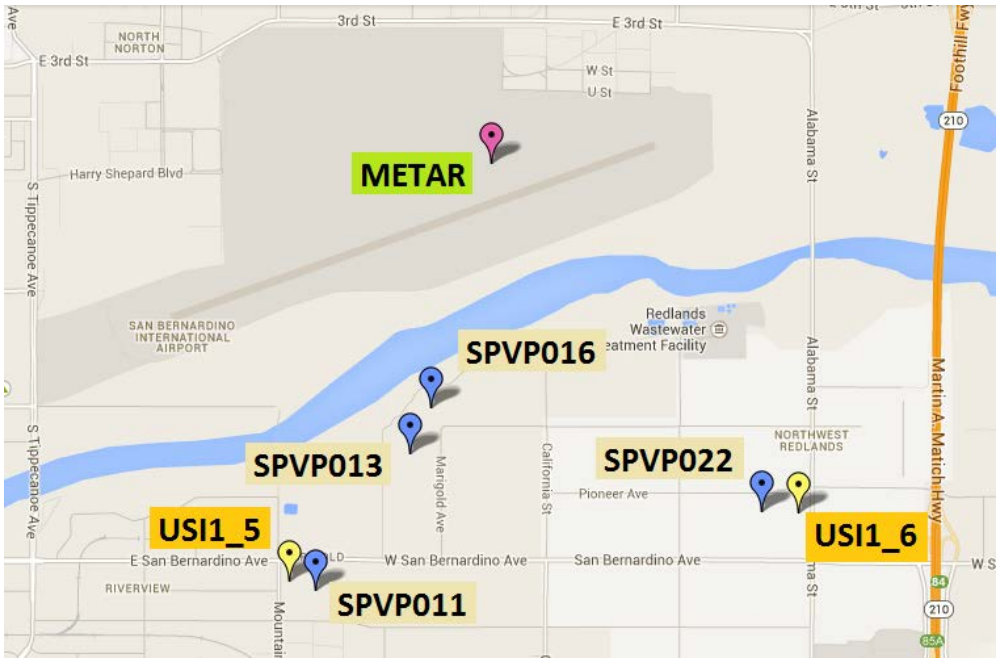

Map data ©2013 Google.

2.2 Sky Imager/Power Data Availability

Available power data provided by SCE along with a complete list of available forecast images for USI1.5 and USI1.6 are given in Table 7. USI1.5 and USI1.6 were installed on December 5th and December 11th, 2012, respectively and imagery was collected through March 31st, 2014. 88 days were missing for USI1.5 and 48 days were missing for USI1.6 resulting in over 400 days of useable imagery for each imager.

The dome of the imagers was cleaned frequently to avoid dust and dirt accumulation, which would otherwise result in poor image quality. There were no persistent technical issues with the operation of the imagers after March 20, 2013. Short outages later in the year were caused by upgrades to rooftop electrical circuits at both sites. Unfortunately, rooftop access was limited, so dust and dirt accumulated on the dome of the imagers, resulting in poorer image quality for many images.

Table 7: Availability of Images for USI1.5 and USI1.6 (2013 – 2014)

	2013 (Day of Year)	2014 (Day of Year)
Power Data	59-130	-
USI1.5	59-63 70-168 191-365	1-90
USI1.6	59-184 193-194 228-305 310-365	1-90

2.3 Sky Imager/Power Data Selection for Further Analysis

To accurately assess the performance of USI solar irradiance forecasting during a variety of sky conditions, the entire months of March and April 2013 were selected for analysis. During these months, 33 of 61 days were clear days with a cloud fraction lower than 1%. There were two overcast days. Neither clear nor overcast days are of interest for sky imager forecasting as the solar power output ramps are small. Eight of these days are further eliminated due to missing power data or sky imager images. The remaining days consisted of partial cloud cover, which are relevant days for testing forecast performance.

2.4 Satellite Data Overview

Clean Power Research (CPR) provided satellite forecast data around the four SPVP sites. The satellite data used in this analysis were centered at 34° 4' 30" N, 117° 14' 42"W (marked as satellite pixel 1 in Figure 49) and 34° 5' 6"N, 117° 14' 6"W (satellite pixel 2 in Figure 49). The spatial coverage of 0.01 degrees for longitude and latitude, which corresponds to about 1 km x 1 km is marked as a red square in Figure 49. SPVP011 was contained in pixel 1, and SPVP013 and SPVP016 were contained in pixel 2. Satellite forecasts are issued with every new satellite image twice per hour at :00 and :30 minutes and the temporal resolution of the forecast horizon is 1 minute out to 30 min. Linear interpolation was used to calculate the forecast GHI every 30 seconds consistent with the sky imager forecasts.

Figure 49: Locations of Satellite Pixels (red squares) Relative to Solar Power Plants

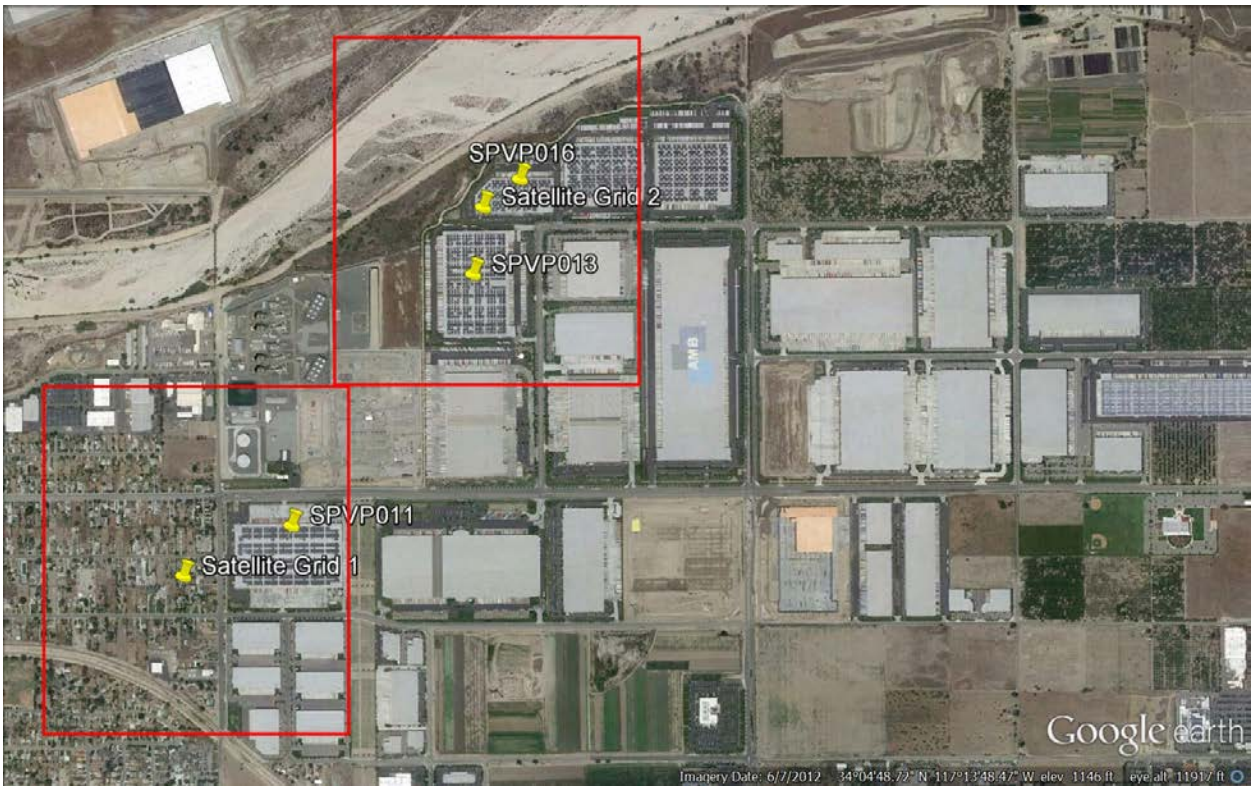

Map data ©2012 Google Earth.

2.5 Satellite Data Selection for Analysis

Satellite data were available for all of 2013, while available power plant and USI data are catalogued in Table 8. USI and satellite forecasts were both available for the 17 days that were not clear or overcast in March and April 2013 (Table 22) and the comparison was performed over this period.

Table 8: Availability of Power Data, USI Images and Satellite Data

Data Type	2013 (Day of Year)
Power Data	59-130
USI1_5	59-63 70-168 191-365
Satellite Data	1-365

2.6 Sky Imager Forecast Procedure

The method used to generate forecasts in this study is an improved implementation of the procedure described in[7]. A brief overview of the USI forecast procedure is presented, with a focus on the major improvements made since the previous iteration of UCSD sky imager forecast software. USI forecast data processing may be considered in two main sections: one which operates purely upon sky imager data, and one which is specific to the location and equipment of the site of interest. A forecast may then be issued after all data processing is complete. A graphical guide of the forecast procedure is shown in Figure 50.

Figure 50: Flowchart of Forecast Procedure

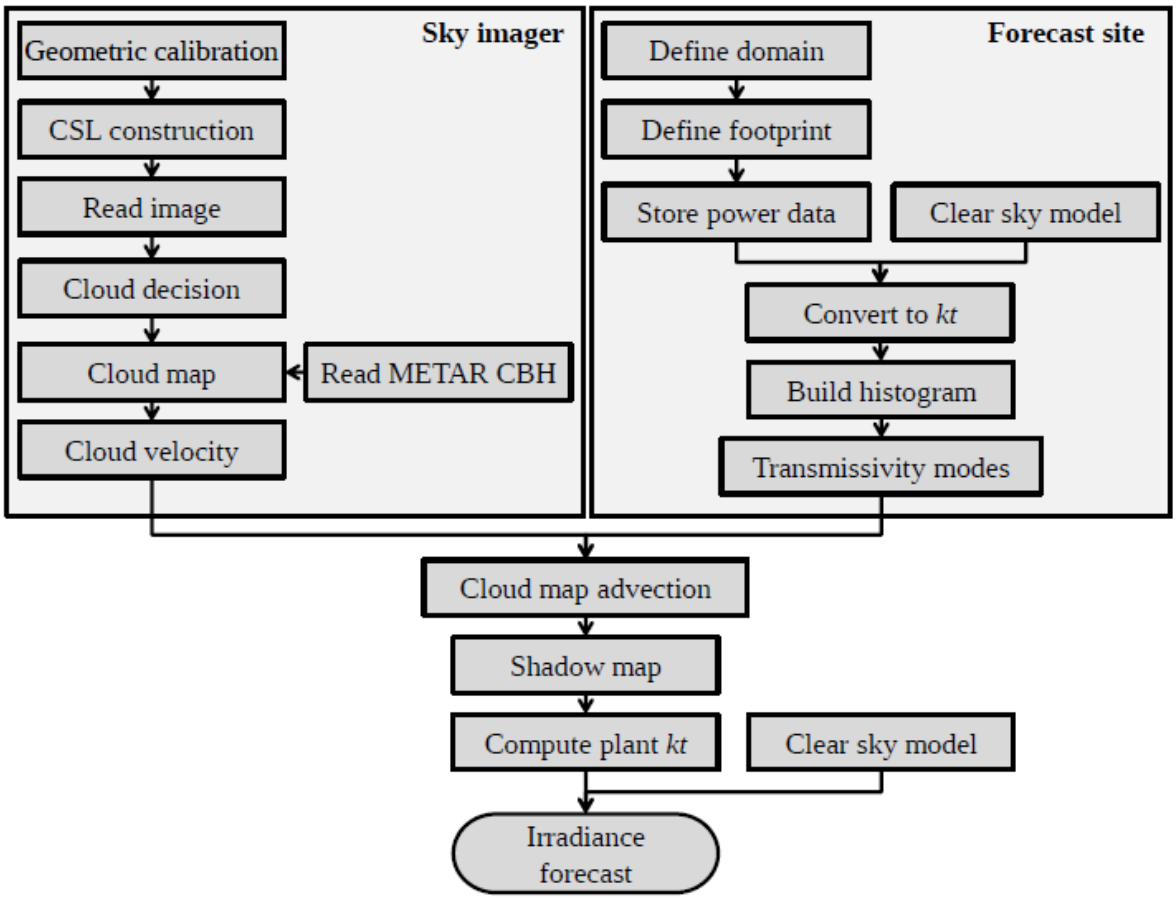

2.6.1 Geometric Calibration and Image Pre-processing

Before image processing, the USI was calibrated to map each image pixel to a geographic azimuth and zenith angle by leveraging the known position of the sun and the (equisolid angle) projection function of the lens. Once the geographic azimuth and zenith angles are known, a "sun-pixel angle" may be computed as the angle between the vector to the sun and the direction vector for a given image pixel.

After calibration maps have been generated (typically performed once per season or following a maintenance operation), images taken by the USI are cropped to remove static objects on the horizon (buildings, trees, etc.), white balanced by a 3x3 color-correction matrix, and treated for any known sensor errors (e.g. dark current noise).

2.6.2 Detecting Clouds

The first objective after reading an image is to determine which regions (if any) of the image contain clouds (Figure 51).

Figure 51: Cloud Decision Procedure

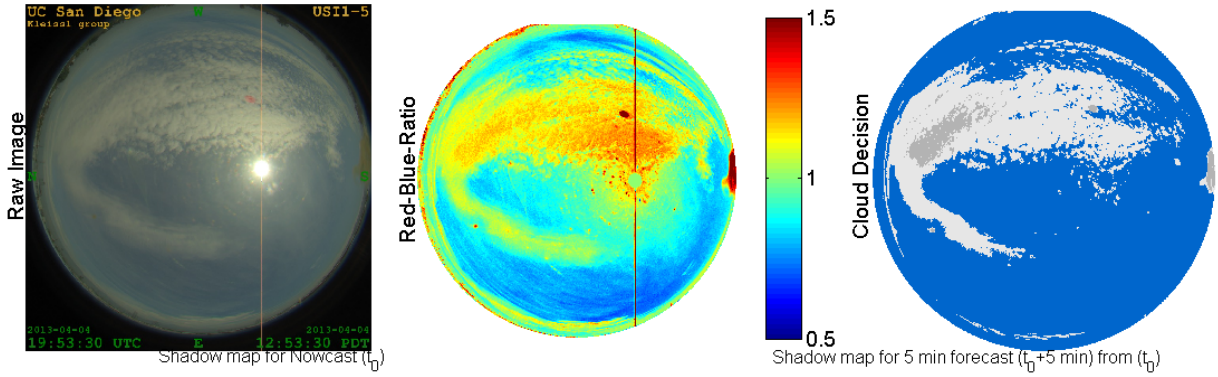

Left: Original image. Center: Red-blue-ratio to enhance cloud contrast. Right: Cloud decision for thin (white) and thick (grey) clouds.

Following the cloud decision algorithm detailed in *A method for cloud detection and opacity classification based on ground based sky imagery*[8], image pixels are classified as clear, thin cloud, or thick cloud based on the ratio of the red image channel to the blue image channel, or red-blue-ratio (RBR). Thresholds are applied on the difference between the RBR of a specific pixel and the clear sky RBR of the same pixel ($\Delta RBR \equiv RBR - RBR_{clear}$), which describe the minimum Δ RBR values representative of thin clouds and thick clouds. To determine the clear sky RBR of image pixels, a Clear Sky Library (CSL) was compiled, which contains the clear sky RBR as a function of image zenith and sun-pixel angles in the form of lookup tables for each solar zenith angle. ΔRBR thin and thick thresholds, thresholds were visually calibrated by comparing resulting cloud decision images with raw images and their ΔRBR images. The CSL was constructed from completely clear days throughout the dataset (March 1st, March 16th, April 3rd, April 9th, April 17th and April 26th).

Additional treatment is required to improve the cloud decision under an overcast condition. The area near the solar disk naturally presents large RBR values in the clear sky library, leading to a low ΔRBR values after subtraction, and a clear decision subsequently. This misclassification is predominant in overcast conditions. To fix this issue several modifications are applied. First, the current cloud decision is overridden with a RBR (instead of a ΔRBR) threshold when the cloud condition is recognized as one of the three following situations:

- Overcast (the overall cloud fraction is over 60%), or
- The cloud fraction within the solar disk is larger than 20%, or

[8] Ghonima, M. S., Urquhart, B., Chow, C. W., Shields, J. E., Cazorla, A., Kleissl, J., 2012. A method for cloud detection and opacity classification based on ground based sky imagery. Atmospheric Measurement Techniques 5, 2881 - 2892.

- The overall cloud fraction is larger than 53% while the cloud fraction within the solar disk is larger than 5% but smaller than 20%.

For the RBR-based cloud decision, the thin and thick thresholds are 1.0 and 1.1, respectively. Second, after applying the cloud decision, the pixels covering the solar disk are reexamined. Saturation is defined for each pixel as the sum of three channel intensities normalized by the sum of the maximum possible values of three channels. Since the pixels in the solar disk are usually saturated if they are unshaded, it was assumed a pixel is clear if its saturation is larger than 96%. This improves the cloud decision within the solar disk and therefore improves the nowcast results. The improvement for mostly cloudy conditions with clear sun pixels is illustrated in Figure 52. The sun is briefly at least partially unobstructed and the saturation check for pixels within the solar disk correctly clears the solar region.

Figure 52: Improved Cloud Decision for Nearly Overcast Conditions

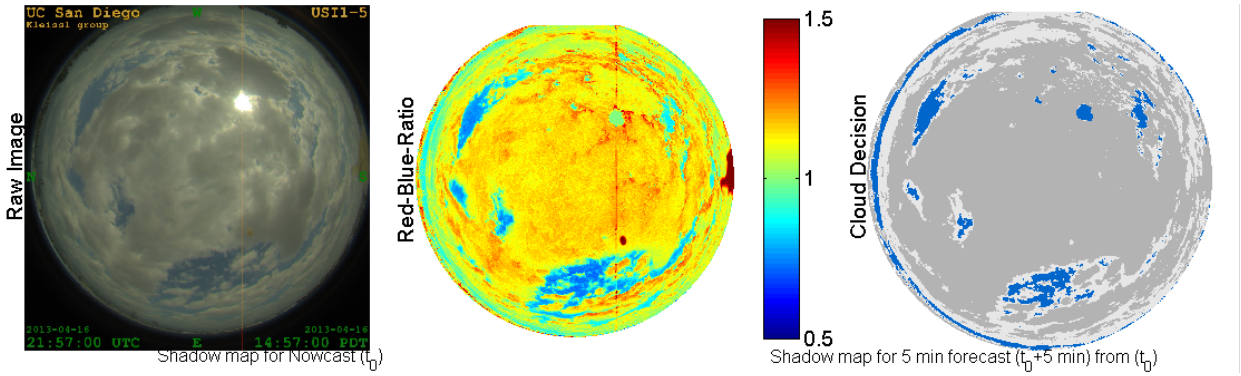

Left: Original image. Center: Red-blue-ratio to enhance cloud contrast. Right: Cloud decision for thin (white) and thick (grey) clouds and clear (blue).

Direct imaging of the sun also requires additional treatment near the solar disk in order to mitigate cloud decision errors. A "CSL bypass" procedure based on the sunshine parameter used by Chow et al. (2011) was developed: when the sun is determined to be obstructed (less than 50% saturated pixels in pixels of sun-pixel angle $< 1^\circ$), the CSL was not used within the region of sun-pixel angle $< 35^\circ$, and only binary cloud decision was performed by assigning pixels with RBR $>$ 0.778 as thick clouds.

Finally, markings such as smudges, soiling, and scratches can possess high RBR values, particularly as the position of the sun in the image approaches these markings. A correction algorithm was applied to remove these false small thick clouds. After all cloud decision and correction algorithms have completed, the blooming stripe is addressed. The blooming stripe is detected in the RGB image by searching near the sun for columns of very uniform brightness. If present, the blooming stripe (typically only about 10 pixels wide) is post-processed by interpolating across the edges of the stripe in the cloud decision image.

2.6.3 Cloud Height, Cloud Map and Cloud Velocity

Cloud base height (CBH) measurements were obtained from historical weather reports of the standardized METAR weather data format. METAR data are typically generated once per hour (sometimes more frequently) at airports or other weather observation stations. In this case, the nearest METAR station was located about 4 km northeast of USI1.5 at the San Bernardino airport (KSBD). A geometric transform, similar to the pseudo-Cartesian transform[9] was then performed to map cloud information to a latitude-longitude grid at the CBH. The resulting "cloud map" is a two-dimensional planar mapping of cloud position at the obtained CBH above the forecast site, centered above the physical location of the USI.

Cloud pixel velocity was obtained by applying the cross-correlation method (CCM) to the RBR of two consecutive cloud maps. The vector field resulting from the CCM contains the cloud speed vector field where vectors with small cross-correlation coefficients have been excluded. The vector field is processed through a series of quality controls to yield a single average cloud velocity vector that is applied to the entire cloud map. In other words, the velocity of all clouds is assumed to be identical.

2.6.4 Forecast Site: Domain and Footprint

While the cloud map is a circle, for simplified processing the forecast domain was defined as a 2.4 x 3.8 km grid at a resolution of 2.5 meters with an elevation from the SRTM1 digital elevation model[10]. The forecast domain contains the georeferenced placement and coverage of the photovoltaic plants, hereby denoted "footprint".

2.6.5 Cloud Transmissivity

The assignment of clear sky indices to clear sky, thin, and thick clouds is based upon persistence forecasts. Measured power output from a moving 2-hour window prior to the time of forecast is processed to derive a clear sky index kt using the modified Kasten clear sky model[11] with Linke turbidity factor from the SoDa database. A histogram is then constructed (Figure 53) and peaks representing modal transmissivities of thin clouds, thick clouds, and clear sky are detected. If a peak cannot be determined within acceptable kt bounds for its given class, a default value, derived from observational data, is assigned (0.42 for thick clouds, 0.70 for thin clouds, and 1.06 for clear sky). To improve the response to changing cloud optical depth for

---

[9] Allmen, M., Kegelmeyer, W., 1996. The computation of cloud-base height from paired whole-sky imaging cameras. Journal of Atmospheric and Oceanic Technology 13, 97 - 113.

[10] Farr, T. G., Rosen, P. A., Caro, E., Crippen, R., Duren, R., Hensley, S., Kobrick, M., Paller, M., Rodriguez, E., Roth, L., Seal, D., Sha_er, S., Shimada, J., Umland, J., Werner, M., Oskin, M., Burbank, D., Alsdorf, D., 2007. The shuttle radar topography mission. Reviews of Geophysics 45 (2).

[11] Ineichen, P., Perez, R., 2002. A new airmass independent formulation for the linke turbidity coefficient. Solar Energy 73, 151 - 157.

homogeneous sky conditions, if cloud fraction is less than 5% (mostly clear) or greater than 95% (mostly overcast), the median kt of the past minute of measured data will be assigned to the clear sky or thick cloud class, respectively.

Figure 53: Histogram of Measured for November 14, 2012

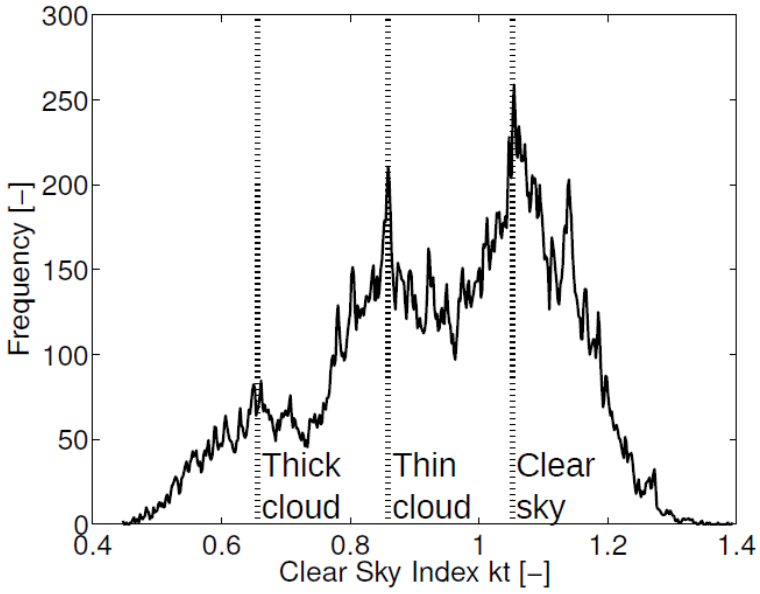

10:00:00 PST through 12:00:00 PST, illustrating three distinct peaks representative of thin clouds, thick clouds, and clear sky

2.6.6 Merge: Cloud Map Advection, Shadow map and Irradiance Forecast

Irradiance forecasts are produced by advecting the current cloud map at the calculated cloud pixel velocity to generate cloud position forecasts at each forecast interval (30 seconds). The locations of ground shadows cast by clouds as defined by their location in each advected cloud map are determined by ray tracing. The resulting estimation of cloud shadows within the forecast domain is termed the "shadow map." For each pixel within the footprint, a modal kt is assigned from the histogram procedure (as described Section 3.1.5). The average modal kt of the pixels within the power plant is then multiplied by the clear sky power output model to produce solar plant power output.

2.7 Error Metrics

2.7.1 Cloud Map Matching Metrics

Two quantities were used to characterize the performance of image-based algorithms: matching error and cloud-advection-versus-persistence (cap) error. The 30-sec forecast cloud map generated at time t_0 was overlaid onto the actual cloud map at time $t_0 + (30\ \mathrm{s})$ in order to determine pixel-by-pixel forecast error, or "matching error." No distinction between thin and

thick clouds was made in determining matching error; a pixel is either cloudy or clear. Matching error was defined as:

$$e_m = \frac{P_{\text{false}}}{P_{\text{total}}} \times 100\%. \quad (1)$$

Matching errors for mostly uniform sky conditions (i.e. completely clear or completely overcast) are by default close to zero and are not an interesting test of forecast skill, so aggregate matching error metrics (e.g. mean and standard deviation) were only computed using matching errors for times corresponding to $5\% <$ cloud fraction $< 95\%$. Similarly, daily cap error, scalar average cloud speed, and average cloud height were computed only for the same time periods. A cap error below 100% indicates that cloud advection outperformed persistence and confirms the potential of the sky imager forecast approach.

Cap error was computed in order to determine whether cloud advection improves forecast performance compared to a naïve forecast by comparing the number of falsely matched pixels of the 30-sec advection forecasts with those of an image persistence forecast. Image persistence means that the cloud map at t_0 remains static until 30 seconds later. Cap error was defined as:

$$e_{\text{cap}} = \frac{P_{\text{false,advection}}}{P_{\text{false,persistence}}} \times 100\%. \quad (2)$$

A cap error of less than 100% indicates that cloud advection improves performance over image persistence forecast.

2.7.2 Aggregate Error Metrics

Time series constructed from 0, 5, 10, and 15 minute forecasts were validated against measured data collected at the four power plants. To avoid disproportional weighting of data near solar noon, validation was also performed on normalized power similar to the clear sky index kt. Instantaneous power output / kt at the image capture times was used as ground truth.

Four error metrics were used to assess the overall performance of the USI forecast system as a function of forecast horizon: relative mean absolute error (rMAE), relative mean bias error (rMBE), and forecast skill (FS). Relative metrics were obtained by normalizing by the temporal and spatial average of the observed kt for each day ($\overline{kt}$). Each metric was computed for each forecast horizon using kt values averaged across the four power plants. In the following equations, N denotes the total number of forecasts generated on a given day. The superscript "obs" denotes an observed value, and "fh" denotes forecast horizon in minutes ($fh = 0, 0.5, 1, \ldots, 15$ min). Therefore, kt_n^{fh} indicates the spatial average of the fh-minute-ahead clear sky index kt forecasts generated at each power plant at time t_n corresponding to the n th forecast of the day.

$$\mathrm{rMAE}(fh) = \frac{1}{N}\sum_{n=1}^{N}\left|kt_n^{fh} - kt_n^{\mathrm{obs}}\right| \times \frac{100\%}{\overline{kt}^{\mathrm{obs}}} \quad (3)$$

$$\mathrm{rMBE}(fh) = \frac{1}{N}\sum_{n=1}^{N}\left(kt_n^{fh} - kt_n^{\mathrm{obs}}\right) \times \frac{100\%}{\overline{kt}^{\mathrm{obs}}} \quad (4)$$

To quantify the relative performance of USI forecasts against a reference metric, a forecast skill was calculated for each forecast horizon. Marquez and Coimbra (2013b) found that the ratio of forecast model RMSE to persistence model RMSE is a measure of general forecast skill that is less affected by location, time, and local variability and can therefore be used to intercompare forecast results. The persistence model used was a persistence forecast generated by assuming power plant measured kt at time t_n persisted for the entire forecast window (i.e. $kt_{n+fh/\Delta t_{\mathrm{images}}}^{fh,\mathrm{persistence}} = kt_n^{\mathrm{obs}}$). Here, rMAE was used to compute forecast skill instead of rRMSE due to the linear nature of rMAE. Thus, forecast skill FS was defined as

$$\mathrm{FS}(fh) = 1 - \frac{\mathrm{rMAE}(fh)}{\mathrm{rMAE}_{\mathrm{p}}(fh)} \quad (5)$$

Positive values of FS therefore indicate USI forecast was superior to power plant persistence forecast, with a maximum possible value of 1.

As an indicator of sample size, the average number of solar plants covered by the shadow map for each forecast horizon was computed. Error metrics were not computed for time series showing average number of stations covered less than 1, because the lack of forecast data for the day and forecast horizon in consideration would make the error metrics not representative. Generally plant coverage was not an issue except for March 3 when the cloud speed was exceptionally high, and thus for longer forecast horizons, like 15 minute horizon, the cloud map had already moved out of the area covered by the power plants.

2.8 Ramp Events

2.8.1 Ramp Event Detection

One of the major roles that sky imagers can play in solar power integration is to enable and improve the use of ramp mitigation tools. USI forecasts of cloud shadow locations should be able to inform users of the timing, magnitude, and duration of upcoming ramp events. This will allow operators to take action to mitigate negative impacts or comply with integration or Power Purchase Agreement (PPA) requirements, especially in areas with high solar penetration.

Ramp rate is defined as the ratio of a certain percentage change in power output over a unit of time, usually minutes. The percentage change is calculated by dividing the change in power output by the nameplate capacity of the power plant. A ramp event is a ramp that exceeds an arbitrarily defined critical value. In order to detect ramp events in power and forecast data, each 0 to 15 minutes forecast and corresponding measured power data set were segmented into parts of 1 min duration. Each of the segments is later fitted with a linear polynomial and the fits,

which exceeded the preset ramp rate value, were marked as 'potential ramp event' (either as ramping up or ramping down event). This procedure was repeated until the starting point of the sub-segments changed to each of the data points in the set one by one. This repetition ensures that a large ramp dataset is created where the choice of specific starting point does not affect the analysis outcome, since the polynomial approximations tend to change slightly with respect to the starting point of the segmentation procedure.

Later, segments marked as potential ramp events which are also neighbors to other marked sub-segments, are appended to each other to form a combined (longer) ramp events. Sample results for a 15 minutes segment are shown in left side of Figure 54 The sky imagers, and the graphs in this report report time in Coordinated Universal Time (UTC) time which is also commonly refered to as Greenwich Mean Time.

The combined ramp events may be further processed to ensure certain user-defined conditions. While minimum or maximum duration thresholds were not used, the ramps are cropped to force beginning and end points of the ramp to show more than 2% increase compared to the following /preceding data point.

Figure 54: Ramp Matching Between Forecast and Measured Data for a USI Forecast

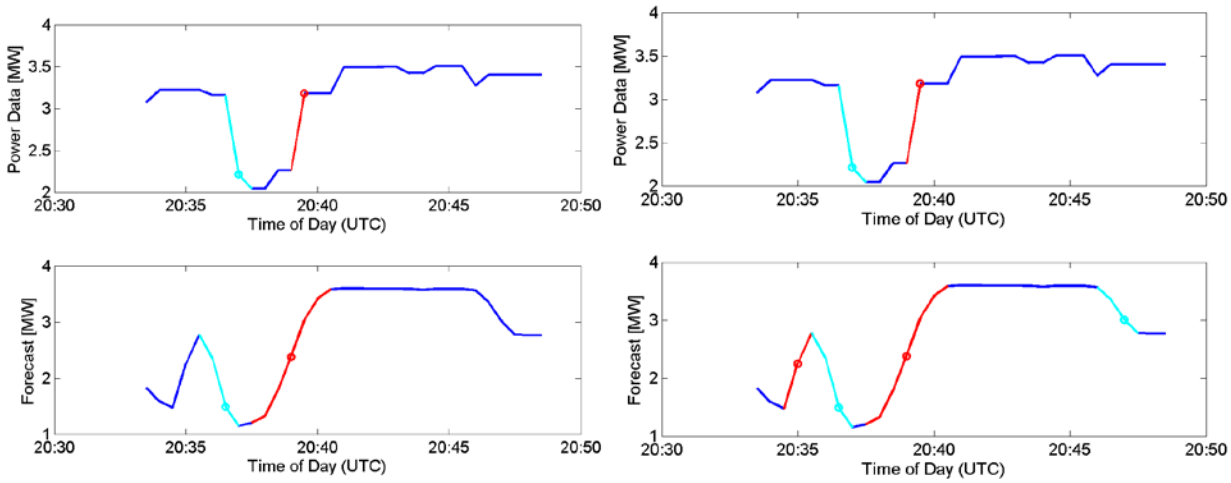

Forecast issued at 20:34 Coordinated Universal Time (UTC). Cyan indicates a ramping down event and Red indicates a ramping up event over 20%.

2.8.2 Ramp Event Matching

After detecting ramps in power and forecast data separately, the research team attempted to match ramps in power data to ramps in forecast data (Figure 55). In Figure 7, Cyan indicates a ramping down event and Red indicates a ramping up event over 20%. All potential ramps that satisfy the 20% threshold criterion are shown on the left. The remaining matched ramps are shown on the right. The down and up ramp between 20:36 and 20:40 are successfully matched. The left-most up-ramp ramp event or right-most down-ramp event are not considered for matching since it is not within three minutes of the observed ramp events

The goal is to create ramp pairs consisting of observed power output ramps that are uniquely matched by ramps in the USI forecast. Three ramp characteristics could be used for matching, in specific the magnitude, duration and time of the event. In this ramp event analysis, a ramp is considered uniquely detected if it occurs within three minutes of the observed ramp event, i.e. up to three minutes before the start of the ramp or three minutes after the end of the ramp. If multiple ramps in forecast data satisfy this condition, the tool selects the forecast ramp whose magnitude most closely matches the actual ramp event.

The duration of the ramp can also be used for ramp comparison but duration is not used in this analysis due to the low temporal resolution of measured power data (typically 30 seconds time step). Since ramp durations are as short as a few seconds to a few minutes, the low temporal resolution prevents accurate quantification of ramp duration.

2.8.3 Ramp Event Forecast Performance

The USI performance in ramp matching is measured by the rate of hits and false alarms in the results. A 'hit' is a successful match of a real ramp event with a forecast ramp event. A 'false alarm' is a USI forecast ramp event that did not happen as a real ramp event. The rate of hits is computed by normalizing the total number of hits for each day by the number of observed ramp events. The false alarms, on the other hand, are normalized by the number of ramps predicted in the forecast data. The objective is for the hit rate to be 100% while the false alarm rate should be zero.

Chapter 3
Feeder Impact Analysis

Integrating the USRE PV generation presents a challenge to utilities in that operating practices and system control responses to disturbances on the distribution feeder levels were developed for conventional generation and need to be reaffirmed or, if necessary, revised to account for the inherent variability of PV generation. Solar data are necessary to accurately predict the system behavior during normal operation and the response of the distribution feeder to disturbances. In previous tasks, historical and forecasted solar data were obtained and a model of the SCE control area was developed to investigate control and planning issues associated with the PV integration on the transmission level. The next logical step, which is documented in this section, is to employ the high-quality solar historical and forecasted data in a detailed electrical study that analyses the distribution feeder impact of the additional PV generation.

3.1 Voltage Control Evaluation

The goal of this task is to evaluate voltage control. Voltage regulation and control operations (i.e., number of tap changes or capacitor switching) were simulated over the profile of load. Measured PV output variations during an n entire year were used to calculate voltage fluctuation. This is important because voltage regulators and capacitor switches may undergo wear and tear due to excessive switching caused by fluctuating generation and load conditions.

3.1.1 Problem Description

Over-/undervoltages can occur during (1) steady-state operation and (2) during momentary disturbance, such as utility switching operation, fault clearing, large motor starts, lightning strikes, etc. In this section, sustained (steady-state) over-/undervoltages are discussed.

The voltage provided to utility customers must be kept within certain limits (1) to ensure correct operation of the customers' equipment that is supplied by the voltage and (2) to prevent safety hazards due to overvoltages. Detrimental effects of sustained over-/undervoltage include

- inhibiting the correct operation of the customers' equipment (e.g., machines running too fast or too slow),
- tripping of sensitive load,
- overheating of induction motors (induction motors operated below rated voltage draw more current, which increases heating losses),
- premature failure (e.g., the life cycle of incandescent lights operated at higher-than-rated voltage decreases),
- increased losses during overvoltage conditions.

Most regulatory entities and utilities in the USA adhere to the voltage limits specified in ANSI C84.1. The standard specifies two different tolerances for two different locations in the power systems. The preferred, more restrictive, voltage range is 'Range A' and the less restrictive voltage range is 'Range B'. 'Range B' voltages that are outside 'Range A' may be acceptable in

"problem systems" but, according to the standard "… corrective measures shall be undertaken within a reasonable time to improve voltages to meet Range A requirements." Both ranges allow for voltages that are outside the specified limits, but these excursions "should be infrequent". ANSI C84.1 specifies limits for the service voltage and the utilization voltages. The service voltage is the voltage at the point where the customer connects to the system (usually at the meter) – maintaining the service voltage within acceptable limits is the utility's responsibility. The utilization voltage is the voltage that is supplied to the customer's equipment (for instance, the voltage at the outlet). The utilization voltage is typically less than the service voltage due to the voltage drop caused by the wiring of the facility, but, if the service voltage is within acceptable limits and the wiring is done according to building codes, which is the customer's responsibility, then the utilization voltage is expected to be within acceptable limits as well. Table 9 lists the ANSI C84.1 service voltage limits for Range A and Range B.

Table 9: Range A and Range B service voltage limits according to ANSI C84.1.

	120 V to 600 V		above 600 V	
	Min	**Max**	**Min**	**Max**
Range A	-5%	+5%	-2.5%	+5%
Range B	-8.3%	+5.8%	-5%	+5.8%

Most utilities control the voltage on the secondary distribution circuit (the low-voltage circuit the customer is directly connected to) by regulating the voltage on the primary circuit (the distribution feeder circuit with typical voltage levels between 4 kV and 35 kV). The service voltage is the stepped-down feeder voltage minus the losses (i.e., service transformer losses and wiring losses). Based on the expected load, utilities can design service transformer sizes and the size and length of a service connection so that the service voltage stays within acceptable limits. Equipment that is at the utilities disposal for regulating the primary circuit voltage includes (1) load tap-changing transformers (LTCs) at the substation and on the line and (2) shunt capacitor banks. In general, any control operation of the voltage regulation equipment (changing of the taps or switching of capacitor steps) is detrimental to the lifetime of the regulation equipment and an excessive number of control operations can dramatically reduce the equipment lifetime.

Inverters used in many DGs usually have power factor correction capabilities. However, IEEE 1547 forbids the DR to actively regulate voltage, which is a somewhat controversial requirement. Opponents of this requirement argue that this restriction is counter innovative in the sense that it curbs the full potential of DR inverter technology. A consequence of IEEE 1547 restriction is that on systems that require active regulation to meet the area service voltage requirements (Table 9), equipment other than the DR must be employed to change the reactive power in direct response to measured voltage conditions. Active regulation can come from, for instance, D-STACOMs, which typically use inverter technology that is similar to the inverter technology employed in modern DRs. The opponents of the IEEE 1547 requirement point out that it is inefficient to use DR inverters to force operation at constant power factor (in response to varying environmental conditions) and then employ D-STATCOMs to provide dynamic power

factor control (in response to the measured voltage fluctuations) instead of using the DR alone to control the power factor in response to varying environmental conditions AND system voltage fluctuations.

There is consensus in the standard-developing community that employing DR for active regulation of the PCC voltage is (1) technically feasible, (2) requires coordination between the DR operator and the area EPS operator to ensure proper operation of regulation equipment operated by the area EPS, and (3) violates the IEEE 1547 requirement and is therefore currently not an option on systems that follow IEEE 1547. This current status quo is in place because the working group that developed the IEEE 1547 standard decided that, at the time the standard was written, the problems associated with active regulation from the DR outweigh the obvious benefits of DR providing active regulation of the PCC voltage. Some of the arguments that led to the acceptance of this IEEE 1547 requirement are listed here:

- The current market structure makes it difficult to provide ancillary services to the area EPS operators because of uniform rules for the public utilities.
- Since IEEE 1547 was published, many manufacturers designed their products to meet IEEE 1547 requirements. Consequently, many current installations that employ these products do not have the capability to actively regulate the area EPS voltage and will not benefit from lifting the IEEE 1547 requirement.
- Active regulation could lead to communication and control interactions between utilities and DR owners, which some DR proponents wished to avoid at the time 1547 was adopted.

3.1.2 Objectives

The objectives of this task is to (1) investigate in simulations if overvoltage conditions exist on the Feeders A and B with today's PV penetration level or future anticipated penetration levels and (2) investigate in simulations and through discussion potential measures that SCE can deploy to mitigate PV-caused overvoltages, such as voltage regulation equipment, and (3) investigate in simulation PV-caused stress on voltage regulation equipment.

3.1.3 Approach

SCE provided a plethora of measured data sets collected at the substations of the modeled Feeders A and B, and the existing PV sites currently installed on these feeders. The provided data sets cover the time period of 13 months ranging from June 28, 2012 to July 2, 2013. Despite the amount of the provided measurements only a few data sets were consistent enough to be suitable for this effort. It is important to note that the type of data required for a study like this one is difficult to obtain. For a thorough investigation, it is essential to use detailed measurements with sub-minute resolutions. Few utilities in North America are collecting and storing wide-area feeder measurements at the high resolution that is required for this type of study.

For this study the following parameters were selected:

Feeder A:

- Substation phase currents: used to develop annual and daily load profiles for all feeder loads
- PV real powers for all three sites: used to develop annual and daily generation profiles for the modeled PV sites
- Irradiance (measured at PV Site #3): used to fill "gaps" in PV generation profiles

Feeder B:

- Substation phase currents: used to develop annual and daily load profiles for all feeder loads
- Substation reactive powers: used to develop annual and daily load profiles for all feeder loads.
- PV real powers for the single site: used to develop annual and daily generation profiles for the modeled PV site

The following Sections describe the analysis, cleaning, and implementation of the received data into the feeder impact analysis task of this study.

3.1.3.1 Data Received for Feeder A

As mentioned above, data sets provided for Feeder A, cover the time period between June 28, 2012 and July 2, 2013 at a time resolution of 15 seconds.

Figure 55 shows the irradiance measured at Feeder A's PV site #3. The irradiance profile required little data-cleaning as it had only a few and short-ranged "gaps" between measured points. The provided irradiance shows a shape that is typical for the activity of the sun in the Northern Hemisphere (i.e., relatively high activity in the time period between late spring and early fall, and relatively low activity for the rest of the year). It is very important to have at least one high resolution irradiance data set measured in the immediate vicinity of the system under study, as high resolution generation profiles tend to have "gaps" between measurements. Using local irradiance data, these "gaps" can be "filled". In this particular case, the two feeders are adjoined with all four PV sites located within an area that is roughly 1.5 square miles Therefore, the provided irradiance profile has a high correlation with all four generation profiles and is suited for replacement of missing data points. Few utilities in North America are collecting and storing wide area-feeder measurements at the high resolution required for this type of study. No individual irradiance was provided for the Feeder B site. Thus the "gap-filling" for the PV system connected to Feeder B had to be performed using the irradiance shown in Figure 56.

As seen in Figure 57 (top) and Figure 58 (top), the generation profiles for Feeder A's site #1 and site #2 are missing data for the first four months of the studied period along with some minor "gaps" (i.e., several hours) in the rest of the data. Using the existing generation profiles together with the irradiance data, the missing data was replenished employing a process called 'Curve Fitting'. Curve Fitting is a mathematical procedure of finding a formula that best fits a given set

of data. In this case, the given data sets are irradiance (input data set) and generation (output data set). By finding individual formulas for each of the two sites, it was assured that the power generated by both PV systems would be slightly different, as it is the case for geographically separated PV plants. Note, in case of site #2 only, the irradiance and generation profiles for the time period between November 2012 and February 2013 were used for the 'Curve Fitting' procedure. The reason for this limitation is that the total rating of this site was increased by 1 MW in mid-February.

Figure 58 (bottom) and Figure 59 (bottom) show edited generation profiles with the missing data added.

Figure 60 (top) shows the generation profile of the third PV system installed on Feeder A. This profile had a few short-ranged "gaps" (i.e., minutes to hours) and required little cleaning. However, due to an inverter malfunction, the site #3 generation profile had 500-kW generation drops throughout the studied period. These drops were corrected by adding 500 kW to the identified periods. Figure 60 (bottom) shows the edited generation profile with missing data added and generation drops corrected. It is interesting to note that the shape of site #3's generation output is significantly different from the generation outputs of sites #1 and #2. There could be several reasons for this behavior: (1) the site is equipped with a tracking system allowing the PV panels to follow the sun throughout the daylight hours, and (2) the DC rating of the system is slightly higher than the AC rating thus forcing the inverters operate close to their maximum rating more often than it is the case for sites #1 and #2. It is most likely that option (1) is being used here as this is the more feasible one from a financial point of view. Table 10 compares the number of hours each PV system is operating at its rating, during the studied time period. Site #3 has by far the most hours.

Figure 55 Irradiance Profile Provided by SCE.

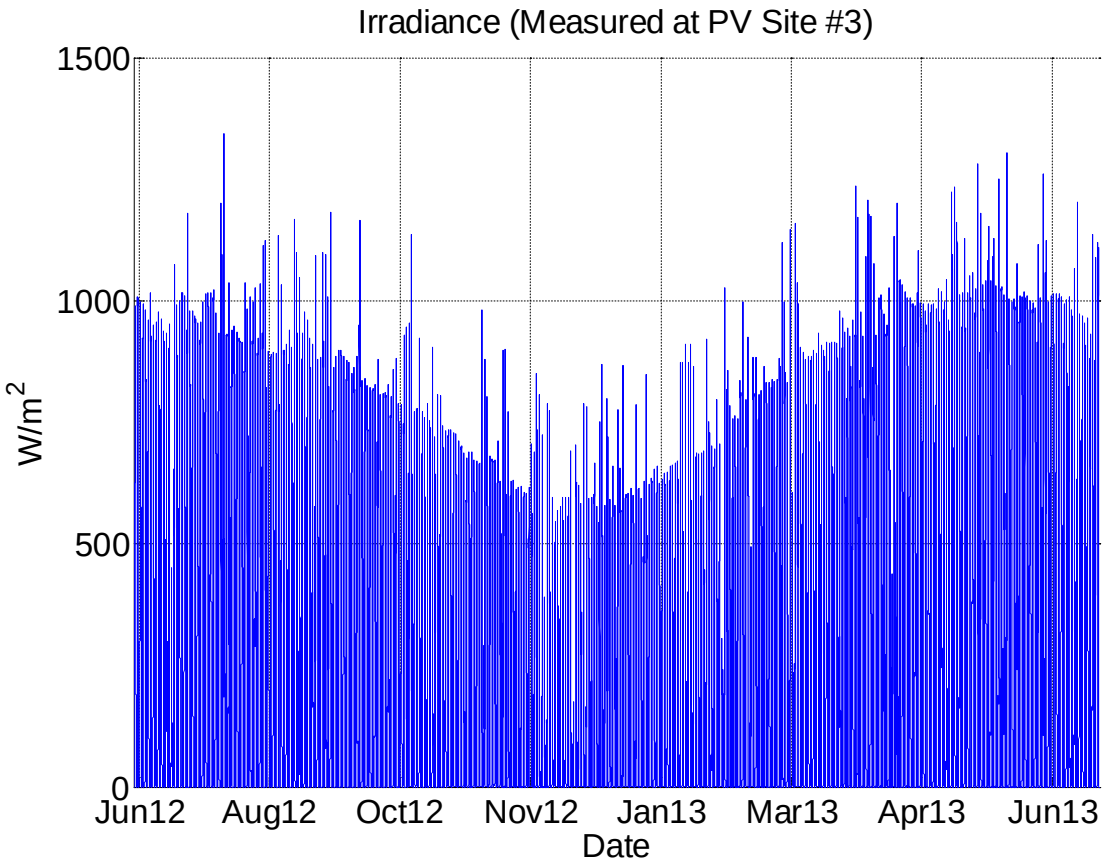

Figure 56: PV-1, Production Profile Provided by SCE

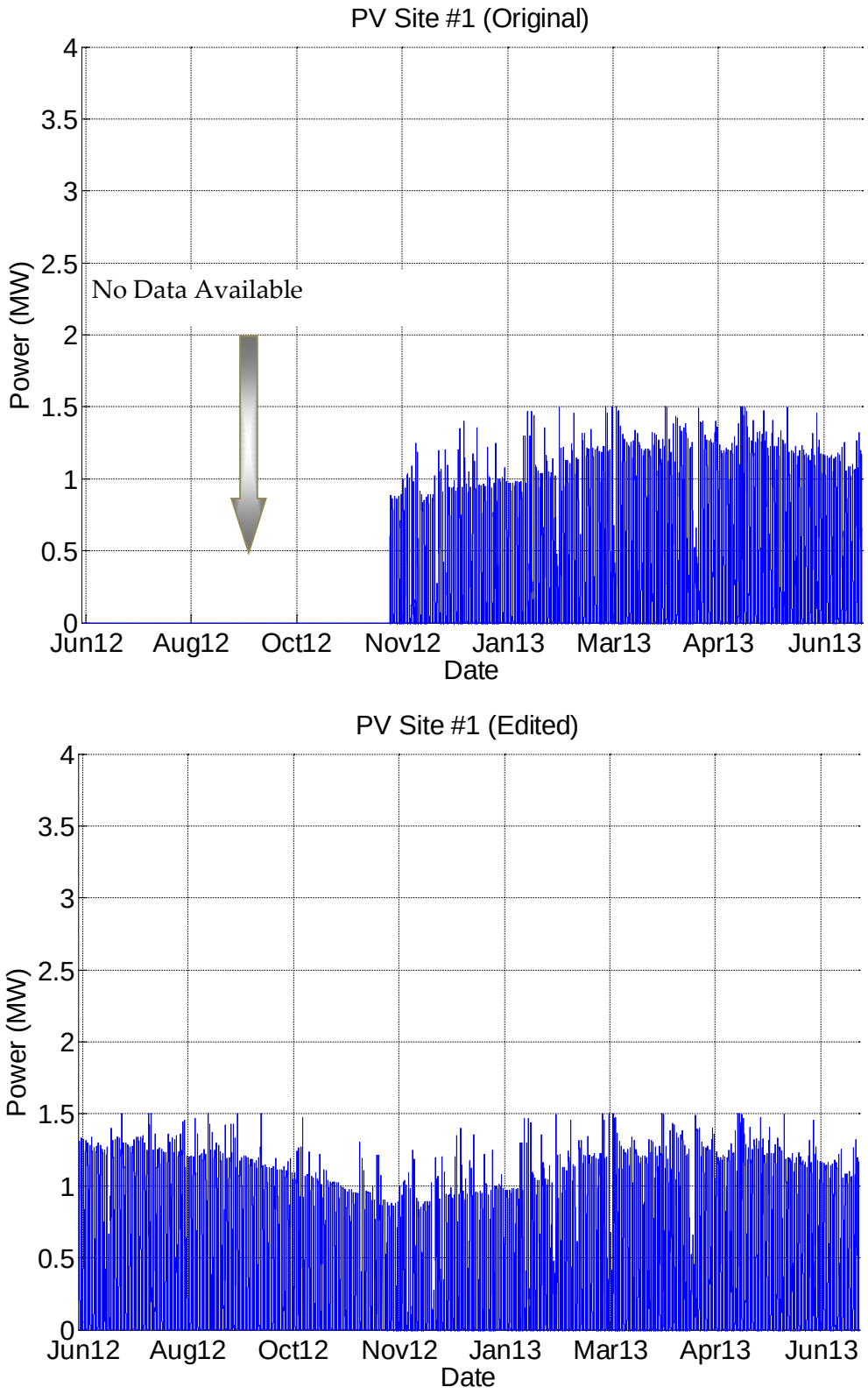

Figure 57: PV-2, Production Profile Provided by SCE

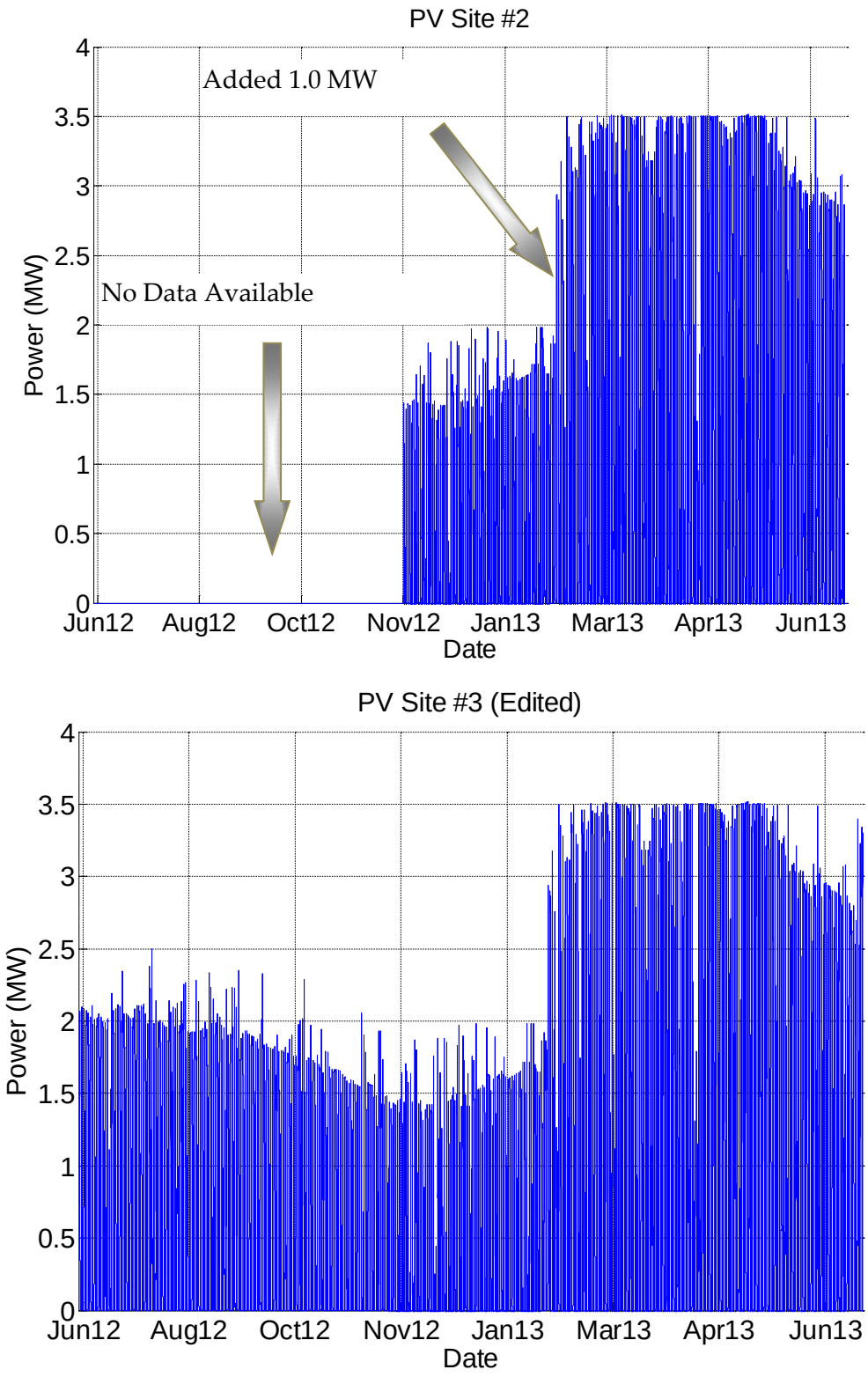

Figure 58: PV-3, Production Profile Provided by SCE

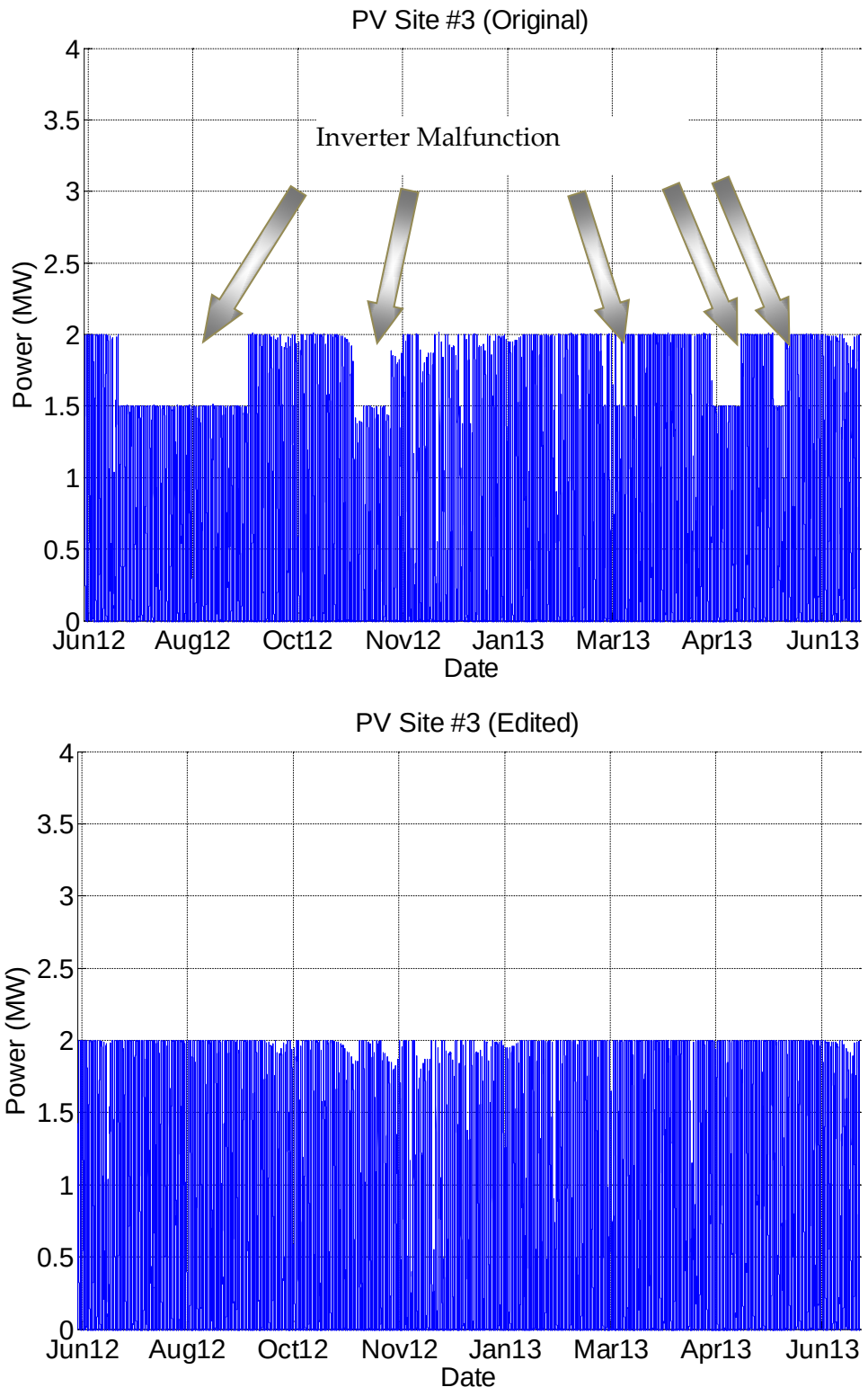

Figure 59 shows the three-phase substation MVA profile, which was calculated using the substation phase current profiles, provided by SCE and the assumption that the line voltage is maintained at a constant 12 kV level. The voltage had to be assumed as a constant value, since no line voltage measurements were provided for Feeder A. In addition to constant voltage, several other assumptions had to be made to incorporate the calculated MVA profile into the simulation efforts. The provided phase current profiles did not contain phase angle measurements, thus making it difficult to separate the active and reactive components. The reason this separation is required is the necessity to determine the actual power consumption from the calculated net-load (Load – PV) values. The calculated MVA values at the substation are already offset by the amount of power generated by the PV systems in the feeder and had to be converted to pre-PV levels to be used in the simulation.

Figure 59: Substation Load Annual Consumption Profile

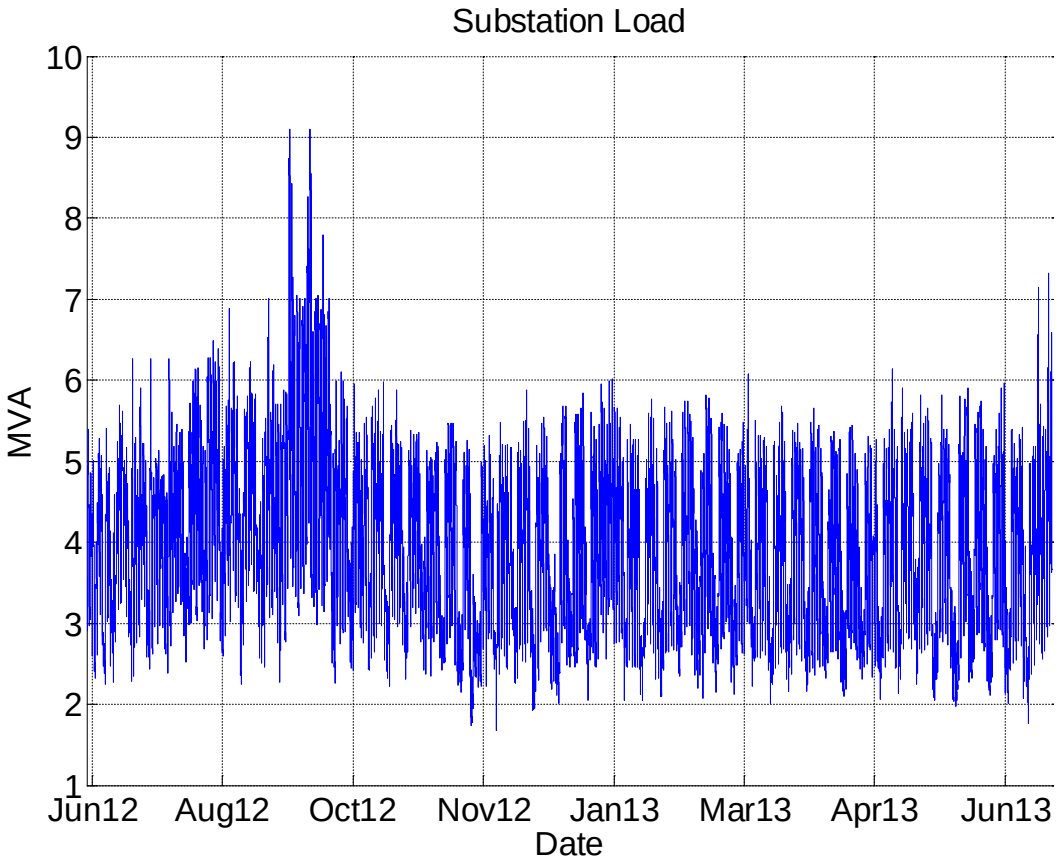

Table 10: Hours Each PV System is Operating at Its Rating.

	Feeder A			Feeder B
	Site #1	Site #2	Site #3	Site #1
# of hours generating at max rating	1	47	528	67

Figure 60 (top) shows a 24 hours substation net-load profile together with the power generated by all three PV systems. As the PV output increases during the daylight hours, it offsets the real power consumed by the loads in the feeder, thus decreasing the amount of real power delivered by the substation. The substation provided power decreases until it reaches an inflection point at which the active power demand in the feeder is entirely covered by the PV systems and the substation is only supplying reactive power to the feeder. As the active power generated by the PV systems continues to grow, so does the net-load curve indicating that at this point the active power generated by the PV systems flows past the substation into the transmission system. That continues until the active power generated by the PV systems starts declining and reaches the point where it measures up to the active power demand of the loads in the feeder. This is indicated by the second inflection point of the substation net-load curve. Past this point the PV generated active power offsets increasingly smaller parts of the demand with the substation supplying the difference. Once the PV generation reaches zero, the substation resumes the supply of the entire feeder demand. To separate the substation's net-load curve into its active and reactive parts, two assumptions regarding the reactive power demand were made: (1) the reactive power demand to the left of the first inflection point and to the right of the second inflection point stays constant at the values defined by the respective inflection points, and (2) the reactive power demand between the inflection points increases linearly. It is important to note that the reactive power rise between the inflection points is partially due to the increased voltage levels in the feeder caused by reversed power flow. However, without any additional information regarding the status of the feeder during this period, it is rather hard to account for the PV influenced increase in reactive power demand. Therefore, a linear approximation appears to be reasonable.

Figure 61 (bottom) shows the assumed reactive power profile, calculated active power profile, and the resulting apparent power profile calculated using the following equation:

$$MVA_{pre-PV} = \sqrt{(MW_{Net-Load} + MW_{PV})^2 + MVAr^2}$$

Also, note that the drops in the PV generation profile around the noon hours are the result of the site #3 inverter malfunctioning, which had to be accounted for during the conversion process.

Similar calculations had to be performed for the majority of the 370 days, worth of provided measurements.

Figure 60: Example of Conversion of Provided Load Data

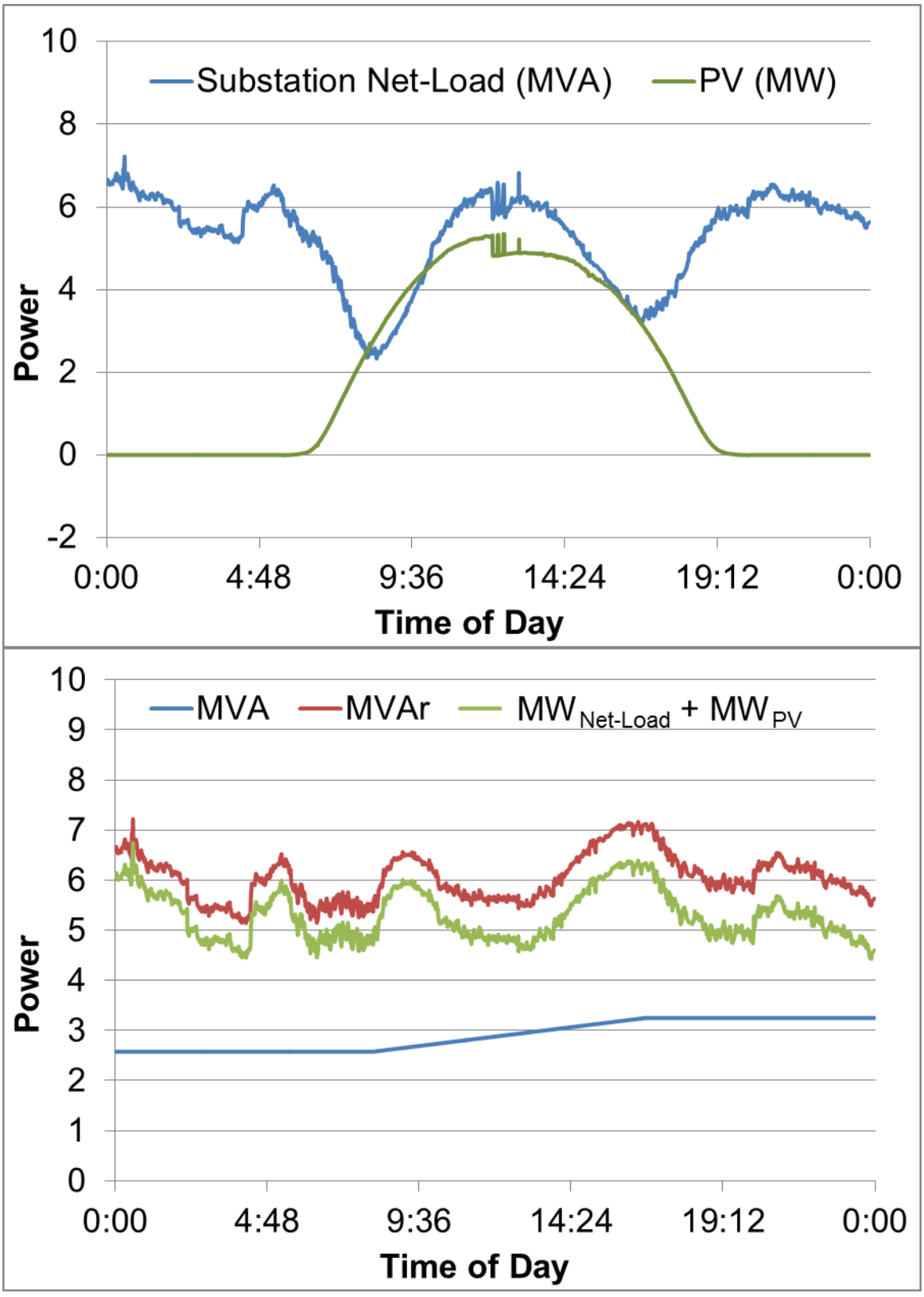

3.1.3.2 Data Received for Feeder B

Similar to Feeder A, SCE provided various measured data sets for Feeder B. The provided data sets cover the time period between June 28, 2012 and July 2, 2013 at a time resolution of 15 seconds. The difference to Feeder A is that no individual irradiance was provided for Feeder B. Another difference is that SCE included a comprehensive reactive power data set, which simplified the conversion of the load profiles to pre-PV levels.

Figure 61 (top) shows the generation profile for Feeder B's single PV site. Similar to the generation profiles provided for Feeder A's sites #1 and #2, several months worth of data are missing. The data "gaps" were filled utilizing the 'Curve Fitting' procedure described previously. Figure 62 (bottom) show the edited generation profile with the missing data added.

Figure 61: PV, Production Profile Provided by SCE

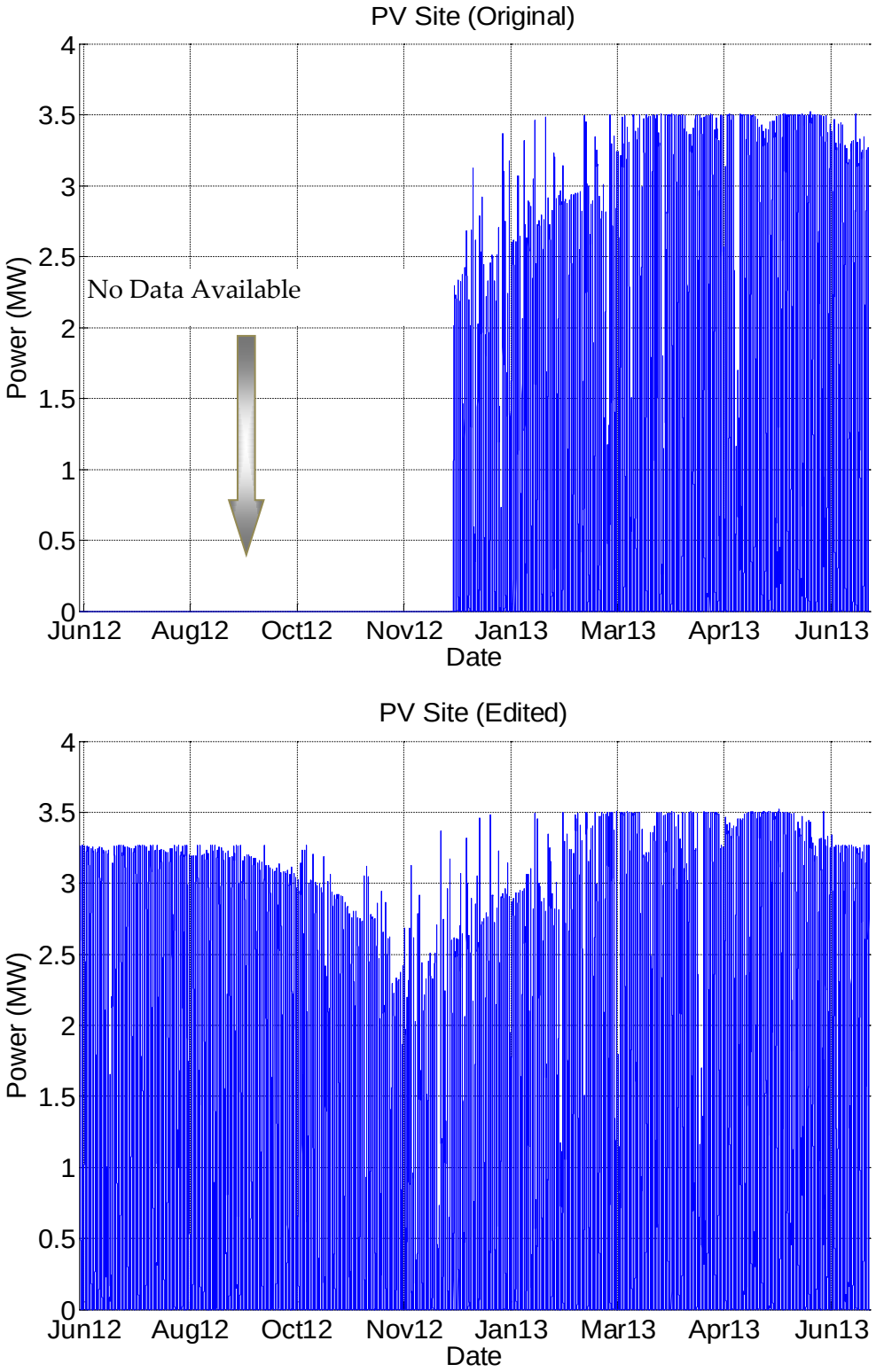

Figure 62 shows the three phase substation MVA profile, which was calculated using the substation phase current profiles provided by SCE. Similar to the calculation for Feeder A, the MVA profile for Feeder B was calculated assuming constant substation voltage levels.

Figure 62: Substation Load, Annual Consumption Profile

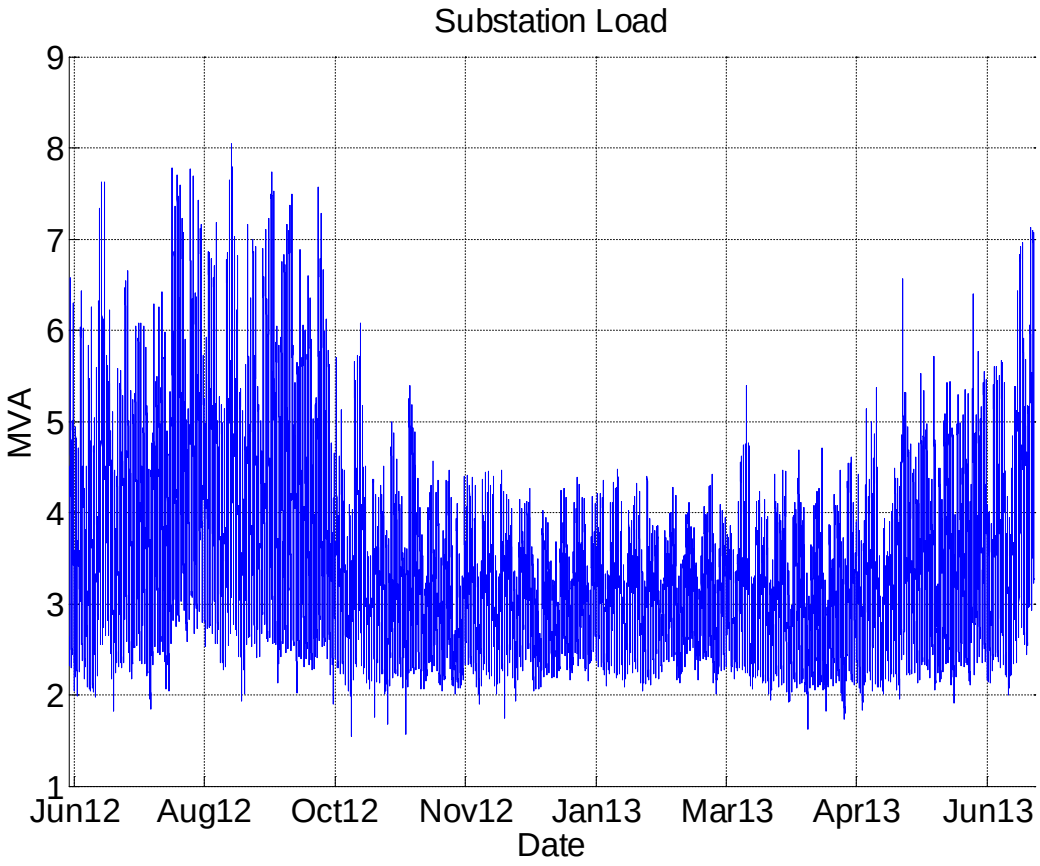

Similar to Feeder A, the substation net-load profile of Feeder B was converted to apparent power profile representing the pre-PV levels. The difference to the conversation procedure described for Feeder A is that the provided data measurements for Feeder B contained a detailed reactive power data set. Thus, no assumptions regarding the reactive power were necessary.

Figure 64 (top) shows a 24 hours substation net-load profile together with the power generated by the PV system and the measured substation reactive power profile. The 1800 kVAr drop in the reactive power around 1 PM is a direct result of a shunt capacitor switching. The capacitor bank stays online until 7 PM when it is taken off-line, right before the power generated by the PV system drops to zero. It is interesting to note that the capacitor bank is taken on-line around the time when the PV system is generating at its peak. The evaluation of Feeder B's data sets has shown that a similar shunt capacitor behavior can be observed for days with high sun activity leading to the conclusion that the capacitor is VAR controlled. However, in the provided CYME model the capacitor is identified as a voltage controlled unit.

Figure 63 (bottom) shows the measured reactive power profile with the 1800 kVAr capacitor rating added to it, calculated active power profile, and the resulting apparent power profile calculated using the same approach used for Feeder A.

Figure 63: Substation Power, Consumption Profile Provided by SCE

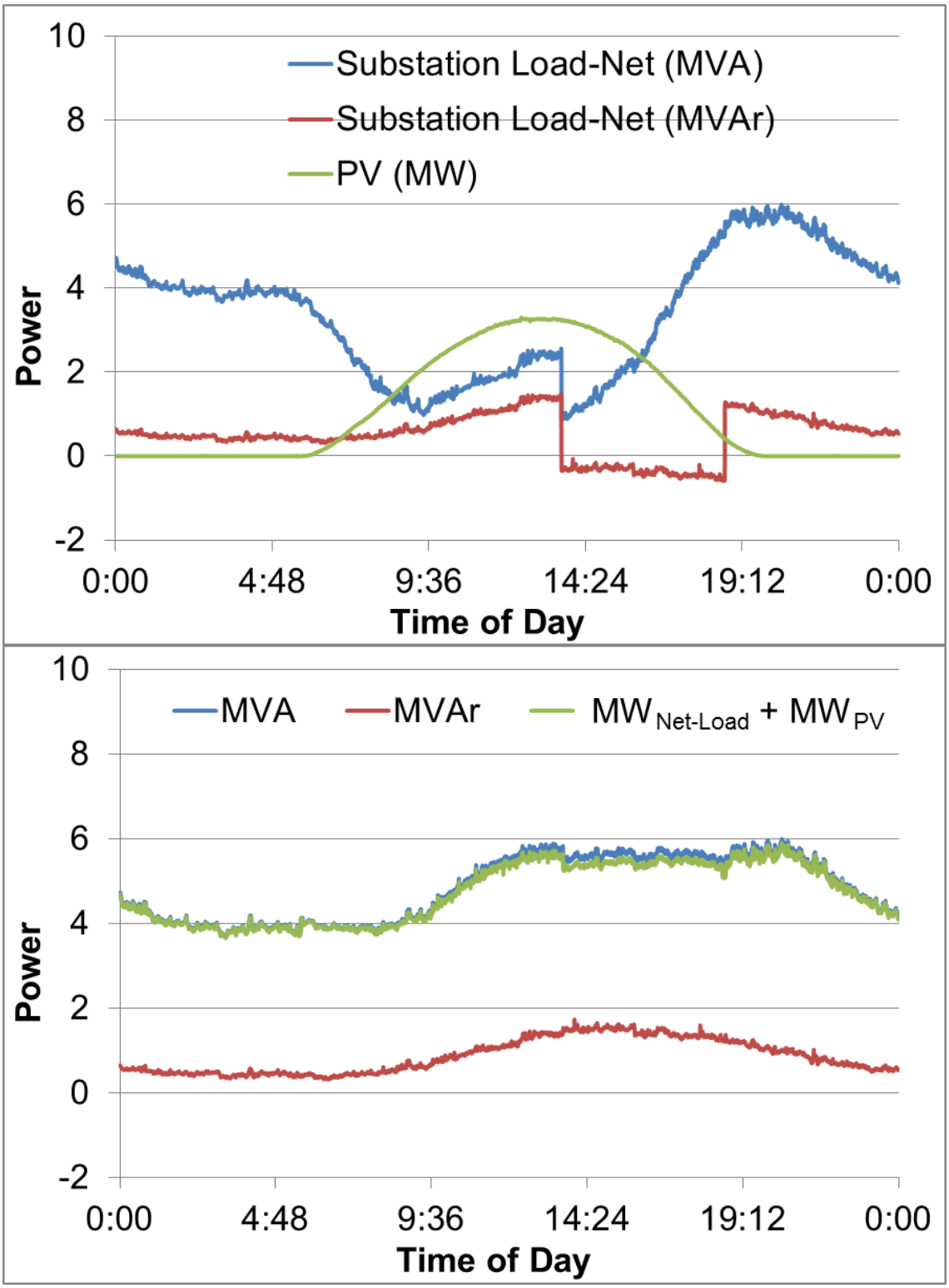

3.1.3.3 Simulation Cases

Two simulation cases were performed to analyze the impact of PV systems on each of the two feeders under study. The first case ('Current PV') was aimed at assessing the impacts under current PV penetration conditions, while the second case ('Increased PV') was aimed at assessing the impacts under a possible future penetration scenario.

As described in previous chapters, the current PV penetrations of Feeders A and B are 7 MW and 3.5 MW, respectively. To properly evaluate the impact of the current PV penetration, it is important to simulate the system 'as is'. In other words, for Feeder A's PV sites #1 and #2 the edited PV generation profiles shown in Figure 57 (bottom) and Figure 58 (bottom) were used while for Feeder B's PV site the edited generation profile shown in Figure 62 (bottom) was implemented. The behavior of Feeder A's PV site #3 was modeled using the unedited generation profile shown in Figure 59 (top).

For the Increased PV case, it was assumed that the combined rating of the currently installed PV systems will be increased to 10.5 MW on the respective feeders. On Feeder A, all three system's ratings were assumed to grow to 3.5 MW each, while on Feeder B the single PV system was assumed to grow to 10.5 MW. Additionally, all four systems were assumed to have tracking systems installed, allowing the PV panels to follow the sun throughout the daylight hours. Considering that Feeder A's site #3 is equipped with a tracking system, its generation profile is the most appropriate one for this simulation case. The addition of the tracking system amplifies the effects of the oversized systems on the feeders. Unfortunately, only one data set, that represents a tracking enhanced system, has been provided. Using this set for all four PV systems at once does bear some disadvantages – e.g., exaggeration of the impact due to synchronized up and down ramps of the installed PV systems. However, as mentioned above, these units are located in near proximity to each other suggesting that the tracking could lead to similar generation profiles.

Figure 64 shows the generation profile used for the three units installed on Feeder A. Figure 65 shows the profile used for the system installed on Feeder B. Essentially, both figures are showing the same profile that is scaled differently due to the different PV penetration levels.

Figure 64: PV – Increased Rating

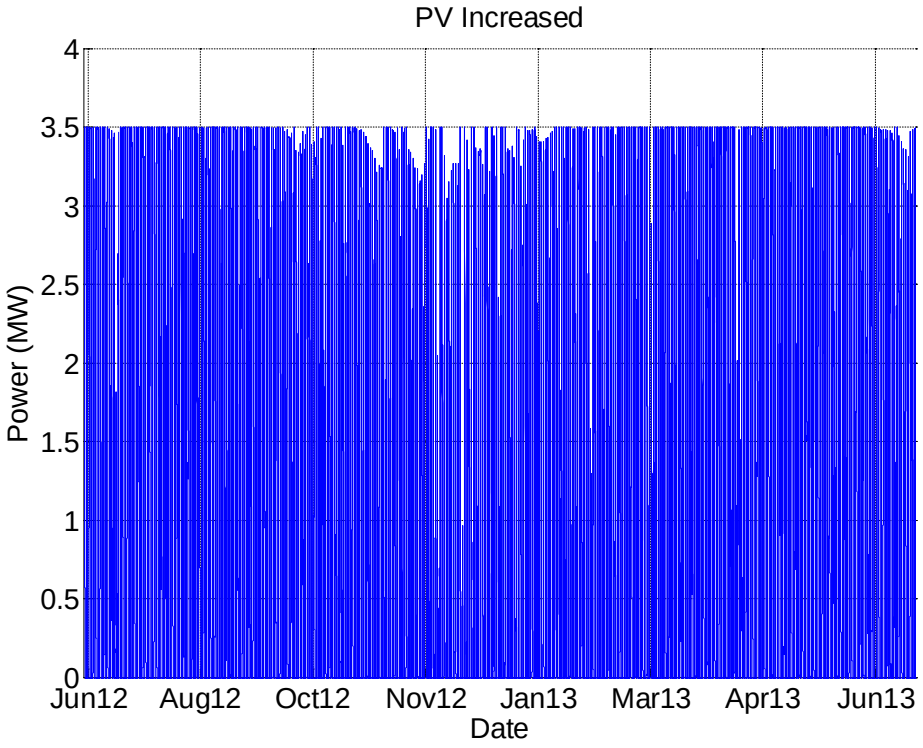

Figure 65: PV – Increased Rating

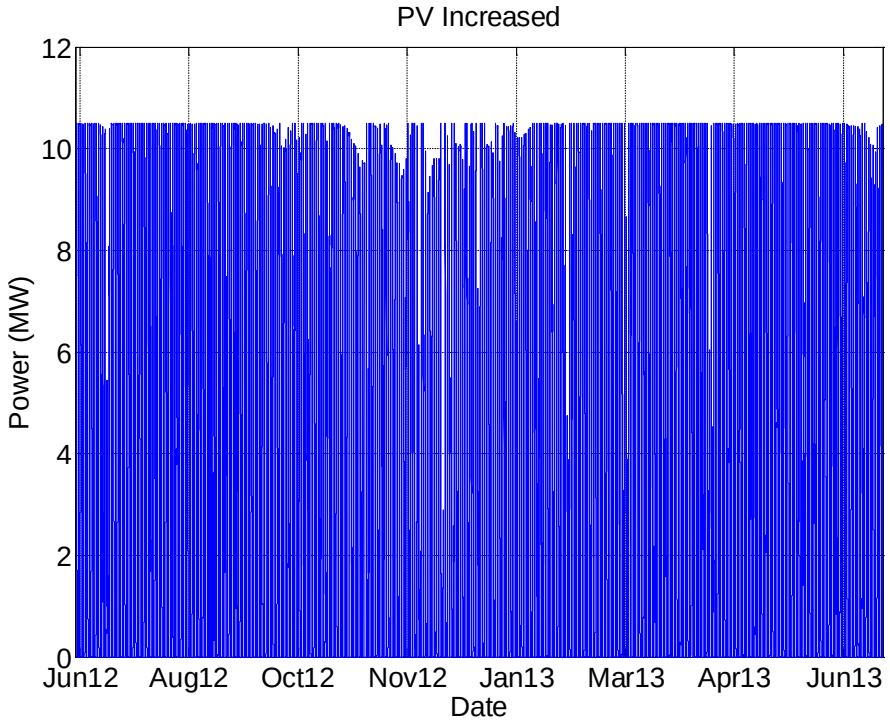

3.1.4 Presentation of Simulation Results

In this Section the simulation results are presented for each of the two cases. In addition to performing simulation runs covering the entire study period, two single 24 hour profiles (one for each feeder) were simulated representing the days with the lowest load to PV ratio. For Feeder A, that day was March 17, 2013 and for Feeder B it was March 23, 2013. The reason behind simulating individual days was to get a better understanding of the PV impacts on the system by investigating days with significant reverse power flow in detail.

3.1.4.1 Feeder A – Current PV Penetration Level

The simulation results for the current PV penetration level at Feeder A are shown in Figure 66 through Figure 70. During the studied period the current penetration level managed to shave off roughly 0.5 MW of the absolute peak and led to a total of 1111 hours of reverse power flow maxing out at 4.4 MW. The feeder voltage levels have remained within a range of 0.97 pu and 1.03 pu, which is a slight increase from the 0.97 pu and 1.02 pu range that has been observed during the simulations with no PV included. The increased voltage levels have not led to a rise of shunt capacitor switching. As a matter of fact, the capacitor bank registered two events[12], which is an increase of one when compared to the No PV scenario.

Figure 66: Substation Power, with Current PV Penetration

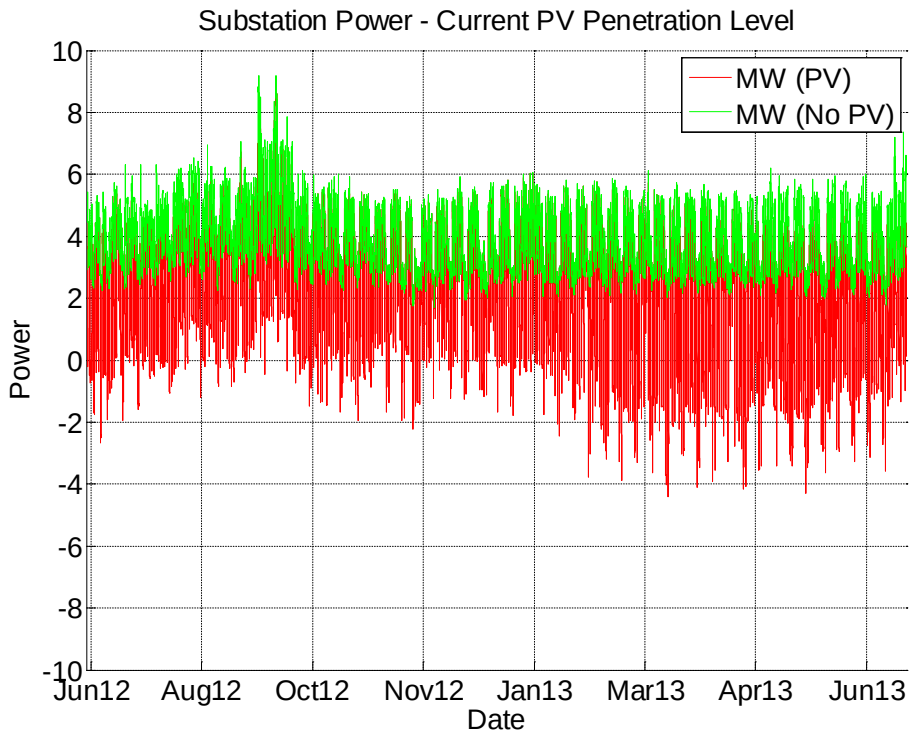

[12] Shunt capacitors 'closing' and 'opening' are counted as events.

Figure 67: Maximum and Minimum Bus Voltages with Current PV Penetration

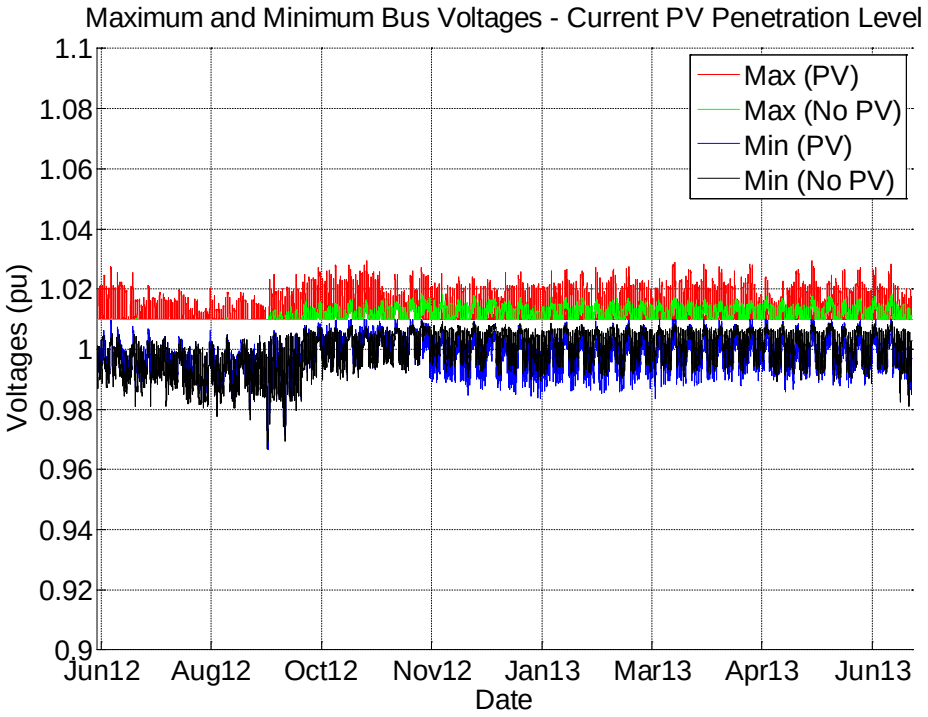

Figure 68: Capacitor Bank Event, with Current PV Penetration Level

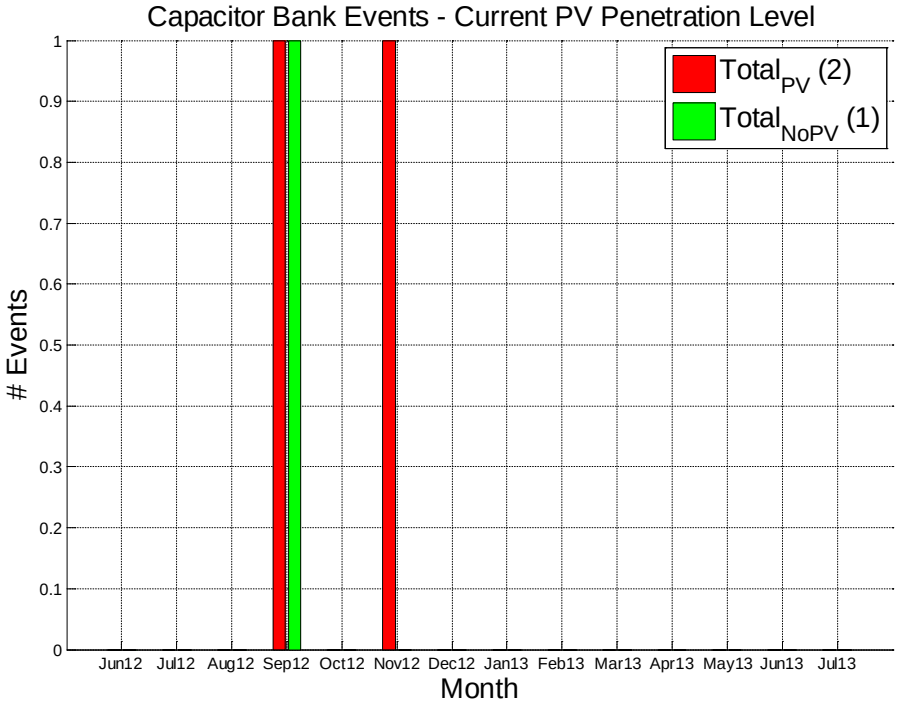

Figure 69: Substation Power with Current PV Penetration (Daily)

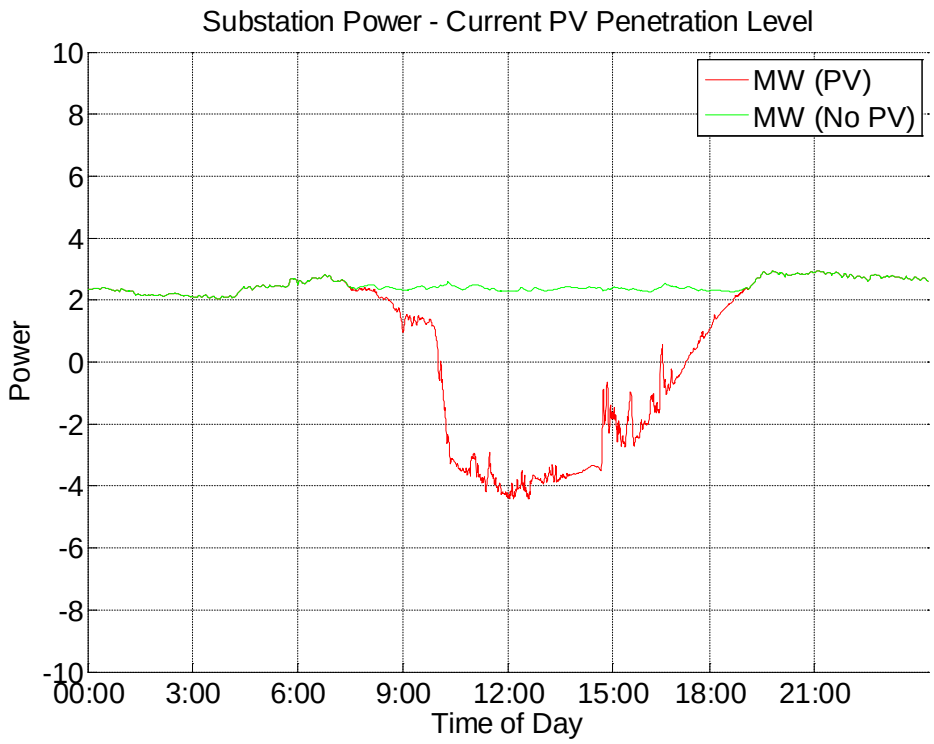

Figure 70: Maximum and Minimum Bus Voltages with Current PV Penetration (Daily)

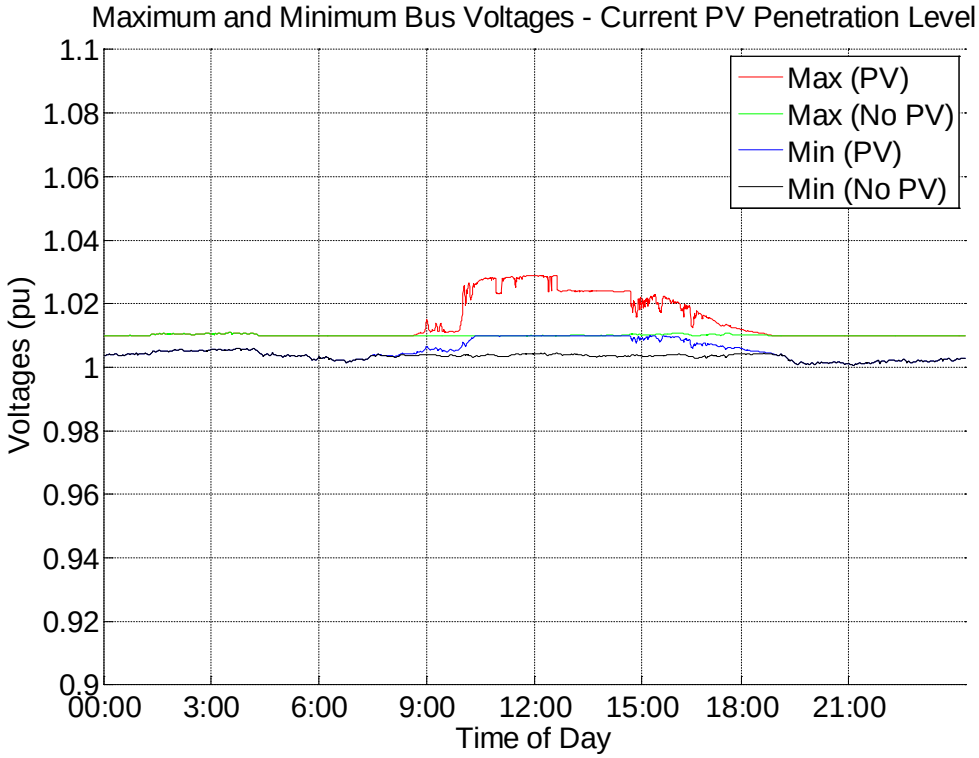

3.1.4.2 Feeder A – Increased PV Penetration Level

The simulation results for the increased PV penetration level at Feeder A are shown in Figures 71-75. During the studied period the potential penetration level managed to shave off roughly 0.6 MW of the absolute peak and led to a total of 2647 hours of reverse power flow maxing out at 8.2 MW. The feeder voltage levels have remained within a range of 0.97 pu and 1.04 pu, which is a slight increase from the 0.97 pu and 1.02 pu range that has been observed during the simulations with no PV included, and roughly 1 % increase from the Current PV level case. The increased voltage levels have not led to a rise of shunt capacitor switching. It peaked at two switching events just like the Current PV level case.

Figure 71: Substation Power with Increased PV Penetration

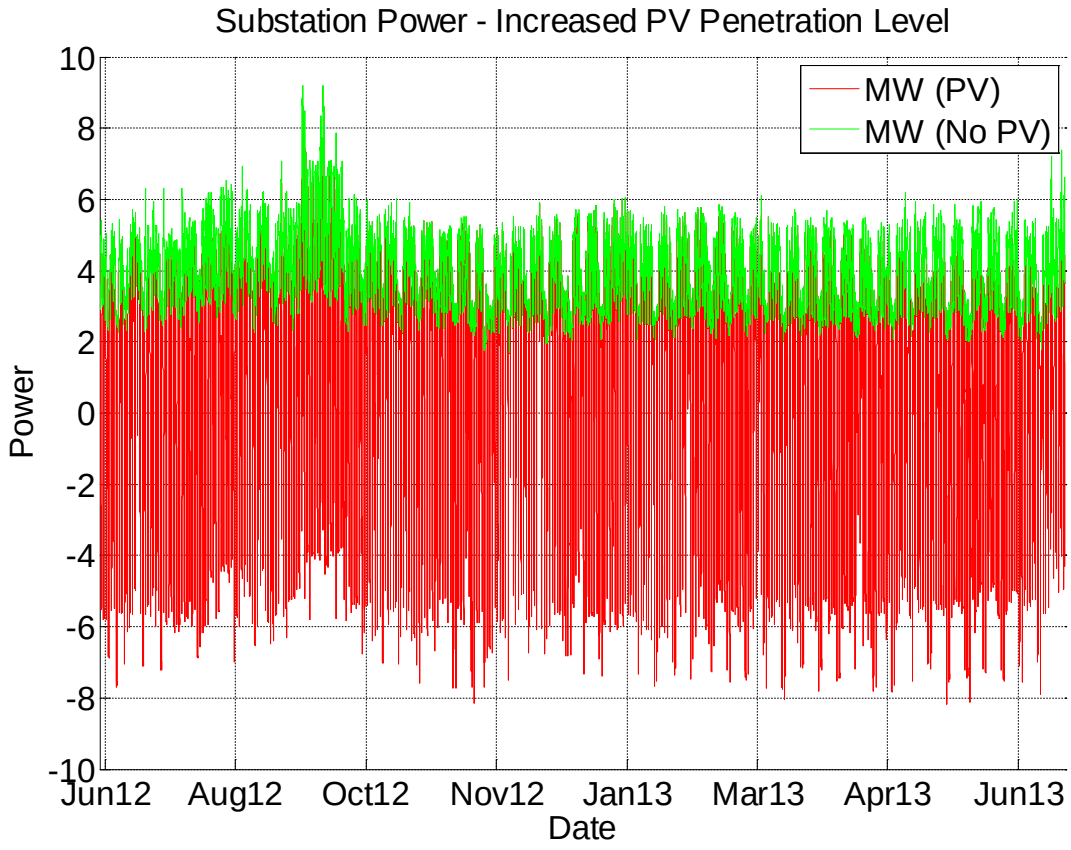

Figure 72: Maximum and Minimum Bus Voltages with Increased PV Penetration

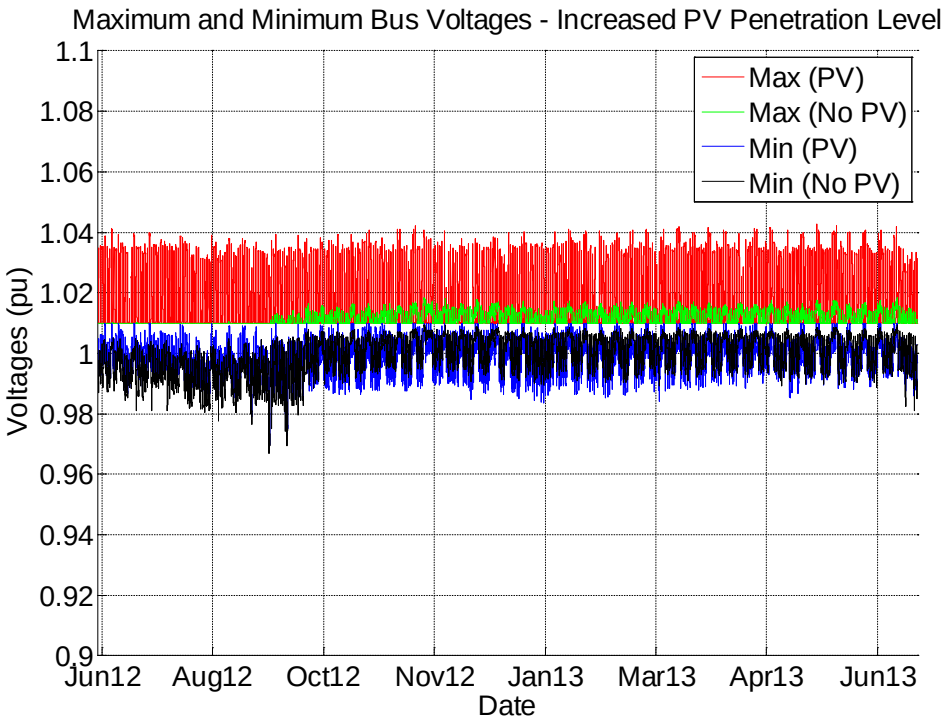

Figure 73: Capacitor Bank Events with Increased PV Penetration Level

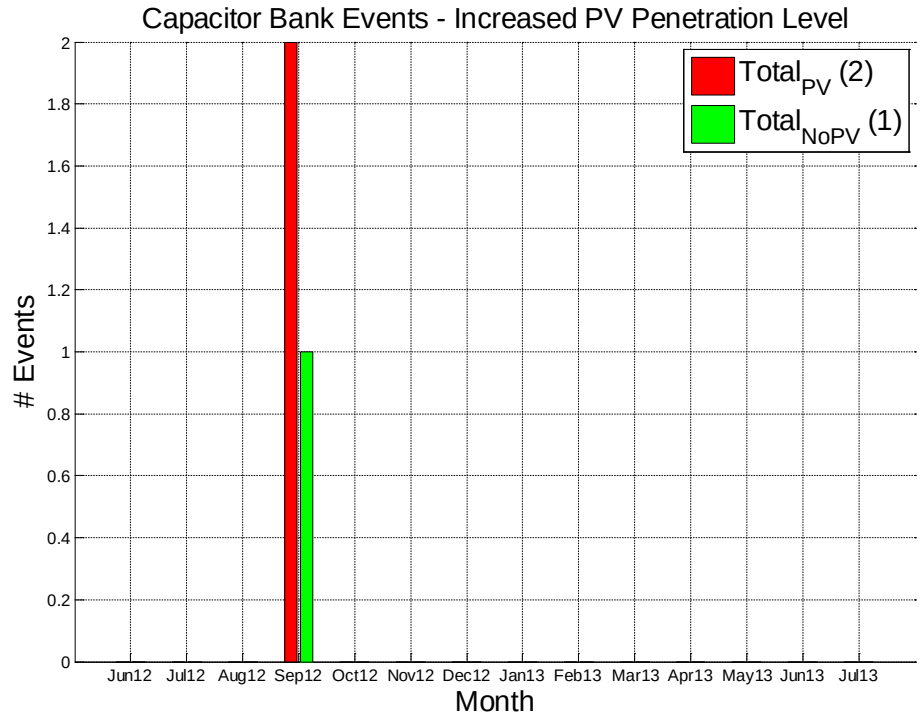

Figure 74: Substation Power with Increased Daily PV Penetration

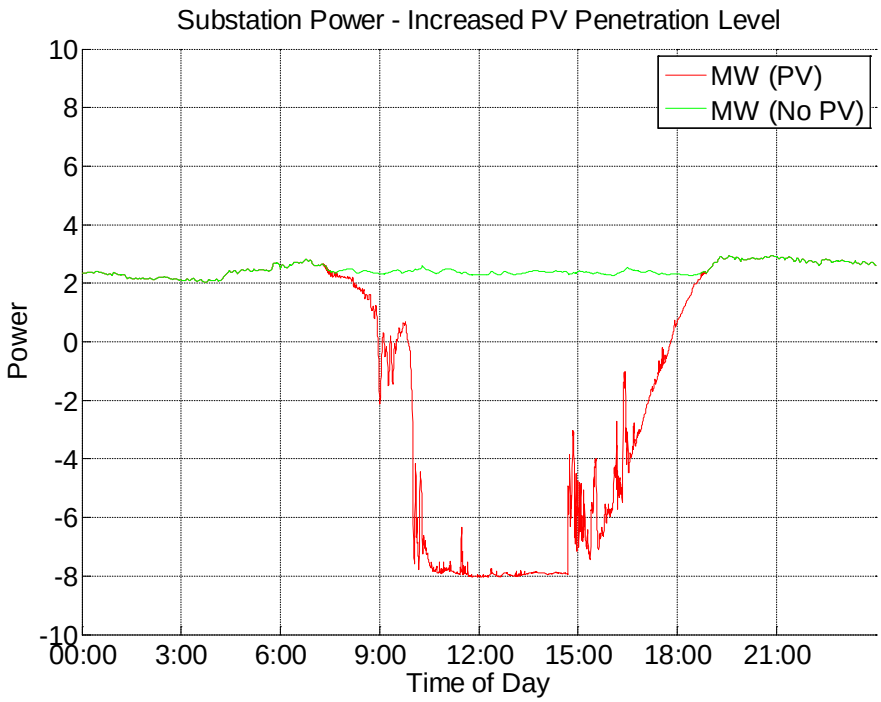

Figure 75: Maximum and Minimum Bus Voltages with Increased PV Penetration (Daily)

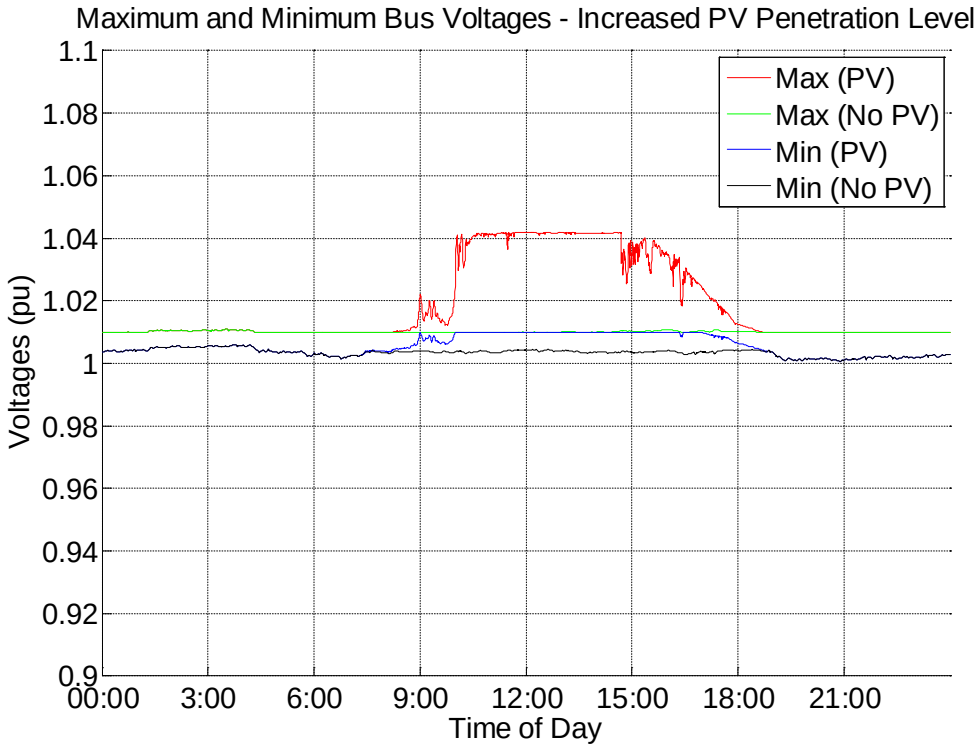

3.1.4.3 Feeder B – Current PV Penetration Level

The simulation results for the current PV penetration level at Feeder B are shown in Figures 77 - 82. During the studied period the current penetration level managed to shave off roughly 1 MW of the absolute peak and led to a total of 124 hours of reverse power flow maxing out at 1.2 MW. The reason the lower PV rating on the Feeder B managed to shave off roughly twice the amount of load observed from simulation results for Feeder A, is that Feeder B's peak occurred during daylight hours. While, Feeder A's peak occurred right around sunset. The feeder voltage levels have remained within a range of 0.98 pu and 1.03 pu, which is a slight increase from the 0.97 pu and 1.025 pu range that has been observed during the simulations with no PV included.

The number of measured shunt capacitor switching events was 265, which was significantly higher than what was observed in the initial simulation results for Feeder B, which assumed voltage controlled capacitors[13]. On the other hand, modeling the capacitor in Feeder B as VAr-controlled as opposed to volt-control provided a very good match between the simulation results and the data on switching operations provided by SCE.

The reason for the increase in switching events when the capacitor is Var-controlled lies in the difference between the two control strategies. With increased PV penetration on the feeder, the overall voltage levels tend to rise, leading to fewer situations when a volt-controlled capacitor has to be operated. On the other hand, the same PV related voltage rises usually lead to an increased reactive power demand within the feeder resulting in more switching events of a VAr-controlled capacitor.

Figures 76 - 81 show the simulation results from simulation runs that model the capacitors as VAr-controlled. The 265 switching events are a slight increase if compared to the 248 events for the No PV case.

[13] Voltage controlled capacitors were assumed in the simulations for Feeder A and were able to successfully match the simulation results to the provided data.

Figure 76: Substation Power with Current PV Penetration

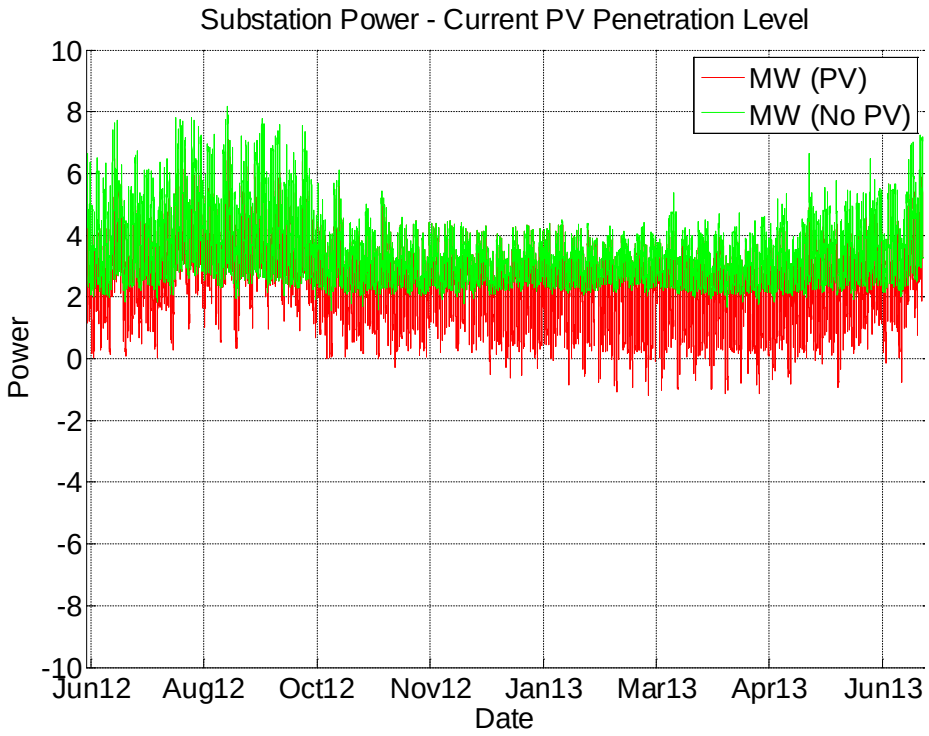

Figure 77: Maximum and Minimum Bus Voltages with Current PV Penetration

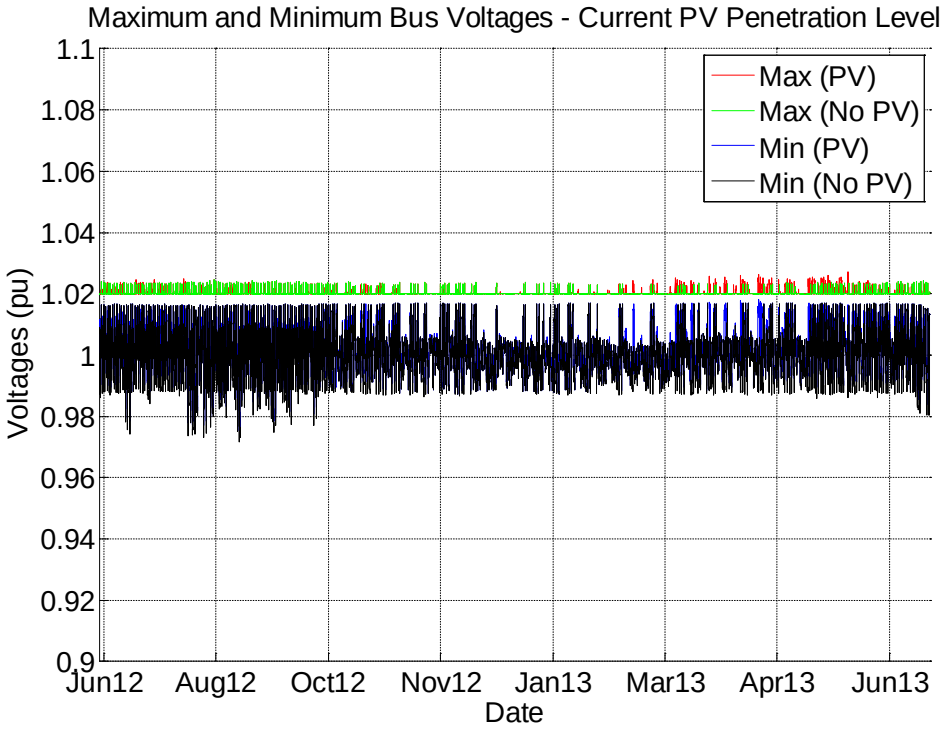

Figure 78: Capacitor Bank Events with Current PV Penetration Level

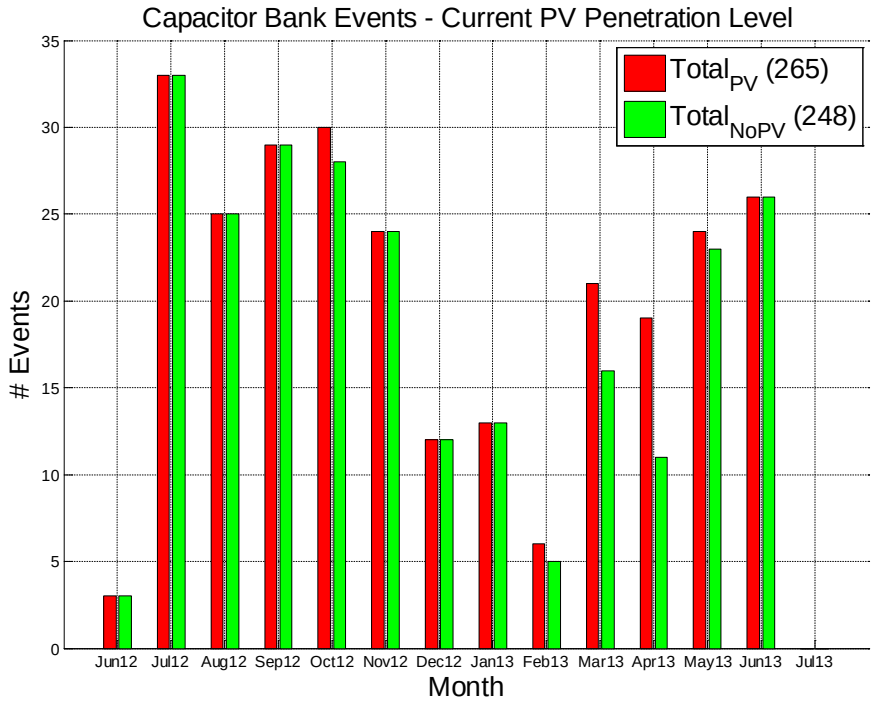

Figure 79: Substation Power with Current Daily PV Penetration

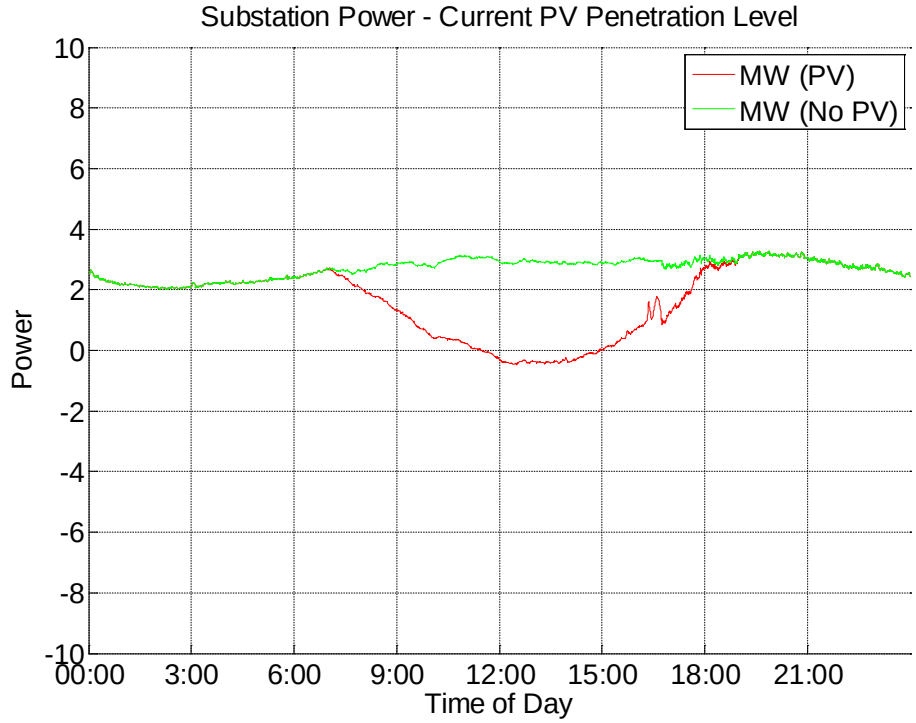

Figure 80: Maximum and Minimum Bus Voltages with Current Daily PV Penetration

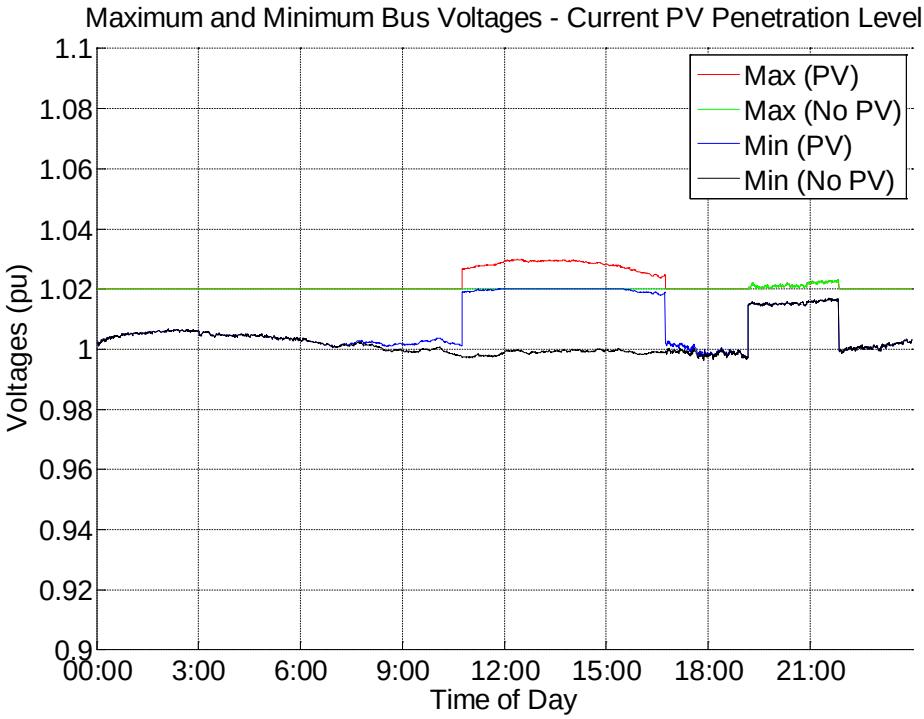

Figure 81: Capacitor Bank Events with Current Daily PV Penetration Level

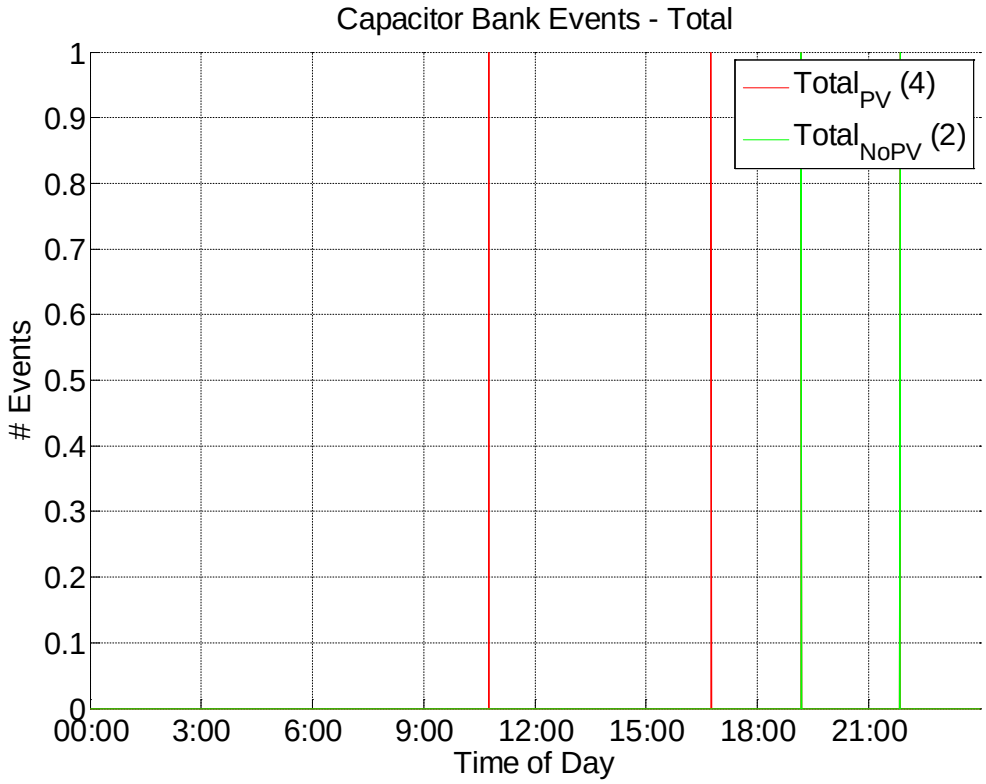

3.1.4.4 Feeder B – Increased PV Penetration Level

The simulation results for the increased PV penetration level at Feeder B are shown in Figures 82 - 87.

During the studied period the potential penetration level managed to shave off roughly 2 MW of the absolute peak and led to a total of 2803 hours of reverse power flow maxing out at 8.1 MW. The feeder voltage levels have remained within a range of 0.98 pu and 1.046 pu, which is a slight increase from the 0.97 pu and 1.025 pu range that has been observed during the simulations with no PV included, and roughly 2 % increase from the Current PV level case. The number of shunt capacitor events increased to 347.

Figure 82: Substation Power with Increased PV Penetration

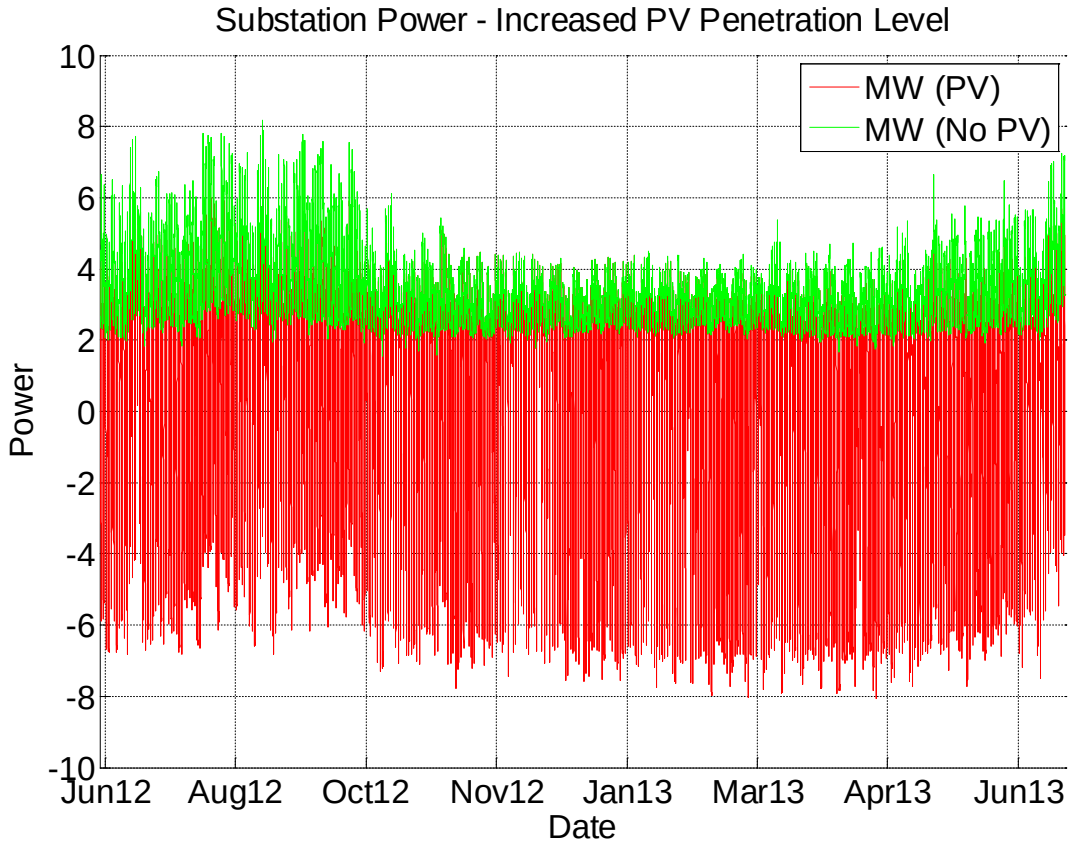

Figure 83: Maximum and Minimum Bus Voltages with Increased PV Penetration

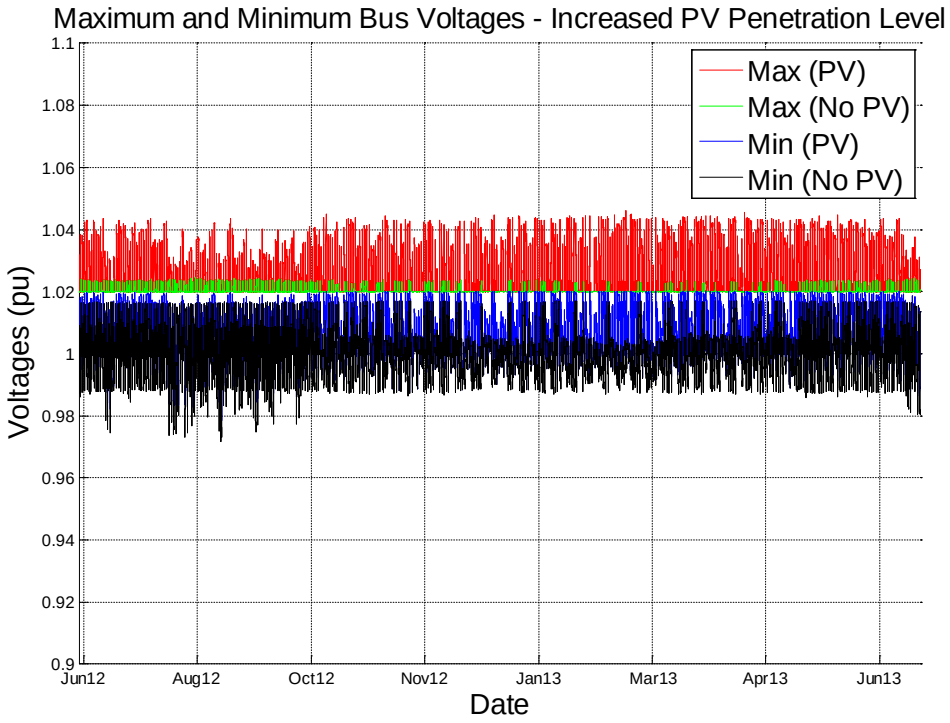

Figure 84: Capacitor Bank Events with Increased PV Penetration Level

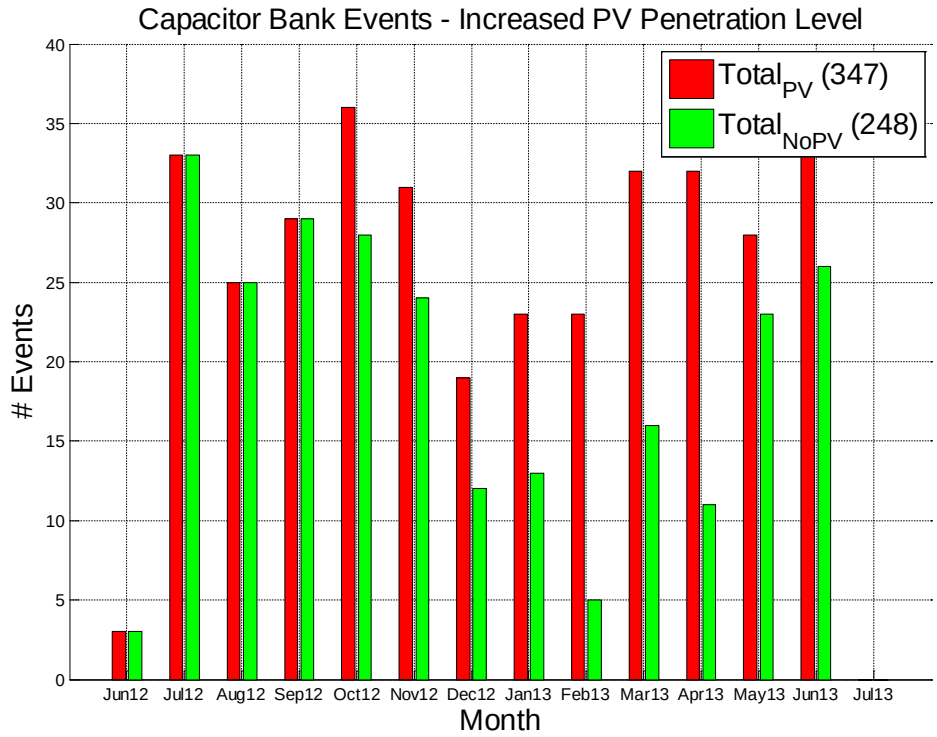

Figure 85: Substation Power, with Current Daily PV Penetration

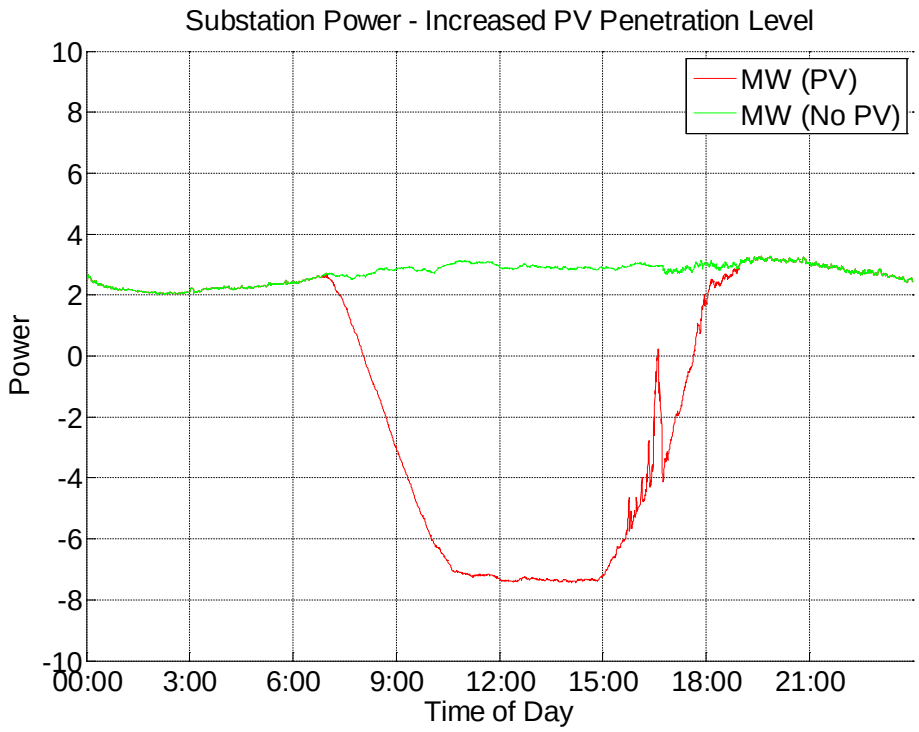

Figure 86: Maximum and Minimum Bus Voltages with Daily Increased PV Penetration

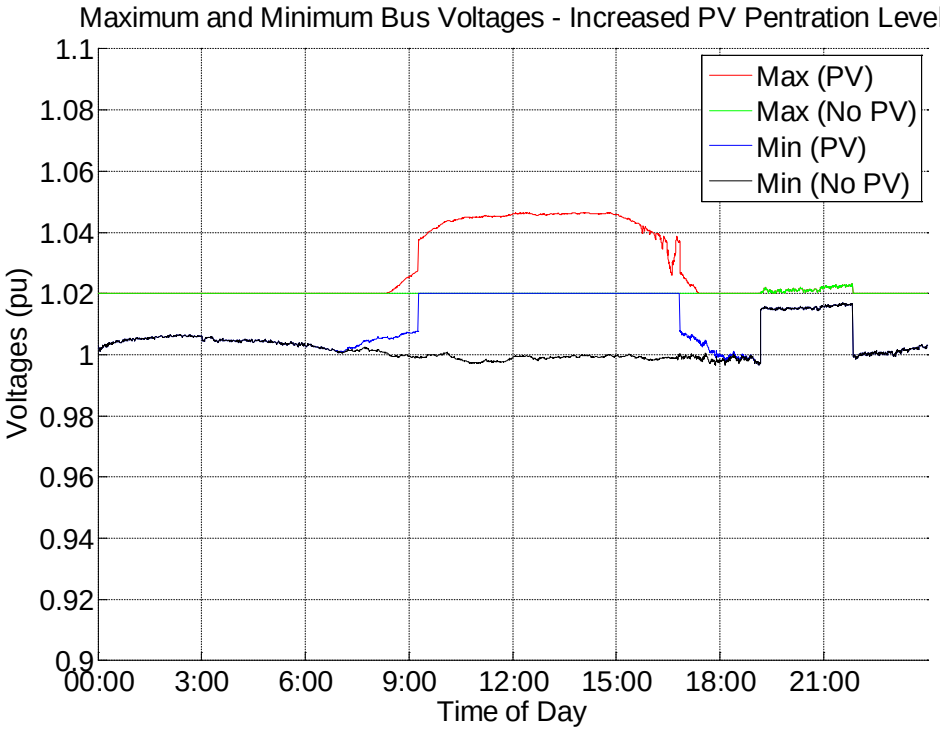

Figure 87: Capacitor Bank Events, with Current Daily PV Penetration Level

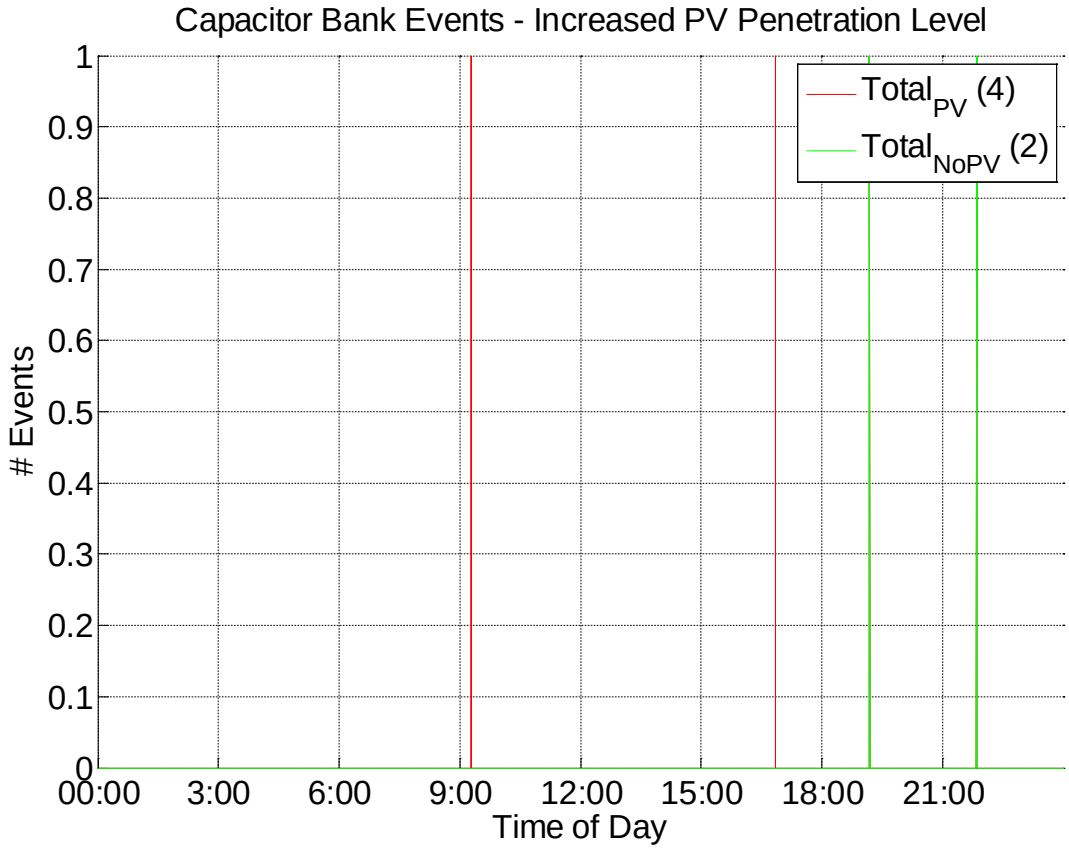

3.1.5 Discussion and Conclusion

Time-series simulations (covering a 13 months study period) of the two provided feeder models to assess possible impacts that the current and potential future PV penetration levels could have on these feeders. The currently installed PV systems on Feeders A and B are 7 MW and 3.5 MW, respectively. It was assumed the potential future PV systems to be 10.5 MW, which is slightly above the ratings of the modeled feeders (10 MW). Additionally, it was assumed that the future systems would be equipped with sun tracking systems allowing the panels to follow the sun throughout the daylight hours.

The simulation results had shown that increasing the PV penetration levels could potentially lead to boosts in feeder voltage levels, rises in capacitor switching events (depending on used capacitor control), and increases in reverse power flow. All these impacts bear potential issues related to reliability and operation cost increases. However, according to the simulation results the impacts do not violate any currently employed utility standards, nor do they seem to be substantial enough to require mitigation measures (even after the PV ratings were increased to match the feeder ratings).

Tables 11 - 14 summarizes several key-parameters obtained from the simulation results.

Table 11: Hours of Reversed Power Flow

	Feeder A	Feeder B
Current PV	1111	124
Increased PV	2647	2803

Table 12: Maximum and Minimum Substation Loads

	Feeder A		Feeder B	
	Max (MW)	Min (MW)	Max (MW)	Min (MW)
No PV	9.2	1.67	8.18	1.55
Current PV	8.66	-4.41	7.1	-1.2
Increased PV	8.6	-8.18	6.11	-8.1

Table 13: Maximum and Minimum per Unit Feeder Voltages

	Feeder A		Feeder B	
	Max (pu)	Min (pu)	Max (pu)	Min (pu)
No PV	1.019	0.97	1.025	0.972
Current PV	1.029	0.97	1.027	0.975
Increased PV	1.043	0.97	1.046	0.979

Table 14: Shunt Capacitor Events

	Feeder A	Feeder B
No PV	1	248
Current PV	2	265
Increased PV	2	347

3.2 Assessment of Islanding Behavior

3.2.1 Problem Description

Islanding refers to the condition where the Distributed Generation (DG) is isolated on a portion of the power system and operates as an "island" separate from the power system. Islanding is often referred to as “loss-of-mains”. Islanding can be either unintentional or intentional. Unintentional islanding has the following implications on electric power system operation:

1) Typically, the utility cannot control voltage and frequency at the customer in an islanded system.
2) Islanding may create a shock hazard to utility workers and customers as the lines in the islanded system are still energized whereas it is assumed otherwise.
3) Typically, the utility cannot control the DG and consequently it cannot always de-energize downed lines, which can compromise public safety.
4) Rotating machines in the islanded part could be damaged when the island is reclosed out-of-phase to the Electric Power System; out-of-phase reclosure can cause heating and stresses on rotor shafts, enough to cause damage.
5) Islanding may interfere with manual or automatic restoration of normal service for the neighboring customers; if the island’s frequency drifts away from that of the rest of the system, it must be brought back into synchronism before all connections can be restored.
6) The islanded system may not be adequately grounded. Unintentional islanding changes the topology of the system, which means the islanded portion may no longer have a correctly engineered ground.
7) Protection systems on the islands are likely to be uncoordinated since the short circuit current availability and direction of flow changes when the system is islanded.

The increasing penetration of DG results in increasing difficulties in meeting anti-islanding requirements, which the DG has to meet before connecting to the utility. The time interval in which islands must be detected and the DG disconnected are often mandated by standards, such as the IEEE Standard 1547 for interconnecting distributed resources with electric power systems. The standards give maximum time frames in which the DG (1) must detect an island and trip and (2) describe test procedures that are designed to ensure that the DG meets these requirements, but these test procedures often do not account for high-penetration scenarios in which the combined power generated by all DGs in the system is sufficient to support the load in an islanded system. In this scenario, many islanding detection methods fail in detecting the islanded state because the voltage and frequency at any given DG in the islanded system is identical to the voltage and frequency at the DG before islanding occurs.

Applicable codes and standards, such as IEEE 1547, UL 1741, and IEC 62116, demand that DG does not energize any portion of the host utility system during islanding. According to IEEE 1547, the DG “shall cease to energize the area EPS within two seconds after the formation of an unintentional island.” This requirement is difficult to achieve if there is generation-load balance in the microgrid, because the changes in voltage and frequency during loss-of-main may be too

small to reliably detect the islanded state. No information about intentional islanding is given in IEEE 1547-2003. The topic is under consideration for a future revision of the standard. The guide IEEE 1547.4-2011 addresses the topic of operation of DR island systems and includes information about the ability of a DR to separate from and reconnect to the grid while providing power to a local island.

3.2.2 Objectives

- Estimate the risk of islanding, as the probability that PV generation lies in the range from 100% to 110% of the actual load on an isolated feeder segment. This at-risk range is a rule of thumb from previous dynamic simulation studies.
- Recommend switching procedures or other design changes to mitigate any problems found.

3.2.3 Approach

The approach used to assess the unintentional islanding risk is based on the guidelines published by Sandia National Laboratory [9]. In a system with IEEE 1547 compliant PV inverters with anti-islanding control based on positive feedback method, the unintentional islanding risk can be ruled out if a number of conditions are met. Passing this initial screening will rule out unintentional islanding thereby making further investigations unnecessary. If the system fails the initial screening, then the islanding risk should be studied in detail by observing the behavior and control settings of the particular system and generators. The screening criteria are four inequalities, were labeled (1) Active Power Inequality, (2) Reactive Power Inequality, (3) Generator Type Inequality, and (4) Inverter Uniformity Inequality and the four criteria are described as:

Active Power Inequality

$$\sum_{i=1}^{n} P_{DGi} \leq \frac{2}{3} \times \sum_{j=1}^{m} P_{Lminj} \quad (1)$$

In Inequality (1), n and m are the total number of DG and loads in the possible island; P_{DGi} is the active power generation from ith DG unit and P_{Lminj} is the minimum active power load of the jth customer in the island. If the total active power generation from the DGs available in the possible island is less than 2/3 of the total minimum active power load as shown in (1), there would be a large active power unbalance that will cause the voltage at the point of common coupling (PCC) of DG to decrease below the 0.88 pu threshold as specified by IEEE 1547. In such a case, inverters complying with IEEE 1547 will trip within two seconds or less and a sustained island formation can be ruled out. Hence, there is no need to check for the remaining conditions. If the DG in the island is only Photovoltaic (PV) generation, the load that is considered in (1) is the minimum load during daylight hours.

Reactive Power Inequality

$$Q_{index} = \frac{\sum_{k=1}^{p} Q_{capk}}{\left(\sum_{i=1}^{n} Q_{DGi} + \sum_{j=1}^{m} Q_{Lj}\right)} < 0.99 \; OR \; Q_{index} = \frac{\sum_{k=1}^{p} Q_{capk}}{\left(\sum_{i=1}^{n} Q_{DGi} + \sum_{j=1}^{m} Q_{Lj}\right)} > 1.01 \; OR \; pf < 0.99 \quad (2)$$

In Inequality (2), p is the total number of capacitor banks in the system and Q_{capk} is the reactive power injection from the kth capacitor bank. The test of sufficiency of reactive power in the possible unintentional island is expressed in (2). If the reactive power generation in the island is not sufficient, the frequency of the island would quickly rise beyond 60.5 Hz, which is the threshold value set by IEEE 1547. This would trigger the protection system of the inverter with positive feedback anti-islanding control and hence, the formation of sustained island is not possible. As shown in (2), if the sum of total VAr generation from DG units and the total reactive load of the possible island are not within 1% of the total aggregate capacitor rating of the island or if the power factor is less than 0.99, there is almost zero possibility that the island would be sustained.

Generator Type Inequality

$$\sum_{i=1}^{x} P_{roti} \leq 25\% \times \sum_{j=1}^{y} P_{DGinvj} \quad (3)$$

In (3), x and y are the total number of rotational generators and inverter based distributed generators respectively in the possible island; P_{roti} is the active power generation from ith rotational generator and P_{DGinvj} is the active power generation from jth inverter based DG. If the percentage of generation from rotating machines is less than the percentage of the total generation from inverter based DGs in the possible island, the control of IEEE 1547 compliant inverters would still be effective in quickly detecting the voltage and frequency increase followed by fast protective actions. Hence, the formation of a sustained unintentional island would be unlikely. This is expressed in (3) in which the condition of ruling out the possibility of island formation is the case when the generation from rotational machines is less than 25% of the total generation from the inverter based DGs.

Inverter Uniformity Inequality

$$\sum_{i=1}^{z} P_{DGiM1} \geq \frac{2}{3} \times \sum P_{island} \quad (4)$$

In (4), z is the total number of inverter based DG from the same manufacturer $M1$ and P_{island} is the total active power generation in the possible unintentional island. If more than 2/3 of the total generation of the possible island is from DGs that employ inverters from the same manufacturer the electrical behavior and controls would be coordinated. With similar Loss of Mains Detection (LOMD) techniques of the inverters, the islanding detection method would be more effective.

If either the first condition or all of the remaining three conditions are satisfied, there is a minimal possibility of sustained islands. However, failing to meet these criteria would require further studies and detailed investigations on the actual system. Figure 88 summarizes the screening methodology for assessing the risk of unintentional islanding. Note that unintentional islanding can be ruled out if only either Inequality (1) or Inequalities (2) through (4) are satisfied. For the case when active power produced by all DGs on the system is less than 2/3 of the total minimum active load consumption, it is certain that the island cannot be sustained because of the large active power mismatch. However, if Inequality (1) is false, that is, there is sufficient

active power source in the potential island, then, it's necessary to check for the remaining three inequalities in succession. If all of these are satisfied, then, again, islanding would be impossible to be sustained.

Figure 88: Flowchart for Unintentional Islanding Screen

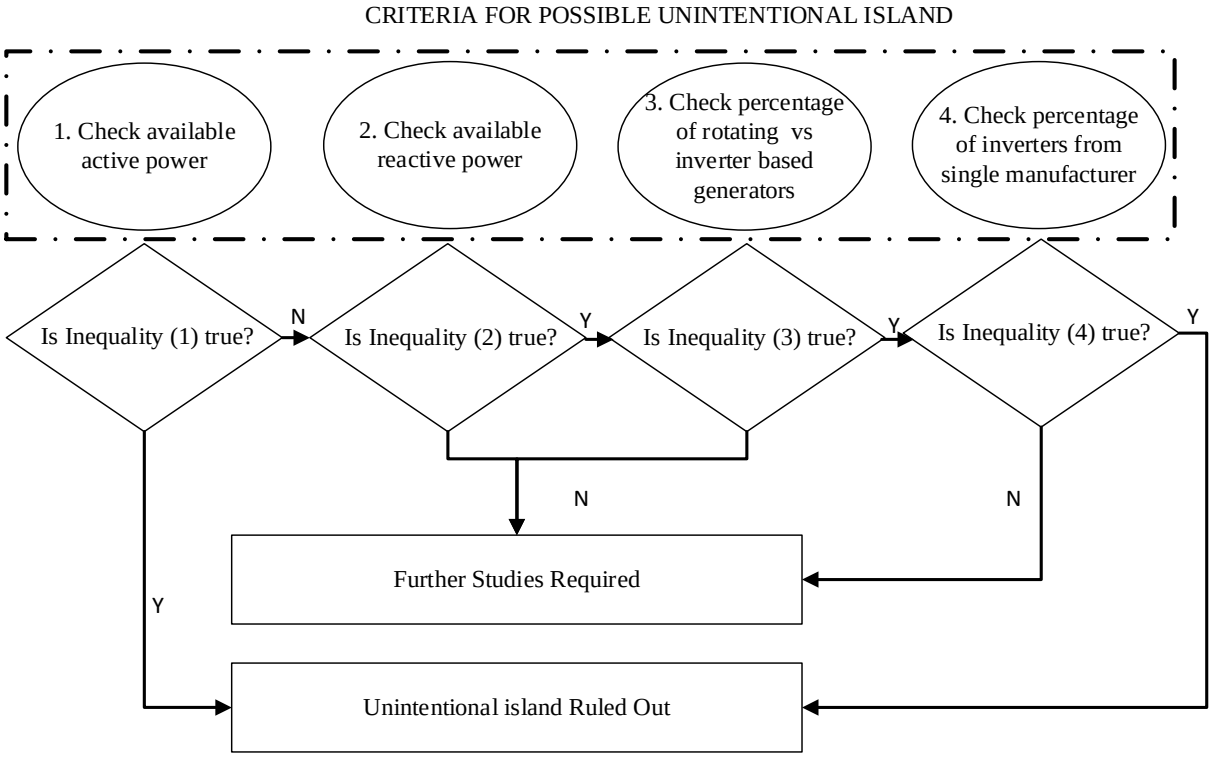

3.2.4 Assessment of Islanding Risk

The methodology described in Section 3.2.3 was employed to assess the possibility of unintentional islanding for the Feeders A and B.

3.2.4.1 Feeder A (Base Case):

Active Power Inequality

The maximum and minimum total load on the Feeder A is 9100.37 kW and 1674.85 kW, respectively. The total available capacity of PV installations on the feeder is 7500 kW. Two-third of the total minimum load is 2/3×1674.85kW= 1116.57 kW. The total available active power from PV while operating at unity power factor is 7500 kW. For this system, the condition expressed in (1) is false during minimum load and maximum generation conditions. It means that the system has sufficient active power availability for sustaining an unintentional island. Therefore, evaluating the remaining three screening criteria is warranted.

Reactive Power Inequality

To assess the reactive power sufficiency in the possible unintentional island in Feeder A, two different scenarios are considered:

1) Scenario 1: PV inverters operating at unity power factor (IEEE 1547 compliant)
2) Scenario 2: PV inverters operating at variable power factor with the capability of injecting/absorbing reactive power as required (IEEE 1547 non-compliant)

In both of the scenarios, the available capacitor banks (fixed 600 kVAr and switchable 600 kVAr units) are considered to be available as needed. Hence, the maximum available reactive power source of the system is 1200 kVAr. The maximum and minimum reactive power loads observed from the yearly load profile of the feeder are 3985.67 kVAr and 733.53 kVAr respectively.

Figure 89a shows the reactive power availability from the capacitor banks in comparison with the total load range for scenario 1. It is clear that capacitor banks are able to supply the reactive power load of the system until the point the maximum limit of 1200 kVAr is reached. The index given in Inequality (2) is named as Q_{index}. As shown in (2), Q_{index} is the ratio of reactive power injection from capacitor banks and the difference between reactive power injection from the available DGs and the reactive power load. For sustained islands, the Q_{index} should lie in the range of 0.99 and 1.01 which ensures the reactive power sufficiency of the island. Q_{index} for the entire range of reactive power load in the Feeder A is shown in Figure 89b.

Figure 89: Assessment of Reactive Power Sufficiency in Feeder A with PV Operating at pf = 1.0.

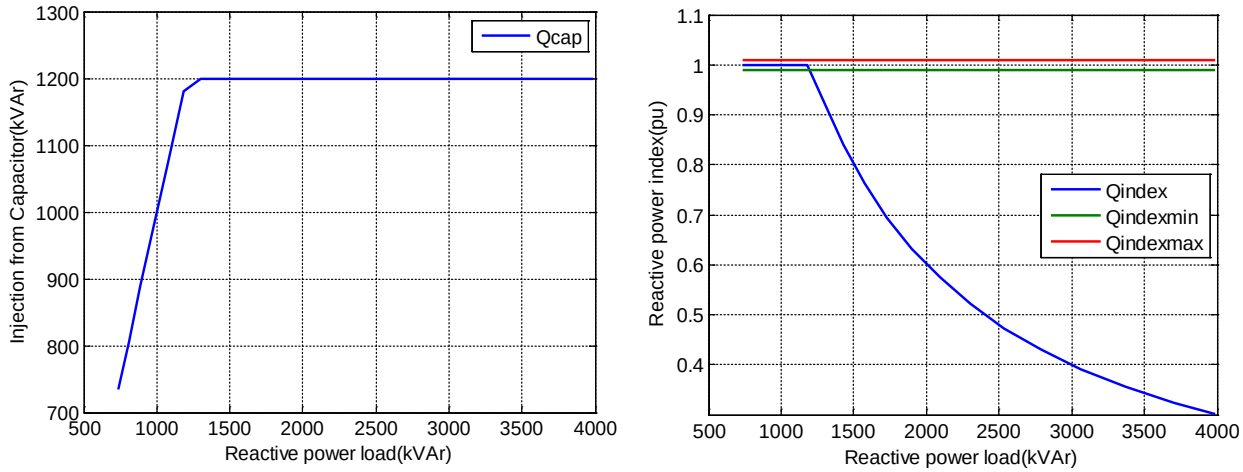

a) Available Reactive power

b) Assessment index

With PV Operating at pf = 1.0.

Next, the assessment is carried out by considering the case in which PV inverters also participate in maintaining the reactive power balance of the possible unintentional island. In this scenario, the capacitor bank injection could be varied from 600 kVAr to a maximum of 1200 kVAr.

The assessment of the reactive power sufficiency is carried out throughout the entire reactive power load range so that reactive power balance of Feeder A is maintained. The reactive injection from PV is calculated such that $Q_{index} = 1$ in Inequality (2). This is done to investigate the contribution from PV generators to maintain the reactive power balance.

Figure 90a shows the variation of reactive power injection from capacitor banks and PV generators with the variation of reactive power load. It can be observed that reactive power injection from PV generators is required as soon as the capacitor banks reach their maximum of 1200 kVAr in order to satisfy the criterion, $Q_{index} = 1$. The capacitor banks are able to supply sufficient reactive power for only around 30% of the entire load range. In other words, reactive power injections from PV inverters are absolutely necessary for the potential island to be sustained in Feeder A. In the ideal case, PV can be assumed to operate at wide range of power factor, that is : 0-1. It means that PV generators can vary active and reactive power in the range of 0-7500 kW and 7500-0 kVAR respectively.

Figure 90b shows the power factor of the PV generator. PV generator has a variable power factor as it is participating in reactive power balance of the feeder as well.

Figure 90: Assessment of Reactive Power Sufficiency in Feeder A

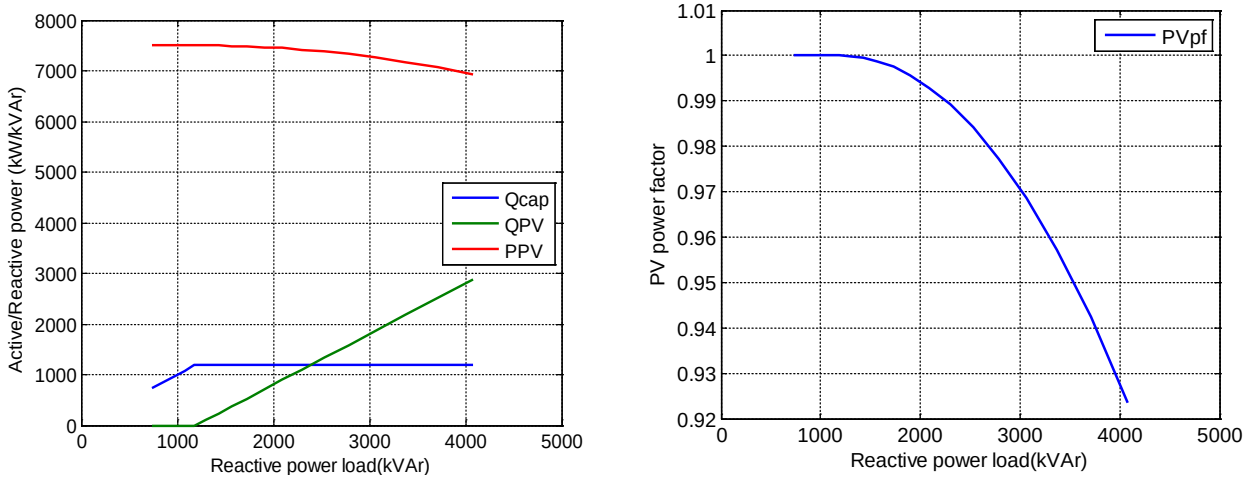

a) Active/Reactive power

b) Power factor

With PV operating at variable pf.

In conclusion, the assessment of the Inequality (2) shows that it is not possible for Feeder A to sustain as an island for the entire load range if PV inverters are entirely IEEE 1547 complaint which is the present situation. However, if PV inverters are allowed to operate at variable power factor so that they actively participate in reactive power balance of the island, then only islanding could be a possibility.

Generator Type Inequality

The generation in the Feeder A is only from the PV systems. There are no other rotating generators available in the system requiring consideration for the assessment of this condition. Inequality (3) is always satisfied for this feeder.

Inverter Uniformity Inequality

All of the PV inverters in this feeder are from a single manufacturer. Hence, Inequality (4) is always satisfied for Feeder A.

The assessment of above conditions for Feeder A indicates that it is not likely to island Feeder A in its present state. With the amendments in IEEE 1547 standard, if PV inverters in the distribution system are allowed to provide necessary reactive power support, then, islanding could be a possibility in the future. Further research and investigation on the behavior of feeder islands are left for the detailed study in future.

3.2.4.2 Feeder A (Load Switching Case):

In this section, the assessment of Feeder A for the possibility of formation of unintentional island is carried out for the condition when either one, any two, or all of the three largest loads are switched out of the feeder. The three largest loads of Feeder A are: P_{Load1A} = 1167.75 kW; P_{Load2A} =778.49 kW; and P_{Load3A} = 778.49 kW.

Active Power Inequality

The assessment of Active Power Inequality from the Base Case scenario shows that there is sufficient penetration of PV in Feeder A, therefore, islanding could be a possibility (that is, Inequality (1) is always false in Feeder A in the present condition).There is no necessity to consider the load switching scenario for the assessment of this inequality as load switching would decrease the total minimum load and the Inequality (1) would still be false. It means that there is sufficient active power generation from PV generators in Feeder A to sustain as a possible island. Further investigation on other Inequality (2) must to be carried out.

Reactive Power Inequality

Similar to the base case analysis, the reactive power inequality assessment is carried out for two scenarios:

1) Scenario 1: PV inverters operating at unity power factor (IEEE 1547 compliant)
2) Scenario 2: PV inverters operating at variable power factor with the capability of injecting/absorbing reactive power as required (IEEE 1547 non-compliant)

The load power factor is assumed to be 0.916 for this feeder. Depending on the requirement, either one, two, or all three largest loads are shed from the system. The corresponding largest reactive power loads considered for switching are Q_{Load1A} = 511.48 kVAr; Q_{Load2A}= 340.95 kVAr and Q_{Load3A} = 340.95 kVAr.

Figure 91a shows the variation of injection from capacitor banks and the switched load with the variation of changed total reactive power load of the system for Scenario 1. Even after all the three biggest loads are taken out of the feeder, the system is still not capable of maintaining reactive power balance with the available maximum reactive injection of 1200 kVAr from the capacitor banks. Figure 91b shows the Q_{index} for the entire range of reactive power load. It can be seen that Q_{index} can remain within the limit of 0.99 to 1.01 for a slightly greater range of load than that in the base case. However, the load switching does not significantly improve reactive power balance on the feeder. Thus, for Feeder A, if PV generators are not allowed to participate

in reactive power balance, there should be a large percentage of load curtailment to sustain as an island which might not be desirable.

Figure 91: Assessment of Reactive Power Sufficiency in Feeder A

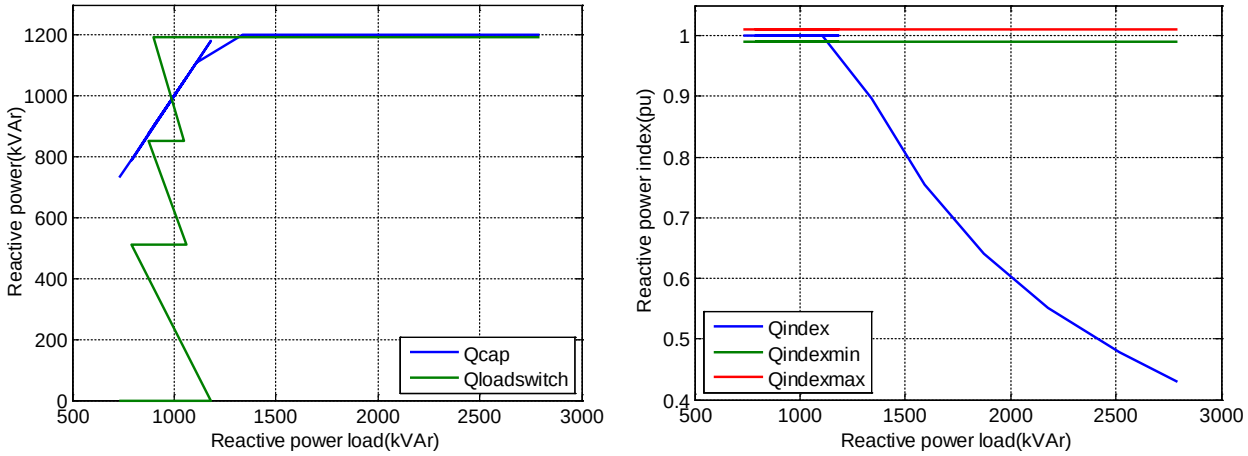

a) Available Reactive power

b) Assessment index

With PV operating at pf = 1.0 (Load Switching Case).

Next, the assessment for the case of PV operating at variable power factor is analyzed. In this case, reactive power injection from PV is calculated by setting $Q_{index} = 1$ at all times for the reason described in the above analysis of the base case. Figure 92a shows reactive power injection from the capacitor banks and active and reactive power injection from the PV generators after load curtailment. It is clear that PV generators start injecting reactive power once the capacitor banks are injecting at their maximum capacity of 1200 kVAr. Here, reactive power injection from PV generators is required for the wider range of reactive power load. Figure 92b shows the variation of power factor of PV generators throughout the range of reactive power load.

Figure 92: Assessment of Reactive Power Sufficiency in Feeder A

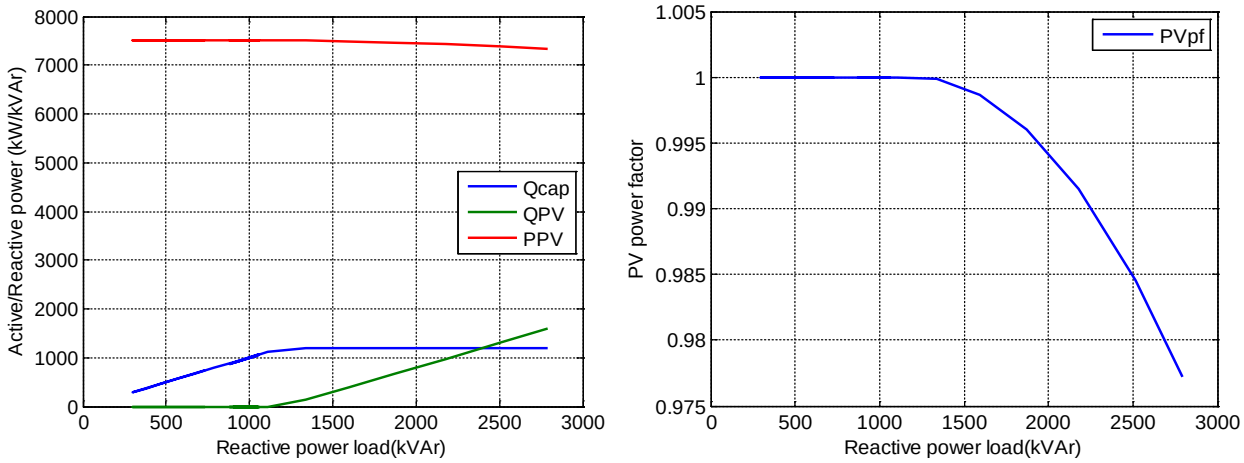

a) Active/Reactive power b) Power factor

With PV operating at variable pf (Load Switching Case).

In conclusion, because of the wider range of reactive power load in Feeder A and relatively small percentage of capacitor banks in the system, formation of an unintentional island is unlikely given the present condition even if the largest loads are disconnected. Even with the load disconnection, Inequality (2) is true for wider load range in this feeder.

Generator Type and Inverter Uniformity Inequalities

The assessment of the Inequality (3) and (4) is not applicable for the load switching case as these inequalities are completely independent of the total load change of the system. Hence, these assessments remain the same as in the base case.

Overall, it can be concluded that Feeder A cannot be sustained as an island unless PV generators are allowed to inject reactive power to the system.

3.2.4.3 Feeder B (Base Case):

Active Power Inequality

The maximum and minimum total active power load on the Feeder B is 8046.399 kW and 1543.532 kW, respectively. Two-third of the total minimum load is 2/3×1543.532 kW = 1029.02 kW. The total available active power from PV, while operating at unity power factor, is 3500 kW. Hence, for this system also, the condition expressed in (1) is false during minimum load and maximum generation conditions. It means that the system has sufficient active power availability for sustaining an unintentional island. Therefore, the evaluation of the remaining three screening criteria is necessary in this case as well.

Reactive Power Inequality

The reactive power sufficiency in the possible unintentional island in Feeder B is also assessed based on the following two scenarios:

1) Scenario 1: PV inverters operating at unity power factor (IEEE 1547 compliant)

2) Scenario 2: PV inverters operating at variable power factor with the capability of injecting/absorbing reactive power as required (IEEE 1547 non-compliant)

In Feeder B, 600 kVAr is a fixed and 1800 kVAr is a switchable capacitor banks. Hence, in both the Scenarios, the reactive injection from the capacitor banks can be varied in the range 600 – 2400 kVAr. The maximum and minimum reactive power load observed from the yearly load profile of the feeder are 4250 kVAr and 730 kVAr respectively. Figure 93a shows the reactive power availability with respect to load for Scenario 1. The only source of reactive power is the capacitor banks since PV inverters are not participating in reactive power support. Similar to the previous section, the Q_{index} is calculated for the Feeder B as well. The Q_{index} for the entire range of reactive power load in the Feeder B is shown Figure 93b. It can be observed that the index is within the range of 0.99 and 1.01 for around 50% of the total range of system reactive power load. Therefore, when PV inverters are generating active power only, the possibility of formation of unintentional island in the Feeder B is around 50% to achieve reactive power sufficiency. This is somewhat greater than the possibility of Feeder A.

Figure 93: Available Reactive Power and Assessment Index Feeder B

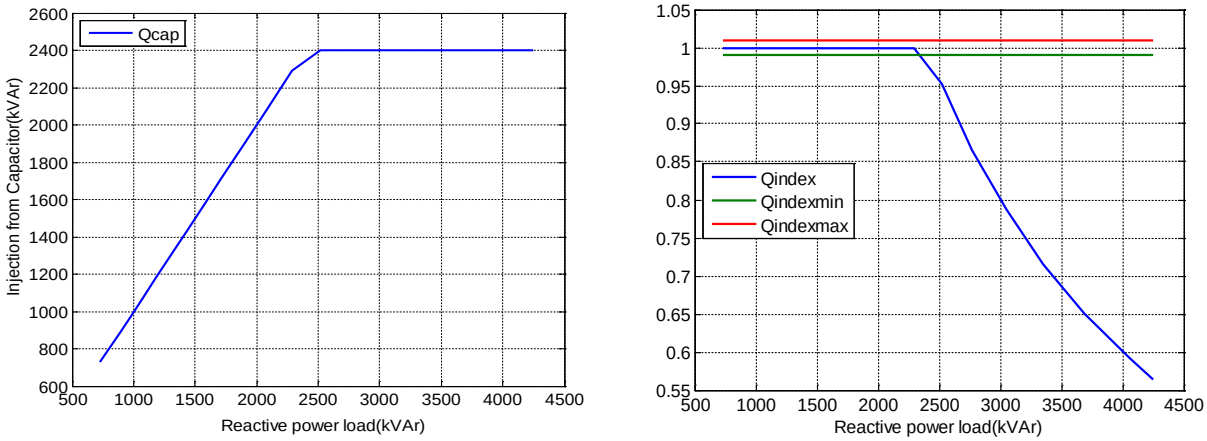

a) Available Reactive power

b) Assessment index

With PV operating at pf = 1.0

Next, the assessment of reactive power inequality is carried out for the case when PV generators also take part in reactive power generation.

Similar to Feeder A, the assessment of the reactive power sufficiency is carried out throughout the entire reactive power load range so that reactive power balance of the Feeder B is maintained. The reactive injection from PV is also calculated in similar manner such that $Q_{index} = 1$ in Inequality (2). It ensures that reactive power sufficiency in the possible island is maintained once PV generators are considered to inject reactive power to the feeder and it is easy to visualize the contribution from PV generators as well. Figure 94 shows the variation of reactive power injection from capacitor banks and PV generators with the variation of reactive power load. It can be observed that reactive power injection from PV generators is required after the capacitor banks reach their maximum of 2400 kVAr to satisfy the criterion, $Q_{index} = 1$. The

capacitor banks are able to supply sufficient reactive power for around 50% of the entire load range. In other words, reactive power injections from PV inverters are necessary for the potential island to be sustained in the Feeder B when it is operating at heavily loaded conditions. In this case also, PV generators are assumed to operate in a wide range of power factor so that the range of active and reactive power injections could be 0-3500 kW and 3500-0 kVAR respectively. For initial 50% of the load range, PV is operating at unity power factor as capacitor banks are capable of supplying the total reactive power load. Once the reactive injection from capacitor banks reaches the maximum rated value, PV starts injecting the necessary amount of reactive power to maintain the power balance of the possible island.

Figure 94: Assessment of Reactive Power Sufficiency in Feeder B

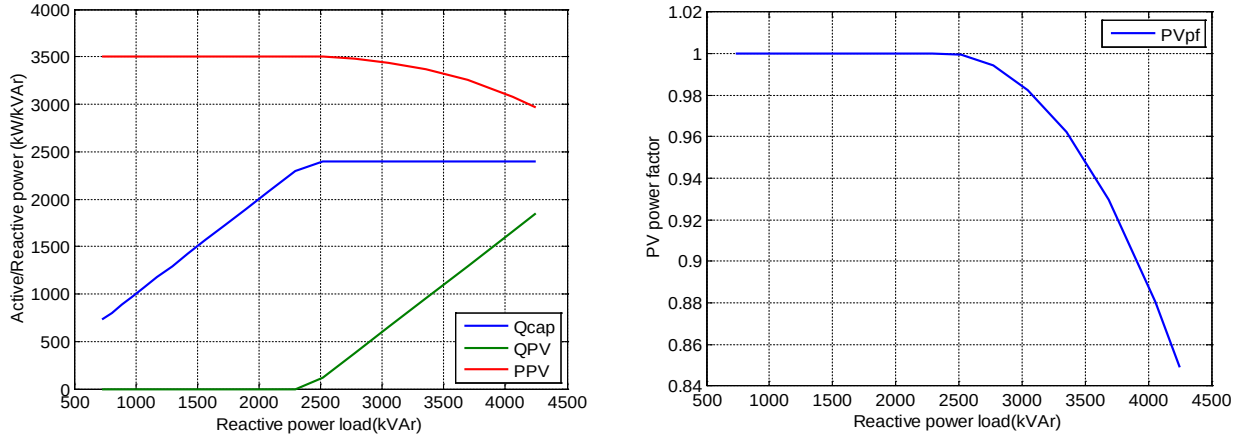

a) Active/Reactive power b) Power factor

With PV operating at variable pf.

Therefore, with the above analysis, it can be concluded that Feeder B is capable of operating as a sustained island with PV generators operating at unity power factor only for around 50% of the current load range of Feeder B. For the rest 50%, the Inequality (2) is always satisfied and hence, there is a least chance of forming sustained island.

Generator Type Inequality

The generation in the Feeder B is only from the PV systems. There are no other rotating generators available in the system that needs to be considered for the assessment of this condition. Hence, Inequality (3) is always satisfied for this feeder as well.

Inverter Uniformity Inequality

All of the PV inverters in this feeder are from a single manufacturer. Hence, Inequality (4) is always satisfied for Feeder B as well.

3.2.4.4 Feeder B (Load Switching Case):

In this section, the assessment of Feeder B for the possibility of formation of unintentional island is carried out when there is a switching out of three biggest loads of the feeder. The three biggest loads of Feeder B are: P_{Load1B} = 852 kW; P_{Load2B} = 342 kW; and P_{Load3B} = 342 kW.

Active Power Inequality

Similar to Feeder A, the assessment of Active Power Inequality from the Base Case scenario shows that there is sufficient penetration of PV in Feeder B so that the inequality (1) is always false in Feeder B in the present condition. Hence, it is not necessary to assess this inequality again after switching out of the loads as it would even decrease the total minimum load and the inequality (1) would still be false. It means that there is sufficient active power generation from PV generators in Feeder B to sustain as a possible island. Hence, further investigation on Inequality (2) is carried out next.

Reactive Power Inequality

As mentioned in the analysis of Feeder A, the reactive power inequality is assessed for Feeder B by switching out either one, two or all three of the corresponding reactive power loads considering a load power factor of 0.895. The corresponding reactive power loads that are considered to be curtailed are: Q_{Load1B} = 424.63 kVAr; Q_{Load2B}= 170.45 kVAr; and Q_{Load3B}= 170.45 kVAr.

Figure 95 shows the reactive power injection from the capacitor banks and the amount of switched reactive power load throughout the reactive power load range of Feeder B for Scenario 1. The amount of load switch is chosen based on the loading condition. The injection from the capacitor banks increases until it reaches the maximum possible rating of 2400 kVAr. The Q_{index} for the entire load range after the load switching is also considered. It can be observed that the index lies within the desirable range of 0.99-1.01 for around 70% of the load range which is an appreciable improvement over the base case values. Hence, inequality (2) would be false for around 70% of the load range even when PV generators do not participate in reactive power generation.

Figure 95: Assessment of Reactive Power Sufficiency in Feeder B

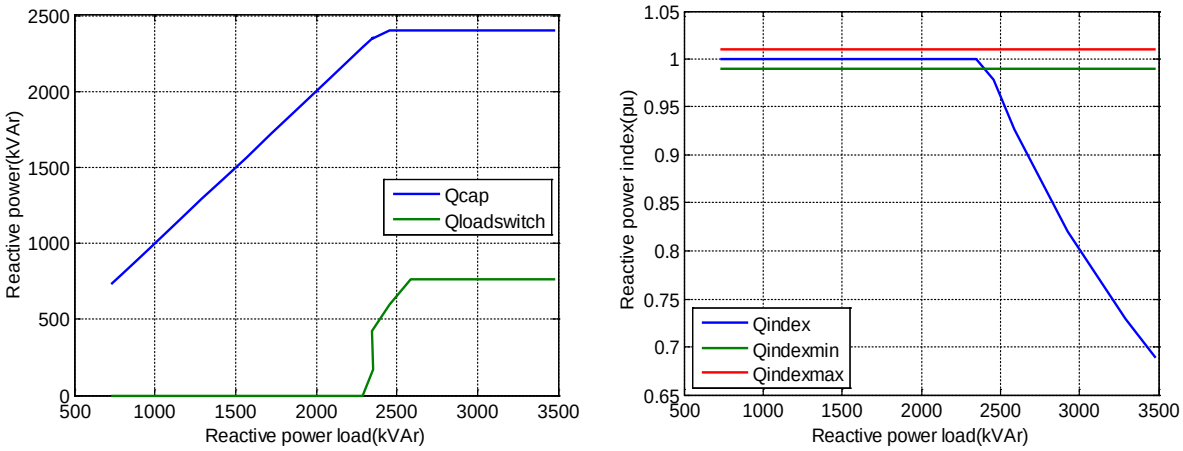

a) Available Reactive power

b) Assessment index

With PV operating at pf = 1.0 (Load Switching Case).

Next, the assessment of Feeder B for the case when PV generators actively participate in reactive power generation is carried out.

Figure 96 shows active and reactive power generation from PV generators and reactive power injection from the capacitor banks of Feeder B. It is clear that PV generators start injecting reactive power to the system once the reactive power injection from capacitor banks is at the maximum value of 2400 kVAr. Also, PV generators are capable of operating at maximum active power injection mode when there is no reactive power injection to the system. The reactive power injection required for Feeder B after load switching is appreciably less than the base case.

Figure 96: Assessment of Reactive Power Sufficiency in Feeder B

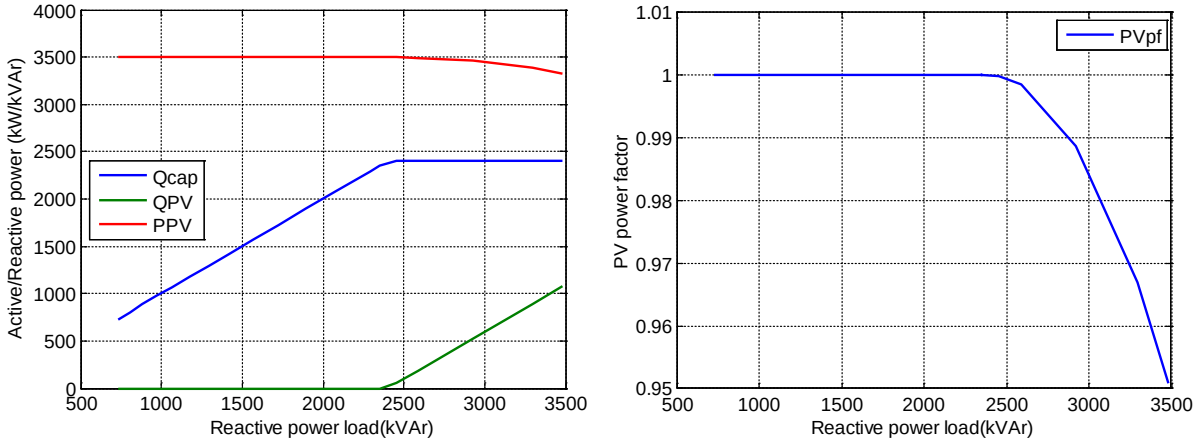

a) Active/Reactive power b) Power factor

With PV Operating at Variable pf (Load Switching Case).

In conclusion, Feeder B could be capable of sustaining as a possible island if there is a proper load curtailment scheme in the present condition since Inequality (2) is false for wider load range in this feeder even when PV generators are operating at unity power factor as a result of load switching.

Generator Type and Inverter Uniformity Inequalities

The assessment of the Inequality(3) and (4) should not be repeated for the load switching case as these inequalities are completely independent of the total load change of the system. Hence, these assessments remain the same as in the base case.

Overall, it can be concluded that Feeder B could be able to sustain as an island for around 70% of the load range while considering the assessment of inequalities (1) and (2) when load switching is considered.

3.2.5 Islanding Mitigation

This section reviews the methods that can be employed for the detection of islands. Once the island is detected, PV inverters can be tripped to prevent any of the islanding issues discussed in Section 3.2.1.

3.2.5.1 Classification of Islanding Detection Methods

Islanding detection methods can be classified mainly into two categories: Local and Remote, as shown in Figure 97. Local methods are further divided into two subcategories as passive and active methods. Local techniques rely on the data that are available at the DG location. Passive methods depend on measuring certain system parameters and they do not interfere with DG operation. Several passive techniques proposed are based on monitoring voltage magnitude, rate of change of frequency, phase angle displacement, and impedance. If the threshold for the monitored quantity is set to too low then nuisance tripping becomes an issue; and if it is set to

too high, islanding will not be detected at all. In active islanding detection methods, DG operation is controlled by using positive feedback of either voltage and/or current.

Figure 97: Types of Islanding Detection Methods

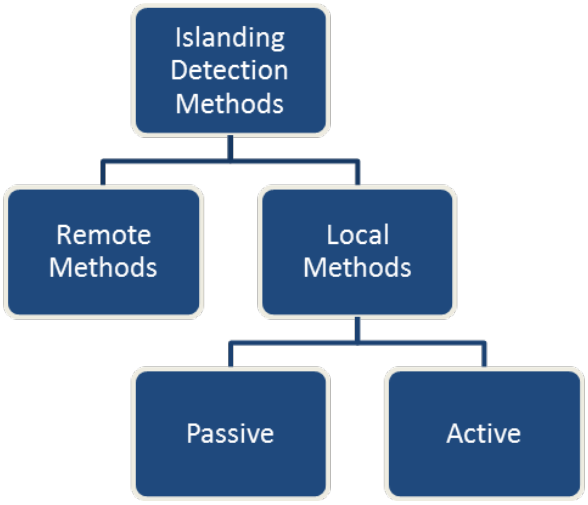

3.2.5.2 Passive Islanding Detection Methods

Passive methods are based on information on the system state that is available at the DG location. The majority of the islanding detection methods proposed early on fall into this category. The following list summarizes commonly used passive methods and provides references from which more detailed information can be obtained:

- **Under-/overvoltage and Under-/overfrequency:**
  These methods detect islanding condition based on changes in voltage and frequency detected by under/over voltage protective relays (UVP/OVP) and under/over frequency protective relays (UFP/OFP). This is one of the earliest islanding detection types. The main disadvantage of this method is the relatively large Non-Detection Zone (NDZ) and the slow detection time. [10] [11] [12]
- **Voltage phase jump detection:**
  This method is based on information about the phase difference between the voltage at the Point of Common Coupling (PCC) and the inverter output current. Under islanding conditions, the inverter output current is unchanged, but the voltage at the PCC is changing. The phase difference exceeding a pre-defined threshold is indicative of an islanded condition. The implementation of this method is relatively easy because Phase-Locked-Loop (PLL) to synchronize the voltage at the PCC and inverter output current is usually available. However, selecting a proper threshold for the phase jump is difficult as a too-low threshold results in nuisance tripping and a too-high threshold results in non-detection of the island. [10] [13]
- **Voltage unbalance and total harmonic distortion:**
  This method is based on information about the voltage unbalance and Total Harmonic

Distortion (THD) of the current. Under islanding conditions, the "stiff" utility source goes away and the loads on the system have to be supplied solely by the DG. Effectively, during islanding the loads are supplied by a weaker source, which increases unbalance and THD. The unbalance and THD exceeding pre-defined thresholds are indicative of an islanded condition. However, similar to the phase jump detection method, selecting proper thresholds is difficult. Also, in scenarios in which most of the loads are supplied by PV before the islanded conditions occur, this method is likely to fail as there would not be a detectable change of unbalance and THD. [14]

3.2.5.3 Active Islanding Detection Methods

In active methods, a disturbance signal is applied to certain parameters at the Point of Common Coupling (PCC) to facilitate the detection of an islanding condition. Active methods involve some kind of feedback technique or control mechanism that detects changes in the frequency or voltage at the PCC. In general, the reliability of islanding detection achieved with active methods is better compared to passive methods and worse compared to remote methods. However, active methods are generally less costly than remote methods and, consequently, they are commonly used for islanding detection. Tables 15 and 16 compare the numerous active methods that are available with regards to (1) the parameters that is observed to determine the islanded state, (2) ease of implementation and detection speed, (3) general reliability of islanding detection, (4) effect on power quality, (5) reliability of islanding detection for systems with multiple inverters, and (6) the potential for standardization. Additional, the tables provide references for each of the islanding detection methods. The references contain detailed descriptions of the methods and results from efforts that evaluated the reliability of them.

Table 15: Summary of Active Islanding Detection Methods, Part 1

Islanding Detection Method & Reference	Parameter Tested to Detect Islanding	Implementation & Speed	Reliability	Maintaining Power Quality	Suitability for Multiple Inverter Operation	Potential for Standard-ization
General Electric Frequency Shift (GEFS) .	Reactive current through frequency estimation algorithm	Medium & fast	High Very small NDZ	Very High, negligible influence on THD	High, but not unlimited. More research required.	High
Automatic Phase Shift (APS) [15]	Frequency of terminal voltage	Medium & fast	High introduces harmonics but THD can be controlled	Medium, PQ is affected as a result distorted inverter output signals	High	High
Sandia Frequency Shift (SFS) [16] [17] [18]	Frequency drift with positive feedback	Difficult & relatively fast	High NDZ exists for high Q-factor but less compared to others	Medium, PQ is affected as a result of continuous drifting	Medium; can be used for parallel operation but PQ is affected.	Medium
Sandia Voltage Shift (SVS) [18] [19]	Voltage Amplitude	Medium & Fast	High, relatively small NDZ exists	Medium, as PQ is affected as a result of continuous drifting	Medium; can be used for parallel operation but PQ is affected.	Medium
Robust Islanding Detection Algorithm [20]	Frequency by varying reactive power	Medium of single inverter but complicated for multi-inverter case & fast	High NDZ exists for high Q loads but less than AFD and SMS	Medium as PQ is affected as a result distorted inverter output signals	Medium may fail for the case of multiple DFPGs with small power ratings operating independently	Medium

Table 16: Summary of Active Islanding Detection Methods, Part 2

Islanding Detection Method & Reference	Parameter Tested to Detect Islanding	Implementation & Speed	Reliability	Maintaining Power Quality	Suitability for Multiple Inverter Operation	Potential for Standard-ization
Current Injection Method [21] [22]	Disturbance signal through d or q axis controller	Difficult & fast	Moderately High NDZ exists for Q>3.0	High no harmonics are injected	Low, as the frequency changes at the PCC can be caused by other inverters	Low poor suitability for parallel operation
Negative Sequence Current Injection [23] [22]	Negative sequence current through VSC controller	Difficult & fast	High Can be used for loads having high Q factors.	High no harmonics are injected	Cannot be determined, as the literature does not discuss application of this method in case of multiple DG's	Cannot be determined
Slip Mode Frequency Shift (SMS) [10] [17] [24]	Phase of PCC voltage	Medium & slow	Medium NDZ exists for high Q-factor	Medium, as PF is affected and no harmonics are injected	Low, as the method cannot handle concurrent detections	Low
Active Frequency Drift (AFD) [15]	Chopping Factor (c.f) i.e. Drift between current and voltage	Easy & medium	Medium NDZ exists for high Q-factor	Medium introduces low-order harmonics	Low, as the method cannot handle concurrent detections	Low
Detection of Impedance at Specific Frequency [10] [25]	Harmonic Voltage and Current	Easy & relatively slow	High NDZ can be eliminated	Low introduces harmonics	Low	Low

3.2.5.4 Remote Methods

Remote islanding detection methods are communication-based methods. Islanding is detected based on status of utility circuit breakers. The signal is then sent to trip the DG unit. Though these techniques are reliable and accurate they are costly and hence not popular. Some of these methods are as follows.

Transfer Trip Scheme

The basic idea of this scheme is to monitor the status of each circuit breaker and recloser between the DG and the utility grid. If a breaker or recloser opens, this information is conveyed to the DG via a communication system and the DG trips. This scheme requires that each breaker/recloser has a receiver and a transmitter that can communicate reliably via a wired connection (e.g., fiber optic cables) or a wireless connection. If the communication infrastructure is not already in place, the costs for implementing this scheme can be very high and, consequently, this scheme is rarely used in distribution systems. However, a transfer trip scheme essentially has a zero NDZ; provided that the communication works reliably.

Power Line Carrier Communication (PLCC)

In this scheme, the power line is utilized as a signal carrier. [26] [27] [28] [29] A signal generator at the substation continuously injects a signal into the line that is sensed by all DGs on the distribution feeder. The loss of the signal at the DG indicates a loss of continuity of the line caused by, for instance, the opening of a breaker. If loss of continuity is detected at the DG location, the DG trips to prevent an islanded situation. Essentially, this scheme is a hybrid of a transfer trip scheme (the information on the state of each breaker is conveyed to the DG via a power line) and an active local detection technique (islanding is determined based on the presence of the low-power signal at the DG). To prevent false trips, the signal injected at the substation needs to reach all DGs downstream at all times as long there is continuity. High-frequency signals are less suitable for this as the attenuation by the system impedance is higher for higher frequencies and, consequently, low-power signals with high frequencies may not reach far enough into the system. Low-frequency signals are better suited for this application as they experience less attenuation and thereby reach farther into the system. Also, to prevent non detection, the signal has to be distinguishable from other signals that are in the islanded system, such as harmonics produced by non-linear loads. If these criteria can be met, then this technique is essentially failsafe (that is, the NDZ is zero).

Apart from the zero NDZ, the PLCC scheme has an additional advantage over active local techniques in that, unlike most active techniques, the power quality (power factor and frequency stability) of the inverter current is not degraded by the scheme. The PLCC signal injected at the substation potentially introduces voltage distortion of the grid supply, but this degradation can be minimized by using low-power, low-frequency signals. In fact, the scheme can potentially be used in such a way that it improves the power quality of the system by, for instance, delaying the trip time of the DG after continuity is lost, so that the DG may ride through temporary disturbances and support the system voltage during the disturbances.

The PLCC scheme is more economical compared to the transfer trip scheme, because (1) only a single signal generator located at the substation is required to provide a signal to all DGs downstream and (2) existing power lines are utilized as communication lines (although the latter could also be done in a "pure" transfer trip scheme). However, the equipment costs (PLCC transmitter at the substation and sensing equipment at the DG) for this scheme are still fairly high, which makes this scheme an expensive option.

3.2.6 Future Technologies

Smart grid technologies offer new opportunities for achieving reliable islanding detection introduces an information layer about the state of each DG unit in the system and the state of the system. The fundamental issue with the DG technology today is that the DG has only a very limited view of the system, that is, it only measures the voltage and current at the DG terminals. Smart grid technology would include a standardized information layer that yields information about the overall system state and events such as loss-of-mains. Loss-of-mains would be communicated to the DG and trigger the desired action, such as the disconnection of the DG. The main difference to already existing remote methods discussed in Section 3.2.5.4 is that the smart grid technology is expected to be included in future DG units as 'default' and, consequently, expensive dedicated islanding detection equipment would become unnecessary. The following list discusses briefly future technologies that can potentially be employed for islanding detection:

- **Solid State Transformer**
  Solid state transformers (SSTs), also known as Power Electronic Transformers (PETs) are power electronics devices that transform a primary high voltage AC voltage to either a lower AC voltage, a DC voltage, or both on the secondary side. SSTs are microprocessor controlled electronics devices that already contain sensing and control equipment, which offer a wide feature set with several possible applications to islanding detection. [30] [31]
- **Phasor Measurement Units**
  Wide Area Measurement Systems (WAMS) employ Phasor Measurement Units (PMUs) to compare phase information across a power system. Islanding detection methods are possible that compare PMU data from outside and from within the potential island. The FNET project currently researched at the University of Tennessee uses one type of PMU that is low enough in cost to be practical for distribution system deployments. FNET uses PMU units called Frequency Disturbance Recorders (FDRs) that plug into conventional 120-V outlets and measure the output voltage. Onboard signal processors compute phase angle and frequency. This information plus GPS time and location information is transmitted to a central server.
- **Electric Vehicle Service Equipment**
  Electric Vehicle Service Equipment (EVSE) is the equipment to which a Plug-in Electric Vehicle (PEV) is connected to charge. EVSE installed as part of a Direct Load Control (DLC) program could be shut off in the case of a suspected island. If the DLC program includes two-way communication allowing the status of the charging load to be seen,

this information could be used to detect an island when EVSE loads are still operating in an area believed to be in an outage.

- **Smart Meters**
  Smart meters are a key component of a smart grid infrastructure. A wide deployment of smart meters can provide data about the state of the distribution circuit and a communication infrastructure that can be used for islanding detection. However, achieving sufficiently fast data reporting frequency and fast processing of the data is critical in order to disconnect PV during islanding in the time frame required by IEEE 1547. Early efforts to use smart meter data to provide some of the necessary data points for fault detection are underway, and methods for using smart meter data to provide some of the information necessary for islanding detection will likely follow.

3.3 Temporary Overvoltage (TOV) Analysis

The goal of this task is to perform an assessment of temporary overvoltage. Overvoltages will be simulated and their effect on surge arresters during generation backfeed conditions will be analyzed.

3.3.1 Problem Description

A Temporary Overvoltage (TOV) is generated within the power system as a result of abnormal system operating conditions. A scenario that can result in TOVs on distribution feeders is as follows:

1) Single-Line-to-Ground (SLG) fault occurs on distribution system causing opening of substation breaker. Feeder disconnected from the ground source provided by substation.
2) PV generators continue to supply energy into the open feeder system until local controls take action to isolate them from system. Additional trip delay caused by Low/Zero Voltage Ridethrough (LVRT/ZVRT) requirements[14].
3) During time window framed by (1) substation breaker opening due to SLG fault and (2) PV disconnecting, collector system is "islanded" and significant TOVs can develop on unfaulted phases.

During this, usually brief period before the PV trips, the DG does not have adequate grounding, which can result in TOVs on the unfaulted phases that have values up to 1.73 times the rated voltage as illustrated in Figure 98. TOVs higher than 1.73 can develop due to (1) ferroresonance conditions, that is, the interaction between the transformer impedance at the PV site and the

[14] LVRT/ZVRT is currently not mandatory for DG. In fact, IEEE 1547 has a trip requirement as opposed to LVRT/ZVRT, which is a no-trip requirement. However, incorporating LVRT/ZVRT into DG is currently being discussed and a future revision of IEEE 1547 may have such a requirement.

Figure 98: Illustration of Voltage Increase on Unfaulted Phases during Single Line-to-Ground Fault

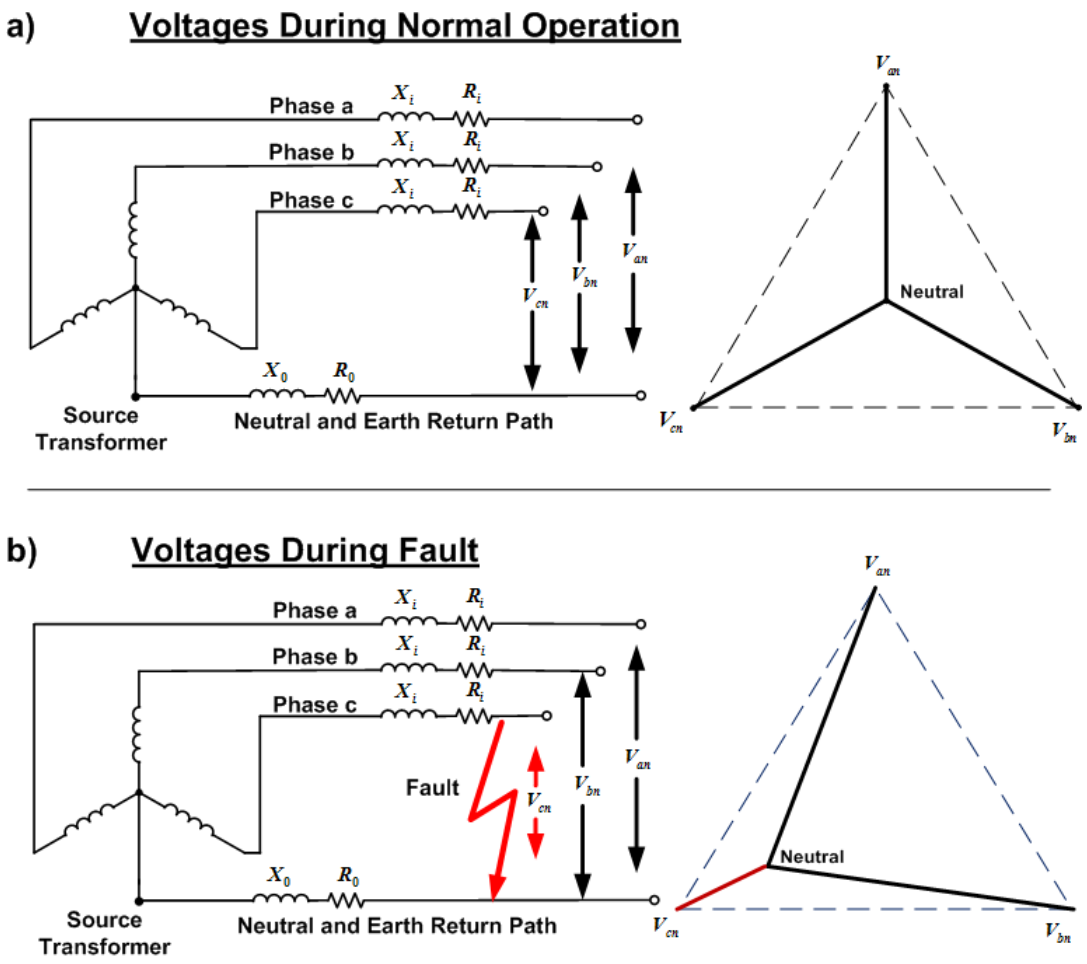

capacitance (cables, capacitor banks) on the feeder system and (2) the control behavior of the PV in response to the fault. These TOVs can last for several milliseconds and can be large enough to damage utility equipment, surge arresters in particular. The problem can be mitigated by ensuring that the feeder has a grounding source in the islanded states, which can be provided through grounding switches or grounding transformers located on the feeder. However, it is important that the grounding source is not too strong, as this will desensitize feeder ground current relay and may result in excessive stress to the grounding equipment during utility faults, load unbalance, and open line conditions. [32] Similarly, SLG faults on collector systems of wind plants can also cause TOVs and many of the concerns and available mitigation measures apply to both the distribution system scenario and the wind plant scenario [33] [34].

Most small three-phase PV generation is connected to the grid through Yg-Yg interface transformer, which acts as an ungrounded source because the PV inverter is 3-wire. Under high penetration this may result in objectionably high levels of TOV during single-phase to ground faults with both the grid and the DG connected in parallel with the fault due to the reasons explained above.

The problem is aggravated if the TOV during the fault results in transformer saturation because a saturated transformer is a source of harmonic currents. The injected harmonics may excite resonance points that are formed by the inductances (primarily the transformer and overhead lines) and capacitances (primarily capacitor banks and cables) in the system, which can result harmonic current and voltage high enough to cause damage to utility and customer equipment.

3.3.2 Objective

The objective of this task is to perform an assessment of Temporary Overvoltage (TOV) concerns for Feeder A. TOVs will be simulated and their effect on utility equipment during generation backfeed conditions will be analyzed. The team recommended grounding or other design features to mitigate any problems found.

3.3.3 Results

Phase A faults were simulated at (1) the feeder head, (2) midsection, and (3) at the feeder end. Two simulation scenarios were considered:

Scenario 1: No PV on the feeder (blue dots in Figure 99)
Scenario 2: PV on the feeder per system description in Section 1.3 (red triangles)

Figure 100 shows the voltages on phase A and phase C with respect to distance from the substation during a single-line-to-ground fault on phase A at various locations for the two scenarios described above. The differences in voltages between the two scenarios at each location are illustrated by red lines connecting the blue-colored no-PV voltage values with the red-colored PV voltage values.

Figure 99: Voltages on Phase A and Phase C

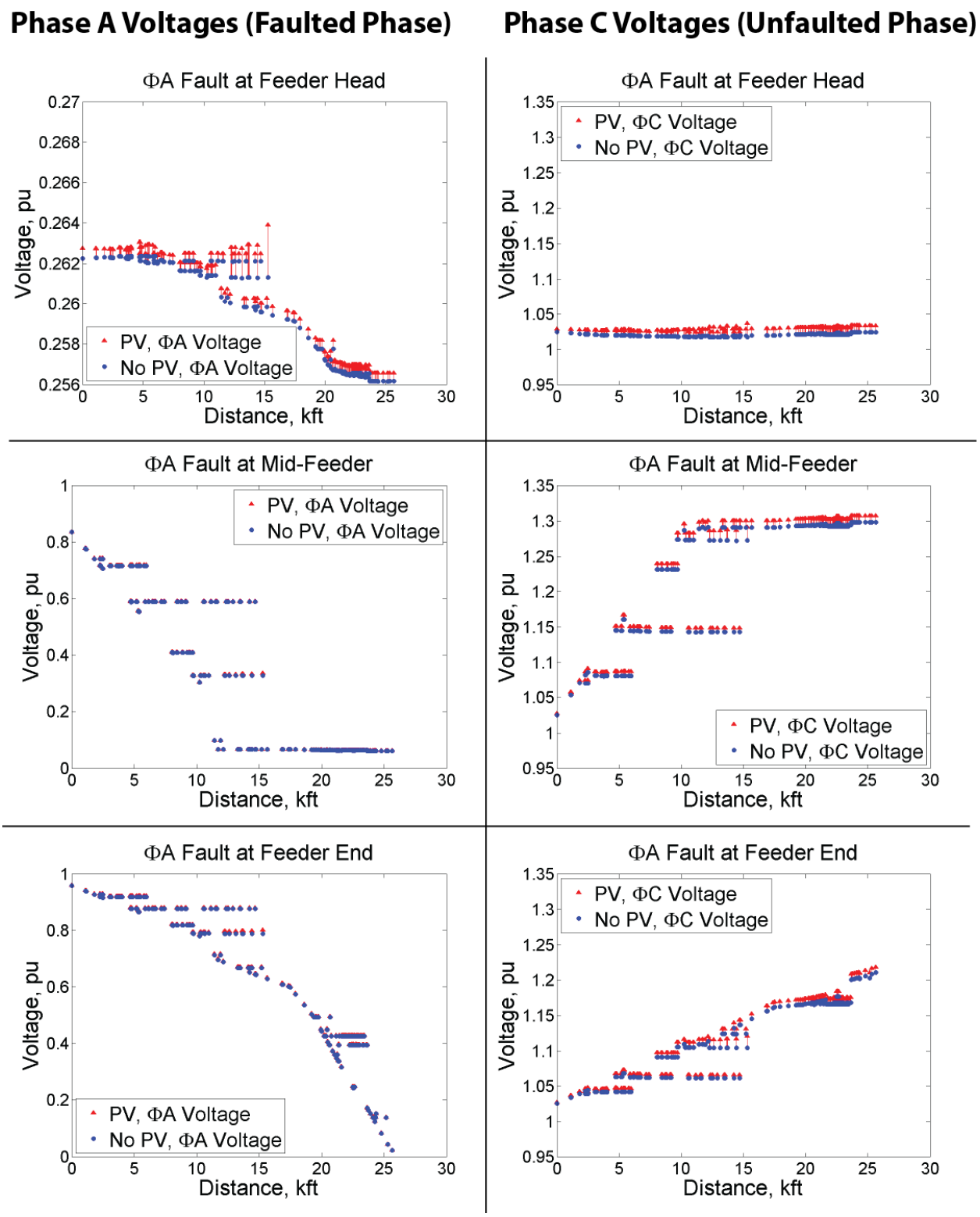

During a single-line-to-ground fault on phase A.

3.3.4 Discussion and Conclusion

The results of the TOV analysis illustrated in Section 3.3.3 show that the simulated single-line-to-ground faults caused TOVs on unfaulted phases of up to 1.3 pu. A single-line-to-ground fault at midsection caused the largest TOVs, which appeared downstream from the fault location on a parallel feeder string. The simulations showed TOVs developed during both Scenario 1 (no PV) and Scenario 2 (PV). TOVs on the unfaulted phase with PV on the system were slightly larger (about 0.02). The duration of the TOV is limited to the time it takes for (1) the feeder breaker to open (disconnecting the utility source) and (2) the PV generators to trip. The former clearing time is governed by the relay protection and is typically 10 cycles or less. IEEE 1547 requires the latter clearing time to be 10 cycles or less for voltages over 1.2 pu and, based on results of inverter testing reviewed, the actual time it takes for the PV inverter to trip once an abnormal voltage condition is detected is much smaller.

In conclusion, the simulations results showed the investigated feeder PV does not significantly aggravate TOV concerns because (1) the model-predicted TOVs on the unfaulted phase with and without PV on the system are similar and (2) PV generators trip during severe overvoltage conditions within 10 cycles or, based on the review of test results with actual inverters, much faster than 10 cycles.

3.4 Overcurrent Analysis and Review Existing Protection Settings

The goal of this task is to perform an analysis on the effect of maximum solar variability on overcurrent protection systems. The effect of overcurrent protection systems for three-phase, line-to-line, line-to-line-to-ground, and single-line-to-ground faults was analyzed. Additionally, the team documented potential problems with protection devices that can be caused due to the presence of PV and review existing relay protection systems to assess if additional generation will actually cause problems on the investigated system.

3.4.1 Problem Description

A distinguishing characteristic of traditional distribution systems compared to transmission systems is that distribution systems are typically radially configured. Another distinguishing characteristic is that the currents in distribution systems can be highly unbalanced due to unbalanced load conditions. Relays in distribution systems typically use the current magnitude to discriminate between fault and load currents –directional sensing is not needed. A characteristic of a radial system is that the short circuit current capacity decreases with distance from the substation. Overcurrent protection devices on distribution systems exploit this pattern and achieve selectivity between different zones by connecting a number of these devices in series with different a time-overcurrent coordination (Figure 100).

Figure 100: Generator Infeed to a Fault

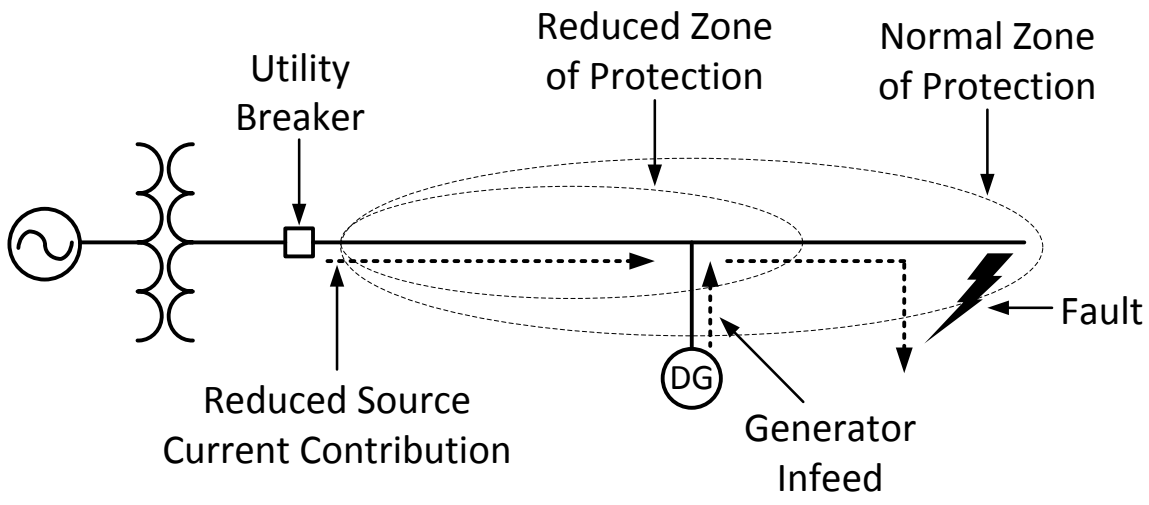

Generator infeed to a fault can limit the distance a utility overcurrent relay can "see" down the feeder.

The overcurrent protection devices protect equipment on the line from being damaged during faults. Some of the commonly used overcurrent protection devices on distribution systems include circuit breakers/reclosers, fuses, and sectionalizers. Typically, a main breaker/recloser is installed at the feeder head. Long feeders have additional breakers/reclosers along the feeder to ensure that faults occurring far away from the substation are sensed and interrupted. Fuses are typically installed on transformers and at the lateral taps in order to avoid that a fault on the lateral causes tripping of the main breaker/recloser, which would cause a service interruption on the whole feeder. Sectionalizers observe the fault response of reclosers and open if the fault persists thereby isolating a faulted section, which is smaller than the section the recloser would isolate if it would stay open permanently. Sectionalizers do not interrupt fault currents, but rather open during the open state of the recloser. Different utilities use varying approaches for the protection coordination of circuit breakers and fuses, such as fuse blowing and fuse saving. For fuse saving coordination, the circuit breaker clears the fault before downstream fuses operate thereby improving reliability by reducing fuse operations. Fuse blowing coordination schemes allow the fuses to blow before the operation of circuit breakers and relays, leading to a sustained interruption [35].

The fundamental problem with the overcurrent protection on distribution feeders in the presence of DG is that protection schemes are typically designed based on the assumption that the system is radial; the energy to supply the loads on the feeder is fed into the feeder at a single location, that is, the substation. The protection scheme will still work for DG penetration levels that do not significantly change fault current levels along the feeder, but for feeders with high DG penetration levels the fault current levels do change and the protection scheme must account for these changes. Specifically, increased DG penetration has the following effects on the feeder protection:

If the DG is located downstream from the overcurrent protection device and the fault occurs downstream, then fault current through the protection device may be reduced resulting in a reduced zone of protection and desensitizing of relays.

If a fuse is located on a lateral and a fault occurs downstream from the protection device, then both the fault current from the grid and the fault current from the DG feed into the fault. This can interfere with fuse-saving protection schemes, because, for this scenario, the fuse may blow before the recloser can protect it (Figure 101).

Figure 101: Recloser Unable to Protect Fuse

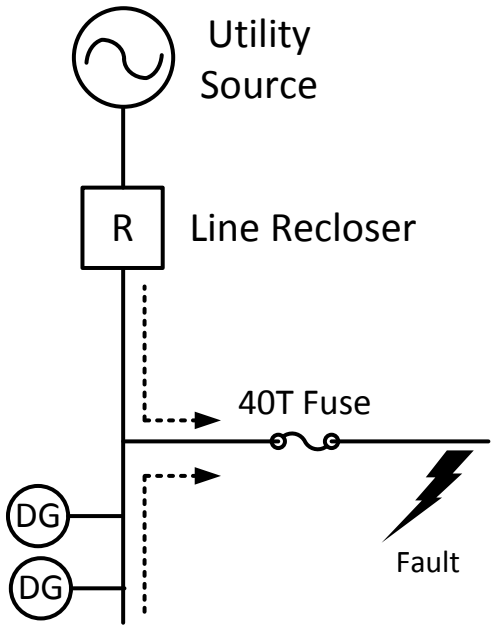

Generator infeed to the fault can blow the fuse before the recloser can protect it

Sympathetic tripping of overcurrent protection devices on unfaulted feeder can occur if two or more radial feeders are fed from a common source and a fault occurs on one of the feeders. If one of the other unfaulted feeders has a significant penetration of PV with a relatively high short-circuit contribution, then the overcurrent relay at the unfaulted feeder would see the fault current from the PV and may trip. However, this can only occur if all of the following conditions are met: (1) the fault current contribution from the PV is sufficiently high so that it can cause the overcurrent relay to trip, (2) the overcurrent relay on the healthy feeder with PV is not able to distinguish between fault current coming from the feeder and fault current coming from the utility source (i.e., it is not set in bi-directional mode), and (3) the overcurrent relay on the healthy feeder is set to trip faster than the overcurrent relay on the feeder with the fault.

Figure 102: Fault on a Parallel Feeder

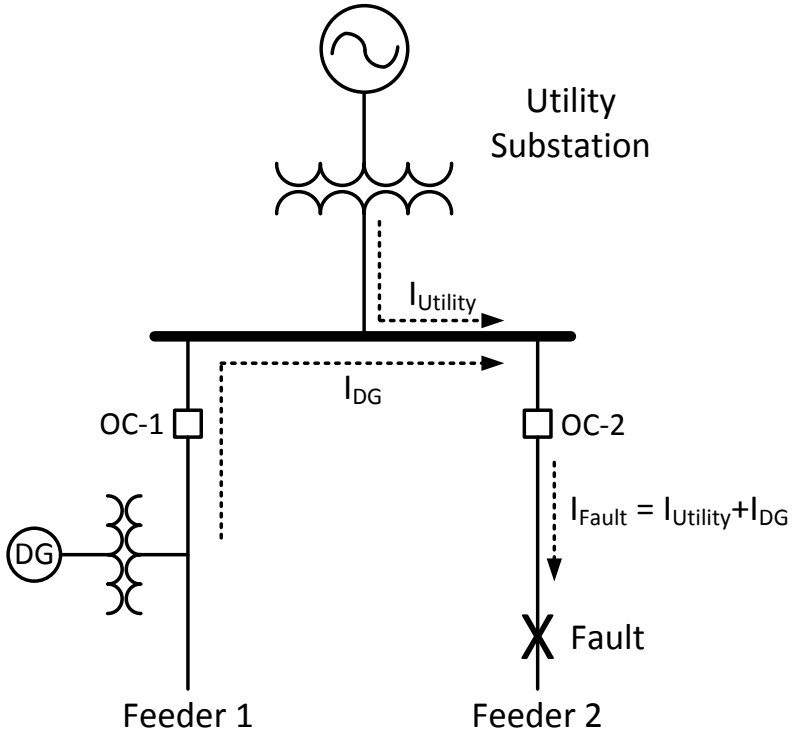

Fault on a parallel feeder can cause sympathetic tripping of protection on PV feeder

The overcurrent protection coordination on the feeder must account for the reduced zone of protection and potential issues related to the fault current increase due to the presence of PV.

3.4.2 Objective

The primary objective of this task is to assess if the presence of PV on the Feeders A will cause protection problems that would require (1) reconfiguration of existing relay protection settings, (2) reduction of reach, or (3) interference with fuse coordination. Specifically, the team will assess if the presence of PV causes (1) reduction of reach, (2) interference with fuse coordination, and (3) sympathetic tripping. A secondary objective is to determine the effect of the short-circuit contribution from PV to three-phase, line-to-line, line-to-line-to-ground, and single-line-to-ground short-circuit levels at all locations on the two feeders. This secondary object is related to the primary objective as changing short-circuit levels due to the presence of PV may require changes of protection settings.

3.4.3 Approach

The research team's approach is to run a short-circuit analysis for the Feeder A for two scenarios. In Scenario 1, the feeder does not have any PV. In Scenario 2, PV penetration levels are modeled as they currently exist on the feeder (see Section 1.3). The approach is to run a short-circuit analysis for Feeder A for two scenarios. In Scenario 1, the feeder does not have any

PV. In Scenario 2, PV penetration levels are modeled as they currently exist on the feeder (see Section 1.3). In addition, a simulation in dynamic mode is run in which simulates the fault behaviors of (1) the substation breaker and (2) the PV inverter. The short-circuit behavior of the PV generators was incorporated in the model to mimic the inverter short-circuit characteristics documented in the SCE test data, that is, during a fault, the PV inverters produce 3 pu of rated current for a duration of about two cycles or less before they trip.

The PV inverters were set to trip during overvoltage and undervoltage conditions in accordance with IEEE 1547. Relay settings provided by SCE were incorporated in the simulations. The overcurrent relay was located at the substation.

3.4.4 Results

Short-Circuit Analysis

One-ohm faults were applied at each bus of Feeder A and the resulting short-circuit current at the bus was recorded. Figure 103 shows the short-circuit currents at each bus during a) a single-phase-to-ground fault, b) a line-to-line fault, and c) a three-phase fault. The figure compares the short-circuit current for Scenario 1 (no PV) with the short-circuit current for Scenario 2 (PV included).

Figure 103: Short-circuit Currents at Each Bus of the Feeder A vs Substation Distance

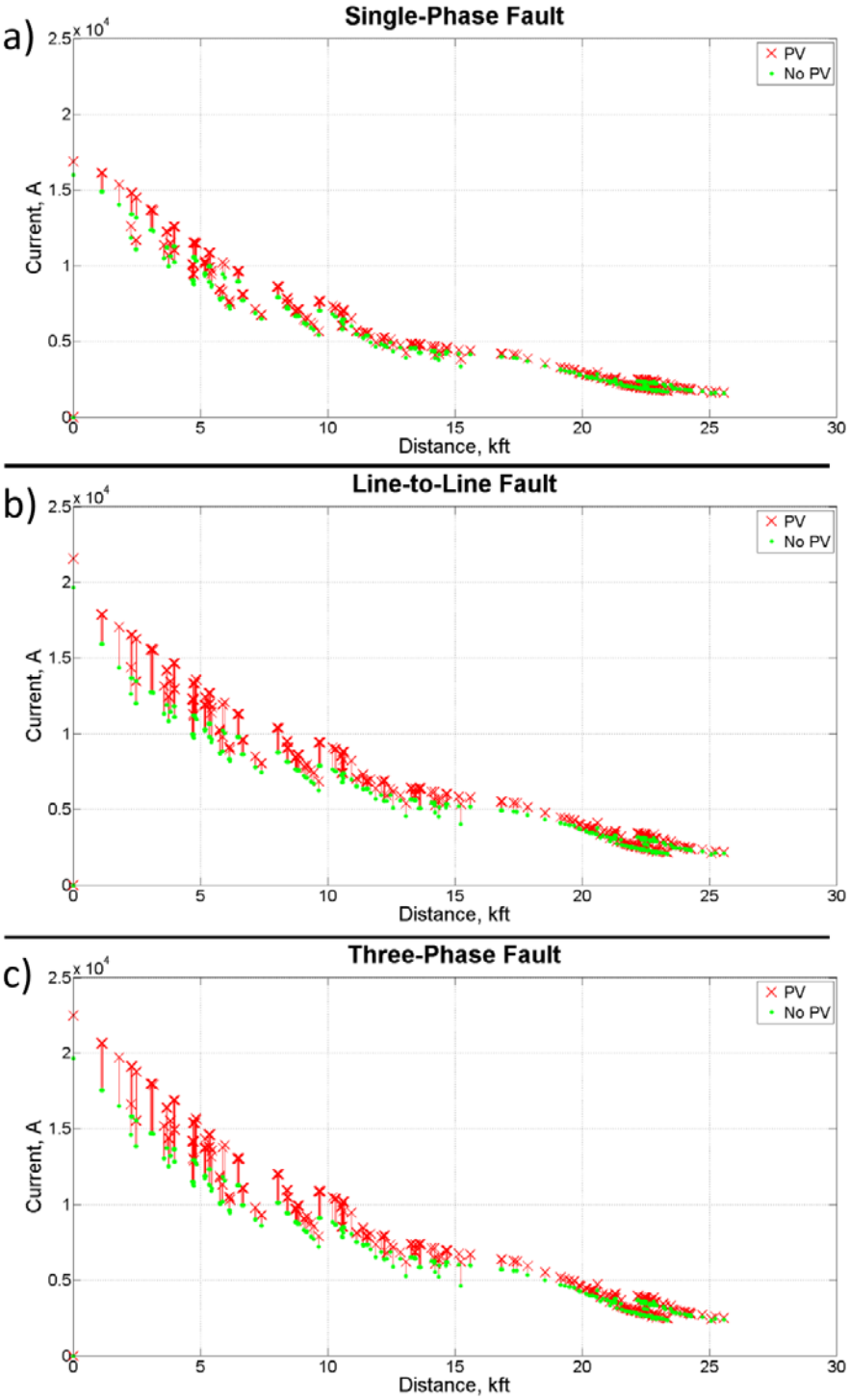

.

Short-circuit currents at each bus of the Feeder A versus distance from the substation. a) Single-phase-to-ground fault, b) line-to-line fault, and c) three-phase fault.

3.4.5 Relay Protection

A bolted three-phase to ground fault was applied at t=1 second at mid-feeder and monitored the voltages and currents at (1) the substation circuit breaker and (2) one of the 13 PV units on the feeder. Figure 104 shows the upstream voltage and current at the substation breaker with PV not present/generating (Scenario 1) and with PV generating at rated power (Scenario 2). Similarly, Figure 105 shows the voltages and currents at one of the 13 PV units for the two scenarios.

For both scenarios, the substation breaker trips on phase overcurrent and locks out within 0.017 seconds as apparent from Figure 104. All PV inverter trip within 10 cycles after the fault was applied, which is illustrated for one of the 13 PV units on the right-hand side of Figure 105.

Figure 104: Voltages and Currents at Substation Circuit Breaker During a Three-phase Bolted Fault

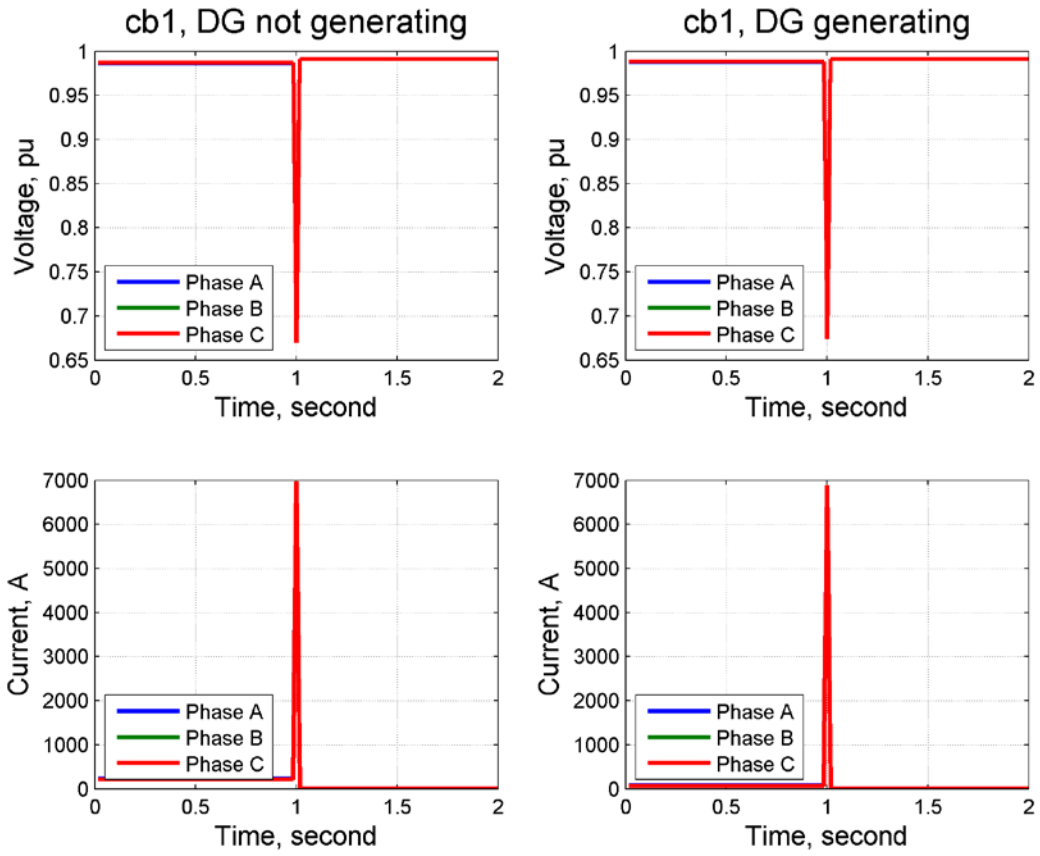

Three-phase bolted fault applied at t=1 second with (1) PV not generating/present (left-hand side) and (2) PV generating (right-hand side).

Figure 105: Voltages and Currents at PV Location During a Three-phase Bolted Fault

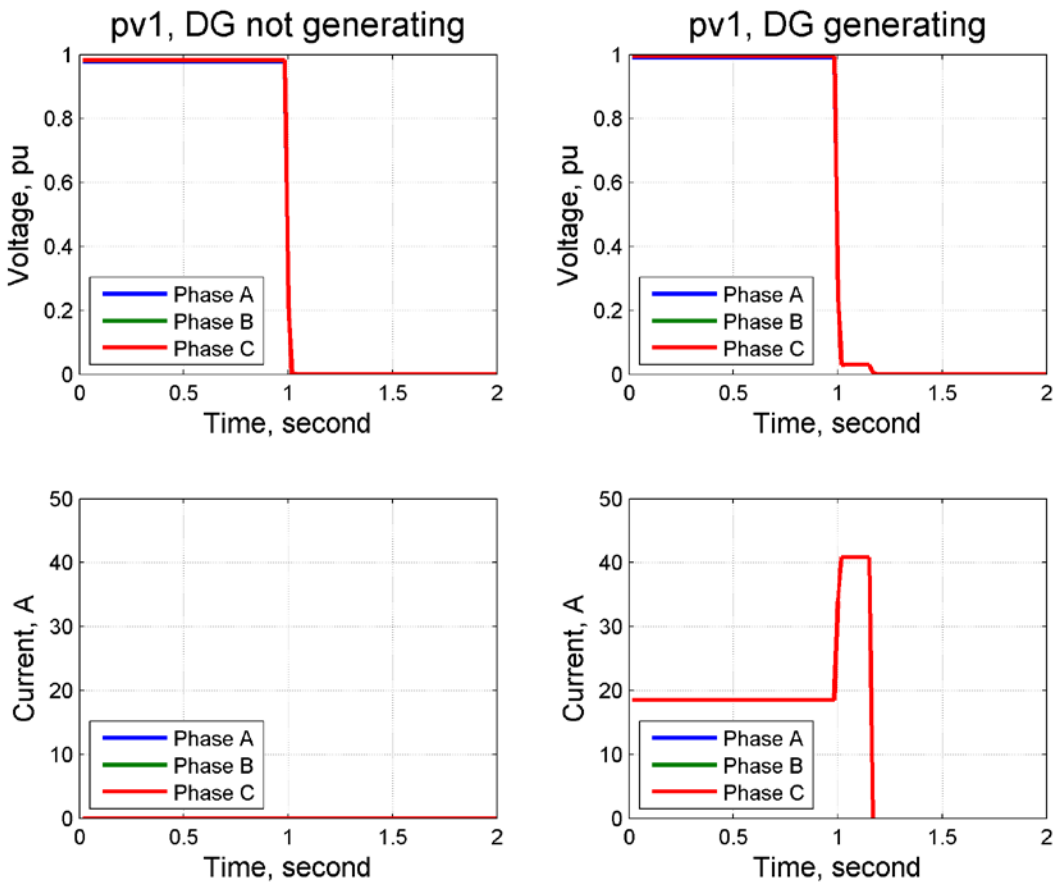

Fault applied at t=1 second with (1) PV not generating/present (left-hand side) and (2) PV generating (right-hand side).

3.4.6 Discussion and Conclusion

PV increases the short-circuit current at the buses significantly. The fault current at the buses near the PV generators is about 20% larger compared to the "no-PV" case. However, based on inverter test data provided by SCE, the PVs trip after about two cycles or faster and, consequently, little impact on relay coordination is expected.

The dynamic simulations illustrate the protection behavior during a three-phase bolted fault at mid-feeder and the consequential tripping of the PV inverters. It was assumed conservatively that the inverters trip within 10 cycles (based on IEEE 1547 requirements), although, as noted, the actual tripping time of the PV inverters is likely much faster. The simulation results show the time it takes for the substation breaker to open is identical for the "no PV generation" scenario and the "PV generating at rated power" scenario. This result is indicative that the presence of PV on Feeder A does not necessitate significant changes of the protection sections. However, simulations for additional fault scenarios are required to support this conclusion.

Chapter 4
Forecasting Results

4.1 Case Studies

USI forecast for two interesting days are examined in greater detail to demonstrate the USI's ability to predict major ramp events. These days are April 4 and 16, 2013. In Figure 106, cloud conditions and respective matching and cap error on April 4 are shown for the power plant SPVP011, where the imager USI1.5 was located. On this day, the morning was overcast with low clouds at 500 meters. Since such low clouds limit the view of the USI, the forecast for any of the solar plants was not available during that time period. At about 16:45, the sky cleared and for the rest of the day, bands of altocumulus clouds pass over the area.

Figure 106: Cloud Conditions on April 4, 2013 with Respective Matching and Cap Error

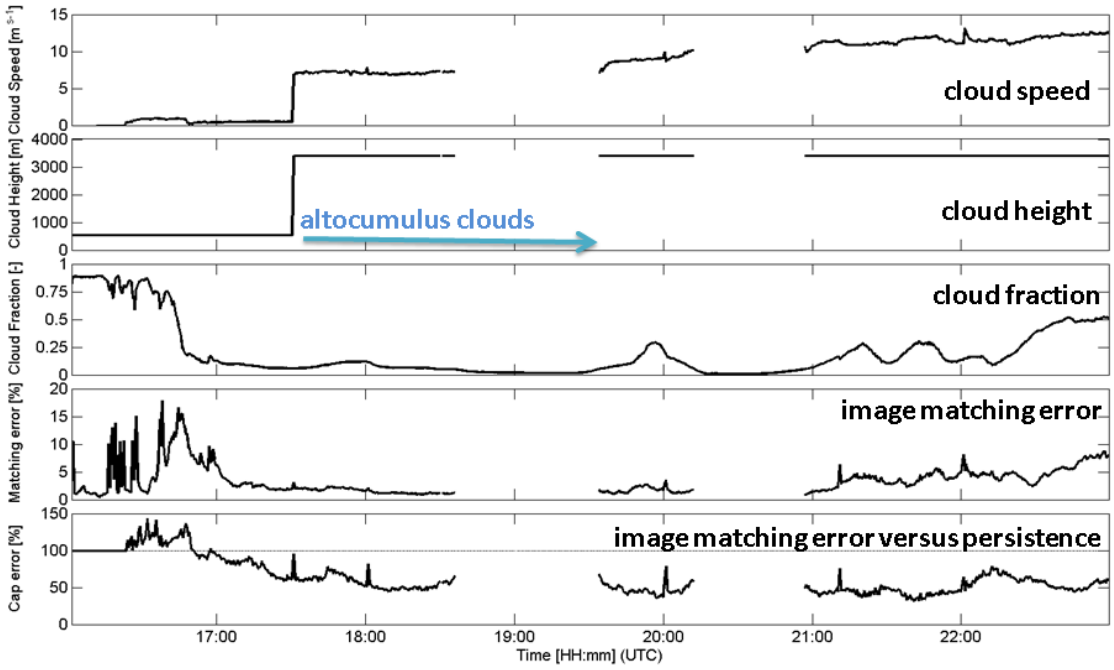

A cap error of less than 100% indicates forecast improvement (skill) over persistence.

Figure 107 shows the five minute power output forecast on April 4. Most of the timing of the variability in the evening was captured, but most notably, the large ramping down events at 19:00 and 20:00 were captured well both in timing and duration. The ramp event at 19:00 is also captured well in magnitude. A smaller isolated ramp event around 19:30 was also correctly predicted. There is no forecast available in the first few hours due to low cloud conditions, which limited the view of the imager and cause the cloud map to be advected out of the scene.

Figure 107: USI Power Forecast for Power Plant SPVP011 on April 4, 2013

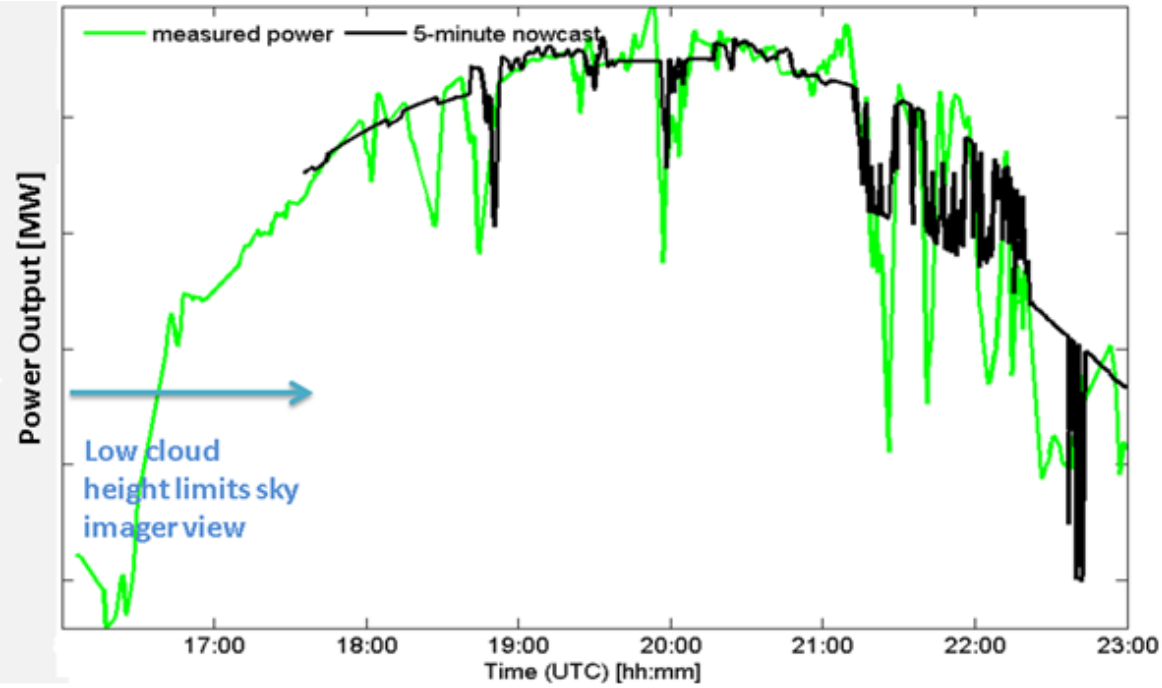

Further investigation reveals that the magnitude and timing of the ramps events are quite different for the four solar power plants under consideration (Figure 108). As the altocumulus cloud band approaches the power plants, a cloud enhancement is observed in the measured power of SPVP011 and SPVP013. Shortly thereafter, when the cloud shadow falls onto these power plants, a large ramp-down is observed. Meanwhile, other solar plants are either not affected by the cloud band, or only experience thinner fringes of the cloud band. The USI forecast could not predict the cloud enhancement but it successfully predicted the timing, duration and magnitude of the event in SPVP011 and the lack thereof at SPVP016 and 022. This demonstrates the ability of the sky imager to resolve small scale spatial variability that would not be resolved by a satellite.

In Figure 109, the power generation forecast for four solar plants is given on the bottom. The green line is measured power, the black line is USI nowcast, which utilizes cloud decision and projection algorithms to create a "0 minute forecast". The red line is USI forecast issued at 19:53, which uses nowcast shadow map and cloud velocity to predict the sky conditions up to 15 minutes in advance. To protect the confidentiality of the data, the y axis labels were removed. The ranges are 1.5 MW for SPVP011, 016, and 022 and 2 MW for plant 013.

Figure 108: Altocumulus Cloud Band Forecast on April 4, 2013

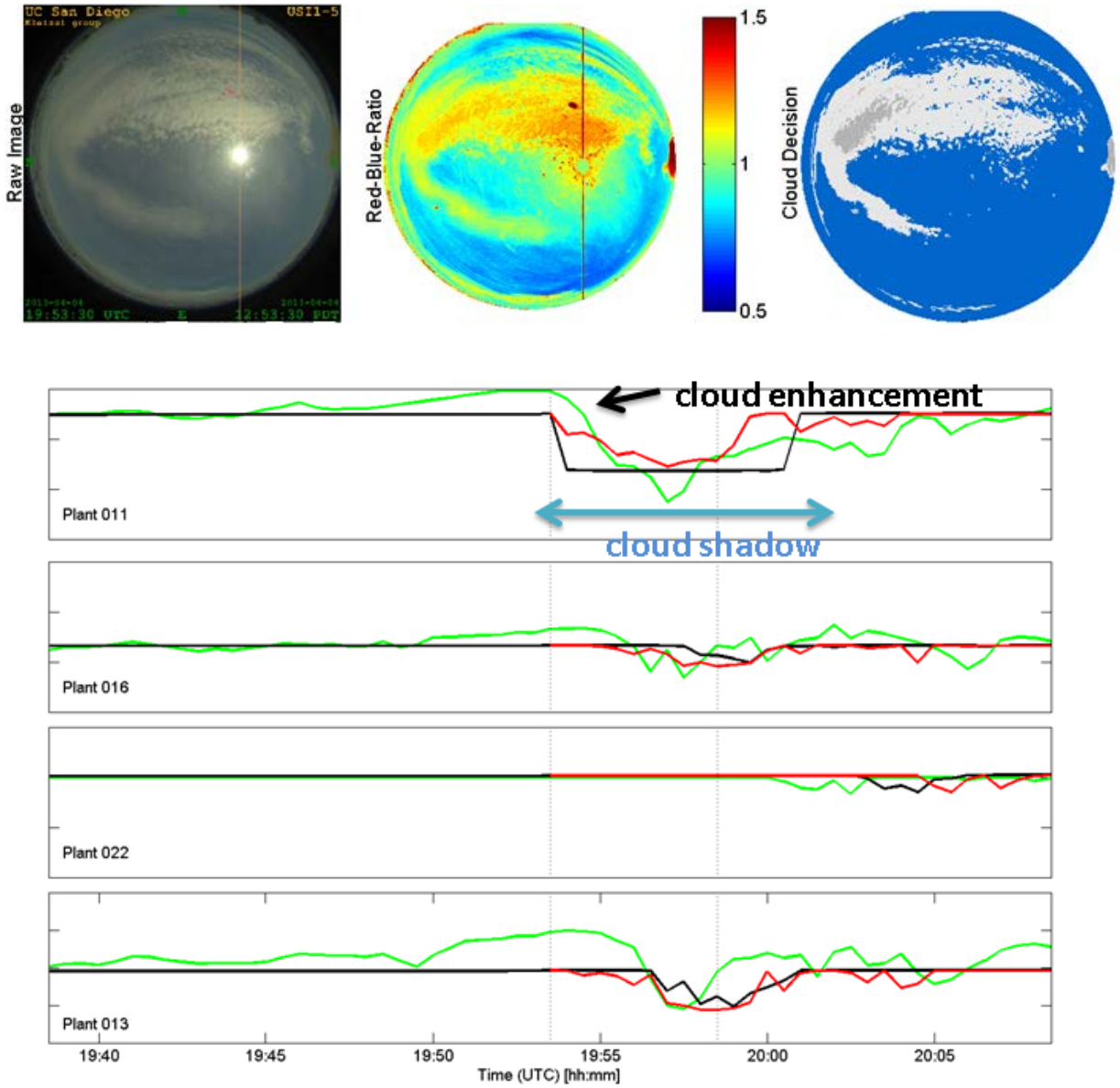

Raw Image, Red-Blue-Ratio (RBR) and cloud decision at 19:53 are shown on top.

The forecast skill for April 4 is generally negative at five minutes, but becomes positive afterwards (Table 16). The forecast skill is greatest at SPVP011 but this trend of greater forecast accuracy with proximity to the USI is not persistent when considering all days.

Table 16: rMAE and Forecast Skill for April 4, 2013

	relative Mean Absolute Error (rMAE) [%]				Forecast Skill [-]		
Forecast Horizon [minutes]	0	5	10	15	5	10	15
Power Error							
SPVP 011	4.3	5.1	5.6	5.9	0.0	0.3	0.3
SPVP 013	5.7	6.7	7.2	7.7	-0.3	0.0	0.0
SPVP 016	5.0	6.1	6.3	6.7	-0.1	0.1	0.2
SPVP 022	4.9	4.9	5.7	7.1	-0.1	-0.1	-0.1
Average	4.0	4.7	5.4	5.8	-0.1	0.2	0.2
kt Error							
SPVP 011	5.7	6.8	7.5	7.8	0.0	0.3	0.3
SPVP 013	7.5	8.9	9.4	10.2	-0.3	0.0	0.0
SPVP 016	7.9	9.8	10.0	10.6	0.0	0.1	0.1
SPVP 022	5.7	5.6	6.5	8.0	0.0	0.0	-0.1
Average	4.6	5.8	6.3	6.9	-0.1	0.1	0.1

April 16 also presents an interesting case study day due to occurrence of both overcast and partly cloudy conditions which lead to large ramps in power output. In Figure 109, cloud conditions and matching and cap error are shown. On this day, the morning was overcast but the cloud decision was still accurate since the CSL was bypassed in the cloud decision step as discussed in Section 3.1.2 (Figure 110). As the sky becomes partly cloudy and clear, the cloud decision automatically reverts back to using the CSL. Throughout the rest of the day, scattered cumulus clouds exist with a tendency to evaporate. The cloud height is constant with one layer until 21:00, and increases to 25:00 m in the afternoon.

Figure 109 Cloud Conditions on April 16, 2013 with Respective Matching and Cap Error

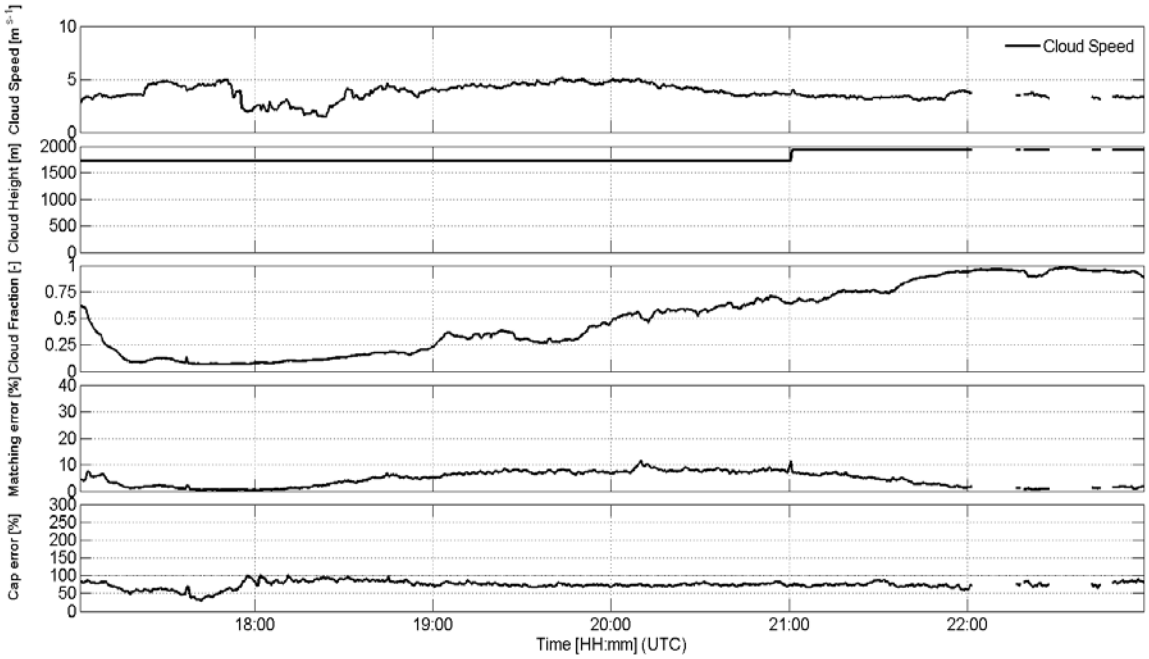

Figure 110: Cloud Decision for Overcast Conditions on April 16, 2013

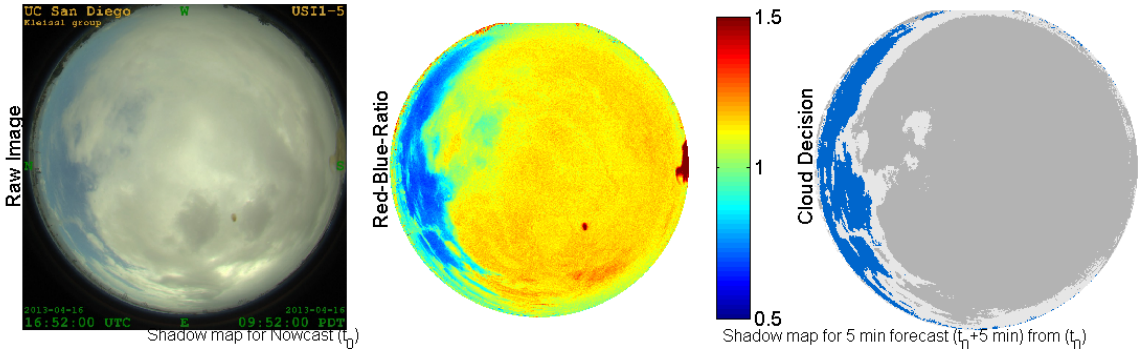

Left: Original image. Center: Red-blue-ratio to enhance cloud contrast. Right: Cloud decision for thin (white) and thick (grey) clouds and clear (blue)

Nowcast power output forecast along with measured power for April 16 is shown in Figure 111. Most of the ramp events in the evening were captured in timing, with a certain degree of magnitude error. At 19:00 and 20:40, the large ramp events were captured well both in timing, duration and magnitude. The ramp events after 21:00 are also captured well in timing but not as good in magnitude.

Figure 111: USI Power Nowcast (0 min forecast) for Power Plant SPVP011 on April 16, 2013

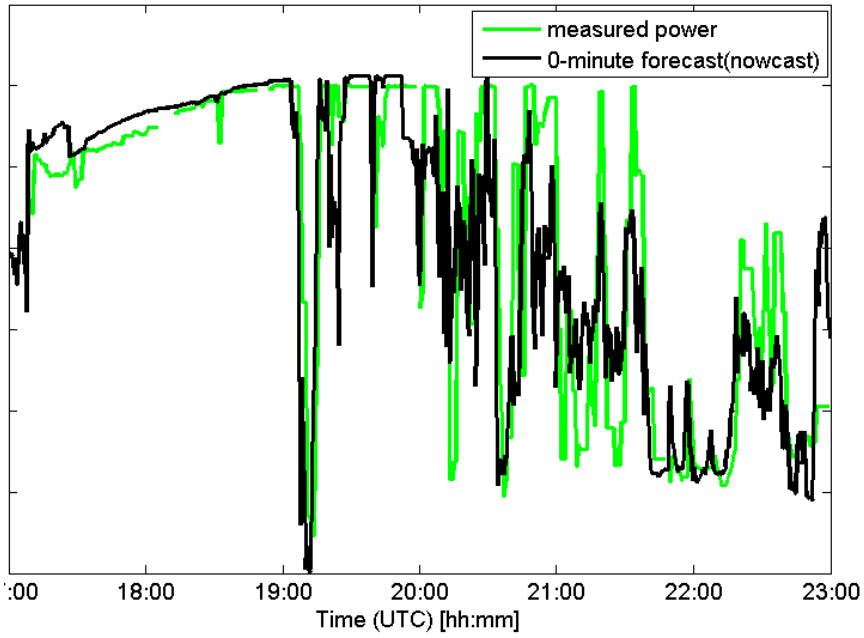

To protect the confidentiality of the data, the y axis labels were removed.

Forecast skill and relative mean absolute error on April 16 is given in Table 17. The forecast skill for this day is generally positive except at SPVP 011. The forecast skill is greatest at SPVP022 and fairly consistent across time horizons.

Table 17: rMAE and Forecast Skill for April 16, 2013

	relative Mean Absolute Error (rMAE) [%]				Forecast Skill [-]		
Forecast Horizon [minutes]	0	5	10	15	5	10	15
Power Error							
SPVP 011	10.2	14.2	14.3	18.0	-0.02	0.20	-0.06
SPVP 013	10.7	15.2	17.4	17.5	0.12	0.21	0.10
SPVP 016	12.8	15.9	15.3	16.6	0.13	0.25	0.22
SPVP 022	10.5	13.	14.2	16.2	0.27	0.20	0.22
Average	7.54	10.6	11.9	12.4	0.15	0.22	0.15

4.2 Aggregate Results

A summary of image-based forecast performance is presented in Table 18 for forecast horizons of 30 seconds and five minutes. The average 30-second cap error of 78% suggests that advection was superior to image persistence, but advection performance weakened for five minute forecast horizons with an average of 97%. Daily cap errors were below 100% for 15 out of 17 days for 30 second forecasts and 13 out of 17 days for five minute forecasts. This suggests the underlying principles and assumptions of the cloud decision and cloud velocity algorithms are consistently valid. Days with cap error exceeding 100% demonstrated adverse conditions, such as stationary clouds (advection performs worse than persistence) and very low, rapidly deforming clouds (near 100%, as advection performs just as poorly as persistence).

Compared with the analysis of an idealized dataset of four days by Chow et al. (2011), the larger validation set analyzed in this paper (61 consecutive days) presented a wider variety of sky conditions including adverse conditions where the assumption of cloud advection does not hold. This is the main reason for a greater range and larger average cap errors compared to Chow et al. (2011), which ranged from 45.0% to 54.6%. Additionally, new features of the USI such as thin cloud detection and an unobstructed circumsolar region (area immediately surrounding the sun) increase power output forecast skill through greater visibility of the sky dome and more accurate kt assignment. However, since thin cloud detection fluctuates more from image to image and there are larger cloud decision errors in the circumsolar region, the total number of false pixels in both advection and image persistence forecasts increases, causing their ratio to be closer to unity.

Table 18: Mean and Standard Deviation of Matching Errors with Total Daily Cap Errors

Date	e_m(%)		**Std.** e_m(%)		e_{cap}(%)		**Avg. cloud fraction (%)**	**Avg. cloud speed (m/s)**	**Avg. CBH (m)**
	30 s	5 min	30 s	5 min	30 s	5 min			
03.02	2.06	9.14	0.55	2.54	34.34	40.7	18.3	12.34	6462
03.03	5.92	24.27	3.74	19.10	57.45	147.4	78.7	25.45	3856
03.04	7.23	27.35	2.44	10.51	94.55	137.5	74.4	2.37	1115
03.15	2.88	11.28	1.80	5.79	58.10	61.21	7.5	9.17	4938
03.18	6.89	21.71	5.90	13.34	89.62	97.48	45.4	2.75	1322
03.31	7.20	27.16	2.95	10.91	65.70	90.70	29.4	5.27	2513
04.01	9.26	31.00	2.06	6.16	84.11	89.82	54.7	3.81	2752
04.02	4.54	17.16	2.91	9.02	49.00	73.62	7.5	7.76	2190
04.04	4.03	19.30	2.52	12.86	59.99	79.95	25.7	8.69	3130
04.05	2.61	8.57	1.45	5.03	88.5	103.5	95.0	4.24	1463
04.06	4.14	12.20	2.69	5.86	75.35	77.02	54.3	2.23	1178
04.07	2.78	8.42	1.22	3.54	63.85	68.70	82.0	13.58	4700
04.08	2.50	9.37	2.72	11.27	89.73	126.4	82.0	3.62	1594
04.12	6.67	29.68	3.02	14.30	101.5	96.9	7.7	1.04	793
04.16	7.60	25.30	4.58	15.40	77.28	93.20	49.1	2.62	1459
04.25	3.50	11.61	4.30	11.40	81.27	84.11	86.3	1.94	1562
04.30	7.67	31.12	4.83	16.69	114.9	95.10	12.3	0.58	640
Average	**5.21**	**19.30**	**2.88**	**10.04**	**77.91**	**97.20**	**49.2**	**4.60**	**2355**

The reported average cloud speed is a scalar average. Average of average cloud fraction does not take clear days into account.

Detailed error metrics for each day are tabulated in Table 19. Average number of stations covered by the nowcast shadow map is listed in the second column. This value is an indicator of the sample size used in the computation of error metrics. Missing days are clear or overcast days, where sky imagers provide no forecast value, and days with missing data.

For five minute USI forecasts, one out of 17 days exhibited a forecast skill of 0 or greater. For 10 minute and 15 minute USI forecasts, three and four out of 17 days exhibited a forecast skill of 0 or greater, respectively. Although ground station persistence forecast outperforms the USI on about half of the days in terms of bulk error metrics, the USI offers more value by being able to predict the occurrence of ramp events. Please refer to Sections 4.3 and 4.4 for details on ramp events analysis.

In addition to accurate cloud decision and CBH, forecast performance is increasingly dependent upon accurate cloud motion as forecast horizon increases. However, depending on cloud height and cloud velocity, circumsolar cloud decision errors, which cause the largest MAE forecast error for 0 minute forecasts especially at plant SPVP011, may no longer affect forecast errors if the circumsolar region is advected out of the footprint. Generally, it was observed that – provided a reasonably accurate nowcast was produced – the performance of five minute USI forecasts is consistently good.

Table 19: Forecasting Nowcast Aggregate Error Metrics

Date	Avg # Stations				rMBE				rMAE				$rMAE_p$			FS		
	0	**5**	**10**	**15**	**0**	**5**	**10**	**15**	**0**	**5**	**10**	**15**	**5**	**10**	**15**	**5**	**10**	**15**
03.02	3.9	3.9	3.9	3.9	3.2	6.6	2.3	1.6	8.3	9.8	7.2	6.8	6.2	9.1	8.9	-0.6	0.2	0.2
03.03	4.0	4.0	1.9	0.4	3.5	-5.7	-11	-9.0	19	25	29	36	2	32	35	-0.2	0.1	-0.0
03.04	3.7	3.7	3.8	3.8	13	3.8	5.3	13	15	26	36	43	15	17	19	-0.7	-1.2	-1.3
03.15	4.0	4.0	4.0	4.0	-3.0	-3.7	-4.1	-3.8	6.2	6.1	5.5	5.3	3.4	4.7	6.0	-0.8	-0.2	0.1
03.18	3.9	3.9	3.8	3.6	-8.8	-5.2	-5.8	-7.1	14	12	14	14	6.7	9.6	11	-0.9	-0.5	-0.3
03.31	4.0	4.0	4.0	4.0	-7.4	-2.6	1.5	1.7	12	16	17	17	8.6	11	11	-0.9	-0.5	-0.5
04.01	4.0	4.0	4.0	4.0	1.8	1.5	1.7	6.0	13	19	22	24	16	19	21	-0.2	-0.1	-0.1
04.02	4.0	4.0	4.0	3.2	0.1	-0.0	0.7	0.2	4.2	4.0	4.2	4.1	3.8	4.0	4.3	-0.1	-0.1	0.1
04.04	3.9	3.8	3.8	3.7	-7.5	-1.4	3.6	8.3	10	11	11	15	5.3	7.3	7.6	-1.3	-0.6	-1.0
04.05	4.0	4.0	4.0	3.8	5.5	18	25	33	20	29	35	40	16	22	22	-0.8	-0.6	-0.8
04.06	4.0	3.9	3.8	3.7	12	11	12	12	17	16	19	19	10	11	11	-0.6	-0.7	-0.7
04.07	4.0	3.0	3.0	2.8	-2.2	0.3	0.8	6.0	13	20	23	23	15	22	22	-0.4	-0.1	-0.1
04.08	4.0	4.0	4.0	4.0	-103	-35	-22	-12	108	52	58	60	24	34	41	-1.2	-0.7	-0.5
04.12	4.0	4.0	3.9	2.7	2.4	2.2	2.0	1.7	2.4	2.4	2.5	1.8	0.5	0.6	0.6	-3.5	-3.3	-2.0
04.16	4.0	4.0	4.0	4.0	1.5	2.0	-1.3	-0.7	10	13	14	14	16	19	18	0.2	0.3	0.2
04.25	4.0	4.0	4.0	4.0	-18	-10	-0.6	-1.3	26	25	25	31	9.2	16	20	-1.7	-0.6	-0.5
04.30	3.8	3.7	3.3	2.8	3.7	3.4	-0.2	-5.3	7.0	7.0	5.6	6.4	3.6	4.1	4.8	-0.9	-0.4	-0.3
AVG	**4.0**	**3.9**	**3.7**	**3.4**	**-6.0**	**-0.8**	**0.6**	**2.6**	**18**	**17**	**19**	**21**	**11**	**14**	**16**	**-0.8**	**-0.5**	**-0.4**

4.3 Ramp Rate Distribution

The variability of the power output can be visualized as a cumulative distribution function (CDF) of ramp rates, which are defined as

$$\mathrm{RR} = \Big(\big\langle P(t+\Delta t)\big\rangle - \big\langle P(t)\big\rangle\Big) \Big/ \Delta t P_{nameplate}\,, \tag{6}$$

where <> indicates a moving average over Δt, $P_{nameplate}$ is the nameplate capacity of the respective power plant. Figure 112 shows the cumulative distribution functions of the measurement data. Ramp rates are normalized by plant DC capacity. In other words, a 10% ramp rate corresponds

to 500 kW min^{-1} for SPVP011, 490 kW min^{-1} for SPVP013, 175 kW min^{-1} for SPVP016 and 310 kW min^{-1} for SPVP022.

More than one 1-minute time steps, ramp rates range up to 25% per minute in SPVP011, 32% per minute in SPVP013, 46% per minute in SPVP016 and 27% per minute in SPVP022. More than 10 minute time steps, ramp rates are less than 10% per minute in SPVP011 (which corresponds to 100% over the 10 minute time step), 5% per minute in SPVP013, 7% per minute in SPVP016 and 6% per minute in SPVP022. While 10 minute ramps do not differ significantly by solar plant size as they are driven by larger cloud systems, one minute ramps are a strong function of capacity. The smallest plant (SPVP016) shows almost twice the largest relative one minute ramps compared to the largest plant.

Figure 112: Cumulative Distribution Function of Ramp Rates in Power Output

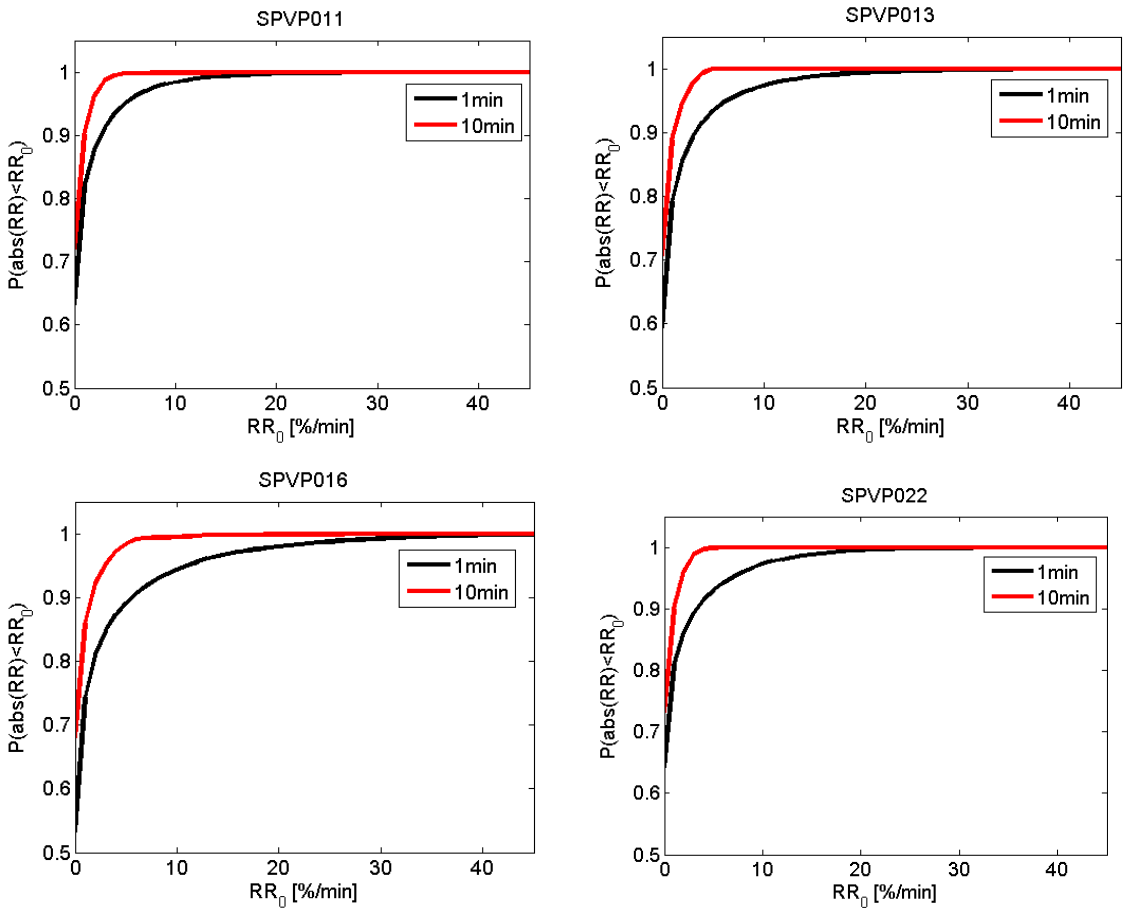

Power output at one minute and 10 minutes intervals for data from Feb 28, 2013 to May 10, 2013.

4.4 Ramp Event Detection

The results for hits and false alarms are shown with error bars in Figure 113. The results are grouped by forecast horizon (0 to 5, 5 to 10, and 10 to 15 minutes) based on the start time of the ramp.

Figure 113: Overall Performance of USI Forecast in Predicting Ramp Events Over 15 Percent

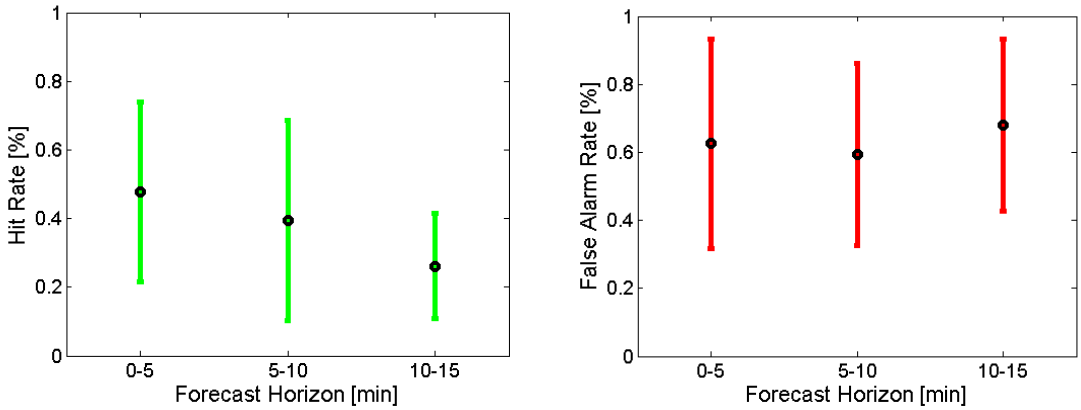

Error bars represent the interquartile range of hit and false alarm percentage among different days.

Magnitude, duration and timing differences are another way to evaluate forecast performance. Sample results for 15% ramp events are shown in Figure 114. The magnitude difference indicates how much larger or smaller the forecast ramp is predicted compared to the observed ramp. Duration difference indicates how much longer or shorter the forecast ramp is compared to the observed ramp. Differences are calculated by subtracting forecast ramp event magnitude/ duration/difference from the observed ramp event magnitude/duration/difference.

Note that the utility of the duration metric is limited, since the data resolution is around 0.6 data points per minute. Nevertheless, it is being reported for reference. Finally, the timing difference indicates how late or early the beginning of a forecast ramp event is predicted compared to the observed ramp. Accurate prediction of the ramp event timing directly influences the operator's ability to react to an upcoming ramp, and therefore, this information is usually more valuable than the other two metrics.

Figure 114: Magnitude, Duration and Timing Difference between Forecast and Actual Ramp Events over 15 Percent

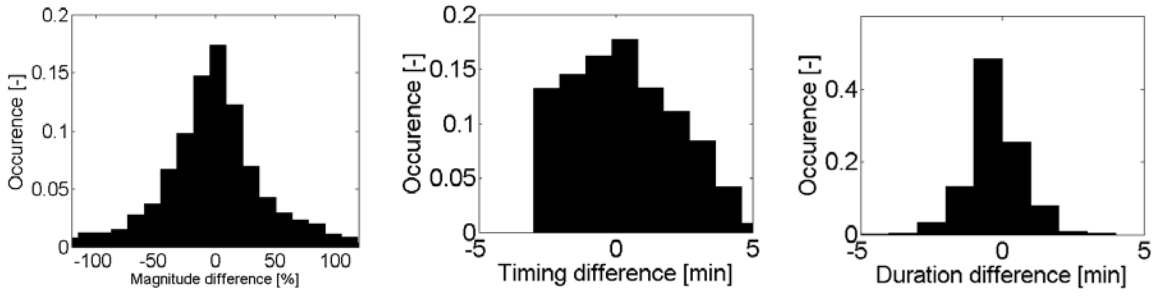

The mean overall performance of USI forecast for 15%, 20% and 25% minimum ramp amplitude is listed in Table 20. The hit percentage is generally around 40%, with accuracy decreasing as the ramp rate threshold is increased from 15% to 25%.

Table 20: Mean Overall Performance of USI Forecast in Predicting Ramp Events

Minimum ramp amplitude	Average # of observed ramps	Average # of forecast ramps	Mean Overall Hit [%]	Mean Overall False Alarm [%]
15%	973	1033	43.8	67.2
20%	875	950	38.9	74.6
25%	781	841	38.8	79.7

Ramp events more than 15%, 20% and 25% of all solar plants and over all days.

The directional tendency of magnitude, duration and timing differences are assessed via the mean bias error (MBE). The typical deviation from zero error for each variable is analyzed by using mean absolute error (MAE)

$$\mathrm{MBE} = \frac{1}{N}\sum_{n=1}^{N}\left(r^{obs} - r^{forecast}\right) \quad (7)$$

$$\mathrm{MAE} = \frac{1}{N}\sum_{n=1}^{N}\left|r^{obs} - r^{forecast}\right| \quad (8)$$

where r is the quantity in question.

MBE and MAE are given in Table 21. The results show that forecasts have a tendency of predicting smaller magnitude which likely stems from the inability of the sky imager to forecast cloud enhancement, i.e. exceedance of clear sky irradiance which often precedes or proceeds large ramp events. The timing and duration error biases are within the uncertainty of the temporal resolution of the data and are therefore insignificant. The magnitude difference has an overall mean of 45-50%, the duration difference is around 0.5 minute and the prediction is made usually 1.5-2 minutes off compared to the actual event.

Table 21: Overall Performance of USI Forecast in Predicting Ramp Events

	Magnitude Difference [%]		Duration Difference [min]		Timing Difference [min]	
Ramp Magnitude	MBE	MAE	MBE	MAE	MBE	MAE
Over 15%	-6.99	44.3	-0.17	0.71	0.23	1.70
Over 20%	-7.36	48.4	-0.10	0.54	0.18	1.65
Over 25%	-6.57	49.5	-0.12	0.43	0.10	1.63

Ramp events more than 15%, 20% and 25%. The difference is defined as forecast minus measured.

The principal limitation of this analysis comes from the nature of the available data. Usually, ramp rate events in solar plants of a few MW in size occur over a few seconds to a minute, which is the time it takes for a cloud to move over the plant. Unfortunately, the temporal resolution used in this study is only 1,183 data points per day on average, which corresponds to a timestep of about 36 seconds, on average. This low resolution limits testing of USI performance for the typical short ramp events. The low resolution also affects the ability to detect and match ramps, since there is no possibility of using detailed temporal evolution of a ramp (i.e. the shape of a ramp) to compare observed events with forecast events. Instead, the low resolution results in similar ramp profiles with sharp slope changes between pairs of data points.

4.5 Forecast Improvements through Cloud Height Correction

An interesting finding on April 16, 2013 data is that when the METAR cloud height data is adjusted through an optimization procedure, there is a large improvement in the forecast, especially in nowcast curves. Figure 115 shows the nowcast results generated with the cloud height data from METAR (black, 1433 meters) and with corrected cloud height data (red, 1733 meters). With the corrected cloud height, the ramping down events around 19:10 for plants SPVP 013 and SPVP 016 are captured with great accuracy. For other time periods, similar improvements are observed primarily in ramp magnitude, but also in ramp timing.

Figure 115: Nowcast Analysis for a Short Segment Around Noon LST on April 16, 2013

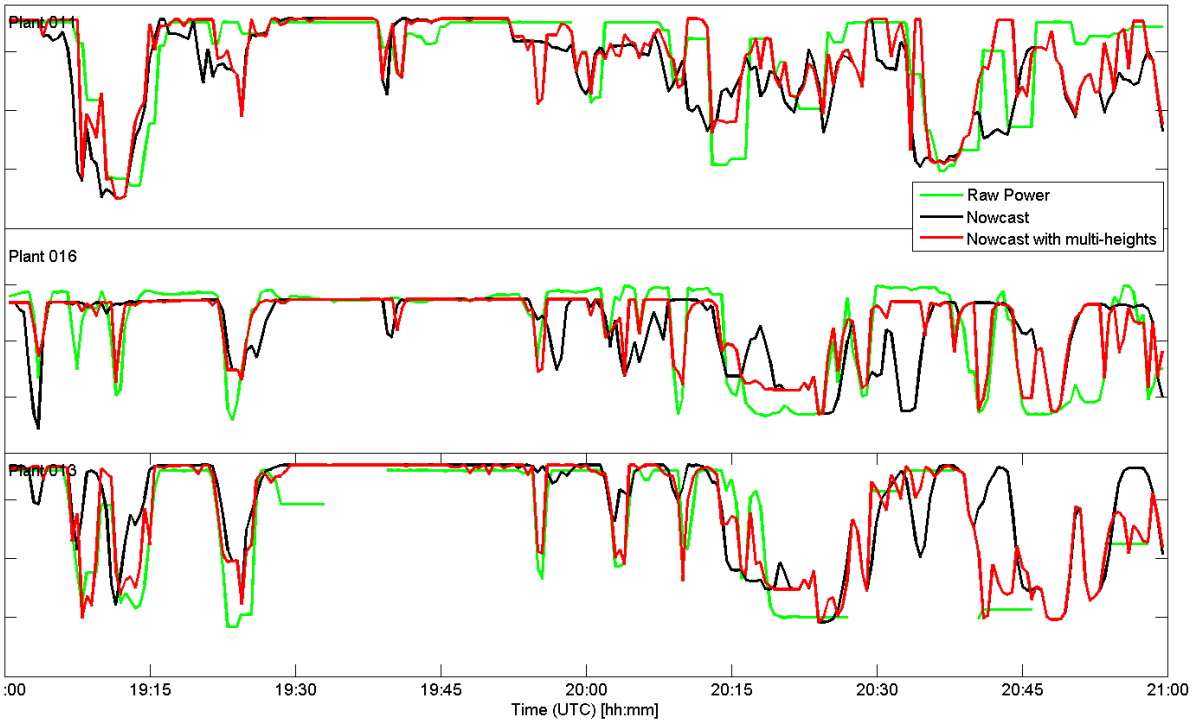

Cloud height of 1433 m from METAR (black) and 1733 m after the correction (red). To protect the confidentiality of the data, the y axis labels were removed.

Cloud height corrections have not been performed in the remainder of this report, since each instance requires manual inspection to ensure improvements in the forecast. Moreover, it is difficult to justify adjustments in the cloud height data without actual measurements. The improvement could simply be a result of 'overfitting' the nowcasts to the measurements and may not actually result in improved forecasts. The nearby METAR site is the only local source of cloud height data. The close proximity of the METAR station and the relatively flat terrain constitute a best-case scenario for cloud height accuracy. Nevertheless, cloud heights are only provided every hour and in practice significant intra-hour variability can occur. It is speculated on-site cloud height measurements should drastically improve the accuracy of USI forecasts.

Chapter 5
Satellite Forecast Performance

5.1 Method for Analyzing Satellite Forecast Performance

The solar power plant data is the ground truth and is provided in MW_{AC}. As described in Section 3.1.5., solar power plant data was converted to clear sky indeces kt^{obs} to facilitate comparison to satellite and sky imager forecasts. Sky imager forecasts are based on clear sky indeces from the histogram method (kt^{USI}) so no further data manipulation is required. Satellite solar resource data are based on cloud indices that are converted to clear sky indices and applied to a clear sky model to obtain GHI, which is provided to the end user. The satellite data GHI was normalized by the Ineichen clear sky model to back-calculate the clear sky index, $kt_n^{Satellite}$.

The USI and ground data are self-consistent as the USI kt is derived from the ground kt data, while kt is calculated independently for the satellite data. As a result, an offset in satellite ktn was observed in clear conditions which would have disadvantaged the satellite forecasts. In order to compare both forecast methods in an objective way, the satellite kt was calibrated so USI kt and satellite kt matched in clear conditions. Temperature and solar altitude changes in March and April causing the calibration factor to vary from 1.05 to 1.16.

Since satellite forecast is issued only twice per hour (at 00 and 30 minutes each hour) only the corresponding USI forecast issue times are considered. The data set is therefore reduced to about 15 realizations per day, which may cause results on specific days not to be representative. However, across the two months a sufficient sample is obtained.

The three error metrics discussed in Section 3.2 were adapted to assess the overall performance of the satellite and sky imager forecasts: relative mean absolute error (rMAE) measures the performance of the USI forecast relative to the power plant data; $rMAE_s$ measures the performace of satellite forecast relative to the power plant data; and forecast skill (FS) measures the performance of the USI relative to the satellite forecasts.

$$\mathrm{rMAE}(fh) = \frac{1}{N}\sum_{n=1}^{N}\left|kt_n^{USI-fh} - kt_n^{\mathrm{obs}}\right| \times \frac{100\%}{\overline{kt}^{\mathrm{obs}}} \qquad (9)$$

$$\mathrm{rMAE_s} = \frac{1}{N}\sum_{n=1}^{N}\left|kt_n^{Satellite} - kt_n^{\mathrm{obs}}\right| \times \frac{100\%}{\overline{kt}^{\mathrm{obs}}} \qquad (10)$$

$$FS^{USI-Sat} = 1 - \frac{\mathrm{rMAE}(fh)}{\mathrm{rMAE_s}} \qquad (11)$$

.

Positive values of FS therefore indicate USI forecast was superior to satellite forecast, with a maximum possible value of 1.

5.2 Satellite Forecast Performance Compared to USI Forecast

Figure 116 illustrates USI and satellite forecast performance for a day when the sky imager performed well. The persistence error increases strongly with forecast horizon in the first eight minutes and then levels off. Both USI and satellite forecasts show a similar trend outperforming or being close to persistence for most of the forecast horizon. There is no consistent winner between the USI and satellite forecasts, but the USI is slightly better overall.

Figure 116: USI (rMAE), Ground Station Persistence (rMAEp), and Satellite (rMAEs) Forecast Error Comparison for April 16, 2013

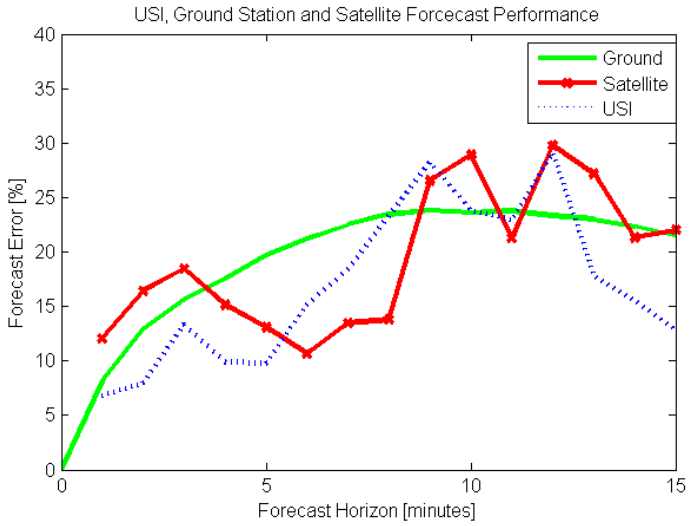

Detailed error metrics for each day are tabulated in Table 22. Given the small number of samples for each day, the performance on individual days may not be representative. Overall the USI shows a slight advantage over the satellite performance both in terms of average (positive forecast skill) and the number of days with positive forecast skill. Specifically, smaller cloud fraction often correlates to stronger forecast skills for the USI compared to the satellite. On mostly clear days the simple and observation-based kt assignment for the USI is advantageous since the clear kt mode in the histogram method is expected to be constant in time. On the other hand, for more overcast days, cloud thickness is more dynamic and can be estimated more accurately from the satellite. The satellite algorithms considers a continuous cloud thickness scale, whereas this algorithm just differentiates into thin/thick/clear. As a result, on days with more expansive clouds, USI forecast performance is lowered.

Table 22: USI and Satellite Aggregate Error Metrics by Forecast Horizon

Date	rMAE				$rMAE_s$			FS			Cloud Fraction (%)
	0	5	10	15	5	10	15	5	10	15	
03.02	8.3	3.6	7.1	8.3	11.2	8.7	11.8	0.68	0.18	0.30	18.3
03.03	19	39.7	6.2	28.5	22.4	32.7	26.9	-0.77	0.81	-0.06	78.7
03.04	15	13.2	23.2	41.6	27.6	27.8	47.0	0.52	0.16	0.12	74.4
03.15	6.2	6.5	6.1	5.1	9.4	10.2	10.8	0.31	0.40	0.53	7.5
03.18	14	17.3	18.6	25.5	16.9	16.6	27.1	-0.02	-0.12	0.06	45.4
03.31	12	24.0	16.6	17.8	17.2	18.5	16.4	-0.40	0.10	-0.08	29.4
04.01	13	32.0	22.4	30.6	18.2	21.0	27.9	-0.76	-0.06	-0.10	54.7
04.02	4.2	5.6	4.6	6.8	6.6	4.9	7.1	0.15	0.06	0.04	7.5
04.04	10	13.4	6.0	16.2	13.0	14.5	21.1	-0.03	0.59	0.23	25.7
04.05	20	33.8	28.7	48.5	22.0	19.0	27.0	-0.54	-0.51	-0.80	95
04.06	17	17.1	22.8	23.9	12.4	14.7	20.7	-0.38	-0.56	-0.16	54.3
04.07	13	28.6	28.2	20.8	29.3	26.6	30.2	0.02	-0.06	0.31	82
04.08	108	49.3	62.2	74.7	40.3	45.9	55.9	-0.22	-0.36	-0.34	82
04.12	2.4	2.0	3.2	2.1	9.0	8.9	8.9	0.78	0.64	0.76	7.7
04.16	10	9.8	23.8	12.9	13.1	32.4	24.3	0.25	0.27	0.47	49.1
04.25	26	21.5	17.0	41.7	23.7	15.8	27.8	0.09	-0.07	-0.50	86.3
04.30	7.0	3.8	3.1	3.0	9.8	6.7	7.4	0.62	0.54	0.60	12.3
AVG	18	18.9	17.6	24.0	17.8	19.1	23.4	0.02	0.12	0.08	

A positive forecast skill indicates that the USI forecast outperforms the satellite forecast.

5.3 Comparison of Sky Imager and Satellite Data Forecasts

In principal, sky imagers have a unique ability to provide accurate forecasts of timing of ramps at utility scale power plants, since the temporal and spatial resolution of other forecast methods is inadequate. However, the present analysis shows that the current sky imager ramp forecasts were insufficient. Two areas that need additional work incluce inaccurate cloud detection in the solar region and inaccurate cloud height specification which likely limit ramp forecast accuracy. Further research is also required to obtain accurate ramp forecasts from sky imagers for

applications such as ramp smoothing and to determine if combining sky imager and satellite images would lead to commercially viable forecasting algorithms.

Zero to fifteen minute power output forecasts for each of the four rooftop solar plants were investigated over two months and two days were analyzed in greater depth. The difficulty of accurate cloud detection in the solar region causes sky imager forecast errors to be larger for five minute horizons. Forecast skill relative to persistence forecasts improves for longer horizons. Specific examples of promising ramp forecast skills were presented, but inaccuracies in cloud height limit ramp forecast accuracy.

USI forecast performance was also analyzed against a one minute resolution satellite forecast. The forecast errors are comparable with slight advantages for the USI. Further improvements in sky imager forecasts will require more accurate atmospheric input measurements of cloud height and cloud optical depth and application of advanced machine learning tools. Additional investigation of forecasts from combined sky imager and satellite images might lead to better overall ramp forecasting.

For the first time, the forecast performance of the newly developed UCSD sky imager has been analyzed. Sky imagers were deployed for a year at a distribution feeder with four utility-scale warehouse rooftop solar plants owned by Southern California Edison. Sky imager data and power output were available every 30 seconds. The largest one minute ramps in power output were 46% of DC capacity for the smallest 1.7 MW plant, while the largest plant (5 MW) only showed ramps up to 25% of PV capacity.

Several other analyses point to the utility of sky imager forecast if forecast accuracy can be improved. The field-of-view was large enough to cover all the plants out to a 10 minute horizon 93% of the time and even at a 15 minute forecast horizon 85% coverage was observed(Table 23. Furthermore, the cloud-advection-versus-persistence (cap) error indicates that cloud advection was 22% superior to persistence at a 30 second forecast horizon, but only a 3% improvement existed at a five minute forecast horizon. A cap error below 100% indicates that cloud advection outperformed persistence and confirms the potential of the sky imager forecast approach.

Table 23: Average Cloud Conditions and Cloud-Advection-versus-Persistence (cap) Error for March and April, 2013.

e_{cap}(%)		Avg % of plants in Field of View	Avg. cloud fraction (%)	Avg. cloud speed (m/s)	Avg. Cloud Base Height (m)
30 s	5 min	0 5 10 15 min			
77.9	**97.2**	100 98 93 85	**49.2**	**4.60**	**2355**

Forecast horizons of 30 seconds and 5 minutes.

USI forecast performance was also analyzed against forecasts derived from satellite imagery. USI and satellite forecast errors are comparable with slight advantages for the USI (Table 24). A positive forecast skill (FS) indicates that the USI forecast outperforms the satellite forecast.

Table 24: USI and Satellite Aggregate Power Output Error Metrics by Forecast Horizon

	rMAE [%]				$rMAE_s$ [%]			FS [%]		
Forecast Horizon [min]	**0**	**5**	**10**	**15**	**5**	**10**	**15**	**5**	**10**	**15**
rMAE [%]	18.0	18.9	17.6	24.0	17.8	19.1	23.4	2	12	8

Chapter 6
Solar Integration Analysis

Solar integration analysis assists SCE by assessing and providing guidance on how many additional solar PV systems SCE can expect in similar areas to areas where the project's solar variability data was gathered. Using the data from the solar monitoring and forecasting data will help the SCE grid accommodate the variable generation output from solar PV systems. The impact of the variable PV output on the grid affects generation resource planning, generation and storage plant siting, and transmission planning.

6.1 Assessment of Current Regulation Costs and Control Performance Impacts

Regulation costs within the SCE control area assess current regulation costs and control performance impacts are primarily dependent on the amount of increased solar PV installed in the SCE control area. EnerNex consulted with SCE to define the specifics of this task. A key parameter in the determination of regulation costs and performance impacts was the amount of solar PV in the SCE control area. This task concentrated on determination of the amount of solar PV which would be economically viable in the control area.

6.2 Evaluation of Increased PV Generations Penetration

The impact of large solar PV systems on the distribution grid is primarily dependent on the penetration level of solar PV on a distribution feeder and also on the location of the solar PV system in relation to the physical layout of the feeder.

The reliability and cost impacts associated with (1) current PV generation levels, (2) the planned PV generation level of 500 MW, and (3) future PV generation levels above 500. It is likely that at some increased penetration level regulating capacity will have to be increased to counter PV variability or forecast error. Figure 117 characterizes the variability of solar generation over a one hour time interval for three different penetration scenarios (15%, 20%, and 25%). These data can be used to facilitate a model of a time-varying reserve profile (Figure 118).

Figure 117: Hourly Generation Changes as Functions of Production Levels Solar Pentration

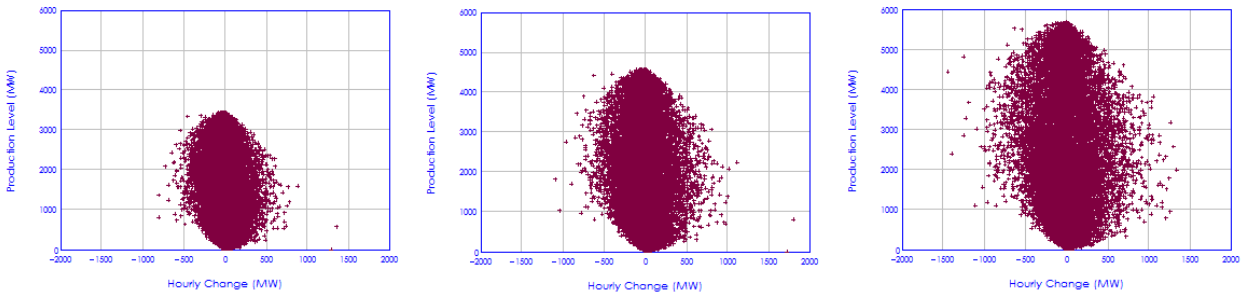

Production levels for 15%, 20%, and 25% solar penetration

Figure 118: Varying "Operating Reserve Margin

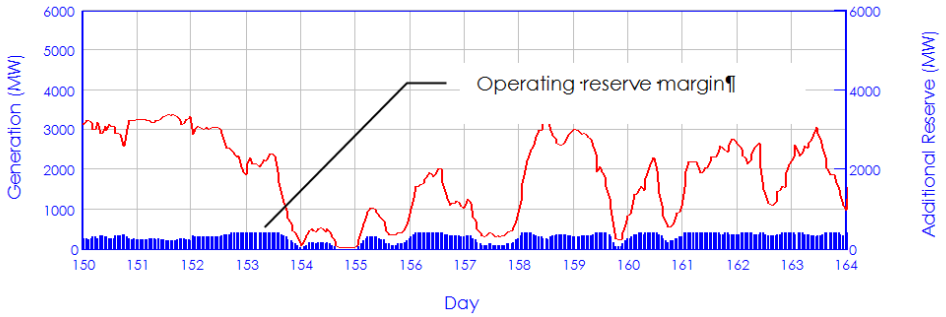

Developed from statistical analysis of hourly distributed generation variations.

6.3 Opportunities for Improved PV Generation Forecasts in Real-Time Operational Planning Functions

Short-term PV generation forecasts can be used to reduce system regulation and other operating costs. The ability to improve PV generation forecasts can result in lower regulation costs as more accurate forecasts can be used to decrease the amount and hence costs of ancillary services including reserves margins needed to compensate for fluctuations in PV output. Control actions based on forecasts from over-the-next-minute to several-hour time frames can be used to optimize the regulation strategy. Currently available optimization techniques used in the control area include the use of tap changers to control voltage fluctuations introduced by solar PV systems, including fluctuations caused by clouds. Other currently available optimization techniques include monitoring the voltage/Var using distribution system sensors, and if the Advanced Meter Infrastructure (AMI) is capable of doing so, of using smart meters to record and transmit feeder voltages to the Distribution Management System. Evolving optimization techniques including energy storage and the use of smart inverters that can be used to control voltage/VAr on distribution lines. The ability to predict fluctuations can assist in real time operations by reducing the need for ancillary services.

Depending on the design of the distribution circuit, large penetrations of solar PV may be acceptable. For example, at times the data collected from the SCE sites indicated that more power was produced by the solar PV systems than the actual real-time demand. Hence reverse power flow was observed; and the SCE feeder design was able to successfully utilize the power produced without producing undesirable power quality degradation such as over-voltage.

Figure 119 shows a distribution of next-hour errors from a persistence forecast. The general response operationally to increased uncertainty in forward time frames is to carry additional reserves. How specifically this would be done in some optimal fashion for PV generation given forecast, forecasted variability, and forecast uncertainty is not yet known. Some control area operators pad their reserves by an amount proportional to what they consider the next hour uncertainty due to load forecast to be. Accurate PV generation forecasts could reduce the uncertainty and hence lower the operational reserve margin.

SCE system operators were consulted in terms of advanced strategies for how forecasting information could be utilized. As PV generation increases, forecasts will take on additional importance. SCE operators identified 45 minute ahead forecasts as the optimum time period for PV generation forecasts to benefit system operations.

Figure 119: Next-hour Deviation from Persistence Forecast – 15% DG Penetration

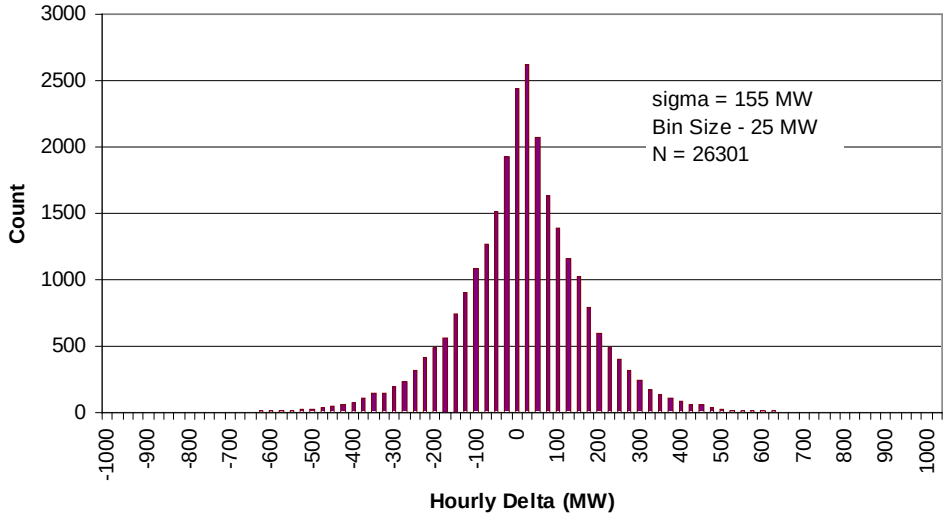

Regulation costs are directly related to the size and geographic diversity of generation in the SCE control area and more broadly for most distribution circuits. Thus to determine the amount of large solar PV systems that would be installed in SCE territory, the likely number of solar PV systems installed by businesses was determined.

This report presents research into estimating a sample size of business establishments in Southern California Edison territory that see economic value in installing Photo Voltaic (PV) systems on their rooftops. The structure of the report is as follows:

- Model system output for 100 kW, 1 MW, 2.5 MW and 5 MW PV systems
  - Estimate payback for these systems
- Review sample size of establishments to estimate potential for PV systems
  - Estimate number of establishments that could install the four categories of PV systems

This report is intended for the utility industry audience who are interested in understanding the economics behind various businesses installing solar PV systems.

6.4 Cost and Control Performance Assessment

Solar Integration Analysis will aid SCE in an operational environment by assessing and providing guidance on how SCE can use the data from the solar monitoring and forecasting activities to help the grid accommodate the variable generation output. The impact of the variable PV output on the grid with regards to generation resource planning, generation and storage plant siting, transmission planning, and the economics will be assessed. Figure 120

illustrates how the effects of variability and uncertainty will be captured in this study, relative to the ancillary service of interest.

Figure 120: Relationship Between the Effects of Variability and Uncertainty

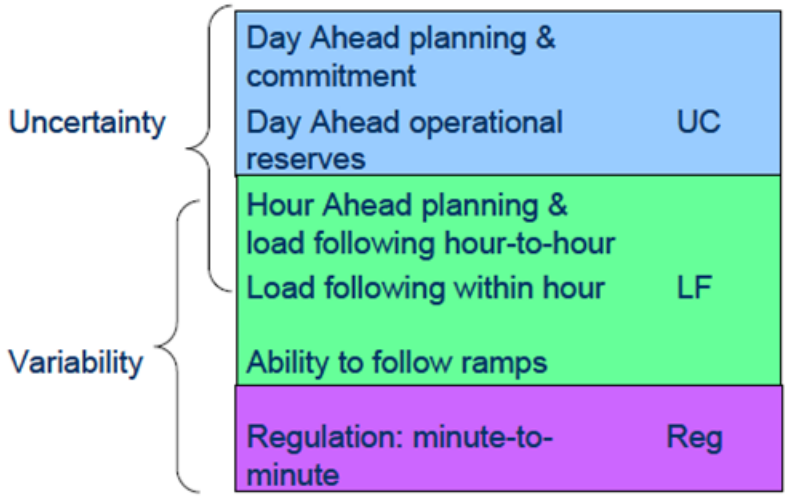

Includes planning functions, and the ancillary services of unit commitment (UC), load following (LF) and regulation (Reg).

The capacity value of PV generation for long term planning analyses is currently a topic of significant discussion in the PV and electric power industries. Characterizing the PV generation to appropriately reflect the historical statistical nature of the generation output on seasonal, daily, and hourly bases is one of the major challenges. In addition to solar power being variable, it is also a challenge to utility planners and operators to accurately predict solar power on the time scales of interest. Day-ahead predictions are necessary for long-term planning of system adequacy, i.e., meeting the system peak load during the year. PV energy is more predictable in the hour-ahead time frame, but even then the uncertainty in PV forecasts must be accounted for in utility operation and dispatching. To minimize negative impacts and maximize benefits, each utility that incorporates solar energy must learn how to accommodate the uncertainty and variability of solar energy in their operational and planning practices, and do so while maintaining system reliability.

6.5 Methodology

The approach for the economic payback for PV systems is based on publicly available information to model PV systems. Four different sizes of PV systems (100 kW, 1 MW, 2.5 MW and 5 MW) were modeled using the National Renewable Energy Laboratory (NREL), System Advisor Model (SAM), to obtain an PV production estimate and payback estimates for the four PV system sizes. SAM utilizes PVWatts Solar array calculator to estimate PV production. This study included modeling PV systems within Southern California Edison (SCE) service territory. It also makes an assumption that these PV systems will primarily be installed as rooftop solar systems by customers in SCE's territory.

The desired data for input into the SAM model includes the following assumptions:

- PV System Location
- PVWatts Solar Array Information
- PV System Cost Assumptions
- Financing Terms
- Incentives
- Depreciation
- SCE Tariff

6.6 Data Modeling Assumptions –

The National Renewable Energy Laboratory's modeling tool, System Advisor Model (SAM), was used to model the customer-owned PV systems of four system capacities (DC)

- 100 kW
- 1 MW
- 2.5 MW
- 5 MW (assumption is that customers having large enough rooftop space on multiple facilities will install this size of a system).

This reports assumes customers having large enough rooftop space on multiple facilities will install these sizes PV systems. SAM requires a climate data file in Typical Metrological Year (TMY2 or TMY3) or Energy Plus Weather (EPW) format. For the purpose of modeling these PV systems, Fontana California was selected as a location. Following is the list of data points that were assumed for PV output and payback estimation:

- PV System Location for modeling PV output
    - Fontana, California
- PVWatts Solar Array Information
    - System nameplate capacity
        - 100 kWdc
        - 1000 kWdc
        - 2500 kWdc
        - 5000 kWdc
    - DC to AC Derate Factor – 80%
    - PV System Configuration
        - Array Tracking – Fixed
        - Tilt – Latitude (34 degrees)
        - Azimuth – 180 degrees (South)

- PV System Cost Assumptions[15]
    - Module Cost - 1.9 $/Wdc
    - Inverter Cost - 0.25 $/Wac
    - Equipment BOS - 0.45 $/Wdc
    - Labor + Miscellaneous - 1.15 $/Wdc
    - Total Installed Cost per capacity - 3.75 $/Wdc
- Financing Terms
    - Loan Term - 10 years
    - Loan Rate – 7%
    - Inflation Rate – 2.5%
    - Sales Tax- 8% (for Fontana)
    - Federal Income Tax Rate – 28%
    - State Income Tax Rate – 9.3%
    - Insurance Rate (Annual) – 0.5% of installed cost
- Incentives
    - Federal Investment Tax Credit (for Solar PV Systems)– 30%
    - California State Production Based Incentive– 0.05 $/kWh (SAM makes a default assumption of 0.05 $/kWh, Current Step 9 for SCE Commercial Customer)
- Depreciation
    - 5 year Modified Accelerated Cost Recovery System (MACRS)
- SCE Rate
    - For 100 kW system - Time of Use, General Service, Demand Metered, Option B: GS-2 TOU B, Three Phase (2kv - 50kV)
        - Energy tiered charge = Generation charge + Delivery charge
        - Time of day demand charges (generation-based) are to be added to the monthly demand charge (Delivery based).
    - For 1000 kW and 2500 kW system - Time-Of-Use - General Service - Large: TOU-8 (2kV-50kV)
        - Tiered energy usage charges are the generation charges + energy delivery charge

[15] "Achieving Low-Cost Solar PV: Industry Workshop Recommendations for Near-Term Balance of System Cost" [2010], http://www.rmi.org/Content/Files/BOSReport.pdf (Accessed 8 May 2014).

        - Critical Peak Event Energy Charge of $1.34519/kWh, to occur 12 times per the summer of calendar year between the hours of 2p.m-6p.m.
        - Demand discount not applicable during CPP event.
    - For 5000 kW system - Time of Use, General Service, Demand Metered, Option B: GS-2 TOU B
        - Energy tiered charge = generation charge + delivery charge
        - Time of day demand charges (generation-based) are to be added to the monthly demand charge(Delivery based).

6.7 Results

This section presents the results of iterations run in SAM that provide the following information for the four different size of PV systems (100 kW, 1000 kW, 2500 kW and 5000 kW) (Figures 121-128):

- Graph of Monthly Energy Output (kWhac)
- Economic Payback information

6.7.1 100 kW (DC) System

Figure 121: Monthly Energy Output (AC) for a 100 kW (DC) System

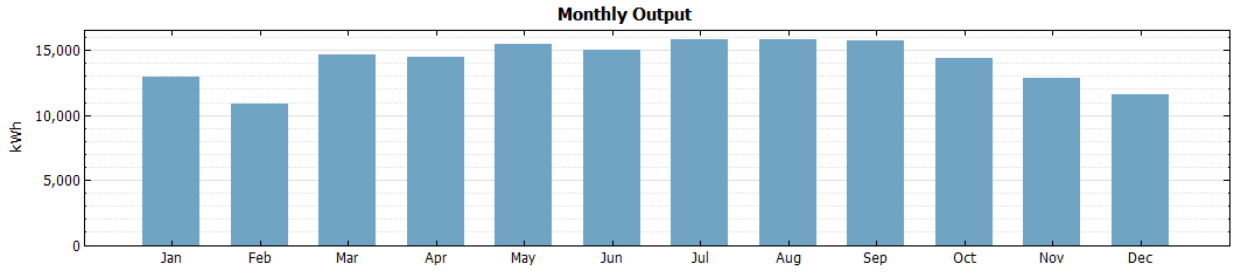

Figure 122: Economic Payback Information for a 100 kW (DC) System

Metric	Value
Annual Energy	169,471 kWh
LCOE Nominal	6.94 ¢/kWh
LCOE Real	6.18 ¢/kWh
Electricity cost without system	$ 30,749.25
Electricity cost with system	$ 11,211.98
Net savings with system	$ 19,537.29
Net present value ($)	$ 10,124.78
Payback (years)	9.36721
Capacity Factor	19.3 %
First year kWhac/kWdc	1,695

6.7.2 1,000 kW (DC) System

Figure 123: Monthly Energy Output (AC) for a 1,000 kW (DC) System

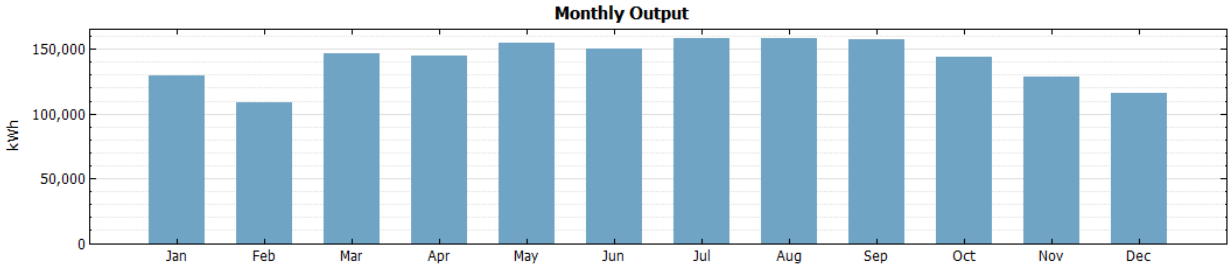

Figure 124: Economic Payback Information for a 1000 kW (DC) System

Metric	Value
Annual Energy	1,694,709 kWh
LCOE Nominal	6.94 ¢/kWh
LCOE Real	6.18 ¢/kWh
Electricity cost without system	$ 343,372.22
Electricity cost with system	$ 128,747.19
Net savings with system	$ 214,624.95
Net present value ($)	$ 172,224.23
Payback (years)	8.74466
Capacity Factor	19.3 %
First year kWhac/kWdc	1,695

6.7.3 2,500 kW (DC) System

Figure 125: Monthly Energy Output (AC) for a ,2500 kW (DC) System

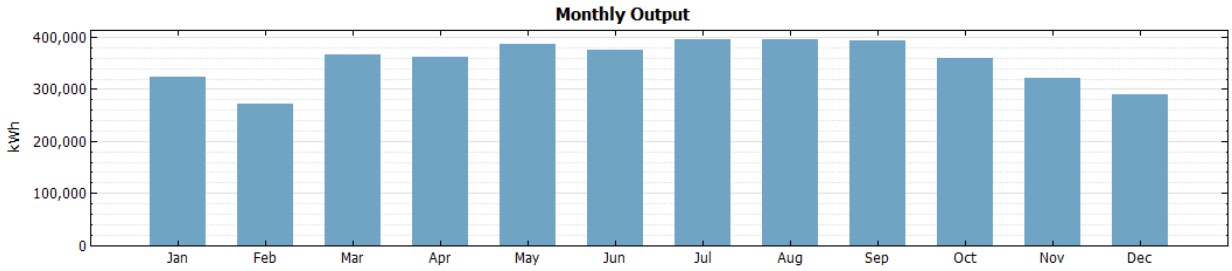

Figure 126: Economic Payback Information for a 2,500 kW (DC) System

Metric	Value
Annual Energy	4,236,773 kWh
LCOE Nominal	6.94 ¢/kWh
LCOE Real	6.18 ¢/kWh
Electricity cost without system	$ 847,381.81
Electricity cost with system	$ 310,819.31
Net savings with system	$ 536,561.88
Net present value ($)	$ 430,559.88
Payback (years)	8.74467
Capacity Factor	19.3 %
First year kWhac/kWdc	1,695

6.7.4 5,000 kW (DC) System

Figure 127: Monthly Energy Output (AC) for a 5000 kW (DC) System

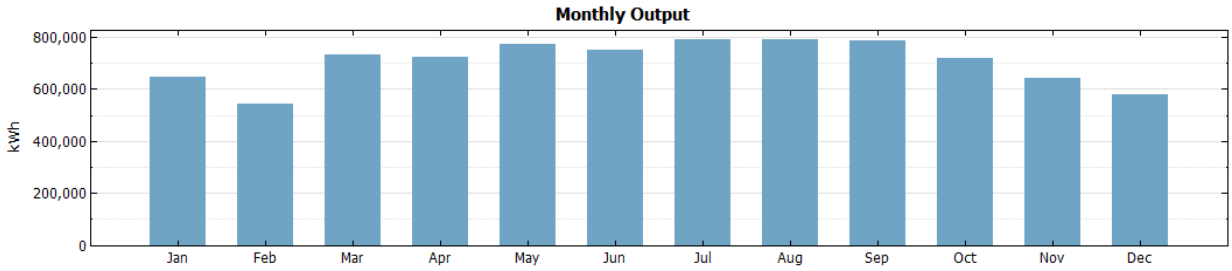

Figure 128: Economic Payback Information for a 5000 kW (DC) System

Metric	Value
Annual Energy	8,473,545 kWh
LCOE Nominal	6.94 ¢/kWh
LCOE Real	6.18 ¢/kWh
Electricity cost without system	$ 1,405,229.88
Electricity cost with system	$ 480,920.66
Net savings with system	$ 924,311.19
Net present value ($)	$ 283,102.81
Payback (years)	9.81469
Capacity Factor	19.3 %
First year kWhac/kWdc	1,695

6.8 Estimating PV System Potential

Research was conducted to estimate the number of establishments in five zip codes located in SCE's territory that would seek the economic benefit of installing PV systems on their roof tops. Census database for commercial buildings was researched for the following five zip codes:

- Fontana – 92335
- Riverside – 92501
- Rowland Heights – 91748
- Pomona – 91766
- Perris – 92570

The 2011 Census[16] database contains business patterns as per the North American Industry Classification System (NAICS) codes. Each zip code contained information for various industries. For the purpose of this study, the following industries were selected:

- Industry Code (48) – Transportation and Warehousing
- Industry Code (42) – Wholesale Trade
- Industry Code (31) – Manufacturing

From the 2011 Census data, Tables 25-29 present the total number of establishments and the number of employees in those establishments for the five zip codes.

[16] "2011 Zip Code Business Patterns (NAICS)" [2011], http://censtats.census.gov/cgi-bin/zbpnaic/zbpsect.pl (Accessed 19 May 2014)

Table 25: Total Number of Establishments Based on Number of Workers – Fontana Zipcode 92335

	Approximate Number of Workers		5	10	15	35	75	175	375	750	1000
	Industry Name	**Industry NAICS Code**	**Number of Establishments**								
Fontana Zipcode 92335	Transportation and warehousing	48----	51	13	10	9	7	5	2	1	1
	Wholesale trade	42----	31	29	21	22	5	2	0	0	0
	Manufacturing	31----	24	23	14	26	6	4	0	1	0
Total Number of Establishments based on Number of Workers			***106***	***65***	***45***	***57***	***18***	***11***	***2***	***2***	***1***

Table 26: Total Number of Establishments Based on Number of Workers – Riverside Zipcode 92501

	Approximate Number of Workers		5	10	15	35	75	175	375	750	1000
	Industry Name	**Industry NAICS Code**	**Number of Establishments**								
Riverside Zipcode 92501	Transportation and warehousing	48----	9	6	4	2	0	1	0	0	0
	Wholesale trade	42----	17	11	7	4	2	0	0	0	0
	Manufacturing	31----	4	3	6	2	3	1	0	0	0
Total Number of Establishments based on Number of Workers			**30**	**20**	**17**	**8**	**5**	**2**	**0**	**0**	**0**

Table 27: Total Number of Establishments Based on Number of Workers – Rowland Heights Zipcode 91748

	Approximate Number of Workers		5	10	15	35	75	175	375	750	1000
	Industry Name	**Industry NAICS Code**	**Number of Establishments**								
Rowland Heights Zipcode 91748	Transportation and warehousing	48----	72	19	12	7	3	2	0	0	0
	Wholesale trade	42----	293	90	83	37	15	4	0	0	0
	Manufacturing	31----	25	8	5	12	13	12	1	0	0
Total Number of Establishments based on Number of Workers			**390**	**117**	**100**	**56**	**31**	**18**	**1**	**0**	**0**

Table 28: Total Number of Establishments Based on Number of Workers – Pomona Zipcode 91766

	Approximate Number of Workers		5	10	15	35	75	175	375	750	1000
	Industry Name	**Industry NAICS Code**	**Number of Establishments**								
Pomona Zipcode 91766	Transportation and warehousing	48----	20	4	5	11	1	1	1	0	0
	Wholesale trade	42----	46	13	13	13	2	3	0	0	0
	Manufacturing	31----	25	16	22	12	4	4	0	0	0
Total Number of Establishments based on Number of Workers			**91**	**33**	**40**	**36**	**7**	**8**	**1**	**0**	**0**

Table 29: Total Number of Establishments Based on Number of Workers – Perris Zipcode 92570

		Approximate Number of Workers	5	10	15	35	75	175	375	750	1000
	Industry Name	Industry NAICS Code	Number of Establishments								
Perris Zipcode 92570	Transportation and warehousing	48----	18	1	6	2	1	1	1	0	1
	Wholesale trade	42----	17	2	2	1	0	1	1	0	0
	Manufacturing	31----	9	7	4	4	6	1	0	0	0
Total Number of Establishments based on Number of Workers			**44**	**10**	**12**	**7**	**7**	**3**	**2**	**0**	**1**

Table 6 summarizes information from the 2011 Census data, presents the total number of establishments based on number of workers in the five zip codes.

Table 30: Total Number of Establishments Based on Number of Workers In All Five Zipcodes

Approximate Number of Workers	5	10	15	35	75	175	375	750	1000
City/Zipcode	*Total Number of Establishments based on Number of Workers*								
Fontana Zipcode 92335	106	65	45	57	18	11	2	2	1
Riverside Zipcode 92501	30	20	17	8	5	2	0	0	0
Rowland Heights Zipcode 91748	390	117	100	56	31	18	1	0	0
Pomona Zipcode 91766	91	33	40	36	7	8	1	0	0
Perris Zipcode 92570	44	10	12	7	7	3	2	0	1
Total Number of Establishments in Five Zipcodes based on Number of Workers	**661**	**245**	**214**	**164**	**68**	**42**	**6**	**2**	**2**

The Commercial Buildings Energy Consumption Survey (CBECS) [17]is a national sample survey that collects information on the stock of U.S. commercial buildings, including their energy-related building characteristics and energy usage data (consumption and expenditures). The CBECS database Table B2 provides summary of employment size category, floor space information and mean square feet per worker based on building type (Table 31).

Mean square feet per worker for building type "Warehouse and Storage" is equal to 1,700. Using this assumption of mean square feet per worker Table 31 is adapted to estimate the available floor space for the number of establishments in the five zip codes under consideration. From the available floor space information following assumptions were made to estimate the roof top space, available roof top space for PV installation, and estimated PV installation capacity (kWdc):

- Mean square feet per worker in SCE territory – 751

[17]"2003 CBECS Survey Data" [2003], http://www.eia.gov/consumption/commercial/data/2003/ (Accessed 23 May 2014)

- Estimated Square Feet Based on Number of Workers = Mean square feet per worker in SCE territory multiplied by the number of workers
- Estimated Roof Top Space (Square Feet) = 75 % of overall estimated square feet of the facility (Assumption is that the facility type is a large single story facility).
- Estimated Roof Top Space for PV Installation (Square Feet) = 75 % of the estimated roof top space
- Estimated PV Installation Capacity (kWdc) is calculated assuming 1 kW per 100 square feet

Table 31: CBECS Table B2

	Number of Buildings (thousand)	Total Floorspace (million square feet)	Total Workers in All Buildings (thousand)	Median Square Feet per Building (thousand)	Median Square Feet per Worker	Median Hours per Week	Median Age of Buildings (years)
Principal Building Activity							
Education	386	9,874	12,489	7.0	854	45	31.5
Food Sales	226	1,255	1,430	2.8	1,094	107	30.5
Food Service	297	1,654	3,129	3.5	550	84	28.5
Health Care	129	3,163	6,317	6.0	540	45	23.5
Inpatient	8	1,905	3,716	106.0	530	168	31.5
Outpatient	121	1,258	2,600	6.0	540	45	23.5
Lodging	142	5,096	2,457	12.5	2,633	168	30.5
Retail (Other Than Mall)	443	4,317	3,463	4.8	1,250	54	35.5
Office	824	12,208	28,154	4.0	525	46	28.5
Public Assembly	277	3,939	2,395	6.7	2,050	42	35.5
Public Order and Safety	71	1,090	1,347	5.0	825	168	16.5
Religious Worship	370	3,754	1,706	6.0	2,400	20	43.5
Service	622	4,050	3,667	2.8	1,160	50	29.5
Warehouse and Storage	597	10,078	4,369	5.2	**1,700**	50	17.5
Other	79	1,738	1,819	4.6	1,200	48	32.5
Vacant	182	2,567	64	3.7	6,625	0	43.5

Table 32 presents the preceeding information for the number of establishments (based on number of workers) in all the five zip codes.

Table 32: PV Installation Capacity Estimation for Warehouse Buildings

Approximate Number of Workers	**5**	**10**	**15**	**35**	**75**	**175**	**375**	**750**	**1000**
Estimated Square Feet Based on Number of Workers	8,500	17,000	25,500	59,500	127,500	297,500	637,500	1,275,000	1,700,000
Estimated Roof Top Space (Square Feet)	6,375	12,750	19,125	44,625	95,625	223,125	478,125	956,250	1,275,000
Estimated Roof Top Space for PV Installation (Square Feet)	4,781	9,563	14,344	33,469	71,719	167,344	358,594	717,188	956,250
Estimated PV Installation Capacity (kWdc) assuming 1 kW = 100 Square Feet	48	96	143	335	717	1,673	3,586	7,172	9,563

From these tables researchers estimated the total number of establishments and the estimated PV capacity for these establishments in the five zip codes. Table 33 provides an estimate of the number of establishments that could potentially install the four PV system sizes (100 kW, 1

MW, 2.5 MW and 5 MW) in the five zip codes of SCE territory. The estimated number of warehouses likely to install PV are sumerized in Table 34.

Table 33: Summary PV Installation Capacity Estimation vs Number of Warehouse Establishments in Five Zipcodes based on Number of Workers

Approximate Number of Workers	5	10	15	35	75	175	375	750	1000
Estimated PV Installation Capacity (kWdc)	48	96	143	335	717	1,673	3,586	7,172	9,563
Total Number of Establishments in Five Zipcodes based on Number of Workers	661	245	214	164	68	42	6	2	2

Table 34: Estimated Number of Warehouse Establishments Likely to Install the four sizes of PV Systems

PV System Size (kWdc)	Number of Warehouse Establishments in the five zip codes
100	743
1000	52
2500	10
5000	4

The calculation for the number of warehouse establishments that are eligible to install the four sizes of PV systems is based on assumption that establishments with a higher PV installation capacity might install a system that is close to the PV system size in consideration. A 100 kW system can be installed by establishments that have the capacity to install PV systems in the range of 96 kW to 5,000 kW. It is important to note that the estimate for number of establishments that might install the four sizes of PV systems is across the three industry categories of transportation and warehousing, wholesale trade and manufacturing.

6.9 Return On Investment (ROI)

Based on the methodology presented in Section 6.4 and the results presented in Section 6.5, which used 2010 PV system cost estimates, Return on Investment (ROI) payback periods for warehouse rooftop solar PV systems are between eight and nine years. Because PV prices are currently lower than in 2010, current typical payback periods will be shorter,however, a key unknown is the future of the 30% federal solar Investment Tax Credit (ITC) which has been extended until 2016. If the ITC is not extended past 2016, significantly fewer warehouse solar PV systems will be installed because the ROI payback period will be longer. Additional factors include state incentive programs like the California Solar Initiative which are capped at certain levels. If these programs are not renewed/extended they might affect the economic calculations for investment in rooftop PV systems.

Based on methodology and results presented in Section 6.5 which includes data from the 2011 Census data the Commercial Buildings Energy Consumption Survey (CBECS) data, the

estimated number of warehouse buildings which could potentially install solar PV section is shown in Figure 129.

Figure 129: Estimated Total Number of Solar PV Installations

PV System Size (kWdc)	Number of Warehouse Establishments in the five zip codes
100	743
1000	52
2500	10
5000	4

Chapter 7
Project Conclusions, Recommendations and Benefits

7.1 Conclusions

High penetration of residential-scale PV introduces unique challenges to the distribution impact study process because (1) the individual PV units are finely distributed, and (2) the variations in output of individual PV units are correlated to a variable degree as a function of geographic separations between their locations. During clear-sky conditions, the output of all PV on a feeder will follow approximately the same smooth diurnal curve over the course of the day. During solidly-overcast conditions, the output is also relatively smooth, following a scaled (20% - 40%) proportion of the clear-sky curve. Impacts of distributed residential PV on voltage during these totally-clear and totally-overcast conditions can be readily evaluated by conventional distribution load-flow analysis techniques because the PV output can be accurately represented as a modifier of the load pattern (i.e., a "negative load").

It is during partly-cloudy conditions, however, that the output of a PV unit is most variable and has the greatest impact in terms of voltage variability and tap-changer duty. The variations in output of an individual PV unit are the result of cloud shadows passing over that location. The size of a typical cloud shadow, during partly-cloudy conditions, is typically much smaller than the geographic footprint of a typical distribution feeder. Therefore, the shadow will usually only affect a portion of the total PV capacity on the feeder at any given time, assuming the PV penetration consists of finely-distributed small residential units. As the shadows move across the landscape at the speed of the wind at cloud height (most typically in the range of 10 – 50 km/h), different areas of the feeder will be shadowed at different times. It is also likely that a feeder's geographic area may experience multiple shadows simultaneously, and as a shadow moves off of the feeder footprint on the downwind side, another shadow may move on to the footprint on the upwind side. The net result is that there will be diversity in the PV output variations.

The diversity of finely-distributed residential-scale PV output variations needs to be appropriately considered when performing PV impact assessment in order to provide results that are neither extremely pessimistic nor extremely optimistic. The degree of PV output correlation is a function of (1) distance between units and (2) the time scale of the PV output power variation; neighboring PV units are highly correlated because they experience the same cloud shadows nearly simultaneously. On the other hand, PV units that are distant from each other will have short-term variability that is substantially uncorrelated. A study performed by the National Renewable Energy Laboratory (NREL) has shown that the coefficient of correlation for two-minute PV output variations drops below 50% if adjacent PV units are displaced by 200 - 300 meters. The correlation is less sensitive to the distance between PV units when looking at variations of a larger time scale; NREL has shown that the correlation of five minute variations begins decreasing when adjacent PV units are displaced by more than approximately one kilometer [63]. Thus, on a feeder-wide basis, the aggregate PV output may be greatly smoothed

by this geo-spatial diversity, while aggregate output within local areas will remain highly variable. Phase balance is also affected because single-phase laterals tend to serve concentrated geographic areas. Clouds may shadow whole laterals at a time, causing erratic changes in phase balance.

As a result of this geo-spatially dependent correlation of PV output variations, the impacts of high-penetration residential-scale PV on distribution voltage, phase balance, and equipment duty cannot be adequately assessed by conventional distribution system analysis techniques and tools. Using a single PV output pattern for all PV units within a feeder will result in voltage variability severity far exceeding that which will occur in reality. While highly conservative, the results will either drive unnecessary system upgrades or unnecessary restrictions on PV interconnection. On the other hand, applying an aggregated output pattern to all PV units will be very optimistic and may not expose significant impacts that may actually occur.

7.2 Recommendations

Additional follow up research is recommended to assess the effects of geo-spatially dependent correlation of PV output. A very rigorous approach to making this assessment of finely-distributed PV impacts is to individually model each of the PV units, as well as the progression of cloud shadows over the feeder footprint, in an extended Quasi-Steady-State (QSS) load-flow simulation [64]. EnerNex has recently performed such an analysis as part of a research project for the California Energy Commission under contract CEC-500-2010-060. Cloud patterns and movement in this study were derived from actual conditions using a recently-developed sky camera and image processing system developed by the University of California at San Diego. This rigorous approach, however, is very time consuming and requires very specialized data. With the tools presently at the typical utility distribution planner's disposal, and the constraints of available time and engineering manpower, such an approach is not practical for routine usage by utilities confronted with high-penetration PV. Instead, a simpler, more efficient methodology is needed.

The objectives of the recommended follow up research are (1) to evaluate the impact of high-penetration residential-scale PV on voltage variability, phase balance, and voltage regulator duty for a range of common scenarios, (2) explore various approximations that can be implemented in the analysis tools used by the industry, (3) validate the approximations against detailed analysis, and (4) provide guidelines for the practical application of the analysis methodology.

7.3 Benefits

During this study, increasingly higher levels of solar PV penetration occurred in California. Understanding the effects of solar PV on the grid will enable higher penetration levels of solar PV to be installed, helping California meet its renewable energy goals. Accurate forecasting of solar PV output in cloudy conditions will allow for more efficient integration and use of solar PV output, helping California reduce GHG emissions.

The research showed that distribution feeders could successfully handle high penetration levels of solar PV including situations where reverse power flows occurred when solar PV production exceeded feeder load. Changes in protection schemes on some distribution feeders would be needed in cases where the additional short circuit contribution from the PV installations is significant. Forecasting ability 15 minutes in the future and ramp rate prediction can help utilities manage solar PV systems operationally.

Chapter 8
Technology Transfer

The project research has two main outputs suitable for technology transfer:

1) Solar forecasting hardware systems and algorithms for intra-hour and other time frames incorporating cloud forecasts

2) Impacts of and recommended protection schemes for high penetration levels of utility scale PV systems, including protection approaches for cases where the additional short circuit contribution from the PV installations is significant.

The USRE cloud location and solar generation prediction algorithms, the sky imagers, and algorithms which can assess the impact of solar PV systems on utility distribution systems and transmission systems are all items which are potentially transferable to industry through several well established mechanisms including technical papers, conference presentations, and commercialization activities.

8.1 Technical Papers

Technical papers will document results and provide referenceable material from the USRE project which will publicize results and facilitate technology transfer. Technical papers accepted for conferences allow a direct transfer of research results to conference attendees. Technical papers have been and will be submitted to the Institute of Electrical and Electronics Engineers (IEEE) Power & Engineering Society (PES).

The process to having a technical paper accepted for publication is to first submit an abstract which is then reviewed by the sponsoring organization's technical committee members. Papers accepted are published in the group's journals or in their publications. In addition, technical papers may be selected for conference presentations, for poster sessions or for other conference events. Once selected, one of the paper's authors is invited to present results at the conference. In addition, the accompanying paper and the presentation are contained in the formal conference journals, allowing them to be accessed, read and potentially leveraged for further efforts.

For the IEEE, the research team has or will submit abstracts to the main Power & Engineering Society and to the Innovative Smart Grid Technologies (ISGT) sub group of the PES. When accepted, papers will be presented to conference attendees in various formats including presentations, panels and poster sessions.

8.1.1 IEEE Organization Overview

The IEEE describes itself as the "world's largest professional association for the advancement of technology." Within the IEEE, the Power & Engineering Society provides the world's largest forum for sharing "technological developments in the electric power industry, for developing standards that guide the development and construction of equipment and systems, and for

educating members of the industry and the general public." Thus the IEEE PES is an appropriate organization for disseminating USRE research results.

8.1.2 IEEE Power & Energy Society General Meetings

PES General Meetings are hosted world-wide. The aim of the PES General Meetings is to provide an international forum for experts to promote, share, and discuss various issues and developments in the field of electrical power engineering.

In 2012, the General Meeting was held in San Diego, California providing wide exposure to results particularly to California-based entities. Specifically the 2012 IEEE Power & Energy Society General Meeting (GM) was held July 22- 26 at the Manchester Grand Hyatt in downtown San Diego. The theme of the conference was New Energy Horizons – Opportunities and Challenges.

An abstract and paper were accepted for the conference and USRE technical results were presented. See APPENDIX A. USRE White Paper Submitted to the 2012 IEEE PES paper. Ms. Kay Stefferud, the USRE Program Manager presented the paper at a poster session at the PES conference.

8.1.3 IEEE Innovative Smart Grid Technologies (ISGT) Conference

The IEEE Innovative Smart Grid Technologies (ISGT) conferences are held annually in the US and also in Europe. Similar to the PES GM meetings, the ISGT conferences offer the opportunity to provide referenceable project results and to present directly to conference attendees.

The 2014 IEEE Conference on Innovative Smart Grid Technologies will be held on February 19-22, at the Washington Grand Hyatt in Washington D.C. The ISGT is a forum for participants to discuss state-of-the-art innovations in smart grid technologies and will feature plenary sessions, multi-track panel discussions, technical papers and poster presentations as well as tutorials by international experts on smart grid applications.

EnerNex and SCE USRE team members collaborated on a paper submitted to the 2014 IEEE ISGT conference. The ISGT paper is summarized in the abstract in Figure 130. The content of the technical paper submitted to the ISGT conference can be found in Appenix B.

Figure 130: USRE ISGT Conference Paper Abstract

Abstract— Distributed large and small-scale renewable generation including solar photovoltaic (PV) installations are rapidly increasing on California residential, commercial, and industrial distribution lines. Utilities have to be prepared for potential issues caused by increased PV penetration on their systems. EnerNex and Southern California Edison are currently conducting a study for the California Energy Commission to investigate the effects of high penetration levels of PV on distribution systems. Part of this investigation is to quantify, through computer simulations and measured solar irradiance data, the effects of an estimated 200 MW commercial-scale PV generation to be installed by 2015 in SCE service territory. The study examines the effects of 3 large rooftops systems totaling 6.5 MWs on an industrial feeders in SCE's southern California territory. Our analyses considered 8 potential issues on high penetration PV distribution feeders. Significant findings include 1) reverse power flows occur during times of high PV generation, 2) voltages remain within permissible ranges even when large loads are dropped and 3) settings for the protective relays need to be adjusted to account for the reverse power flows.

8.1.4 Conference Presentations

Conferences offer the opportunity to present results to technical experts. Conference presentations are archived and distributed to participants and sometimes to organization members. The distinguishing difference between conference presentations and technical papers, is that conference presentations are typically documented in PowerPoint format, while technical papers are formally written as research papers.

Abstracts for conference presentations have or will be submitted to the Utility Variable-Generation Integration Group (UVIG), to DistribuTECH Brasil, to the main DistribuTECH held in the United States.

The process of presenting at a conference is to first submit an abstract which is then reviewed by the sponsoring organization's technical committee members. Abstracts may be selected for conference presentations, for technical expert panels, for poster sessions or for other conference events. Once selected, one of the abstracts authors is invited to present results at the conference. In addition, the presentation is contained in the formal conference journals and frequently on-line, allowing project results to be accessed, read and potentially leveraged for further efforts.

8.1.5 UVIG Organization Overview

The Utility Variable-Generation Integration Group (UVIG), previously known as the Utility Wind Integration Group (UWIG), was established in 1989 to provide a forum for the critical analysis of solar and wind technology for utility applications and to serve as a source of credible

information on the status of solar and wind technology and deployment. UVIG's mission is to accelerate the development and application of good engineering and operational practices supporting the appropriate integration and reliable operation of variable renewable generation on the electric power system.

8.1.6 UVIG Fall Technical Workshop

The 2013 Utility Variable Integration Group (UVIG) Fall Technical Workshop will provide attendees with an expanded perspective on the status of wind and solar integration and interconnection to utility systems in the United States and other countries. The UVIG technical workshop focuses on topics related to integration and interconnection of wind and solar generation. Events include meetings of the UVIG User Groups focusing on variable generation operating impacts, market operation and transmission planning, variable generation modeling and interconnection, and distributed generation. The technical workshop agenda covers variable generation integration studies, distribution system issues, variable generation forecasting, VG integration topics, energy storage, and industry updates. Thus UVIG Technical Workshops are appropriate avenues to disseminate USRE project results.

The 2013 UVIG Fall Technical Workshop will be held on October 29-31, at the DoubleTree by Hilton Hotel in Portland, Oregon. EnerNex submitted an abstract to the conference (Figure 131).

Figure 131: Abstract Submitted to the UVIG 2013 Fall Technical Meeting

U

Impact of High Photovoltaic Penetration on Distribution Feeders in the United States

***Abstract*—**

Small-scale renewable generation is being incentivized in the United States and globally resulting in increasing numbers of photovoltaic (PV) installations in residential, commercial, and industrial buildings. Utilities have to be prepared for potential issues caused by increased PV penetration on their systems. EnerNex, the University of California in San Diego, and Southern California Edison are currently conducting a study for the California Energy Commission to investigate these issues. Part of this investigation is to quantify, through computer simulations and measured solar irradiance data, the effect of the 250 MW commercial-scale PV generation to be installed by 2015 in SCE service territory.

We have modeled and validated two SCE distribution circuits with high penetration levels of PV. The generation levels of each of the PV generators were individually determined from irradiance data taken from field measurements.

Aggregation is a common engineering modeling practice to lump individual generators and loads together into fewer parts. Aggregation applied to PV integration studies artificially reduce the variability in the system resulting in non-conservative simulation results for assessments of PV caused wear-and-tear on voltage regulation equipment. In our modeling approach, we do not use aggregation techniques and use measured irradiance data at individual locations. The data collection period has been over 1 year and accounts for seasonal changes and cloud shading. Consequently, we capture the time-of-day variation of the power generated by each PV generator in a highly realistic fashion.

We applied the model to investigate the following effects of the PV installed on the SCE distribution feeder: (1) voltage control, (2) the most probable n-1 contingency effects, and (3) overcurrent and relay protection.

UVIG states that their forecasting workshop is the leading workshop on wind and solar forecasting. The workshop is intended for utility, wind and solar industry personnel associated with producing and using variable generation (VG) plant output forecasts for power system operation. The workshop:

- Developed a better understanding of the value of VG forecasting in the day-ahead, hour-ahead and real-time periods.
- Explored the practical aspects of the use of VG forecasting models to the scheduling and operation of power systems.
- Developed a better understanding of VG forecasting developments on the horizon.
- Continued an ongoing dialog between the VG forecasting.

The emphasis on forecasting at the workshop makes this conference a particularly fitting avenue for disseminating USRE forecasting results. The USRE project team will submit one or more abstracts to the UVIG Forecasting Conference. The UVIG Forecasting Conference will be held February 25-26, 2014 in Tucson, Arizona at the Westin La Paloma.

8.1.7 DistribuTECH Conferences

The organizers bill DistribuTECH as the utility industry's leading annual transmission and distribution event, covering automation and control systems, energy efficiency, demand response, renewable energy integration, advanced metering, T&D system operation and reliability, power delivery equipment, commercial and industrial energy management technology and water utility technology. DistribuTECH is widely viewed as the most important utility commercially-orientated conference. As such, it is more difficult to present at a DistribuTECH conference than at other conferences.

The USRE project team will submit or has submitted abstracts to the 2012, 2013 and 2014 DistribuTECH conferences held in the United States and in Brazil. The USRE abstracts were accepted for the 2012 and 2013 Brazilian DistribuTECH conferences.

For 2013, results from both the CEC USRE project and a California Solar Initiative (CSI) study will be briefed at DistribuTECH Brazil. Sample presentation charts from the 2013 DistribuTECH Brazilian conference are shown in Figure 132. In the figure, System B represents the SCE feeder analyzed for this USRE project with the three solar PV systems totaling 6.5 MWs.

Figure 132: Brazil DistribuTECH Sample Charts

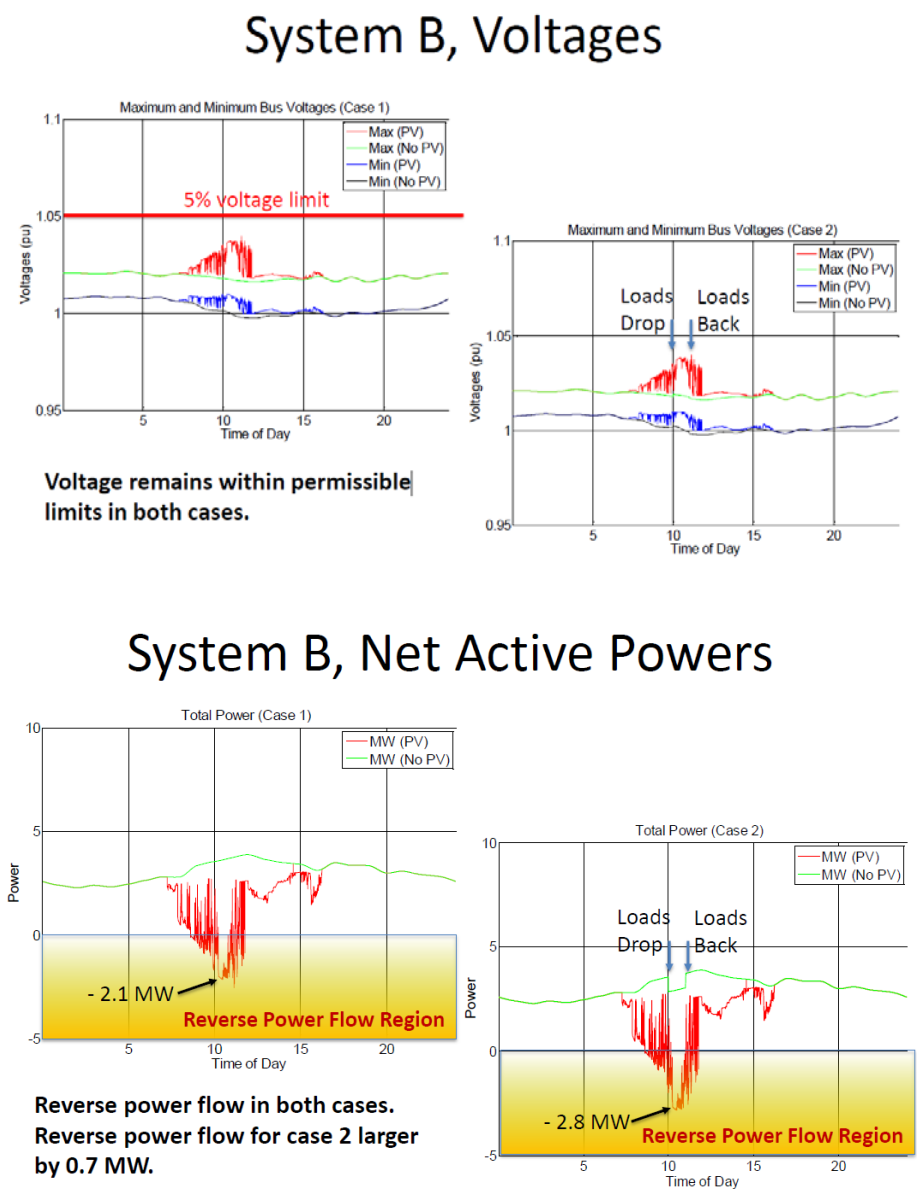

8.2 Commercialization Potential

In addition to presenting technical results in papers and at conferences, the USRE project team is exploring commercialization efforts. Potentially, the USRE cloud location and solar generation prediction algorithms, the sky imagers, and the algorithms which can assess the impact of solar PV systems on distribution and transmission systems are all items which are potentially transferable to industry.

8.2.1 USRE Project Opportunity Background

As California marches forward toward meeting its mandated Renewables Portfolio Strategy (RPS) target of 33% by 2020 and the Governor's additional renewables mandate of 12GW, a number of challenges have arisen as PV and other renewables penetration rates have increased. Projected capacity for California-wide customer-installed PV systems is projected to be more than 3GW in 2016. With SDG&E reporting a 3% monthly increase in solar capacity and SCE reporting greater than 100% solar penetration on some distribution lines, the impact of distributed energy resources (DER) must be addressed. Further protection schemes and real time operational procedures need be revised to accommodate existing and future distributed energy resources.

The existing electric grid was designed and created to safely and reliably distribute power from a few concentrated power generation sources through highly monitored and controlled transmission lines to typically radially distributed loads. Distributed Generation (DG) puts new demands on this existing electric infrastructure by introducing electric generation sources distributed throughout the distribution grid. Today's power distribution networks have limited visibility, diagnostic, control and forecasting capabilities. Distribution grid operator's visibility to distributed level penetrations of PV is limited to either sites with integrated SCADA (generally larger > 1 MW), or assumptions based upon irradiance measurements at nearby locations. Operators are blind to locations with highly distributed PV and no communication or measurement of irradiance in close proximity. In addition, as penetration rates increase on distribution circuits, they introduce new challenges that range from reverse power flows, to inverter control loop feedback, to potential instability and sub-optimal performance. As solar PV systems proliferate, synergistic PV forecasting and control strategies can help not only integrate solar PV into the grid but can also help optimize local distribution grid performance.

The detrimental impact of large volumes of PV on an unprepared grid involve (1) voltage violations (2) flicker and other power quality issues, (3) reverse power flow and protection coordination issues, (4) increased wear on utility equipment, and (5) real and reactive power imbalances. The SkyCam system in concert with distribution circuit operating controls can help mitigate the impact and compensate for relevant conditions and anomalies on distribution circuits including transient and dynamic voltage fluctuations, reverse power flow, unintentional islanding and local thermal impacts.

Variability in ground-level solar irradiance makes regulating and maintaining power both challenging and costly, as the uncertainty requires larger regulation and spinning reserve

capacities to meet ancillary service requirements. Reduction in the uncertainty of solar power using solar forecasting methods can not only reduce the more expensive operating costs of ancillary services, but also allow utilities, CAISO, and energy traders to plan for and make more reliable bids in the wholesale energy markets to mitigate solar PV volatility. Of particular interest to the energy industry are sudden changes in irradiance, termed "ramp events" (Pfister et al., 2003). Ramp events in turn require ancillary services to ramp up or down to meet the change in electrical supply and maintain power quality. Clouds can result in such ramp events causing reductions in output by 50 to 80% within the time period it takes a large cloud to cover a solar array, typically on the order of 5-10 seconds. Short-term irradiance changes can cause voltage fluctuations that can trigger automated line equipment e.g. tap changers on distribution feeders leading to larger maintenance costs for utilities. Given constant load, counteracting such fluctuations would require dynamic inverter VAR control or a secondary power source e.g. energy storage that could ramp up or down at high frequencies to provide load following services. Such ancillary services are costly to operate, so reducing short-term variation is essential. Longer scale variations caused by cloud groups or weather fronts are also problematic as they lead to a large consistent reduction in power generation over a large area. These long-term fluctuations are easier to forecast and can be mitigated by slower ramping with larger supplementary power sources, but the ramping and scheduling of power plants also adds costs to the operation of the electric grid. Grid operators are often concerned with worst-case scenarios, and it is important to understand the behavior of PV power output fluctuations over various timescales.

Therefore, solar forecasting plays a critical role in the integration of utility scale renewable energy (USRE). Accurate forecasts would allow load-following generation that is required to counteract ramps from USRE to be scheduled in the lower cost day-ahead market. Recent integration studies by National Renewable Energy Laboratory (NREL) and General Electric (GE) using 2020 renewable integration scenarios have shown economic values of renewable forecasting of $5 billion/year under 2020 USRE scenarios for the Western Electricity Coordinating Council (WECC) alone. With the advance of smart grid efforts the once autonomous operation of distribution system will also benefit from solar forecasting and solar resource variability analysis.

8.2.2 Overall USRE Project Market Opportunities

California's three Investor Owned Utilities (IOUs) have more than 10,000 distribution circuits operating between 2.4kV-34kV with another 8,000 distribution circuits operated by the state's forty Publicly Owned Utilities (POUs). These distribution circuits represent a wide range of rural, suburban, and urban typologies from long 'flexible' rural/mountain/desert circuits (e.g. 50 miles) to fully blended residential, commercial, and industrial usage with current PV penetration rates approaching 30-50% and projected PV penetration rates equaling total distribution circuit capacity. SCE has estimated that for their territory (four million customers) the cost difference for upgrading their distribution circuits to manage just their portion of California's additional 12GW mandate will have financial impacts that will range from $2.1 billion to as much as $4.5 billion (depending upon location, concentration, and specific circuits).

Studies performed by EPRI suggests even higher impacts to handle DER on distribution circuits that could range from $2-3.5 million/circuit. Additionally, studies performed by Navigant on behalf of CEC showed that at PV penetration rates of 50%, many urban and most rural distribution circuits will experience either voltage or capacity violations. Finally, the impact of PV penetration is also a strong function of its relative distribution on the circuit and that the costs to integrate and/or mitigate high levels of PV penetration can double for clustered PV locations, as would be the case for large PV farms.

Total U.S. electric consumption in 2011 was 4,200 GWh (290 GWh for California) and is valued at approximately $450 billion annually ($50 billion annually for California). Nationally, solar PV accounts for only .03% of total electric production while wind accounts for 2.3%. In contrast, for California, solar PV accounted for over 0.5% of electric energy production with over 440 MW of capacity compared to CAISO's 54 GW of controlled capacity for the state (excludes LADWP's 8 GW). The Energy Commission is projecting that by 2016, California will have more than 3GW of installed solar PV. Dozens of other states also have aggressive RPS mandates; consequently, they will also experience similar distribution upgrade costs as California, perhaps delayed in time. Nationally, the costs for distribution circuit upgrades to handle high penetration PV is estimated to be in the range of $350-650 billion during the next ten years. Although preliminary, estimates for the impact of better PV forecasting, algorithms, and distribution operations that reduce capital expenditures for compensating equipment and protective devices as well as ancillary services for grid support range from 5-15% or from $15-100 billion potential impact over the next ten years for an annualized market opportunity of $1.5-$10 billion/year. Expressed on a per distribution circuit basis indicates that on average the SkyCam system may impact

Several aspects of the project have potential commercial value especially forecasting and control algorithms. The following sections describe the commercial potential of various outputs from the USRE project.

8.2.3 Distribution Control Algorithms

Solar PV systems, particularly at high penetration levels, can cause issues on the grid such as difficulties controlling voltage and frequency, particularly for systems located at the end of distribution lines. However, solar inverters with advanced feature capabilities can also provide benefits to the grid. For example, inverters could be used to control the power ratio of real and reactive power generated from solar PV systems. Thus solar inverters with advanced functionality could improve power quality and help control voltage and frequency on distribution lines.

Using the solar inverters, future versions of Distribution Management Systems (DMSs) could monitor solar production and issue commands in real time to improve efficiency by raising or lowering voltage. Alternatively DMSs could sound alarms to distributions operations personnel who could then manually take action to modify solar generation or distribution equipment functions. Thus control algorithms implemented in DMS system could improve grid operations and reduce costs.

Distribution control can also be implemented using autonomous settings e.g. by setting control parameters in solar inverters or on distribution control devices such as tap changers and capacitors. In addition to potentially improving distribution line power characteristics, control settings could potentially reduce the amount of wear and tear on control equipment.

The potential commercialization aspects of distribution control algorithms include the possibility of embedding algorithms in DMSs, in solar inverters, in distribution operations applications, and in distribution planning systems. Algorithms could be used to predict optimal equipment settings during modeling and planning for distribution line upgrades, for generating alarms in real time for distribution operations personnel, and for optimizing solar production of marketable ancillary services such as volt/VAr control.

8.2.4 Transmission Control Algorithms

Large utility scale PV systems, for example those in the 50 MW AC range, can connect directly to transmission lines, typically with a dedicated substation. These large utility-scale solar plants need to operate in a similar fashion to traditional generation and also in a similar fashion as large wind farms. For example, large PV plants can reduce ramps rates caused by clouds.

The ability to forecast production is an identified gap capability for commercial solar product manufacturers and for solar system installers within California and world-wide. The ability to forecast production could potentially help to determine when solar ramp restrictions are needed. Further generation estimates enhanced with increased accuracy from the maximum ramp rate changes, a project research output, can help in development of commercial products including master inverter controllers, large utility scale inverters roughly defined as those larger than 1MW AC, and in modeling and simulation products which can help estimate the size of energy storage devices.

The potential commercialization aspects of transmission control algorithms include the possibility of embedding algorithms in large solar inverters, in master inverter controllers, in solar generation monitoring and control systems and in Energy Management Systems (EMSs) for solar plants.

8.2.5 Sky Cameras and Forecasting Algorithms

The sky cameras and forecasting algorithms (SkyCam) partially developed under the USRE project can be used in commercial solar forecasting products similar to existing applications for wind farms. Currently SCE uses manual methods which employ meteorologists to predict generation and ramp rates from solar PV systems. Solar forecasting applications are needed by utilities and by the CAISO. Of particular applicability to the USRE project, are applications which can predict intra-hour solar production and solar ramp rates.

Because ramp rates largely determine the amount of backup spinning reserves or energy storage systems needed to modulate solar variability, the economic value of solar forecasting of ramp rates and solar generation is significant. Commercialization of the forecasting algorithms could be performed by commercial companies such as AWS TruePower and Garrad Hassan.

In proceeding with potential commercialization activities for the SkyCam system, it is important to identify the key elements of intellectual property, competitive advantages, and market drivers that could potentially be used as a basis for commercialization. Appendix C provides a proposed Table of Contents for a business plan for the SkyCam System followed by descriptions of some of the more important commercialization discussion areas. Development of a full business plan is beyond the scope of the USRE project; however UCSD and EnerNex are collaborating on the initial stages of business plan development.

8.2.6 Commercialization of USRE Project Results

To pursue commercialization, EnerNex, Advantech and UCSD will develop a business plan which will cover basic elements needed to determine the viability of commercialization of USRE results. One possible avenue to pursue is venture capitalist funding from companies in California. Other avenues to pursue are transfer of the technology to forecasting applications, to utility applications and to CAISO applications.

To successfully transfer technology, relevant business analyses including determining the value proposition, marketing potential, competitive advantage, changing PV needs, market size, market opportunities, manufacturing considerations, Intellectual Property (IP), financial analyses and Return on Investment (ROI) need to be considered. The USRE project results may be used to provide the proof of concept and the working prototypes needed to pursue market development. If the business analyses indicate commercialization is potentially viable, EnerNex will contact venture capitalists (VCs) in California to determine if there is interest in funding further commercialization efforts.

GLOSSARY

Term	Definition
AC	Alternating Current
AFD	Active Frequency Drift
AMI	Advanced Meter Infrastructure
APS	Automatic Phase Shift
BOM	Bill of Materials
BOS	Balance of System
c.f.	Chopping Factor
CAISO	California Independent System Operator
CAP	Cloud-Advection-versus-Persistence
CAPEX	Capital Expenditures
CBECS	Commercial Buildings Energy Consumption Survey
CBH	Cloud Base Height
CBM	Conditioned-Based Maintenance
CCD	Charge-Coupled Device
CDF	Cumulative Distribution Function
CEC	California Energy Commission
CIMIS	California Irrigation Management Information System
CPP	Critical Peak Pricing
CPR	Clean Power Research
CPR	Critical Project Review
CPUC	California Public Utilities Commission
CSI	California Solar Initiative
CSL	Clear Sky Library
D-STACOM	Distribution Static Compensator
DC	Direct Current
DER	Distributed Energy Resources
DG	Distributed Generation
DLC	Direct Load Control
DMS	Distribution Management System
DR	Distributed Resource
EMS	Energy Management System
EMT	Electromagnetic Transient
EPRI	Electric Power Research Institute
EPW	Energy Plus Weather
EPS	Electric Power System
ESP	Energy Service Provider
EVSE	Electric Vehicle Service Equipment

Term	Definition
FDR	Frequency Disturbance Recorder
FS	Forecast Skill
GE	General Electric
GEFS	GEFS
GM	General Meeting
GPS	Global Positioning System
HDR	High Dynamic Range
IEEE	Institute of Electrical and Electronics Engineers
IOU	Investor Owned Utility
IP	Intellectual Property
ISGT	Innovative Smart Grid Technologies
ISO	Independent System Operator
ITC	Investment Tax Credit
Km	Kilometer
KSBD	San Bernardino airport
kV	Kilovolts
kVAr	Kilovolt-amperes reactive
kW	Kilowatt
LADWP	Los Angeles Department of Water and Power
LF	Load Following
LOMD	Loss of Mains Detection
LTC	Load Tap Changer
LVRT/ZVRT	Low/Zero Voltage Ridethrough
MAE	Mean Absolute Error
MBR	Mean Bias Error
MACRS	Modified Accelerated Cost Recovery System
METAR	MEteorological Terminal Aviation Routine Weather Report
MPP	Maximum Power Point
MPPT	Maximum-Power-Point Tracking
MVAr	Mega Volt Ampere Reactive
MW	Megawatt
NAICS	North American Industry Classification System
NDZ	Non-Detection Zone
NREL	National Renewable Energy Laboratory
NSRDB	National Solar Radiation Data Base
NWP	Numerical Weather Prediction
O&M	Operations and Maintenance
PAR	Project Authorization Request
PCC	Point of Common Connection

Term	Definition
PES	Power & Engineering Society
PET	Power Electronic Transformer
PEV	Plug-in Electric Vehicle
PF	Power Factor
PIRP	Participating Intermittent Resource Program
PLL	Phase-Locked-Loop
PLLC	Power Line Carrier Communication
PMU	Phasor Measurement Unit
PNG	Portable Network Graphics
POU	Publicly Owned Utility
PPA	Power Purchase Agreement
pu	Power Unit
PV	Photovoltaic
RBR	Red Blue Ratio
RGB	Red Green Blue
rMAE	Relative Mean Absolute Error
rMBE	Relative Mean Bias Error
RMS	Root-Mean-Square
ROI	Return On Investment
RPS	Renewables Portfolio Strategy
RTO	Regional Transmission Organization
SAM	System Advisor Model
SCADA	Supervisory Control And Data Acquisition
SCE	Southern California Edison
SFS	Sandia Frequency Shift
SIWG	Smart Inverter Working Group
SLG	Single-Line-to-Ground
SMS	Slip Mode Frequency Shift
SPVP	Solar Photovoltaic Program
SST	Solid State Transformer
SVS	Sandia Voltage Shift
THD	Total Harmonic Distortion
TOC	Table of Contents
TOU	Time of Use
TOV	Temporary Over Voltage
TMY	Typical Meteorological Year
UC	Unit Commitment
UCSD	University of California San Diego
UFP/OFP	Under/Over Frequency Protective Relay
USI	UCSD Sky Imagers

Term	Definition
USRE	Utility Scale Renewable Energy
UTC	Coordinated Universal Time
UVIG	Utility Variable-Generation Integration Group
UVP/OVP	Under/Over Frequency Protective Relay
UWIG	Utility Wind Integration Group
V	Volts
Var	Volt Ampere Reactive
VC	Venture Capitalist
vdc	Voltage DC
VG	Variable Generation
VSI	Voltage Source Inverter
WAMS	Wide Area Measurement Systems
WECC	Western Electricity Coordinating Council

REFERENCES

Following information in the public domain was reviewed for this report.

http://censtats.census.gov/cgi-bin/zbpnaic/zbpsect.pl

http://www1.eere.energy.gov/solar/sunshot/pdfs/dpw_white_paper.pdf

http://www.eia.gov/consumption/commercial/data/2003/#b1

http://emp.lbl.gov/sites/all/files/lbnl-5919e.pdf

http://www.energy.ca.gov/2013publications/CEC-400-2013-005/CEC-400-2013-005-D.pdf

http://www.greentechmedia.com/articles/read/solar-pv-bos-cost-trends-in-the-u.s

http://www.nrel.gov/docs/fy13osti/56776.pdf

http://www.rmi.org/Content/Files/BOSReport.pdf

APPENDIX A: USRE White Paper Submitted to the 2012 IEEE PES General Meeting

Solar Forecasting and Variability Analyses using Sky Camera Cloud Detection & Motion Vectors

K. Stefferud, *Member, IEEE*, J. Kleissl, *Member, IEEE*, and J. Schoene, *Member, IEEE*

***Abstract*—Prediction of cloud location greatly increases the accuracy of solar generation forecasts when used in conjunction with regional meteorological data and historic data. Novel granular forecast techniques reduce intra-hour and minute-by-minute solar forecasting error by 50% compared to persistence models [3]. Our work creates cloud shadow maps on the ground to forecast power production ramps geospatially tagged and circuit topographically located to individual sites and aggregately to all sites on a distribution feeder. These forecasting data may be used to (1) reduce the detrimental impact on distribution systems due to voltage fluctuation caused by high PV penetration and (2) optimize utility operational and planning practices in the presence of high generation variability due to the presence of PV.**

***Index Terms*—photovoltaic, power generation, renewable energy, solar, power distribution lines**

I. Introduction

Solar power and other Utility Scale Renewable Energy (USRE) present a significant challenge because of high variability and uncertainty [1] compared to conventional generation, while at the same time solar generation is subject to environmental factors which are not controllable. Increasing amounts of solar generation is being installed and planned in California which currently has 1,000 MW of rooftop solar power installed [6]. Grid operators are often concerned with worst-case scenarios, and it is important to understand the behavior of photovoltaic (PV) power output fluctuations over various timescales.

Opaque clouds cause reductions in output by 50 to 80% within the time period it takes a large cloud to cover an array, which typically ranges from a few seconds for a kW facility to a few minutes for a hundreds of MW utility scale plant [7]. Short-term irradiance fluctuations can cause voltage fluctuations that can trigger automated line equipment (e.g., tap changers) on distribution feeders leading to higher maintenance costs for utilities due to equipment wear [13]. Given constant load, counteracting such fluctuations would require dynamic inverter var control or a secondary power source (e.g., energy storage) that could ramp up or down at high frequencies to provide load following services. Energy storage is costly and dynamic var control is currently not (yet) permitted through IEEE 1547 [8, 9], so reducing short-term variation is essential.

Longer scale variations caused by cloud groups or weather fronts are problematic as they lead to a large reduction in power generation over a large area. Long-term fluctuations are easier to forecast and can be mitigated by slower ramping (but larger) supplementary power sources, but the ramping and scheduling of power plants also adds costs to the operation of the electric grid.

Solar forecasting plays a critical role in the integration of USRE. Accurate forecasts would allow generation that is required to counteract long-term variability from USRE to be scheduled in the lower cost day-ahead market. Recent integration studies by NREL and GE using 2020 renewable integration scenarios have shown economic values of wind and solar forecasting of $5 billion/year under 2020 USRE scenarios in WECC alone [5].

Utility infrastructure upgrades and the use of smart inverters on the distribution system will enable applications of solar forecasting and solar resource variability analysis on shorter time scales. Our research addresses the need to accurately forecast the output from solar PV and determine the maximum amount of variability or ramp rate of solar output. Techniques described here are based on the use of a sky imager to locate clouds [3]. Fig. 1 shows the installed sky camera used in this research.

Fig. 1 UC San Diego Sky Imager installed on a rooftop in La Jolla, California.

This work is supported in part by the California Energy Commission under contract PIR-08-043.

J. Kleissl is with the University of California, San Diego 92093 USA (e-mail: jkleissl@ucsd.edu).

J. Schoene is with EnerNex LLC, Knoxville TN 37932 USA (e-mail: jens@enernex.com).

K. Stefferud is with EnerNex LLC, Knoxville TN 37932 USA (e-mail: kay@enernex.com).

II. Cloud Detection Methodology

Sky Imagers can resolve clouds in the sky covering an area of up to 15 square miles, depending on cloud height. Fig. 2 shows a sample sky image and red-blue-ratio (RBR) color enhancement used for cloud detection. Based on images from clear days, the expected RBR is determined and stored in a clear sky library. On cloudy days, the RBR (Fig. 2b) is compared against the clear sky library. If the RBR exceeds the clear sky library by more than 0.18, a pixel is classified as cloudy.

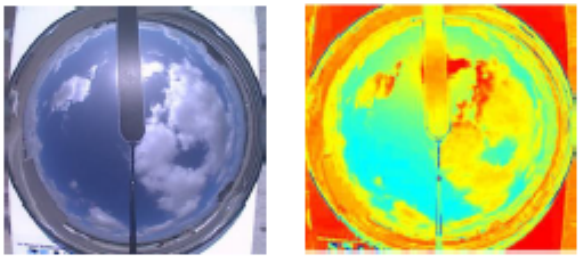

Fig. 2a and 2b: Sample sky image in (a) true color and (b) showing the red-blue-ratio to enhance the contract between clouds and clear sky for automated cloud detection.

III. Cloud Velocity and Shadow Forecast

Cloud velocity is used to advect the clouds detected in Section II forward in time to project shadow locations. Fig. 3 illustrates a cross-correlation method using two images on October 4, 2009 at 161830 and 161900 h. A region of pixels from (a) is correlated to (b) within a search distance. The location of the highest correlation is found and a motion vector is defined. The box is looped over the entire image to obtain a motion vector field and the average of that vector field is determined. In this case the cloud speed was found to be 5 meters per second.

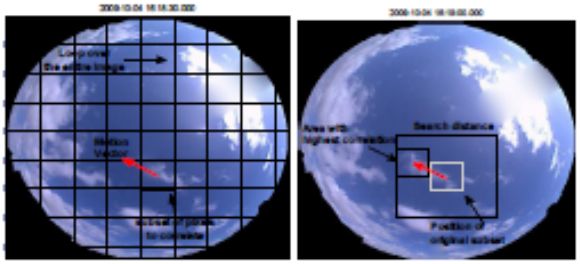

Fig. 3 Cross correlation method used to determine cloud velocity

After advecting the cloud map using the velocity determined in Fig. 3, a binary cloud and clear map is generated. Cloud shadows are then projected onto the ground using the solar azimuth and elevation angles to determine shading of PV systems as shown in Fig. 4. The solar azimuth and elevation angles allow projecting the cloud map onto the ground.

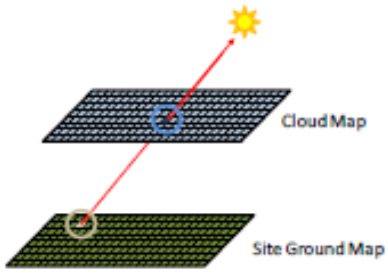

Fig. 4. Cloud forecast map determined from the sky imager.

IV. Power Output and Implementation

Ultimately power output of PV systems must be forecast. With increased granularity, the impact of small clouds and temporary shading can be forecast using the sky imager technique. To do this, the cloud shadow is used to determine which PV systems are affected by clouds. However, irradiances are not measured directly so a cloud optical depth has to be provided. Currently the optical depth is determined from separate irradiance measurements and all clouds are assumed to have the same optical depth. In the case shown in Fig. 5, cloudy periods are assumed to bring about a 60% reduction in irradiance. Fig. 5 shows a comparison of the solar irradiance calculated from the sky imager methodology versus an irradiance sensor measurement.

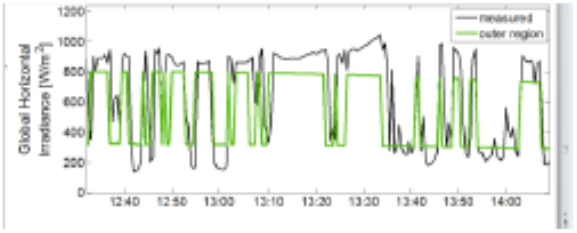

Figure 5: Evaluation of the sky imager forecast (green line) against an irradiance sensor for a 1 hour period on October 4, 2009, at UC San Diego.

V. PV Variability and Forecast Uncertainty

Ramp rate forecast is the key to predicting the variability of solar output. The ramp rate forecast RR [fraction per second] as a function of cloud speed V and cloud optical depth (Δkt) for a single PV site is

$$RR \sim \Delta kt \; V / A^{1/2},$$

where A is the area of the PV array. Given a fixed PV array area, fast-moving and optically thick clouds will cause the largest ramp rates. However, it is extremely unlikely that a cloud will shadow each PV array distributed over a feeder at the same time. So to quantify the variability of a fleet of PV systems, the correlation of power output fluctuations between different PV sites also has to be considered. The correlation is computed separately for different time scales of variability.

Effects from small clouds will be reflected in variability on the order of a few seconds, while effects from large weather systems will be observed in variability over several hours.

Correlations between different sites at different timescales have been quantified at the UC San Diego solar energy testbed [1]. Fluctuation power index (fpi, which is similar to a variance) is used as a measure of relative variability. If the fpi for the average output of a fleet of *n* systems were to be equal to a single system, then the power output variability of the fleet of systems would be *n* times the variability of the single system. In other words, geographic smoothing would not help to reduce the growth in variability.

Fig. 6 shows fpi over different time scales for 1 PV site (black line) and an average of 6 PV sites (red line) spread over 2 square miles at UC San Diego. The number above the black line indicates the reduction in variability. An fpi factor of 6 indicates that the sites are independent and the ramp events at different sites are uncorrelated. This is the case for time scales of up to 2 minutes. For longer timescales (>2 min) the sites become more correlated and the variability is reduced as time scale increases. In general geographic dispersion helps as the relative solar variability decreases as the number of sites increases as can be seen by the decreased (lower) variability for the 6 sites for all time periods. Relative variability of USRE solar PV generation decreases as the size of the plant area increases or as the time scale increases [7].

Given location, size, and distances between the USRE plants, the geographic smoothing effects can be modeled and compared to actual data. It is important to note that these models only consider the typical reduction in variability, but not worst-case scenarios. Such models are mostly useful in economic modeling and long-term operational planning. For example, the effect of the fleet output of the USRE systems could be simulated to determine the typical number of load tap changer operations at a substation in order to schedule maintenance and plan capital expenditures.

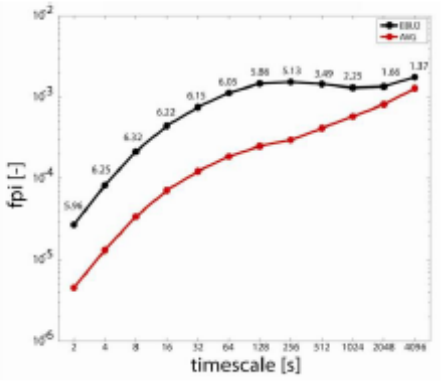

Fig. 6 Relative solar variability at different time scales at a single site (black line) and for the average of 6 separate sites (red line). The numbers above the black line show the factor variability reduction factor.

VI. Impact of Solar Variability on Voltage Fluctuation and Utility Operation Practices

Most utilities control the voltage on the secondary distribution circuit (the low-voltage circuit the customer is directly connected to) by regulating the voltage on the primary circuit (the distribution feeder circuit with typical voltage levels between 4 kV and 35 kV). The service voltage is the stepped-down feeder voltage minus the losses (i.e., service transformer losses and wiring losses). Based on the expected load, utilities design service transformer sizes and the size and length of a service line so that the service voltage stays within acceptable limits. Most regulatory entities and utilities in the USA adhere to the voltage limits specified in ANSI C84.1. Equipment that is at the utilities disposal for regulating the primary circuit voltage includes (1) load tap-changing transformers (LTCs) line and (2) shunt capacitor banks (see Fig. 7).

In general, any control operation of the voltage regulation equipment (tap changing or switching of capacitor steps) is detrimental to the lifetime of the regulation equipment. Voltage fluctuations caused by the presence of PV on the system can cause an excessive number of control operations that can dramatically reduce the equipment lifetime [14].

Another consequence of the more frequent operation of voltage regulation equipment due to the presence of PV is the increasing fluctuation of the reactive power. This has an economic impact on subtransmission and transmission systems. For instance, for a scenario in which PV penetration on the distribution feeder is high and widespread and the capacitor bank is disconnected, some reactive power may have to be supplied from the transmission system. Supplying reactive power from the transmission system is generally more expensive than supplying reactive power locally.

Inverters used in PV and other distributed resources usually have power factor correction capabilities[1]. However, currently IEEE 1547 [8, 9] forbids the distributed resource from actively regulating voltage, which is a somewhat controversial requirement. Opponents of the IEEE 1547 requirement argue that the active PV voltage regulation restriction is counter innovative in that it curbs the full potential of PV inverter technology. A consequence of the IEEE 1547 restriction is that on systems that require active voltage regulation to meet the area electric power system service voltage requirements, equipment other than PVs must be employed to change the reactive power in direct response to measured voltage conditions. Future versions of IEEE 1547 currently under development and review [10] are addressing the possibility of using inverters to assist in power quality control including control of reactive power.

[1] The Distributed Resource (DR) inverters are used to maintain a constant power factor during variable environmental conditions, such as variations in wind speed (in the case of generation from wind) and cloud shadowing (in the case of PV generation).

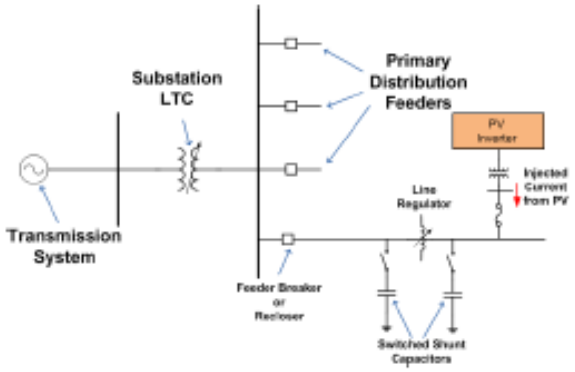

Fig. 7 Radial distribution feeder with voltage regulators and PV.

Voltage fluctuation caused by PV happens on different time scales and the time scale governs (1) the mitigation strategy for which forecasting data may be employed, (2) the forecasting interval that is required, and (3) the type of PV model needed to assess the effectiveness of the mitigation strategy.
Small time-scale voltage fluctuation is caused by cloud transients, that is, the step change of irradiation happening at the transition from one steady-state (e.g., PV generation during clear-sky condition) to another steady-state (e.g., PV generation during cloud shading).

For instance, changing PV generation levels caused by fast changes of irradiation levels due to cloud shading can result in low-frequency voltage fluctuation on the distribution system, which is perceived by the customer in the form of changing light intensity and commonly referred to as "flicker". Complex models of the PV that are capable of simulating the transient response of the inverter are required to simulate the flicker effect and assess the effectiveness of mitigation options. High time resolution forecasting data for a given PV location may be employed for mitigation – the forecasting data would yield information of an oncoming cloud and ramp down the PV output just before the cloud shades the PV thereby avoiding a large step change of PV generation and excessive voltage fluctuation during the transition period from "clear-sky condition" to "cloud shading". After the cloud has passed, the PV output can be ramped up again slowly and in a controlled manner in order to minimize voltage fluctuation.

Large-time scale voltage fluctuation resulting in reactive power fluctuations and operation of voltage regulation equipment is also caused by clouds, but the transition period from high irradiation to low irradiation (or vice versa) is of less importance. Instead, the voltage fluctuates because of changing steady-state generation levels (e.g., full generation during clear-sky condition and reduced generation during cloud shading). Voltage regulation equipment adjustments according to the PV generation levels and frequent changes of the generation level (e.g., during scattered fast-moving clouds) will result in a large number of operations of the regulators, in particular in weak systems and/or systems with large PV penetration. Forecasting data in conjunction with storage may be employed in a control strategy to reduce the number of voltage control operations. A simple quasi steady state PV model where the generation output is scaled according to the insolation level is sufficient for an investigation of the system impact with regards to voltage fluctuation and assessments of mitigation options.

VII. Impacts of Solar Variability on Unit Commitment and Generation Resource Planning

The impact of the variable PV output on the grid affects ancillary services of unit commitment, load following and regulation relevant to generation resource planning, generation and storage plant siting, transmission planning, and economics. Fig. 8 illustrates the effects of variability and uncertainty relative to the ancillary services.

Fig. 8 Relationship between the effects of variability and uncertainty, planning functions, and the ancillary services of unit commitment (UC), load following (LF) and regulation (Reg).

Solar generation variability occurs on a wide range of time frames of utility operation – from real-time minute-to-minute fluctuations through yearly variations affecting long term planning. Solar forecasting must consider both the direct impact of variability and the associated uncertainty which directly impacts costs [5]. Fig. 9 shows the effect of solar variability on a utility's operating reserve margin.

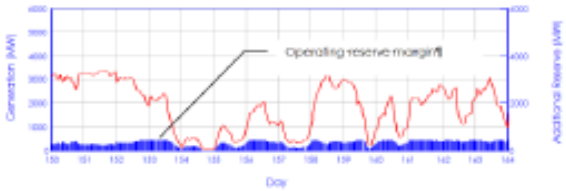

Figure 9: Time varying "operating reserve margin" developed from statistical analysis of hourly distributed generation variations.

The capacity value of PV generation for long term planning analyses is currently a topic of significant discussion in the PV and electric power industries. Characterizing the PV generation to appropriately reflect the historical statistical nature of the generation output on seasonal, daily, and hourly bases is one of the major challenges. In addition to solar power being variable, it is also a challenge to utility planners and operators to accurately predict solar power on the time scales

of interest. Day-ahead predictions are necessary for long-term planning of system adequacy, i.e., meeting the system peak load during the year. PV energy is more predictable in the hour-ahead time frame, but even then the uncertainty in PV forecasts must be accounted for in utility operation and dispatching. In order to minimize negative impacts and maximize benefits, each utility that incorporates solar energy must learn how to accommodate the uncertainty and variability of solar energy in their operational and planning practices, and do so while maintaining system reliability.

VIII. Conclusions

We described sky camera cloud detection, shadow forecasting and cloud motion vector methodology which can be used to estimate the solar PV ramp rate variability of USRE. We reviewed how forecasting data may be employed to reduce the detrimental impact on distribution systems due to voltage fluctuation caused by high PV penetration. Lastly, we discuss the effects of solar variability and uncertainty on ancillary services and the role of solar forecasting data in utility operational and planning practices.

IX. References

Periodicals:

[1] M. Lave, J. Kleissl, Arias-Castro, E., High-frequency fluctuations in clear-sky index, *Solar Energy*, doi:10.1016/j.solener.2011.06.031, August 2011

[2] P. Mathiesen, J. Kleissl, Evaluation of numerical weather prediction for intra-day hourly solar irradiance forecasting in the CONUS, *Solar Energy*, 85(5): 967-977, 2011

[3] C. W. Chow, B. Urquhart, J. Kleissl, M. Lave, A. Dominguez, J. Shields, B. Washom, Intra-hour forecasting with a total sky imager at the UC San Diego solar energy testbed, *Solar Energy*, doi:10.1016/j.solener.2011.08.025, September 2011

[4] R. A. Walling, R. Saint, R. C. Dugan, J. Burke and L. A. Kojovic, "Summary of Distributed Resources Impact on Power Delivery Systems", Working Group on Distributed Generation Integration, , IEEE Transactions on Power Delivery, Vol. 23, No, 3, p1636-1644, July 2008

Technical Reports:

[5] D. Lew and R. Piwko, "Western Wind and Solar Integration Study:Executive Summary", The National Renewable Energy Laboratory, Golden, Colorado, October 2010

[6] T. Madsen, M. Kinman and B. Del Chiaro, "Building a Brighter Future, California's Progress toward a Million Solar Roofs", Environment California Research & Policy Center, Los Angeles, California, November 2011

[7] A. Mills, M. Ahlstrom, M. Brower, A. Ellis, R. George, T. Hoff, B. Kroposki, C. Lenox, N. Miller, J. Stein, and Y-H Wan, "Understanding Variability and Uncertainty of Photovoltaics for Integration with the Electric Power System", Ernest Orlando Lawrence Berkley National Laboratory, December 2009

Standards:

[8] IEEE Std. 1547.1-2005: IEEE Standard Conformance Test Procedures for Equipment Interconnecting Distributed Resources With Electric Power Systems, July 2005

[9] IEEE Std. 1547.3-2007: IEEE Guide for Monitoring, Information Exchange, and Control of Distributed Resources Interconnected With Electric Power Systems, 16 November 2007

[10] IEEE Std. 1547.7: Draft Guide to Conducting Distribution Impact Studies for Distributed Resource Interconnection (under development)

Papers from Conference Proceedings (Published):

[11] M. Hassanzadeh, M. Etezadi-Amoli and M.S. Fadali, Practical Approach for Sub-hourly and Hourly Prediction of PV Power Output, North American Power Symposium (NAPS), 2010, pp 1-5

[12] T. E. McDermott, "Voltage Control and Voltage Fluctuations in Distributed Resource Interconnection Projects", Transmission and Distribution Conference and Exposition, 2010 IEEE PES, pp 1-4

Internet:

[13] J. T. Schwarz, "On load tap changer in Service – Maintenance aspects", http://www.nersa.org.za/Admin/Document/Editor/file/Electricity/Compliance%20Monitoring/Jurgen%20Schwarz.pdf, June 11, 2008, [November 28, 2011]]

[14] P. Kumar, "Guide Book Electrical System, Chapter 3" ,http://www.em-ea.org/Guide%20Books/book-3/Chapter%203.1%20Elecrical%20Systems%20.pdf, Chapter 3.1 Electrical System, February 17, 2005 [November 28, 2011]

Kay Stefferud joined EnerNex as a Principal Consultant in February 2010. She has been a member of both the IEEE Computer and Power Engineering Societies. Kay has written specifications for integrated DER, premise networks, microgrids and demand response systems.

Kay specializes in transitioning new technology from the R&D phase into innovative products. Kay has worked on smart meters, demand response systems, operational flight software, real-time planning systems, medical systems, back bone, router, network appliances, and cyber security products.

Jens Schoene (M'07) is the Director of Research Projects and Modeling at EnerNex LLC in Knoxville, TN. Jens has conducted a large variety of projects including (1) transient, harmonic, and TOV simulations on wind plants and other power systems, (2) distributed generation interconnection studies, (3) power quality measurements, (4) induction studies on transmission and distribution systems, and (5) arc flash studies. He received the Ph.D. degree and the M.S. degree in Electrical Engineering in May 2007 and March 2002, respectively, from the University of Florida, Gainesville. During this time he worked at the International Center for Lightning Research and Testing (ICLRT) at Camp Blanding, Florida where he conducted research on the responses of power distribution systems to direct and nearby lightning strikes, lightning induced currents in grounding structures, and the modeling of the lightning return stroke process. In 1999 he received the Dipl. Ing. degree from the Department of Electrical Engineering, University of Paderborn, Soest. He published eight scientific papers as main-author and ten scientific papers as co-author in peer-reviewed journals and has been the main or co-author of over 20 technical articles and conference proceedings.

Jan Kleissl is an assistant professor at the Dept. of Mechanical and Aerospace Engineering at the University of California, San Diego (UCSD) and Associate Director, UCSD Center for Energy Research. Kleissl received a Ph.D. in 2004 from Johns Hopkins University in Environmental Engineering and joined UC San Diego in 2006. Kleissl

APPENDIX B

USRE White Paper Submitted to the 2012 IEEE ISGT Conference

Large Scale Solar PV System Impact Analyses

E. Gunther, *Fellow, IEEE,* D. Houseman, *Member, IEEE,* G. Rodriquez *Member, IEEE,* J. Schoene, *Member, IEEE,* S. Shaw, *Member, IEEE,* K. Stefferud, *Member, IEEE,* and Vadim Zheglov, *IEEE Member*

***Abstract*— Distributed large and small-scale renewable generation including solar photovoltaic (PV) installations are rapidly increasing on California residential, commercial, and industrial distribution lines. Utilities have to be prepared for potential issues caused by increased PV penetration on their systems. EnerNex and Southern California Edison are currently conducting a study for the California Energy Commission to investigate the effects of high penetration levels of PV on distribution systems. Part of this investigation is to quantify, through computer simulations and measured solar irradiance data, the effects of an estimated 200 MW commercial-scale PV generation to be installed by 2015 in SCE service territory. The study examines the effects of 3 large rooftops systems totaling 6.5 MWs on an industrial feeders in SCE's southern California territory. Our analyses considered 8 potential issues on high penetration PV distribution feeders. Significant findings include 1) reverse power flows occur during times of high PV generation, 2) voltages remain within permissible ranges even when large loads are dropped and 3) settings for the protective relays need to be adjusted to account for the reverse power flows.**

***Index Terms*—photovoltaic, power generation, renewable energy, solar, power distribution lines**

I. Introduction

For this study we modeled and validated two SCE distribution circuits with high penetration levels of PV. The generation levels of each of the PV generators were individually determined from irradiance data taken from field measurements. Modeling scenarios included the loss of the two largest loads during high solar production periods augmenting reverse power flows. We applied the model to investigate the following effects of the PV installed on the SCE distribution feeder: (1) voltage control, (2) effects of losing large loads, and (3) overcurrent and relay protection.

The data collection period has been over 1 year and accounts for seasonal changes and cloud shading. Consequently, we capture the time-of-day variation of the power generated by each PV generator in a highly realistic fashion. The distribution feeder with the 3 large scale PV systems (2 MW, 2 MW and 2.5 MW) and the two largest loads which total 934 MVA are shown below in Fig. 1.

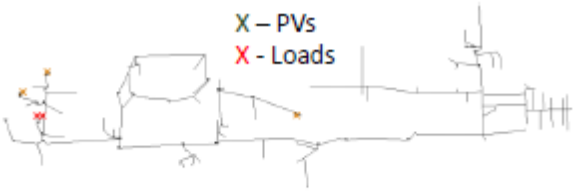

Fig. 1 Distribution feeder with 6.5 MW PV at 3 sites.

II. Impact of Solar Variability on Voltage Fluctuation and Utility Operation Practices

Most utilities control the voltage on the secondary distribution circuit (the low-voltage circuit the customer is directly connected to) by regulating the voltage on the primary circuit (the distribution feeder circuit with typical voltage levels between 4 kV and 35 kV). The service voltage is the stepped-down feeder voltage minus the losses (i.e., service transformer losses and wiring losses). Based on the expected load, utilities design service transformer sizes and the size and length of a service line so that the service voltage stays within acceptable limits. Most regulatory entities and utilities in the USA adhere to the voltage limits specified in ANSI C84.1. Equipment that is at the utilities disposal for regulating the primary circuit voltage includes (1) load tap-changing transformers (LTCs) line and (2) shunt capacitor banks (see Fig. 2).

In general, any control operation of the voltage regulation equipment (tap changing or switching of capacitor steps) is detrimental to the lifetime of the regulation equipment. Voltage fluctuations caused by the presence of PV on the system can cause an excessive number of control operations that can dramatically reduce the equipment lifetime [4].

Another consequence of the more frequent operation of voltage regulation equipment due to the presence of PV is the increasing fluctuation of the reactive power. This has an

This work is supported in part by the California Energy Commission under contract PIR-08-043.

E. Gunther is with EnerNex LLC, Knoxville TN 37932 USA (e-mail: erich@enernex.com).

D. Houseman is with EnerNex LLC, Knoxville TN 37932 USA (e-mail: doug@enernex.com).

George Rodriquez is with SCE, Pomona CA 91767, (email: George.Rodriguez@sce.com).

Sunil Shah is with SCE, Pomona CA 91767, (email: Sunil.Shah@sce.com).

J. Schoene is with EnerNex LLC, Knoxville TN 37932 USA (e-mail: jens@enernex.com).

K. Stefferud is with EnerNex LLC, Knoxville TN 37932 USA (e-mail: kay@enernex.com).

V. Zheglov is with EnerNex LLC, Knoxville TN 37932 USA (e-mail: vadim@enernex.com).

economic impact on subtransmission and transmission systems. For instance, for a scenario in which PV penetration on the distribution feeder is high and widespread and the capacitor bank is disconnected, some reactive power may have to be supplied from the transmission system. Supplying reactive power from the transmission system is generally more expensive than supplying reactive power locally.

Inverters used in PV and other distributed resources usually have power factor correction capabilities[1]. However, currently IEEE 1547 [1, 2] forbids the distributed resource from actively regulating voltage, which is a somewhat controversial requirement. Opponents of the IEEE 1547 requirement argue that the active PV voltage regulation restriction is counter innovative in that it curbs the full potential of PV inverter technology. A consequence of the IEEE 1547 restriction is that on systems that require active voltage regulation to meet the area electric power system service voltage requirements, equipment other than PVs must be employed to change the reactive power in direct response to measured voltage conditions. Future versions of IEEE 1547 currently under development and review [3] are addressing the possibility of using inverters to assist in power quality control including control of reactive power. Changes to voltage regulation, voltage ride through, and frequency ride through requirements have been proposed in IEEE 1547 Amendment A.

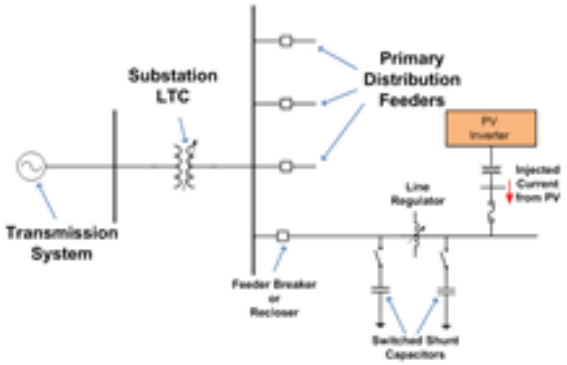

Fig. 2 Radial distribution feeder with voltage regulators and PV.

Voltage fluctuation caused by PV happens on different time scales and the hence the time scale and type of PV model needed to assess the effectiveness of the mitigation strategy. Small time-scale voltage fluctuation is caused by cloud transients, that is, the step change of irradiation happening at the transition from one steady-state (e.g., PV generation during clear-sky condition) to another steady-state (e.g., PV generation during cloud shading).

For instance, changing PV generation levels caused by fast changes of irradiation levels due to cloud shading can result in low-frequency voltage fluctuation on the distribution system, which is perceived by the customer in the form of changing light intensity and commonly referred to as "flicker". Complex models of the PV that are capable of simulating the transient response of the inverter are required to simulate the flicker effect and assess the effectiveness of mitigation options. High time resolution forecasting data for a given PV location may be employed for mitigation – the forecasting data would yield information of an oncoming cloud and ramp down the PV output just before the cloud shades the PV thereby avoiding a large step change of PV generation and excessive voltage fluctuation during the transition period from "clear-sky condition" to "cloud shading". After the cloud has passed, the PV output can be ramped up again slowly and in a controlled manner in order to minimize voltage fluctuation. To accomplish control of the PV output, advanced inverter functions are required as well as an equitable method to compensate solar systems owners for lost power output.

Large-time scale voltage fluctuation resulting in reactive power fluctuations and operation of voltage regulation equipment is also caused by clouds, but the transition period from high irradiation to low irradiation (or vice versa) is of less importance. Instead, the voltage fluctuates because of changing steady-state generation levels (e.g., full generation during clear-sky condition and reduced generation during cloud shading). Voltage regulation equipment adjustments according to the PV generation levels and frequent changes of the generation level (e.g., during scattered fast-moving clouds) will result in a large number of operations of the regulators, in particular in weak systems and/or systems with large PV penetration. Forecasting data in conjunction with storage may be employed in a control strategy to reduce the number of voltage control operations. A simple quasi steady state PV model where the generation output is scaled according to the insolation level is sufficient for an investigation of the system impact with regards to voltage fluctuation and assessments of mitigation options.

III. Analyzes Overview

The study's analyses considered two scenarios: 1) Actual SCE industrial feeder with 3 large rooftops systems totaling 6.5 MWs and 2) Simulated loss of the feeder's two largest loads totaling 934 MVA during a period of high solar generation. Our analyses considered 8 potential issues on high penetration PV distribution feeders. Fig. 3 categorizes and summaries the 8 analyses performed and potential issues associated with each.

IV. Findings

Analyses of the simulation results, recorded voltages and actual events on the feeders indicate 3 significant findings: 1) reverse power flows occur during times of high PV penetration, 2) voltages remain within permissible ranges even when large loads are dropped 3) settings for the protective relays need to be adjusted to account for the reverse power flows.

[1] The Distributed Resource (DR) inverters are used to maintain a constant power factor during variable environmental conditions, such as variations in wind speed (in the case of generation from wind) and cloud shadowing (in the case of PV generation).

APPENDIX C:Sky Camera and Solar Forecasting Algorithms Business Plan

The sky cameras and forecasting algorithms (SkyCam) developed as part of the USRE project can be used in commercial solar forecasting products similar to existing applications for wind farms. Currently SCE uses manual methods which employ meteorologists to predict generation and ramp rates from solar PV systems. Solar forecasting applications are needed by utilities and by the CAISO. Of particular applicability to the USRE project, are applications which can predict intra-hour solar production and solar ramp rates.

Because ramp rates largely determine the amount of backup spinning reserves or energy storage systems needed to modulate solar variability, the economic value of solar forecasting of ramp rates and solar generation is significant. Commercialization of the forecasting algorithms could be performed by commercial companies such as AWS TruePower and Garrad Hassan.

In proceeding with potential commercialization activities for the SkyCam system, it is important to identify the key elements of intellectual property, competitive advantages, and market drivers that will be used as a basis for commercialization. The following excerpt provides a proposed Table of Contents for a 'Mini Business Plan' for the SkyCam System followed by descriptions of some of the more important commercialization discussion areas.

SkyCam Technologies Business Plan Outline (TOC)

EXECUTIVE SUMMARY

- Overview
- Market Opportunity
- Competition
- Overall Strategy
- Marketing, Sales, & Distribution
- Technology and Product Development
- Manufacturing
- Management
- Summary Financial Projections
- Conclusion

Section 2. OPPORTUNITY HIGHLIGHTS

- Background
- The Technology & Intellectual Property
- Market Opportunity
- Value Proposition
- Key Market Applications
- Scope of Initial Applications

- Key Financials
- Milestones

Section 3. COMPANY DESCRIPTION AND OVERVIEW

- Genesis
- Technology Overview
- Intellectual Property
- Initial Product Line Description
- Marketing & Sales Strategy
- Manufacturing
- Research & Development
- Staffing Plans
- Initial Executive Staff
- Permanent Staff
- OEM Development Partners
- Key Alliances
- National distributors/installers
- Energy Service Providers (ESPs)
- Strategic Partnerships
- Competition
- Competitive Responses
- Equipment Trials
- Risk Management

Section 4. SUMMARY PROJECTED FINANCIAL STATEMENTS

- Scenario Descriptions
- Financial Assumptions
- Capital Requirements & CashFlow Needs
- Financial Summary & Results

Section 5. CONCLUSION

Appendix A: Intellectual Property Overview and Strategy

Appendix B: Financial Assumptions and Summary Results

Appendix C: Quarterly/Annual Projected Financial Statements

Appendix D: Key Market Data

Appendix E: Market & Competitive Drivers

- Market Benefit Drivers
- Key U.S./ROW Competitors
- Competitive Technologies
- Competitive Comparison By Key Attribute

Appendix F: Product Requirements Summary

Appendix G: Glossary of Terms and Abbreviations

Market Connection:

The target market for SkyCam systems include a range of prospective customers: utilities, system integrators and PV system manufacturers, ESPs, large PV farm owners/operators, and others. Utilities are a natural target segment given that they are estimated to invest between $350-630B on upgrading, protecting, and controlling their U.S. distribution circuits. Within distribution circuits, "target rich" circuits would include (1) those that already have or are projected to have very high PV penetration rates, (2) those that have high PV clustering, (3) those where large solar PV systems are located on the end of the distribution line and (4) those that look electrically like 'weak sources' (e.g. long lines). ESPs, system integrators, PV system manufacturers, and owner/operators will likely realize additional benefits through incorporation of SkyCam systems as the market more fully matures and develops to include more stringent performance guarantees on not only total energy production (AC kwh) but on other metrics as well e.g. power quality, power volatility and predictability.

Competition:

The SkyCam system addresses the need to accurately forecast the output from solar PV using sky imagery and determine the maximum amount of variability or ramp rate of solar output. The system and solar forecasting model was developed and validated with generation data from SCE USRE systems. In addition, statistical analysis of power output data yields the maximum amount of output variability in the form of ramp up/down rates. These are key metrics that must be addressed by any system that is addressing the needs of the solar forecasting marketplace.

Deterministic measurement-based forecasting typically involves measurements obtained from satellites or ground-based sky imagers. However, deterministic forecasting using sky imagers is still in its infancy, and approaches thus far include intra-hour DNI (Marquez and Coimbra, 2013a), solar irradiance (Chow et al., 2011) forecasting using a Total Sky Imager (TSI) produced by Yankee Environmental Systems, and real AC power forecasting for 48 MW of photovoltaics (Urquhart et al., 2012). Other competitive systems and their system attributes may be available as well.

Competitive Advantages:

The SkyCam system has several key attributes that distinguishes it from existing competitive offerings and provide it a sustainable competitive advantage. These key features need to be clearly delineated.

Potential Market Barriers

One of the biggest technical barriers to integration of high penetration levels of PV is that the magnitude of impacts and the level of understanding is relatively nascent. Statistically, PV systems tend to be clustered together which as discussed previously nearly doubles the cost for distribution circuit upgrades, protection, and compensation, but the full extent of their impacts are just now beginning to be understood. For example, EnerNex analyzed existing SCE feeders where peak solar generation from PV systems clustered on warehouses already exceeds loads, as part of their CEC Utility Scale Solar Forecasting, Analysis and Modeling project (Agreement Number 500-10-060). The protection schemes on these SCE distribution feeders are able to successfully operate. Meanwhile SDG&E reported problems with excess wear on tap changers for PV systems at a much lower PV concentration, but with the PV systems located at the end of the distribution feeder. Clearly both the design of the feeders and the location of the PV systems on the feeders impacts the ability to incorporate high levels of PV. Also, it is not clear what the impact will be of incorporating smart inverter features for PV systems since being able to control real and reactive power through volt-VAR control may improve circuit PV capacity substantially based on EPRI estimates.

Full utilization and realization of the SkyCam value proposition is highly dependent on the many other interactions and long-term benefits of other alternative distribution circuit technologies. For instance, there is little understanding of the impact of high percentages of PV on grid stability or on power quality in terms of feeder configurations and control scheme design. Additionally there is little information on the dynamics of the grid and the impact pre and post solar PV installation to help provide a benchmark for adoption. Evaluating fault protection equipment for effects from adverse power flow and evaluating voltage control equipment for spatial variations attendant with the location of PV will both help determine the potential value contribution of a SkyCam-type system. Although new studies of these impacts and distribution circuit archetypes and typologies are being developed, the full extent of these interactions and the relative value of different types of control and mitigation compared to implementing SkyCam-type systems is difficult to estimate.

SkyCam Benefits:

SkyCam technologies will improve the economies of solar technology by improving the operation of solar on the grid in some of the following ways;

- Validates pro-active monitoring and forecasting algorithms for 1-15 minute look-ahead PV power production
- Provides accurate timing, magnitude, and duration of ramp events (both output power increases and decreases)

- Provides look-ahead forecasts to both owner/operators and local utility companies to allow them to proactively manage variable power output especially ramp events (both up and down)
- Optimizes mitigation techniques for high penetration of renewables with improved visibility benefiting both the PV owner and utility
- Improves capacity and stability margins of distribution circuits through proactive command and control and ultimately even curtailment commands for circuit protection purposes
- Provide utilities additional technology and control alternatives in managing both each distribution circuit optimally for both efficiency and grid stability as well as overall regional optimization allowing them to embrace higher PV penetration levels
- Provides scientifically validated basis for 'grid supporting' functions utilizing aggregated PV power and ramp event forecasts for regional optimization and control (e.g. utility and possibly CASIO in the future). These techniques would directly impact regulatory guidelines found in both IEEE 1547 as well as California's Rule 21.
- Provide additional engineering data and guidelines on control and operation of dense PV

In general, additional value streams can be identified as the SkyCam system capabilities are further refined and explored. These features will assist utilities in future scenarios to be able to transform many of their challenges into opportunities. IOUs/POUs will be able to proactively embrace/affect future policy and investment plans thus saving both CAPEX and OPEX funds by avoiding stranded assets, by improving operating efficiency and capacities of existing circuits, and by more efficient use of current assets and equipment. In addition, replacement/upgrade strategies, conditioned-based maintenance (CBM) responses, proactive identification of likely circuit failures, transformer utilization and life cycle costs and strategies for circuit healing and fault location can all be addressed. Real utility financial impacts and benefits will be further developed.

Commercialization Milestones:

There are a variety of potential performance and cost milestones that must be met including:

The state-wide benefits were calculated using average capital and O&M cost per distribution circuit mile. Project performance and cost objectives include:

1) Successful demonstration of the SkyCam measurement and forecasting capability according to each of the following metrics: 1-15 minute forecasts of output power, ramp events, and other relevant data.

2) Creation of detailed utility-oriented business case identified by the most likely beneficial distribution circuit typologies.

3). Creation of detailed ESP/Owner/Operator business case based on value of information and timing including participation in CAISO (or other RTO/ISO equivalent) ancillary services energy markets and other identified value streams.

4) Creation and validation of enhanced performance models of distribution circuit operations and how they could best take advantage of SkyCam-based forecasts e.g. provide input to the evolving utility interconnection process based on better tools, more 'controls', and smarter algorithms.

5). Thorough manufacturing Bill of Materials (BOM) and labor analyses with value engineering performed at several projected production volume levels to determine gross manufacturing profit and contribution margins (to be used in projected financial statements).

6). Estimation of cash flow and capital requirements under several business scenarios.

7) Other potential benefits that require additional analysis and quantification:

- Avoided costs of compensation and/or protective equipment on circuit
- More effective distribution circuit asset utilization (e.g. capacitor banks, transformers, protection equipment, etc.)
- Potential percentage improvement in distribution circuit load factor and available capacity,
- Potential reduction in distribution circuit CAPEX costs and O&M reduction
- Potential value of utility (or Owner/Operator) being able to statistically diversify and forecast accordingly many distributed large PV sites to help reduce required mitigation for ramp events as well as reduce possible ancillary services purchases.

Intellectual Property:

The SkyCam system is composed of both remotely-based equipment and centrally-located processing capability. The remote system is composed of a specialty camera system and optics, on-board Linux-based real-time operating system running a variety of floating-point software algorithms on a microprocessor and with associated data storage, communications, and power supplies. In cooperation with Sanyo Electric Co. (now Panasonic), LTD., Smart Energy Systems Division, the University of California, San Diego designed and developed a sky imager system specifically for short-term solar forecasting applications. The SkyCam design was also partially informed by extensive work with the Yankee Environmental Systems Total Sky Imager, along with consulting from Janet Shields who developed the world class Whole Sky Imager. The SkyCam contains a high quality large format 12-bit CCD sensor coupled with an equisolid angle fisheye lens. The optical system is supported by an onboard embedded computer and a suite of sensors to monitor system status and health. The system takes images at a 30 second rate with images ranging in size from 7-12MB which means the bandwidth can potentially be up to 3.2

Mbits/sec. Consequently, a cellular connection can only be used for monitoring operations, system health (including temperature and humidity), and image quality and not for higher bandwidth data transmission which would require either a high-speed internet connection (ideally) or require monthly swapping of portable hard drives resident in the SkyCam system.

The centrally-located processing receives all data from all remote locations, archives this data, and performs a variety of higher-level processing and forecasting algorithms. At the present time, most algorithms are only processing on a standalone remote basis to determine 1-15 minute forecast power outputs, however, additional 'multi-remote' processing is being developed which will combine SkyCam remote locations to obtain effective stereoscopic views of the same clouds to help determine their real cloud height (currently determined by using standard meteorological data for each type of cloud cover). A determination must be made as to the intellectual property rights (if any) of Sanyo, Yankee Group, and Janet Shields in the SkyCam system both for any proprietary hardware or optical development (none expected) and any contributions to optical processing algorithms. It is expected that both CEC and UCSD would require their standard range of potential royalty rights (which have been assumed in projected financials).

The SkyCam camera system is calibrated so that the pointing angle in 3D space of every pixel is known. This way, when clouds are detected, their angular location is known. Using stereography between two USIs, the depth of the cloud field is determined giving the quasi-three-dimensional location of the clouds in the sky. The cloud locations are georeferenced (registered with respect to earth coordinates) so that their shadows can be ray traced to the surface. After taking multiple images, the speed and direction of the clouds is determined, their future locations are forecast, and the shadows they will cast is computed. Simultaneously, using complimentary power and irradiance ground measurements, the thickness of the clouds is estimated. The spatial distribution of the shadows over the solar collectors and the optical thickness of the clouds are then used to estimate power output at a granular resolution.

The SkyCam is designed to continuously capture high resolution images of the sky hemisphere. The optical system uses a high quality large format CCD camera coupled with a high dynamic range algorithm which enables the USI to capture the large range of light intensities existing within the sky hemisphere. The SkyCam has a complete thermal control and monitoring system to maintain suitable operating temperatures for the electronics, even in the harshest of environments, such as the hot southwest deserts. A thermal control system includes two large thermoelectric coolers and dome heaters to prevent condensation on the external optical surface. The operating software combines multiple images with different exposure lengths to generate a single 48-bit high dynamic range image for use with processing algorithms.

A more detailed description of the SkyCam system and operation follows. The USI captures images using an upward-facing charge-coupled device (CCD) image sensor sensing RGB channels at 12 bit intensity resolution per channel. A 4.5 mm focal length circular fisheye lens allows imaging of the entire sky hemisphere. Utilizing high dynamic range (HDR) imaging, the USI outputs images at 16 bits per channel with a dynamic range of over 80 dB (Urquhart et al.,

2013). Lossless PNG compression is used to store and transmit images for forecast analysis. This large dynamic range is a key feature of the SkyCam system.

Since cloud cover near the sun provides vital information for short-term solar forecasting, the SkyCam does not employ a solar occulting device. The increased resolution and dynamic range, combined with the ability to image the entire sky hemisphere, has allowed the USI to overcome the primary shortcomings of the previous imaging system a commercially-available TSI. These features are several key intellectual property rights of the SkyCam system. The proven ability of the SkyCam system to predict the occurrence of ramp events and timing holds considerable value for this developing industry. Although it is not possible to forecast a large majority of short ramps accurately (although progress is being made to refine these as well), the 5 minute USI forecast accurately predicted many of the larger ramp events quite well across a large variety of sky conditions. Comparison of forecast time series against measured time series showed a forecast horizon of 10 minutes to be about the most accurate forecast horizon. 15 minute forecasts exhibit slightly larger errors but the performance of 15 minute forecast skill is promising.

Prior Art Impacts on Intellectual Property:

A key activity that must be further analyzed in any intellectual property assessment is the relative roles and contributions of other individuals and entities to the working implementation of a prototype. Especially important is whether those contributions were obtained publicly (e.g. trade shows and conference venues) and whether any intellectual property rights were established (e.g. copyrights, patent pending, etc.). The following discussion is included to outline both additional SkyCam intellectual property as well as all known possible intellectual property rights that would need to be ascertained in the near future.

The method used to generate forecasts in this study is an improved implementation of the procedure described in Chow et al. (2011), which was developed for the TSI. A brief overview of the USI forecast procedure will be presented, with a focus on the major improvements made since the previous iteration of UCSD sky imager forecast software. USI forecast data processing may be considered in two main sections: one which operates purely upon sky imager data, and one which is specific to the location and equipment of the site of interest. A forecast may then be issued after all data processing is complete. The sky imagery-based algorithms are explained in great detail in Chow et al. (2011) and Ghonima et al.

The first objective after reading an image is to determine which regions (if any) of the image contain clouds (Fig. 3). Following the cloud decision algorithm detailed in Ghonima et al. (2012), image pixels are classified as clear, thin cloud, or thick cloud based on the ratio of the red image channel to the blue image channel, or red-blue-ratio (RBR). Thresholds are applied on the difference between the RBR of a specific pixel and the clear sky RBR of the same pixel (let RBR RBR - RBR), which describe the minimum RBR values representative of thin clouds and thick clouds. To determine the clear sky RBR of image pixels, a "clear sky library" (CSL) was compiled, which contains the clear sky RBR as a function of image zenith and sun-pixel angles in the form of lookup tables for each solar zenith angle. RBR thin and thick thresholds,

thresholds were visually calibrated by comparing resulting cloud decision images with raw images and their RBR images. The CSL was constructed from one completely clear day close to the dataset on March 22. Thin and thick thresholds for this day were 0.3084 and 0.5290.

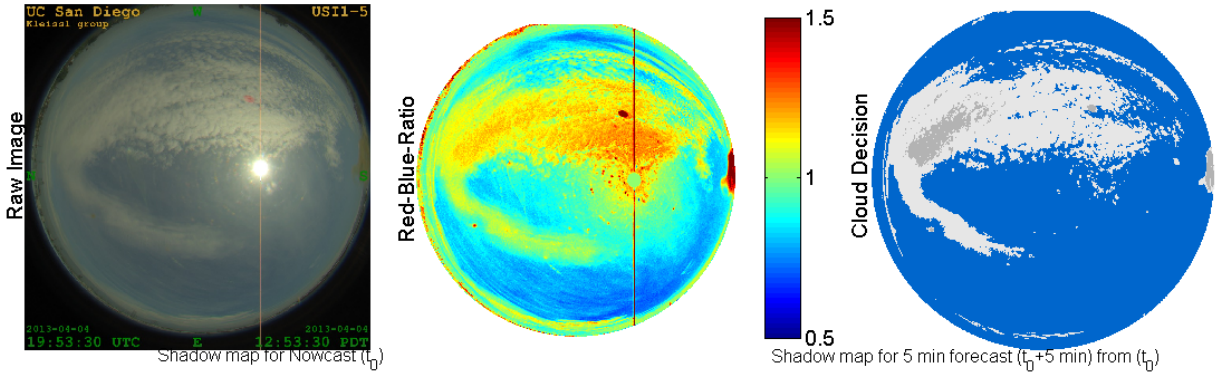

Figure: Cloud decision procedure. Left: Original image. Center: Red-blue-ratio to enhance cloud contrast. Right: Cloud decision for thin (white) and thick (grey) clouds.

Cloud base height (CBH) measurements were obtained from historical weather reports of the standardized METAR weather data format, which are typically generated once per hour (sometimes more frequently) at airports or weather observation stations. In this case, the nearest METAR station was located about 4 km northeast of the USI at the San Bernardino airport (KSBD). A geometric transform, similar to the pseudo-Cartesian transform of Allmen and Kegelmeyer (1996) was then performed to map cloud information to a latitude-longitude grid at the CBH. The resulting "cloud map" is a two-dimensional planar mapping of cloud position at the obtained CBH above the forecast site, centered above the physical location of the USI.

Cloud pixel velocity was obtained by applying the cross-correlation method (CCM) to the RBR of two consecutive cloud maps (Chow et al., 2011). The vector field resulting from the CCM contains the wind vector field where vectors with small cross-correlation coefficients have been excluded. The vector field is processed through a series of quality controls to yield a single average cloud velocity vector that is applied to the entire cloud map. In other words, the velocity of all clouds is assumed to be homogeneous.

Irradiance forecasts are produced by advecting the current cloud map at the calculated cloud pixel velocity to generate cloud position forecasts at each forecast interval (30 seconds). The locations of ground shadows cast by clouds as defined by their location in each advected cloud map are determined by ray tracing. The resulting estimation of cloud shadows within the forecast domain is termed the "shadow map." For each pixel within the footprint, a modal is assigned from the histogram procedure based on whether the pixel is covered by clear sky, thin cloud, or thick cloud. The average modal of the pixels within the power plant is then multiplied by the clear sky power output model to produce plant power out